Elucidating the Molecular Mechanisms by which Arboviruses Hijack Cellular Pathways

by

Adriana Marcela Airo

A thesis submitted in partial fulfillment of the requirements for the degree of

Doctor of Philosophy

in

Virology

Department of Medical Microbiology and Immunology
University of Alberta

© Adriana Marcela Airo, 2020

Abstract

Despite their small size and apparent simplicity, viruses are capable of causing mass casualties, political turmoil, and global economic shut down. Due to their minimal genome (~10–12 kb), arboviruses such as Zika (ZIKV), Dengue (DENV), and Mayaro (MAYV) depend on many host molecules for replication and have evolved multiple strategies to subvert host innate immune defense mechanisms. Currently, few vaccines and limited treatment options exist.

The main function of flavivirus capsid proteins is to protect the viral genome, however, accumulating evidence suggests that in addition to this function, capsid can modulate the host cell to create a favourable environment for viral replication. A major finding in this thesis was that flavivirus capsids play a role in evasion of antiviral systems. Strategies employed by capsid include inhibition of apoptosis and activation of the master regulator Akt. Moreover, I examined the global transcriptome changes in capsid expressing cells by RNA-Seq and identified a potential mechanism by which flavivirus capsids suppress the production of type I interferon.

Very little is known about the interactions of MAYV with human cells, therefore, in this thesis I examine MAYV tropism and characterize MAYV-infection in primary human macrophages. RNA-Seq data revealed that MAYV causes drastic changes in the transcriptome of infected macrophages and suggests an important role for macrophages in MAYV-induced inflammation and disease pathology.

Collectively, this thesis provides insight into arbovirus-host interactions. Understanding the consequences of the interactions between viral proteins and cellular factors may reveal novel therapeutic targets.

Preface

A version of Chapter 3 was published as Airo AM, Urbanowski MD, Lopez-Orozco J, You JH, Skene-Arnold TD, Holmes C, Yamshchikov V, Malik-Soni N, Frappier L, Hobman TC. 2018. "Expression of flavivirus capsids enhance the cellular environment for viral replication by activating Akt-signalling pathways". *Virology*. 516:147-157. This project was originally conceived by M Urbanowski and T Hobman. J Lopez-Orozco and J You assisted with experimental design, data collection and analysis. T Skene-Arnold helped with the Microcystin-Sepharose pulldowns. T Skene-Arnold, C Holmes and V Yamshchikov supplied reagents and intellectual input. N Malik-Soni and L Frappier performed and provided data for affinity purification mass spectrometry. I was responsible for experimental design, data collection and analysis as well as manuscript composition and revisions. M Urbanowski contributed to data collection, analysis and manuscript composition. T Hobman was the supervisory author and contributed to concept formation and manuscript composition.

The use of Peripheral blood mononuclear cells (PBMCs) from healthy volunteer blood donors was approved by the Health Research Ethics Board at the University of Alberta (University of Alberta human ethics protocol 00079034) and written informed consent was received for all samples.

Permission/license was obtained for all published figures used in this thesis.

Figure 1.2B was reprinted with permission from Shang, Z., et al. (2018). “Crystal structure of the capsid protein from Zika virus”. Journal of Molecular Biology **430**(7), 948-962. License Number: 4833740219179. Licensed Content Publisher: Elsevier.

Figure 1.2C was reprinted with permission from Barrows, N. J., et al. (2018). "Biochemistry and molecular biology of flaviviruses." Chemical reviews **118**(8): 4448-4482. Copyright (2018) American Chemical Society.

Dedication

In memory of my father

Acknowledgements

To my supervisor Dr. Tom Hobman, thank you for the opportunity to gain research experience and for your continued support throughout my PhD. I am very grateful to you for providing an environment that permitted me to branch out and conduct my research independently. To my committee members, Dr. Jim Smiley and Dr. Maya Shmulevitz, thank you for the valuable feedback and continued support. Thank you to Dr. Rob Ingham and Dr. Eric Jan for serving as my PhD defence examiners.

Many thanks to past and present members of the Hobman lab with special mention to Valeria Mancinelli for experimental support, Eileen Reklow for technical support, Colleen Reid, Alberto Felix Lopez, Drs. Joaquin Lopez-Orozco, Zaikun Xu and Jae Hwan You for helpful feedback and contributions to my research.

Thank you to the Department of MMI and the MMI students for being such a wonderful group. Thank you to Dr. Deanna Santer for scientific discussions and helping me set up primary macrophage cultures. Thank you to the Ingham and Evans lab members for sharing reagents and technical advice. Thank you to Dr. Juan Jovel for help with analysis of RNA-Seq data. Lastly, thank you to Dr. Debby Burshtyn for convincing me that U of A was the place to undertake my graduate studies.

To my amazing parents – thank you for teaching me integrity, encouraging curiosity, demonstrating perseverance, and providing support. It is thanks to you and your sacrifices that I am privileged enough to pursue my interests. Thank you to my big brothers for their tremendous support and for always helping me. I feel very lucky to be a part of such a wonderful family.

To my significant other/best friend/most valued colleague, Patrick. Almost every experiment in this thesis was discussed with you at one point and you always offered valuable insight. Your support throughout the years has kept me afloat. I couldn't have done this without you.

To my dad – an engineer by training but a scientist at heart – you were always my role model and although you cannot read this, I thank you for all that you did and I dedicate this thesis to you.

Table of Contents

Abstract ii

Preface iii

Dedication v

Acknowledgements vi

List of Tables xiv

List of Figures xv

Abbreviations xviii

Chapter 1 Introduction 1

1.1 Overview 2

1.2 Flaviviruses 3

1.2.1 DENV 3

1.2.2 ZIKV 6

1.2.3 Flavivirus virion and genome organization 7

1.2.4 Flavivirus replication 10

1.2.4.1 Viral Entry and Cellular Tropism 10

1.2.4.2. Translation and Replication 12

1.2.4.3. Virion Assembly and Egress 14

1.3 Subversion of cellular pathways by ZIKV and other flaviviruses 14

1.3.1 Apoptosis 15

1.3.1.1 Extrinsic Apoptosis 17

1.3.1.2 Intrinsic apoptosis 18

1.3.2 Viral modulation of apoptosis 20

1.3.3 The PI3K/Akt Signalling pathway can prevent apoptosis initiated by Fas 21

1.3.3.1 Phosphatases that regulate the PI3K/Akt pathway 23

1.3.4 Interferon 26

1.3.4.1 The IFN system 26

1.3.4.2 The IFN induction pathway 28

1.3.4.3 Subversion of IFN induction by ZIKV and other flaviviruses 33

1.4 Alphaviruses 36

1.4.1 CHIKV and MAYV 37

1.4.2 Alphavirus virion and genome organization 39

1.4.3 Alphavirus replication 42

1.4.3.1 Viral entry and cellular tropism 42

1.4.3.2 Translation and replication 44

1.4.3.3 Virion assembly and exit 45

1.4.4 Mechanisms of virus-induced arthralgia 46

1.5 Objectives of Thesis 48

Chapter 2 Materials and Methods 50

2.1 Materials 51

2.1.1 Reagents 51

2.2 Methods 62

2.2.1 Molecular Biology 62

2.2.1.1 Purification of Plasmid DNA from E.coli 62

2.2.1.2 Polymerase chain reaction 63

2.2.1.3 Restriction endonuclease digestion 63

2.2.1.4 Agarose Gel electrophoresis 63

2.2.1.5 Purification of DNA fragments 64

2.2.1.6 Ligation of DNA fragments 64

2.2.1.7 Transformation of E. coli 64

2.2.1.8 Construction of recombinant plasmids 65

2.2.2 RNA techniques 66

2.2.2.1 RNA isolation 66

2.2.2.2 Quantification of RNA 67

2.2.3 Cell Culture, transfection, and transduction of mammalian cell lines 67

2.2.3.1 Cell line maintenance 67

2.2.3.2 Transfection of cell lines 68

2.2.3.3 Generation of AcGFP-Myc-ZIKV capsid expressing stable cell lines 68

2.2.3.4 Polyionosinic:Polycytidylic Acid (Poly(I:C)) stimulation 69

2.2.3.5 RNA interference 69

2.2.3.6 Cell viability assays 69

2.2.4 Virology techniques 70

2.2.4.1 Production of lentivirus 70

2.2.4.2 Transduction of mammalian cells with lentivirus 70

2.2.4.3 Determination of lentivirus yield 71

2.2.4.4 Virus infection and quantification 72

2.2.5 SDS-Page and Immunoblotting 72

2.2.6 Immunofluorescence Microscopy 73

2.2.7 Analysis of protein-protein interactions 74

2.2.7.1 Microcystin-Sepharose pulldowns 74

2.2.7.2 Co-immunoprecipitation of PP-1 and ZIKV C 75

2.2.7.3 Co-immunoprecipitation of TRIM25 and ZIKV C 76

2.2.8 RNA sequencing 76

2.2.8.1 Sample prep for RNA-sequencing 76

2.2.8.2 Ion Torrent Next-generation sequencing 77

2.2.8.3 Analysis of RNA-Seq (Differential gene expression analysis) 78

2.2.9 Isolation of primary cells from blood 78

2.2.9.1 Gradient density centrifugation for purification of PBMC cells 78

2.2.9.2 Isolation of CD14^{+} monocytes and MDM differentiation 79

2.2.10 Flow cytometry 79

2.2.10.1 Detection of activated caspase-3 and caspase-8 in transduced cells 79

2.2.10.2 Detection of caspase-3 in cells co-expressing capsid and WNV replicon 80

2.2.10.3 Flow cytometry analysis of ZIKV-infected cells 81

2.2.10.4 Flow cytometry analysis of MAYV-infected cells 82

Chapter 3 Expression of Flavivirus capsids enhance the cellular environment for viral replication by activating Akt-signalling pathways 83

3.1 Rationale 84

3.2 Results 85

3.2.1 Myc-tagged flavivirus capsids localize to cytoplasmic reticular elements and nuclei 85

3.2.2 Expression of flavivirus capsids protects cells from Fas-dependent apoptosis 85

3.2.3 Capsid expression confers a modest but significant protective effect against Fas-dependent apoptosis in replicon-transfected cells 87

3.2.4 Flavivirus capsids enhance phosphorylation of Akt at serine 473 89

3.2.5 Inhibition of PI3K reduces anti-apoptotic activity of flavivirus capsid proteins 93

3.2.6 Flavivirus capsid expressing cells are more metabolically active 93

3.2.7 Expression of flavivirus capsid proteins increases expression of GLUT1 . 95

3.2.8 Dengue virus capsid interacts with protein phosphatase 1 97

3.2.9 Zika virus capsid protects cells from Fas-dependent apoptosis and interacts with protein phosphatase 1 98

3.2.10 Protein sequence alignment of flavivirus capsid proteins 103

3.3 Summary 105

Chapter 4 RNA-sequencing of flavivirus capsid expressing cells reveals novel insights into capsid-mediated subversion of host innate immune responses 107

4.1 Rationale 108

4.2 Results 109

4.2.1 Global gene expression changes in capsid-expressing cells 109

4.2.2 QPCR validates transcriptomic changes from RNA-sequencing 111

4.2.3 Cells transduced with lentiviral vectors encoding ZIKV capsid suppress IFN-β and are susceptible to infection 118

4.2.4 ZIKV capsid expressing cells subvert IFN induction 121

4.2.5 ZIKV capsid interacts with TRIM25 123

4.2.6 TRIM25 protein levels are not significantly changed during ZIKV-infection 125

4.2.7 Knockdown of TRIM25 enhances ZIKV replication 125

4.3 Summary 129

Chapter 5 Characterization of Mayaro virus infection in primary human macrophages 131

5.1 Rationale 132

5.2 Results 133

5.2.1. MAYV replicates in Vero and A549 cell lines 133

5.2.2 Flow cytometric analysis of MAYV-infected cells in peripheral blood mononuclear cells 135

5.2.3 Monocyte-derived macrophages (MDMs) are susceptible to MAYV 135

5.2.4 Global gene expression changes in MAYV-infected MDMs 137

5.2.5 Gene ontology enrichment analysis of upregulated DEGs in MDMs 144

5.2.6 Gene ontology enrichment analysis of downregulated DEGs in MDMs . 144

5.2.7 LAMP3/CD63 is upregulated in MAYV-infected cells 148

5.2.8 LAMP3 protein levels persist despite small interfering RNA-mediated knockdown 151

5.3 Summary 154

Chapter 6 Discussion and Perspectives 156

6.1 Synopsis 157

6.2 Viral activation of PI3K/Akt-signalling 158

6.2.1 Viral entry 158

6.2.2 Cell survival 159

6.2.3 Metabolism 162

6.2.4 Perspective: the role of flavivirus capsids in the PI3K/Akt pathway 163

6.3 Subversion of interferon induction by flaviviruses 165

6.3.1 Subversion of Type I IFN induction by ZIKV and other flaviviruses 165

6.3.2. Flavivirus capsids subvert IFN induction 167

6.3.3 Perspective: Examining the role of Flavivirus capsids on evasion of innate immunity 169

6.4 Characterization of MAYV infection in primary human macrophages.. 171

6.4.1 Macrophages are target cells of MAYV-infection 171

6.4.2 Examining the role of MAYV-infected macrophages in arthralgia 174

6.4.3 The role of LAMP3/CD63 on alphavirus infection 176

6.4.2 Perspective: Physiological consequences of macrophage infection 178

6.5 Concluding remarks..... 179

REFERENCES..... 180

List of Tables

Table 1.1 Viral proteins that interact with Protein Phosphatase-1 (PP-1) 25

Table 2.1 Commercially prepared reagents 51

Table 2.2 Molecular Size Standards..... 53

Table 2.3 DNA/RNA modifying enzymes and buffers..... 53

Table 2.4 Detection Systems..... 54

Table 2.5 Multicomponent Systems..... 54

Table 2.6 Commonly used buffers 55

Table 2.7 Oligonucleotides 56

Table 2.8 Plasmid vectors 58

Table 2.9 Primary Antibodies 59

Table 2.10 Secondary Antibodies 61

Table 2.11 Mammalian cell lines 61

Table 2.12 Viruses 62

Table 4.1 List of top 20 down-regulated differentially expressed genes 113

Table 4.2 List of top 20 up-regulated differentially expressed genes 114

Table 5.1 List of top 20 up-regulated differentially expressed genes 146

Table 5.2 List of top 20 down-regulated differentially expressed genes 149

List of Figures

Figure 1.1 Global distribution of DENV and ZIKV 5

Figure 1.2 Flavivirus virion and genome organization 8

Figure 1.3 Model of flavivirus replication cycle 11

Figure 1.4 Extrinsic and intrinsic apoptosis pathways..... 16

Figure 1.5 PI3K/Akt signalling antagonizes apoptosis initiated by FasL..... 22

Figure 1.6 The type I IFN response 29

Figure 1.7 Model of RIG-I activation 32

Figure 1.8 Global distribution of CHKV and MAYV 38

Figure 1.9 Alphavirus virion and genome organization 40

Figure 1.10 Model of Alphavirus replication cycle 43

Figure 1.11 Alphavirus-induced arthritis 47

Figure 2.1 Plasmid map of pTRIP-MCS-AcGFP-myc-Capsid..... 65

Figure 3.1 Expression and localization of myc-tagged flavivirus capsid proteins 86

Figure 3.2 Expression of flavivirus capsids protects cells from anti-Fas challenge.. 88

Figure 3.3 Capsid expression confers a modest but significant protective effect against Fas-dependent apoptosis in replicon-transfected cells..... 90

Figure 3.4 Flavivirus capsid expression promotes Akt activation 92

Figure 3.5 Inhibition of PI3K reduces protection by flavivirus capsid proteins to anti-Fas 94

Figure 3.6 Capsid-expressing cells are more metabolically active..... 96

Figure 3.7 Dengue virus capsid interacts with protein phosphatase 1 99

Figure 3.8 Expression of Zika virus capsid increases phospho-Akt and protects cells from anti-Fas challenge 101

Figure 3.9 Zika virus capsid interacts with protein phosphatase 1 102

Figure 3.10 Protein sequence alignment of the flavivirus capsids..... 104

Figure 4.1 Expression of myc-tagged capsid proteins 110

Figure 4.2 Global gene expression changes in capsid expressing cells 112

Figure 4.3 Top 30 down-regulated genes in cells transduced with flavivirus capsids 115

Figure 4.4 Gene ontology enrichment analysis of common differentially expressed genes (DEGs) among capsids 116

Figure 4.5 Visualization of gene ontology enrichment analysis of common down-regulated differentially expressed genes (DEGs) in capsid-expressing cells 117

Figure 4.6 Validation of RNA-Sequencing 119

Figure 4.7 ZIKV capsid expressing cells suppress IFN-β and are highly susceptible to infection 120

Figure 4.8 ZIKV capsid expressing cells suppress IFN induction..... 122

Figure 4.9 ZIKV capsid interacts with TRIM25..... 124

Figure 4.10 TRIM25 is not degraded during ZIKV infection 126

Figure 4.11 Knockdown of TRIM25 enhances ZIKV replication..... 127

Figure 5.1 MAYV replication in cell lines 134

Figure 5.2 Monocyte-derived macrophages (MDMs) are susceptible to MAYV ... 136

Figure 5.3 Growth curves of MAYV-infected MDMs 138

Figure 5.4 Diagram of sample preparation used for RNA-sequencing 140

Figure 5.5 MDMs from eight healthy donors show different levels of susceptibility to MAYV 141

Figure 5.6 MAYV induces dramatic changes in the transcriptome of macrophages 142

Figure 5.7 Scatter Plot of common DEGs between female and male donors 143

Figure 5.8 Gene Ontology enrichment analysis of up-regulated DEGs in MAYV-infected MDMs 145

Figure 5.9 Gene Ontology enrichment analysis of down-regulated DEGs in MAYV-infected MDMs 147

Figure 5.10 LAMP3/CD63 is transcriptionally upregulated in MAYV-infected cells 150

Figure 5.11 LAMP3/CD63 is upregulated in MAYV-infected cells 152

Figure 5.12 siRNA mediated knockdown of LAMP3 153

Figure 6.1 Model of how flavivirus capsid proteins increase levels of phospho-Akt 161

Figure 6.2 Depiction of how ZIKV non-structural proteins inhibit IFN-induction. 166

Figure 6.3 Model for how flavivirus capsid proteins inhibit innate immune responses 170

Abbreviations

A549	Human alveolar basal epithelial 549 cells
AcGFP	*Aquorea corelescens* Green Fluorescent Protein
ATP	Adenosine triphosphate
BSA	Bovine serum albumin
C	Capsid
CARD	Caspase activation and recruitment domain
cDNA	Complementary Deoxyribonucleic Acid
cGAS	Cyclic GMP-AMP synthase
CHIKV	Chikungunya virus
DAPI	4',6-diamidino-2-phenylindole
DCs	Dendritic cells
DEGs	Differentially expressed genes
DENV	Dengue virus
DMEM	Dulbecco's Modified Eagle Medium
DMSO	Dimethyl Sulfoxide
dNTPs	Deoxynucleotide Triphosphates
dsRNA	Double stranded RNA
E	Envelope
EDTA	Ethylenediaminetetraacetic acid
HCV	Hepatitis C virus
HEK 293T	Human embryonic kidney 293T cells
HIV-1	Human immunodeficiency virus type 1
IFN	Interferon
ISGs	Interferon stimulated genes
JEV	Japanese encephalitis virus
kDa	Kilodaltons
LAMP3	Lysosomal Associated Membrane Protein 3
MAYV	Mayaro virus

MDMs	Monocyte derived macrophages
MOI	Multiplicity of infection
MVEV	Murray Valley Encephalitis Virus
ORF	Open reading frame
PBMCs	Peripheral Blood mononuclear cells
PCD	Programmed Cell Death
PCR	Polymerase Chain Reaction
PP-1	Protein Phosphatase 1
PVDF	Polyvinylidene fluoride
RIG-I	Retinoic acid-inducible gene I
RLR	RIG-I-like receptor
RRV	Ross River virus
SDS-PAGE	Sodium Dodecyl Sulfate Polyacrylamide Gel Electrophoresis
SFV	Semliki forest virus
siRNA	Small-interfering RNA
SLEV	St. Louis Encephalitis Virus
TBEV	Tick-borne encephalitis virus
TLR	Toll like receptor
TRIM25	Tripartite motif-containing protein 25
UTR	Untranslated Region
WNV	West Nile virus
YFV	Yellow fever virus
ZIKV	Zika virus

Chapter 1

Introduction

1.1 Overview

Arboviruses such as Zika virus (ZIKV), Dengue virus (DENV), Mayaro virus (MAYV) and Chikungunya virus (CHIKV) cause significant morbidity and mortality worldwide. Like most other viruses, their genomes (positive-sense ~10–12 kb) have very limited coding capacity and therefore these viruses depend on many host molecules for replication and have evolved multiple strategies to hijack cellular pathways and cause disease. Understanding the consequences of the interactions between viral proteins with cellular factors may provide insight into virus-host defense evasion strategies thus revealing novel therapeutic targets.

Arboviruses are spread by arthropod vectors such as mosquito or ticks and therefore are present in almost every inhabitable place on the planet. DENV for example, is so widespread that approximately 2.5 billion people live in countries where this virus is endemic and ~ 390 million DENV infections occur annually (World-Health-Organization et al., 2009). Global warming, international travel, and urbanization are all factors that contribute to the spread of viral infections and can lead to cross-over transmission events that led to the ZIKV epidemic in 2015/16 for example. Unfortunately, treatment options for most arboviral infections are limited and as such research focused on understanding how these viruses cause disease is critical to the development of novel therapeutics and vaccines.

1.2 Flaviviruses

Flaviviruses are arboviruses that belong to the family *Flaviviridae*. The word Flavivirus is derived from the Latin word "flavi", meaning "yellow", due to the jaundice caused by the prototypic flavivirus Yellow Fever virus (YFV). The genus is comprised of over 70 viruses and includes medically important mosquito-transmitted viruses such as DENV, ZIKV, Japanese encephalitis virus (JEV), Saint Louis encephalitis virus (SLEV), Murray Valley encephalitis virus (MVEV) and West Nile virus (WNV). To provide a general overview of flaviviruses, the following sections will discuss flavivirus pathogenesis, genome structure and replication with a focus on two prominent flaviviruses most relevant to this thesis, DENV and ZIKV.

1.2.1 DENV

Infection with DENV generally results in acute self-limiting illness ranging from mild flu-like symptoms to more intense symptoms such as headache, fever, rash, muscle and joint pain. There are an estimated 390 million DENV infections worldwide per year but only a small subset (~5%) of infections progress to DENV shock syndrome (DSS) or DENV hemorrhagic fever (DHF) which require formal medical care (Bhatt et al., 2013). In a subset of cases, DSS or DHF can lead to electrolyte imbalance, multi-organ failure and ultimately, death.

Transmission is mainly through *Aedes aegypti* and *Aedes albopictus* mosquito species, which generally bite during the daytime hours, breed well indoors and in clean

stagnant water (such as in flowerpots). DENV regularly causes large-scale outbreaks in many countries (**Figure 1.1A**). Currently, the countries with the most DENV cases are Brazil, Mexico, Nicaragua, the Philippines and Malaysia. Of note, Singapore had ~2,100 DENV cases during the first six weeks of 2020 – representing a 60% increase in DENV infections over the same period last year (World Health Organization). The Philippines reported their worst DENV outbreak in years with an estimated 1000 deaths in 2019 (World Health Organization). DENV is divided into four serotypes (DENV 1-4) and while lifelong immunity against an infecting serotype typically occurs, subsequent infections by a different DENV serotype is associated with a greater risk for severe dengue. This results in "waves" of different DENV serotypes in each region that switch every couple of years and individuals who have been infected with DENV numerous times.

Treatment for DENV is supportive as there are no specific antivirals. A vaccine called "Dengvaxia" has recently been licenced and is available in some countries, but it has limited value as it performs differently in DENV seropositive versus seronegative individuals. Specifically, there is an increased risk of hospitalization and severe DENV in seronegative individuals who receive this vaccine, and thus is only recommended for individuals with a previously confirmed DENV infection. Fortunately, a new vaccine candidate "TAK-003" has shown promise in phase 3 clinical trials and this protection appears to be irrespective of previous dengue exposure (Biswal et al., 2019).

A.

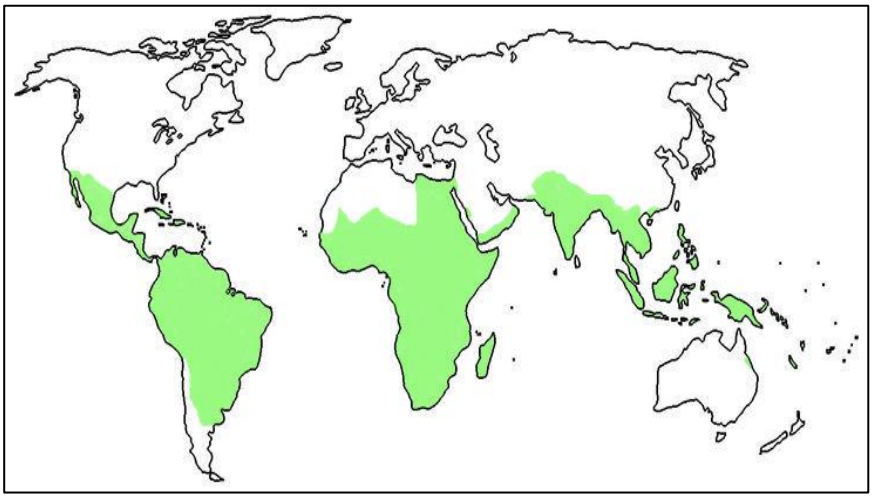

B.

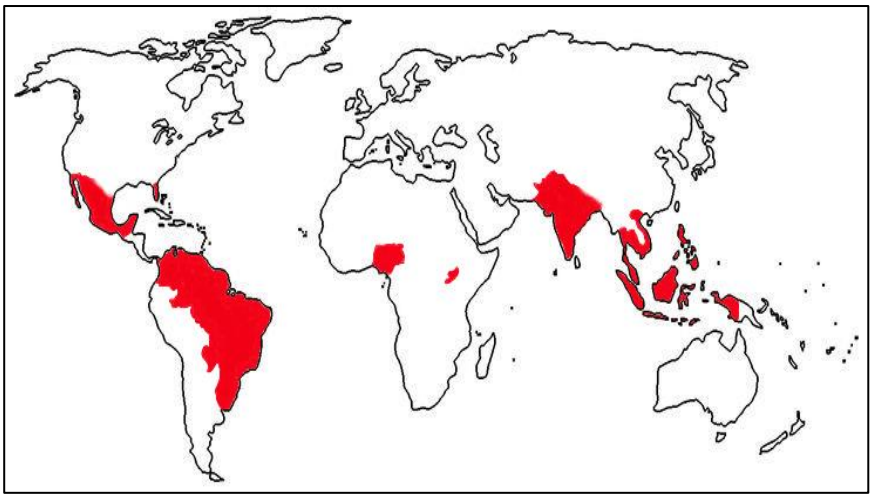

Figure 1.1 Global distribution of A. DENV and B. ZIKV as of 2020.

1.2.2 ZIKV

ZIKV is an emerging arbovirus that came to rapid international attention in 2015. Although infection with ZIKV can be asymptomatic or accompanied by a self-limiting flu-like illness, it is now known to be associated with microcephaly and other fetal development abnormalities (Lee and Shin, 2019) as well as with the neurological disorder Guillain-Barré syndrome (Krauer et al., 2017).

ZIKV was originally isolated in 1947 from a rhesus monkey caged in the Zika forest in Uganda (Dick et al., 1952). For ~60 years, ZIKV silently circulated in Africa and Asia (Gubler et al., 2017). The first known epidemic of ZIKV occurred in 2007 on Yap Island, Federated States of Micronesia (Duffy et al., 2009) and was followed by epidemics in the Pacific Islands including French Polynesia (Cao-Lormeau et al., 2014). Studies suggest that ZIKV was introduced into Brazil in late 2013 or early 2014 (Faria et al., 2016; Faria et al., 2017) and has since rapidly spread throughout the Americas (**Figure 1.1B**). Given the unprecedented rise of ZIKV in the Americas, it is critical to understand the mechanisms by which ZIKV and other flaviviruses cause disease so that urgently needed therapeutics and treatments can be discovered.

Of note, there are several vaccines in Phase 1 clinical trials including live-attenuated, inactivated, and a DENV-vectored vaccine expressing ZIKV premembrane/membrane and envelope proteins as well as many others in early-stage research (Poland et al., 2019).

1.2.3 Flavivirus virion and genome organization

Flaviviruses are small, enveloped viruses with a single-stranded RNA genome of positive polarity (~11 kb) and a diameter of ~50 nm (**Figure 1.2**). The genomic RNA has a 5' cap but lacks a 3' poly A-tail and encodes for a single open reading frame (ORF) of about 10 kb long. The single ORF is flanked by 5' and 3' noncoding regions or untranslated regions (UTRs) that have structural roles necessary for replication (Villordo and Gamarnik, 2009). The genome is translated as a single large polyprotein that is then cleaved by both cellular and viral proteases into three structural (C, prM, E) and seven non-structural proteins (NS1, NS2A, NS2B, NS3, NS4A, NS4B, NS5).

The capsid protein is a small protein (~13 kDa) mainly responsible for encapsidation and protection of viral RNA (Zhang et al., 2017). The capsid protein structure contains four α helices and forms dimers (Shang et al., 2018) (**Figure 1.2B**). The gene that encodes the capsid protein is located at the furthermost 5'end of the ORF, and therefore capsid is the first viral protein translated inside an infected cell (**Figure 1.2C**). Capsid then undergoes two cleavage events; the NS2B/NS3 protease catalyzes the cleavage of capsid at the cytosolic side (Amberg and Rice, 1999) resulting in its release from the membrane and capsid is cleaved by a signal peptidase in the lumen of the ER (Barrows et al., 2018; Stocks and Lobigs, 1998). The current model suggests that signal peptidase cleavage remains inefficient until NS2B/NS3 cleavage has occurred (Lobigs and Lee, 2004). It has also been shown that only the mature capsid, and not the membrane-anchored form of capsid, is found in infected cells (Urbanowski and Hobman, 2013).

A.

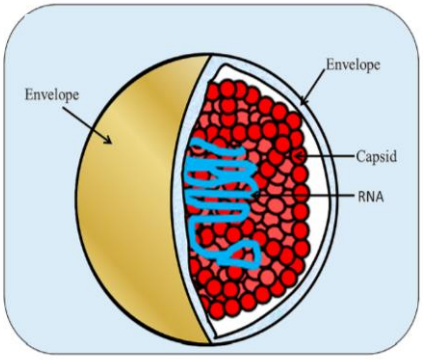

B.

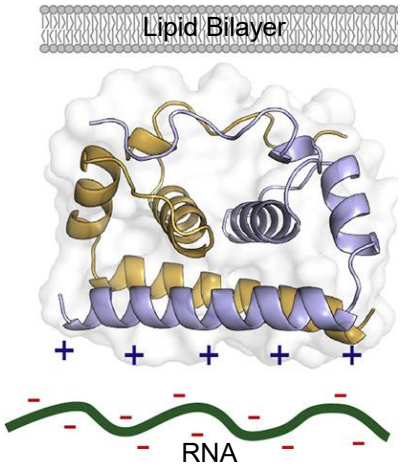

C.

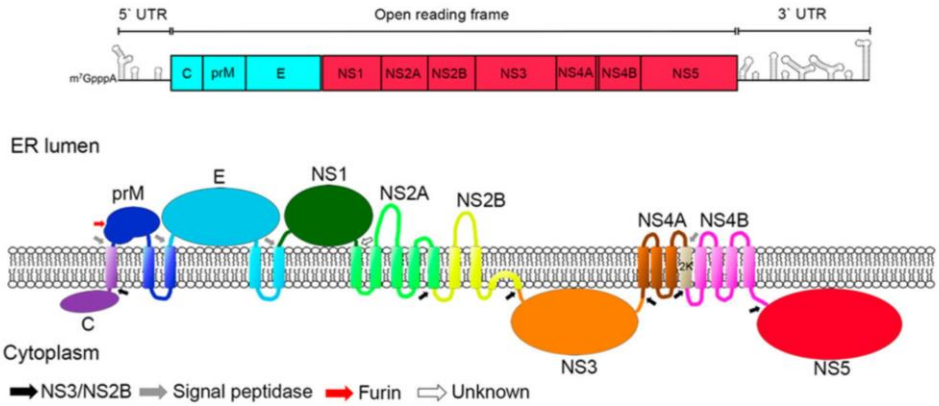

Figure 1.2. Flavivirus virion and genome organization. A. A schematic of a generic flavivirus virion (~50 nm diameter) is shown. (Modified from Zhang et al., 2017) **B.** Model of the dimer structures of ZIKV C interacting with RNA. (Modified from Shang et al., 2018). **C.** Schematic representation of the flavivirus genome (~11 kb). The genome contains a type I cap structure (m^7 GpppAm) at the 5' UTR. The 3'UTR lacks a polyadenylated (polyA) tail which can be found on other positive sense RNA virus genomes. The ORF encodes for 3 structural proteins (C, prM and E) and 7 non-structural proteins (NS1, NS2A, NS2B, NS3, NS4A, NS4B, and NS5) (Barrows et al., 2018).

The flavivirus envelope contains two proteins: E and M, the latter which is synthesized as a precursor called prM. The E glycoprotein is the primary viral protein that facilitates receptor-binding and membrane fusion between virions and host cells (Harrison, 2008).

The non-structural proteins are involved in virus replication, formation of the replication complexes (RCs), and modulation of antiviral defense pathways. Among them, NS3 and NS5 harbor multiple enzymatic activities. NS3 is a multifunctional protein that acts as a viral protease, helicase/NTPase and RNA 5'-triphosphatase (Assenberg et al., 2009). NS5 is the most highly conserved and largest protein (~100 kDa) consisting of two domains; the methyltransferase domain which is involved in capping the nascent viral RNA and the RNA-dependent RNA polymerase domain which produces negative and positive sense viral genomes (Ackermann and Padmanabhan, 2001; Nomaguchi et al., 2004).

The membrane proteins (NS2A, NS2B, NS4A and NS4B) are relatively poorly characterized. NS2A plays an essential role in virus assembly (Liu et al., 2003; Xie et al., 2019) and orchestrates virus morphogenesis (Zhang et al., 2019). NS2B is important for recruitment of NS3 to the ER and activating its protease activity (Xing et al., 2020). NS4A is a membrane-associated protein consisting of four transmembrane helices and an N-terminal cytosolic region which is also part of the replication complex. This was determined from studies that showed interaction of NS4A with the replicative intermediates double-stranded RNA (dsRNA), NS1, NS2A, and NS5 (Mackenzie et al., 1998). NS4B is a hydrophobic protein that appears to play an important role in

replication by facilitating the formation of the viral replication complexes (Zmurko et al., 2015).

Lastly, NS1 is a viral glycoprotein that localizes to the lumen of the ER, on the cell surface, or is secreted into the extracellular space (Gutsche et al., 2011). The intracellular dimer form of NS1 plays a role in genome replication whereas secreted NS1 triggers cytokine release and contributes directly to vascular leakage during DENV infection (Beatty et al., 2015; Modhiran et al., 2015; Thomas, 2015).

1.2.4 Flavivirus replication

Flaviviruses, like all viruses, are reliant on host cellular processes in order to replicate and to spread to new hosts. The flavivirus replication cycle can be divided into 3 stages: viral entry, translation and replication, virion assembly and viral egress (**Figure 1.3**).

1.2.4.1 Viral Entry and Cellular Tropism

Flaviviruses have a wide cellular tropism, which is advantageous because it allows them to replicate in a variety of hosts including insects, reptiles, birds, and mammals. This broad tropism is attributed to the numerous cellular factors such as glycosaminoglycans (Hilgard and Stockert, 2000), DC-SIGN (Davis et al., 2006), tubulin and tubulin-like proteins (Chee and AbuBakar, 2004), Hsp70/90 (Reyes-del Valle et al., 2005; Srisutthisamphan et al., 2018), mannose-6-phosphate receptor

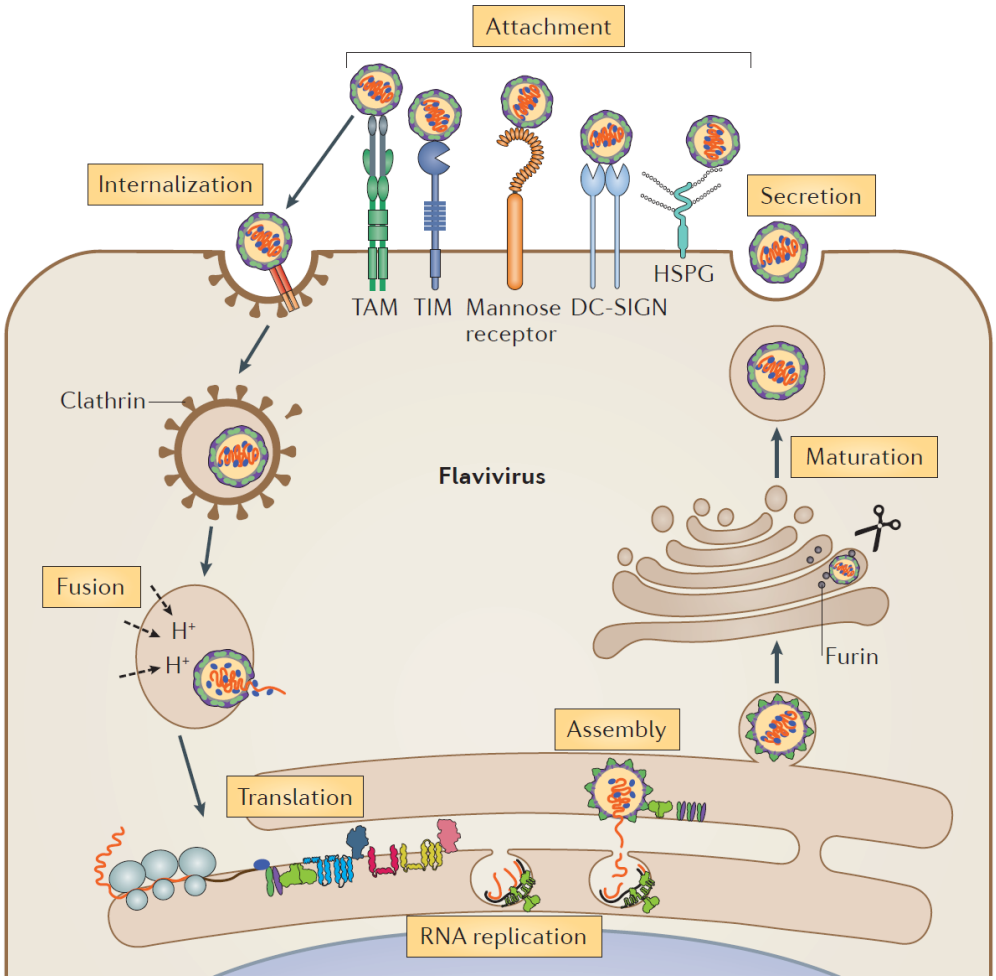

Figure 1.3. Model of flavivirus replication cycle. Virions attach to a receptor on the cell surface and enter via clathrin-mediated endocytosis. Acidification of virion-containing vesicles induces conformational changes in the viral envelope proteins resulting in fusion between the viral and the endosomal membranes and virus particle disassembly. The released positive-sense RNA can be directly translated into a single polyprotein that is processed by both viral and host proteases. Genome replication occurs inside invaginations of the ER membrane. Virus assembly occurs on the surface of the ER membrane. The immature viral particle is transported through the Golgi and trans-Golgi network and virion maturation occurs upon cleavage by the host protease furin, resulting in infectious virus particles. Mature virions are subsequently released by exocytosis. (Neufeldt., et al 2018)

(Miller et al., 2008), and TIM/TAM (Meertens et al., 2012) that serve as receptors and co-receptors. Binding to host receptors by the flavivirus E protein facilitates viral entry into the cell via receptor-mediated clathrin-dependent endocytosis (Acosta et al., 2011; Smit et al., 2011), or less commonly in immune cell subtypes via phagocytic internalization of antibody-virus complexes (Halstead et al., 1977; Hawkes, 1964). Internalized virions transit through endosomes where the lower pH environment leads to structural conformation changes in the E protein (Stiasny et al., 2011; Van Der Schaar et al., 2008). This permits the E protein to facilitate the fusion of the viral envelope with the endosomal membrane, leading to the formation of a fusion pore through which the viral RNA is released into the host cell cytoplasm (Gollins and Porterfield, 1986).

1.2.4.2. Translation and Replication

The uncoated positive-sense RNA genomes of flaviviruses act directly as mRNA for the translation of the viral polyprotein, but also serve as templates for subsequent genome replication via antisense intermediates (reviewed in (Mazeaud et al., 2018)).

Translation of the viral polyprotein occurs following trafficking of the RNA genome to ribosomes on the endoplasmic reticulum (ER) membrane (Gillespie et al., 2010). The viral polyprotein is processed on the ER membrane by host and viral proteases, producing three structural and seven non-structural viral proteins. The non-

structural proteins, specifically NS1, NS4A and NS4B, induce the formation of an ER-derived membranous replication complex (reviewed in (Neufeldt et al., 2018)). It is not fully understood how a switch from translation of the genome to replication of the genome occurs, however there are two prevailing hypotheses. The first is that a large stem loop structure at the 5' UTR acts as the promoter for the RNA Dependent RNA polymerase (RdRp) NS5; 11 kb away from the 3' initiation site. A conformation change of the viral RNA occurs via long range RNA-RNA interactions where cyclization of the RNA genome brings the 5' and 3' ends into proximity, allowing for NS5 to reach the 3' end of the genome and initiate negative-sense strand synthesis (summarized in (Villordo and Gamarnik, 2009)). A second hypothesis states that continued accumulation of NS5 on genomic RNA physically blocks the access of cellular translation initiation factors (Garcia-Blanco et al., 2016). Together these hypotheses point to a switch from translation to genome replication following an initial buildup of the necessary factors for replication and virion assembly.

Replication of the viral RNA is dependent on the RNA-dependent RNA polymerase activity of NS5 to first produce an antisense RNA strand that serves as the template for subsequent rounds of replication. The production of (+)sense RNA is favoured over antisense RNA by a mechanism that is unclear, resulting in many more viral genome copies being available to be packaged as progeny virions (Lindenbach et al., 2007).

1.2.4.3. Virion Assembly and Egress

To date, the mechanisms by which nascent (+)sense RNAs are assembled into virions remains undefined. It is known that nucleocapsids form from capsid proteins interacting with nascent viral genomes, while omitting cellular mRNA (despite the absence of unique packaging sequences) (Khromykh et al., 2001).

Following encapsidation of genomic RNA, the RNA-capsid complex buds into the ER lumen acquiring a host derived envelope and the viral E and prM proteins. The E and prM glycoproteins are sufficient to complete budding through the ER membranes, as over-expressing only E and prM results in production of subviral particles lacking the nucleocapsid (Schalich et al., 1996). Newly budded intracellular virions are non-infectious because the E protein is not in a fusion-competent conformation (Elshuber et al., 2003; Guirakhoo et al., 1991). However, as the immature virions transit the *trans*-Golgi, a cellular protease, furin, cleaves prM protein to its mature M form and together with the acidic pH of this compartment which results in a conformational change in the E protein such that the fusion peptide can be exposed (Stadler et al., 1997). These conformational changes result in the formation of mature infectious virions which are then released from cells via exocytosis.

1.3 Subversion of cellular pathways by ZIKV and other flaviviruses

In order to cause infection, viruses depend on many host molecules for replication and have evolved multiple strategies to hijack cellular pathways in order to

produce an environment favourable for replication. Some of the pathways that are relevant to this thesis include: apoptosis pathways, the PI3K/Akt pathway, and the type I IFN induction pathway.

1.3.1 Apoptosis

The multiple mechanisms that orchestrate cell death pathways are complex and have been studied in detail for decades (reviewed in (Galluzzi et al., 2018)). Accidental cell death can occur as a result of extreme physical, chemical, or mechanical injury. In contrast, apoptosis, is an orderly and highly regulated process.

Apoptosis is critical activity for many cellular processes including normal cell turnover, proper development and functioning of the immune system. Therefore, it is no surprise that dysregulated apoptosis is a factor in many human conditions including autoimmune disorders and cancer. There are two main apoptotic pathways: the extrinsic (death receptor-mediated) pathway and the intrinsic (mitochondrial-dependent) pathway (**Figure 1.4**). Generally speaking, the extrinsic pathway can be triggered by virus-induced expression of death receptors or as part of the cytotoxic T cell response, whereas the intrinsic pathway can be activated as an early-warning system to induce suicide of the infected cell before the virus has a chance to replicate and escape to other sites (Fitzsimmons et al., 2019; Loreto et al., 2014).

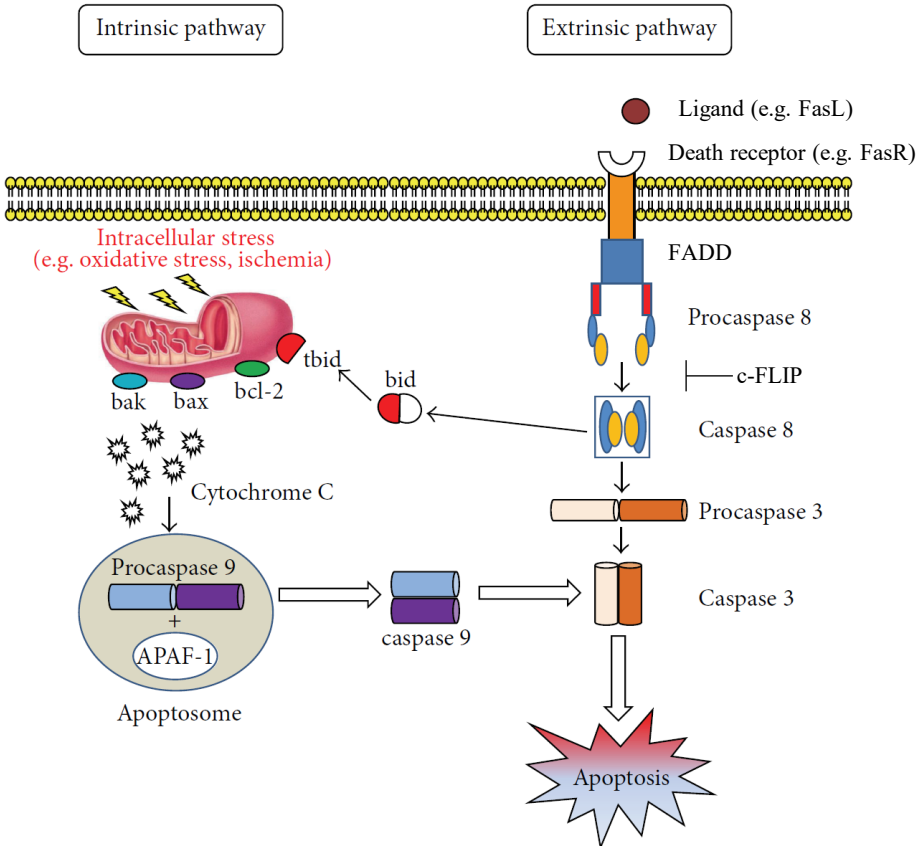

Figure 1.4. Extrinsic and intrinsic apoptosis pathways. The extrinsic (death receptor-mediated) pathway is initiated by binding of a specific death receptor (e.g. FasR) to its ligand (e.g. FasL). This initiates cytoplasmic interaction of Fas-associated protein with death domain (FADD) to the death receptor resulting in clustering and activation of caspase-8. Activated caspase-8 can induce apoptosis by directly activating caspase-3 or by cleavage of Bid to produce truncated Bid (tBid), which results in release of cytochrome *c* from mitochondria and activation of caspases-9 and -3. Intrinsic (mitochondria-dependent) apoptosis is induced by intracellular stress. The pathway is regulated by Bcl-2 family members associated with mitochondrial membranes including Bax and Bcl-2. Bak, Bax and Bid are proapoptotic proteins that promote release of cytochrome *c* from the mitochondria. Cytochrome *c* binds to apoptotic protease activating factor (APAF-1) and triggers formation of the apoptosome. Procaspase-9 is activated and in turn can activate caspase-3 and results in apoptosis. (Modified from Loreto., et al 2014)

1.3.1.1 Extrinsic Apoptosis

Extrinsic or death receptor-mediated apoptosis is initiated by oligomerization of death receptors by their ligands. One such type of receptor is the Fas cell surface death receptor (FasR) (Walczak and Krammer, 2000). FasR belongs to the tumor necrosis factor receptor (TNFR) superfamily and consists of an extracellular cysteine-rich domain, a transmembrane domain, and intracellular death domain. The cognate ligand for FasR is Fas ligand (FasL), which belongs to the tumor necrosis factor (TNF) family and is a type II transmembrane protein that is expressed on cytotoxic T lymphocytes (Krammer, 2000). The binding of FasL to FasR on the target cell induces receptor death domain trimerization and formation of the death inducing signalling complex (DISC). The receptor complex is internalized via the cellular endosomal machinery and a protein called the "Fas associated protein with death domain" (FADD) binds to FasR via the death domains. FADD has a death effector domain that permits recruitment and binding of the inactive form of the initiator caspase-8 (pro-caspase-8). Caspase-8 then undergoes autocatalytic cleavage to produce a shorter active form that is released from DISC into the cytosol where it directly cleaves and activates executioner caspases.

This pathway can be regulated by Cellular FLICE (FADD-like IL-1β-converting enzyme)-inhibitory protein (c-FLIP). c-FLIP binds to FADD and/or caspase-8 and forms an apoptosis inhibitory complex (AIC) (Safa, 2012) which in turn prevents DISC formation and thus inhibits apoptosis.

1.3.1.2 Intrinsic apoptosis

Intrinsic apoptosis is dependent upon permeabilization of the mitochondria and release of cytochrome *c* (Kaufmann and Earnshaw, 2000) and can be initiated by a wide variety of stimuli and including cell stresses such as growth factor withdrawal, DNA damage, ER stress, reactive oxygen species (ROS) overload, viral infections, or mitotic defects (Galluzzi et al., 2018). Loss of mitochondrial transmembrane potential (i.e. damaged mitochondria) and prompt release of the pro-apoptotic protein cytochrome *c* from the mitochondrial intermembrane space into the cytosol are early events in the intrinsic apoptosis pathway (Elmore, 2007). Cytosolic cytochrome *c* binds to Apaf-1 and triggers the formation of the apoptosome; a large multiprotein complex that recruits and activates the initiator caspase-9. Active caspase-9 then initiates what many consider an irreversible step in the apoptotic cascade, endoproteolyic activation of the executioner caspase-3.

The intrinsic apoptosis pathway is regulated by Bcl-2 proteins; a large family of proteins that includes pro-apoptotic and anti-apoptotic members. These proteins contain conserved Bcl-2 homology (BH) domains (BH1-4) that can be used to divide the Bcl-2 family into three subgroups: i) the multidomain anti-apoptotic members (e.g., Bcl-2, Bcl-xL); ii) the multidomain pro-apoptotic members (e.g., Bax, Bak, Bok); and iii) the pro-apoptotic members with only a single BH3 domain (e.g., Bad, Bid, Bik) (Popgeorgiev et al., 2018). The Bcl-2 family of proteins controls apoptosis primarily by direct binding interactions among Bcl-2 family members. For example, the proapoptotic proteins Bak and Bax form oligomers and induce mitochondrial outer

membrane permeabilization and subsequent initiation of the caspase cascade. Anti-apoptotic Bcl-2 proteins can inhibit mitochondrial outer membrane permeabilization by direct binding to Bak and Bax. However, the regulation of apoptosis by Bcl-2 family proteins is still controversial with respect to exactly how the Bcl-2 family proteins exert their pro- or anti-apoptotic effect (reviewed in (Kale et al., 2018)).

Finally, although the two apoptotic pathways can function completely separately, crosstalk between the intrinsic and extrinsic pathways can occur when death receptor activation by FasL induces caspase-8 mediated cleavage of the Bcl-2 family pro-apoptotic protein Bid. This is important because Bid cleavage on the mitochondria is essential for caspase-8-induced cytochrome *c* release (Schug et al., 2011) and induction of intrinsic apoptosis.

Extrinsic and intrinsic apoptosis pathways share parallel functioning components. Specifically, both employ initiator (caspases-2, -8, -9 and -10) and effector/executioner (caspases-3, -6 and -7) to activate apoptosis. The main difference among the two types of caspases is that initiator caspases auto-proteolytically cleave (i.e. self-activate) and once activated produce an amplifying chain reaction to activate executioner caspases. Executioner caspases must be cleaved by initiator caspases in order to become active. Activated caspases cleave a wide variety of target proteins in the cell resulting in destruction of cellular organelles and structural components of the cells.

1.3.2 Viral modulation of apoptosis

Apoptosis is important for tissue homeostasis when new cells are produced, old cells must be turned over. It also serves as a critical antiviral defense mechanism as infected cells often commit to apoptosis as a means of interrupting viral replication and spread. Not surprisingly, many viruses have evolved mechanisms to counteract programmed cell death pathways.

Some mammalian viruses encode orthologs of the anti-apoptotic regulators in the Bcl-2 family. Such is the case with the DNA virus Epstein Barr virus which encodes two proteins (BHRF1 and BALF1) that share sequence and structural homology with cellular Bcl-2 proteins. BHRF1 interacts with cellular pro-apoptotic Bcl-2 proteins, Bim, Bid, and Bak to inhibit apoptosis whereas the role of BALF1 remains controversial (Fitzsimmons et al., 2019). Similarly, Kaposi's sarcoma–associated γ-herpesvirus (KSHV) expresses the Bcl-2 homolog KSbcl-2, which serves to block apoptosis (Cheng et al., 1997). Other viruses encode proteins that inhibit apoptosis by modulating the transcriptional level of Bcl-2 family members or by post-translational modifications of these proteins. For example, HIV Nef induces the phosphorylation and inactivation of the pro-apoptotic Bad protein resulting in the suppression of apoptosis in T cells (Wolf et al., 2001).

Another mechanism used by viruses to interfere with apoptosis is to block death receptor mediated signalling. Several DNA viruses have evolved elegant strategies to modulate this signalling. For example, secretion of the TNFR2 ortholog expressed by Shope fibroma virus (rabbit poxvirus) binds to the ligands TNFα and TNFβ, thus

blocking death receptor signalling and compromising the antiviral effects of TNF (Smith et al., 1991).

1.3.3 The PI3K/Akt Signalling pathway can prevent apoptosis initiated by Fas

The PI3K/Akt pathway is a survival signalling pathway that is highly conserved and whose activation is controlled by multiple cellular processes. The signalling pathway begins with activation of a receptor tyrosine kinase (RTK) by a growth factor (such as insulin) (**Figure 1.5**). Ligand binding stimulates phosphatidylinositol 3-kinase (PI3K) to convert phosphatidylinositol (3,4)-bis-phosphate (PIP2) to phosphatidylinositol (3,4,5)-tris-phosphate (PIP3) and triggers the recruitment of Akt (also known as Protein Kinase B or PKB) to the plasma membrane. Akt is a serine/threonine-specific protein kinase that regulates many cellular regulatory processes including apoptosis and glucose metabolism. It binds to PIP3 at the plasma membrane where it interacts with its activating kinases, PDK1 and PDK2 (mTORC2). Two sequential phosphorylation events are needed to fully activate Akt; PDK1 phosphorylates Akt at T308 (Alessi et al., 1997), followed by phosphorylation of S473 by PDK2 (Hart and Vogt, 2011). Akt then dissociates from the plasma membrane and phosphorylates a plethora of proteins involved in cell cycle regulation and metabolism (reviewed in (Manning and Toker, 2017)). For example, PI3K/Akt regulates expression of c-FLIP (Panka et al., 2001), a protein that forms an apoptosis inhibitory complex (AIC) to block Fas-mediated apoptosis. Akt also phosphorylates Bad, which

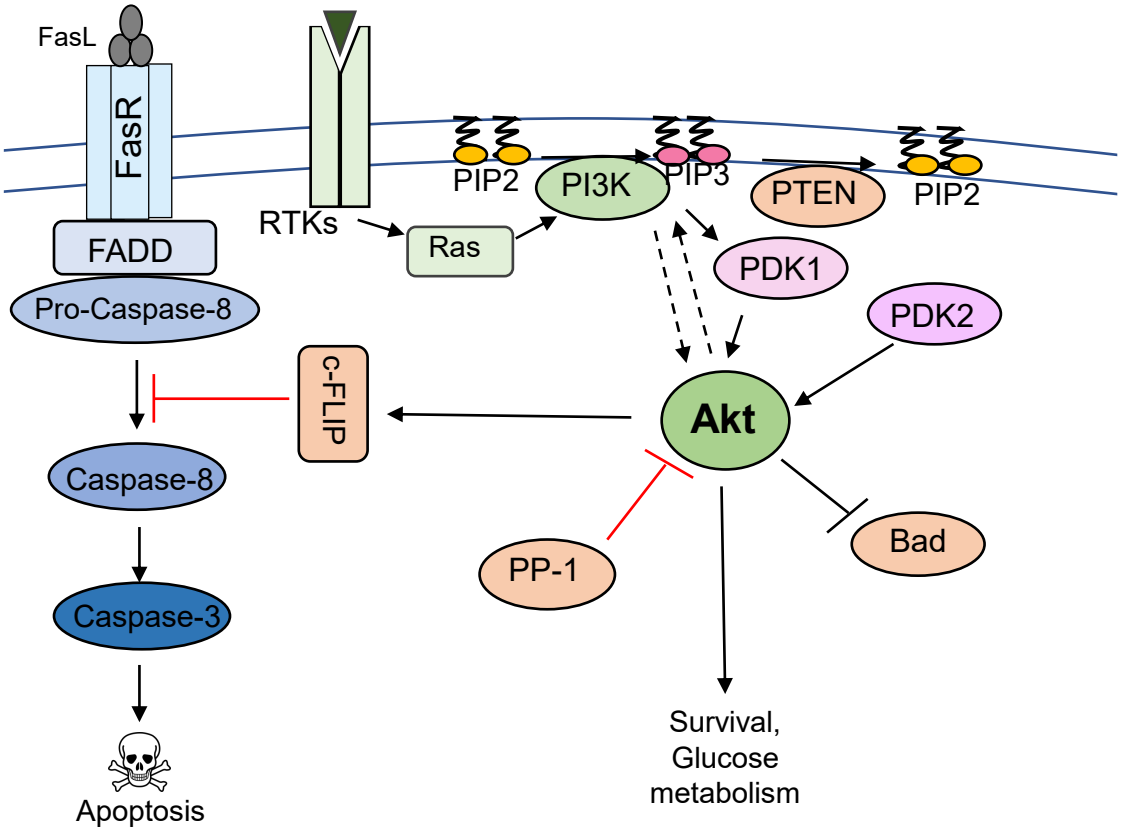

Figure 1.5. PI3K/Akt signalling antagonizes apoptosis initiated by FasL. Stimulation of the PI3K/Akt pathway results in phosphorylation and activation of Akt at T308 and S473 by PDK1 and PDK2 (mTORC2), respectively. Activated Akt phosphorylates a plethora of proteins involved in cell cycle regulation and metabolism, including inhibitory phosphorylation of the pro-apoptotic protein Bad. Akt regulates c-FLIP expression and c-FLIP can inhibit Fas-mediated apoptosis. Akt can be inactivated by protein phosphatase-1 (PP-1).

permits 14-3-3 isoforms to bind to and inhibit the pro-apoptotic activity of Bad (Datta et al., 2000).

A common strategy used by DNA and RNA viruses involves activation of the pro-survival kinase Akt (Buchkovich et al., 2008; Diehl and Schaal, 2013). Flaviviruses such as JEV and DENV activate Akt within 1 hour post-infection and when PI3K was blocked using an inhibitor, apoptosis occurred at an early stage of infection (Lee et al., 2005). The activation of PI3K/Akt by flaviviruses is rapid, thus binding of virion to host cell receptors appears to be sufficient for PI3K/Akt activation and it is likely that engagement of cell surface receptors following virion binding triggers this event and is followed by a more sustained phase later in infection.

Previous research in our lab showed that expression of WNV capsid protein results in increased phosphorylation of Akt and that capsid-dependent phosphorylation of Akt was abrogated by a PI3K inhibitor (Urbanowski and Hobman, 2013). Moreover, the capsid protein of WNV protected cells from Fas-mediated apoptosis (Urbanowski and Hobman, 2013) however, the specific mechanism by which capsid protein affects levels of phopho-Akt, and if the anti-apoptotic mechanism is conserved among flavivirus capsids were not addressed.

1.3.3.1 Phosphatases that regulate the PI3K/Akt pathway

The PI3K/Akt pathway can be controlled by several important regulatory proteins. One such protein is the Phosphatase and tensin homolog (PTEN) tumor

suppressor protein. PIP3 formation is negatively regulated by PTEN-mediated dephosphorylation of PIP3 converting it to PIP2. Other proteins that regulate Akt are some of the most abundant phosphatases in the cell; Protein Phosphatase 1 (PP-1) and protein phosphatase 2A (PP2A). PP-1 is a serine/threonine phosphatase that interacts with many regulatory subunits to confer specificity for hundreds of substrate proteins including Akt. Dephosphorylation of Akt by PP-1 down-regulates the activity of this kinase (Xiao et al., 2010).

PP-1 is composed of a catalytic subunit and at least one regulatory subunit. The catalytic subunit is highly conserved among all eukaryotes and consists of a 30 kDa single domain protein. In mammals, four distinct catalytic subunits of PP-1 exist: PP1α, PP1β/δ and the splice variants PP1γ1 and PP1γ2. Most PP-1 regulatory proteins and some PP-1 substrates contain a variant of the PP-1 binding motif, the "RVxF" motif (Peti et al., 2013). Several viruses utilize PP-1 to promote their replication. For example, the ICP34.5 protein of HSV-1 binds PP-1 through its carboxyl-terminal domain that contains the consensus binding motif (RVxF). This binding serves to bring PP-1 and translation initiation factor eIF2 (eIF2α) together facilitating the specific dephosphorylation of eIF2α by PP-1 (Li et al., 2011). The phosphorylated form of eIF2α is antiviral but the non-phosphorylated form is essential for protein synthesis, thus, dephosphorylation of eIF2α permits continued viral protein synthesis and replication. A list of viruses that use PP-1 to regulate cellular functions is shown in **Table 1.1**.

Virus	Viral protein	Mechanism
HIV-1	Tat	Binds PP-1 in cytoplasm, translocate to nucleus. In nucleus PP-1 dephosphorylates CDK9 and promotes HIV-1 transcription (Ammosova., et al 2011)
Ebola	VP30	PP-1 controls VP30 dephosphorylation – required for genome replication (Ilinykh., et al 2014)
Enterovirus 71	2C	PP-1 dephosphorylates IKK, results in the inhibition of the NF-κB signalling pathway (Li, Zheng et al. 2016)
Measles virus	V	PP-1 mediated dephosphorylation of MDA5, results in suppression of interferon induction (Davis., et al 2014)
HSV-1	ICP34.5	ICP34.5 binds PP-1 and PP-1 dephosphorylates eIF2α to enable continued protein synthesis and viral replication (Li, Zhang et al. 2011)
African swine fever virus	DP71L	PP-1 dephosphorylates eIF2α to enable continued protein synthesis (Rivera., et al 2007)
DENV and ZIKV	C	Capsid binds to PP-1, prevents dephosphorylation of Akt (in this thesis (Airo, Urbanowski., et al 2018))

Table 1.1 Viral proteins that interact with Protein Phosphatase-1 (PP-1)

1.3.4 Interferon

The interferons are a family of autocrine and paracrine cytokines used mainly to alert neighbouring cells of potential invaders. They are critical for establishing robust innate and adaptive immune responses to pathogens. As such, most if not all viruses have evolved mechanisms to subvert the IFN response.

1.3.4.1 The IFN system

Three types of IFN have been identified in humans: type I IFN (IFN α/β/κ/ε/ω), type II IFN (IFNγ), and type III IFN (IFNλ1, IFNλ2, IFNλ3, IFNλ4). All IFN molecules bind to cognate receptors and initiate signalling cascades that lead to the transcriptional regulation of hundreds of IFN stimulated genes (ISGs). This serves to reprogram and prime cells in an autocrine or paracrine manner to enhance detection of and mount effective defenses against pathogens (for a review on ISGs and viral infection please see (Schneider et al., 2014)).

In most cell types, infection results in the production of type I IFN (IFNα or IFNβ). The quick and robust expression of IFN is pivotal to mount an effective immune response for controlling viral infections. This is evidenced by experiments showing that knockout mice lacking the ability to induce IFNα/β or downstream response pathways exhibit enhanced susceptibility to infection by flaviviruses (Johnson and Roehrig, 1999; Lazear et al., 2016; Meier et al., 2009; Morrison and Diamond, 2017; Samuel and Diamond, 2005; Shresta et al., 2004).

The receptors for type I IFN are interferon alpha and beta receptor subunit 1 (IFNAR1) and interferon alpha and beta receptor subunit 2 (IFNAR2). These receptors are ubiquitously expressed but some cells secrete more IFNα/β than others. For example, dendritic cells, epithelial cells and macrophages secrete large amounts of type I IFN and thus are considered a primary source of IFNα/β for antiviral responses (Swiecki and Colonna, 2011). Type II IFNs are predominantly produced by natural killer cells, macrophages and activated T cells during infection (Orange et al., 1995) and play key roles in activation of macrophages and regulation of T cell polarization (Tewari et al., 2007). Type III IFN also plays important roles in antiviral activity, but is limited as only cells of epithelial origin contain the receptors for type III IFN (Lazear et al., 2015).

The interferon response can be divided into two stages, induction and signalling. The induction phase involves pathogen recognition, activation of cellular pattern recognition receptors (PRRs), and expression and release of IFN. The signalling phase involves binding of IFN to cognate receptor in an autocrine or paracrine manner. This results in the activation of the Janus kinase signal transducer and activator of transcription (JAK-STAT) signalling pathway which then triggers production of IFN and the transcription of hundreds of ISGs. ISGs are required to generate an effective antiviral response and many are involved in limiting viral replication (e.g. OAS, IFITs and RNAse L). For example, IFIT1 exerts its antiviral activity by binding directly to the 5' end of foreign RNA (Pichlmair et al., 2011). This impairs the recruitment of the

cap-binding eukaryotic translation initiation factor 4F thus inhibiting translation (Habjan et al., 2013).

In this thesis, only IFN induction will be explored in further detail but it is worth noting that many *Flaviviridae* members including WNV, DENV, and ZIKV block multiple stages in the IFN induction and IFN signalling pathways. For example, we and others showed that ZIKV NS5 protein degrades STAT2 to inhibit type I IFN signalling and ISG expression (Grant et al., 2016; Kumar et al., 2016). Similarly, DENV NS5 protein also induces degradation of STAT2 (Ashour et al., 2009). Through a different mechanism, the WNV NS5 protein supresses the maturation and cell surface expression of IFNAR1 (Lubick et al., 2015) as a means to antagonize type I IFN signalling.

1.3.4.2 The IFN induction pathway

The first step in IFN induction is recognition of a pathogen component by a PRR which upon activation induces a signalling cascade through the use of adaptor proteins and kinases to stimulate the transcription of IFN genes (**Figure 1.6**). Two complementary pattern recognition receptor (PRR) systems account for most viral responses: the toll-like receptors (TLR) and the RIG-I-like receptors (RLR). In addition, the cytosolic DNA sensor cGAS (cyclic GMP-AMP synthase) is activated during flavivirus infection (Schoggins et al., 2014). The specific details of how RNA viruses activate a DNA sensor are not clear, but one possibility is that cGAS detects

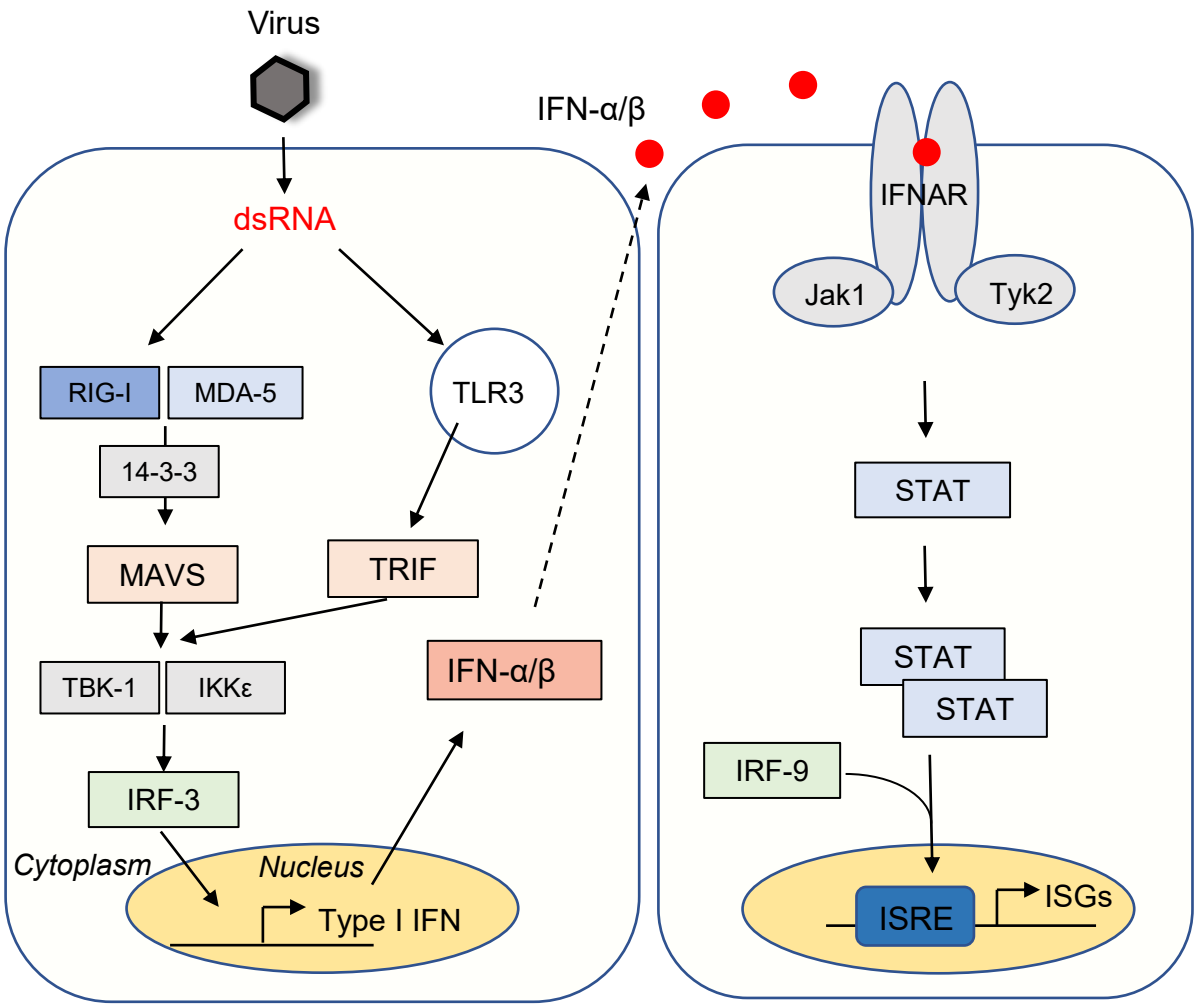

Figure 1.6. The type I IFN response. The IFN induction pathway can be initiated by detection of viral RNA by cytoplasmic helicase receptors (RIG-I and MDA5) and endosomal transmembrane Toll-like receptors (TLR3). The 14-3-3 chaperone proteins are required for translocation of activated RIG-I and MDA-5 from the cytosol to MAVS on the mitochondria. Activation of TLR3 results in interaction with the adaptor protein TRIF. Both pathways activate distinct signalling pathways that converge on the activation of kinases TBK1 and IKKε followed by subsequent phosphorylation of the transcription factor IRF-3. Activated IRF-3 can enter the nucleus and initiate transcription of IFN-α/β genes. The IFN signalling pathway is initiated upon binding of IFN-α/β to IFN-α receptor (IFNAR). This results in activation of the Janus kinase/signal transducers and activators of transcription (JAK-STAT) signalling pathway, dimerization of the STAT proteins and translocation to the cell nucleus. In the nucleus, STAT proteins bind to the IFN-stimulated response element (ISRE) resulting in transcription of IFN stimulated genes (ISGs).

PAMPs associated with RNA viruses by crosstalk with the RIG-I/MDA5 pathway (Zevini et al., 2017). Moreover, it has been shown that the release of mitochondrial DNA during DENV infection provides an endogenous source of cytosolic DNA to induce cGAS signalling (Sun et al., 2017a). For the purpose of this thesis, only the RNA-sensors will be discussed in further detail.

TLRs are mainly found on the cell surface or in intracellular compartments such as the ER, endosomes, or lysosomes and are highly expressed on innate immune cells such as DCs and macrophages (reviewed in (Kawasaki and Kawai, 2014)). TLRs are classified broadly into two categories: cell surface expressed TLRs and intracellular TLRs. Cell surface TLRs recognize cell wall components of bacterial pathogens whereas intracellular TLRs recognize nucleic acids. TLR3 recognizes dsRNA whereas TLR7 and TLR8 detect ssRNA. An important distinction is that TLRs sample material coming in from the outside and cannot detect a viral infection within the host cell. For example, TLR 3, 7 and 9 signal from within an acidified endosome compartment and thus can detect viral infection upon virus entry and uncoating (which exposes the nucleic acid). TLR3 can also sample phagosomes as they are engulfed after apoptotic cell death (Schulz et al., 2005).

The RLRs are ubiquitously expressed cytosolic receptors that detect viral nucleic acids. Only three RLR members have been identified so far; RIG-I (retinoic acid-inducible gene I), MDA5 (melanoma differentiation associated factor 5) and LGP2 (laboratory of genetics and physiology 2). The importance of these sensors is illustrated by the fact that RIG-I and MDA5 knock out mice exhibited increased

pathogenicity in response to infection by WNV, JEV and other RNA viruses (Errett et al., 2013; Kato et al., 2006). RIG-I and MDA5 are RNA helicases that contain two caspase-activation and recruitment domains (2CARDs) in their N-terminal regions, a DExD/H Box helicase domain, and a C-terminal regulatory domain (RD) (Saito et al., 2007; Yoneyama et al., 2004). Both RIG-I and MDA-5 are stimulated by single-stranded 5'-triphosphorylated and dsRNA as well as the dsRNA mimic poly (I:C). Although flavivirus genomes can be recognized by both RIG-I and MDA5, it appears that RIG-I plays a more important role than MDA5 in mediating early IFN antiviral responses to flaviviruses (Chazal et al., 2018). This is demonstrated by studies of WNV infection in RIG-I$^{-/-}$ or MDA5$^{-/-}$ mouse embryonic fibroblasts that suggest that RIG-I is activated early during infection whereas MDA5 is required for enhancing and sustaining type I IFN and ISG expression (Fredericksen et al., 2008).

The current model for RIG-I activation stipulates that in the absence of viral infection, RIG-I exists in a phosphorylated and inactive conformation (**Figure 1.7**). Binding of the helicase domain and RD to viral RNA induces a conformational change that exposes the two CARD domains and induces oligomerization of RIG-I. Following de-phosphorylation of the CARD domains by the phosphatase PP1-α/γ (Wies et al., 2013) RIG-I is polyubiquitinated at lysine site 172 by the E3 ubiquitin ligase Tripartite motif-containing protein 25 (TRIM25). This is essential for RIG-I activation (Gack et al., 2007). Recently, it was reported that Riplet rather than TRIM25 was primarily responsible for ubiquitinating and activating RIG-I (Hayman et al., 2019). It is worth point out that this remains controversial as multiple previous studies showed TRIM25

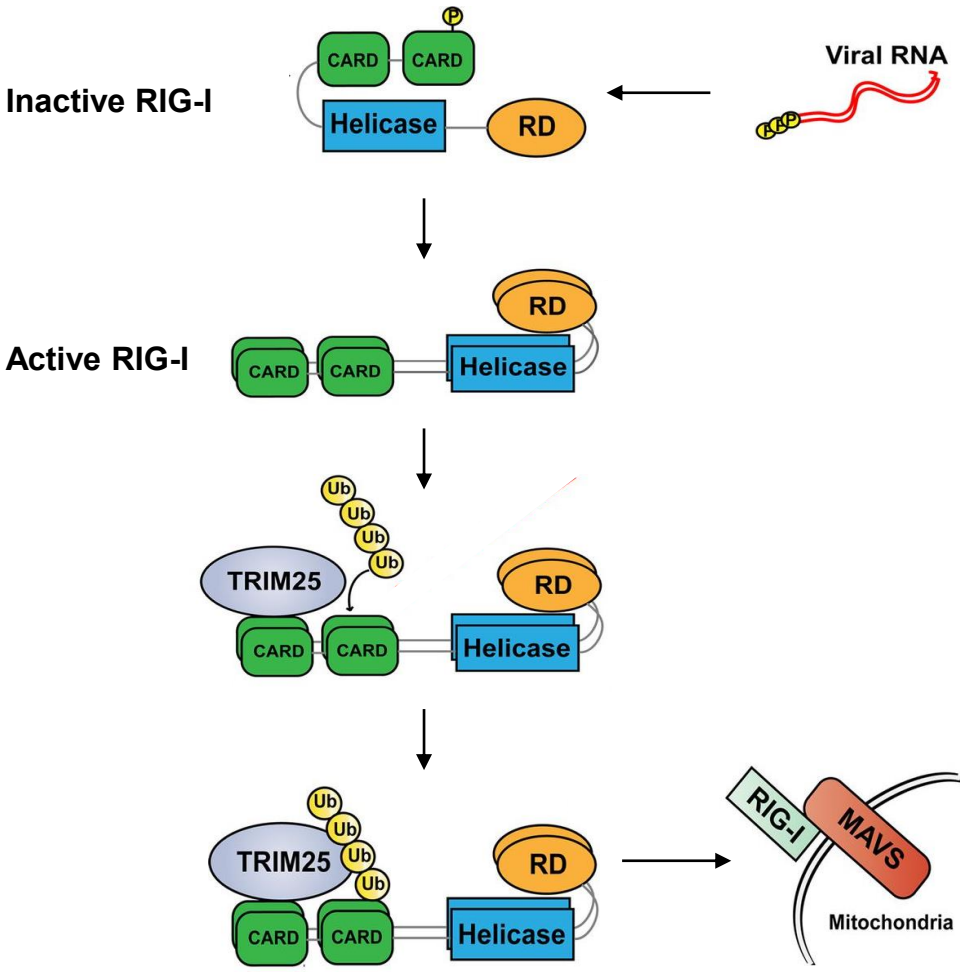

Figure 1.7. Model of RIG-I activation. In the absence of viral infection RIG-I exists in a phosphorylated and inactive conformation. Binding of viral RNA to the helicase and c-terminal regulatory domain (RD) induces a conformational change that exposes the CARD domains and RIG-I homomultimerizes on RNA. TRIM25 polyubiquitinates RIG-I and this facilitates the interaction with MAVS on mitochondria. (Modified from Sánchez-Aparicio, Feinman et al. 2018)

is essential for RIG-I activation and IFN signalling (Gack et al., 2007; Martín-Vicente et al., 2017; Sanchez et al., 2016). Polyubiquitination and oligomerization of RIG-I is required for subsequent interaction with the mitochondrial antiviral-signalling protein (MAVS), which is localized on mitochondria and peroxisomes. The chaperone protein 14-3-3ε is required for the translocation of activated RIG-I from the cytosol to MAVS on the mitochondria. MAVS interacts with a series of adapter and kinase proteins including TRAF3, TBK1, IKKε and this leads to the activation of IRF-3 (**Figure 1.6**) (Nan et al., 2014). Activated IRF-3 then enters the nucleus and initiates the production of interferon-beta and antiviral activity (Gack et al., 2007; Okamoto et al., 2018).

Of note, Protein Kinase R (PKR) is also a PRR that is activated by the presence of viral dsRNA, however the mechanism by which PKR mediates IFN induction is unclear. However, it has been reported that PKR activation enhances MDA5-mediated IFN production (Pham et al., 2016).

1.3.4.3 Subversion of IFN induction by ZIKV and other flaviviruses

As mentioned above, flaviviruses have evolved effective mechanisms for antagonizing the host IFN response. The evasion mechanisms employed by DENV and WNV (and other flaviviruses) have been intensely studied and can be separated into three main categories: i) Direct inhibition/inactivation of specific PRRs; ii) Sequestration of 14-3-3 scaffold proteins that control the subcellular localization of PRRs; and iii) Inhibition of IFN induction by blocking downstream signalling

molecules in the pathway (Serman and Gack, 2019). Compared to DENV and WNV, the mechanisms by which ZIKV subverts IFN production have only recently come into focus.

The NS4A protein which is a small hydrophobic protein consisting of four transmembrane helices and an N-terminal cytosolic region, has been reported to antagonize the IFN response (Ma et al., 2018; Ngan et al., 2019). The main mechanism of RLR-NS4A interaction is thought to involve direct binding of the N-terminal cytosolic region of NS4A to the N-terminal CARD domain of MAVS. This interaction was confirmed by co-immunoprecipitation assays which showed that NS4A interacts with MAVS but not to RIG-I or MDA5 (Ma et al., 2018). In addition, ectopic overexpression of NS4A reduced the interaction of overexpressed MDA5 or RIG-I with endogenous MAVS in HEK293T cells and co-localizations studies showed that upon poly (I:C) stimulation the interaction of MAVS and MDA5 was significantly reduced in the presence of NS4A. Interestingly, binding of NS4A to MAVS did not block its activation, instead it is presumed that NS4A-binding blocks RIG-I/MDA5 binding to the MAVS CARD domain that is required for activation. Whether this interaction is actually blocked during ZIKV infection is unknown.

The NS3 protein of ZIKV is also implicated in evasion of RLR-signalling. It contains a “RLDP” motif that mimics substrates of the chaperone 14-3-3ε (Riedl et al., 2019). 14-3-3ε is required for translocation of activated RIG-I from the cytosol to the mitochondria, and binding of NS3 to 14-3-3ε blocks 14-3-3-mediated cytosol to mitochondria translocation of RIG-I thereby inhibiting RLR-signalling.

In addition to inhibition of PRRs or adaptor proteins, the NS1 and NS4B proteins of ZIKV inhibit IFN induction by direct interaction and inhibition of the kinase TBK1. NS1 and NS4B inhibit TBK1 oligomerization which is required for IFN induction (Wu et al., 2017). However, these observations were made solely from co-immunoprecipitation studies and how/where NS1 or NS4B proteins bind TBK1 is unknown.

The ZIKV NS5 protein inhibits the IFN induction pathway by interaction with IKKε, a protein upstream of IRF-3 (Lundberg et al., 2019). While further experiments are warranted to elucidate the mechanism, one possibility is that NS5 binds to and blocks IKKε kinase activity, as has been reported with DENV proteins NS2B/NS3 (Angleró-Rodríguez et al., 2014). Alternatively, it may inhibit the formation of MAVS and IKKε complexes.

Lastly, two recent papers suggest a role for flavivirus capsids in subverting IFN induction, albeit by different mechanisms. Kumar *et al*., identified DEAD Box Helicase 3 X-linked (DDX3X) as a DENV capsid-interacting protein (Kumar et al., 2018a). One of the roles of DDX3X is as an effector of TBK1 that is necessary for type I IFN induction (Soulat et al., 2008). However, in this study, knock-down of DDX3X did not affect induction of type I IFN during DENV infection. The authors concluded that the antiviral effect of DDX3X in DENV infection is independent of IFN induction pathways and no further investigation or experiments examining the role of capsid on IFN induction were performed. Conversely, Samuel *et al*. concluded that flavivirus capsid are viral suppressors of RNA silencing in the mosquito *Aedes aegypti* (Samuel et al., 2016). Specifically, they proposed that capsid proteins antagonize RNA

silencing by binding long dsRNAs with high affinity thus interfering with efficient processing by the endoribonuclease Dicer. Dicer is an indispensable antiviral protein in many organisms but such antiviral activity has not yet been clearly demonstrated in mammals (MacKay et al., 2014).

1.4 Alphaviruses

Alphaviruses are small enveloped viruses that contain a single-stranded positive sense RNA genome. *Alphaviruses* belong to the family *Togaviridae* and is comprised of at least 30 members that are separated into New World and Old World viruses. The New World viruses evolved separately and include viruses that can cause severe encephalitis in humans and animals. Notable pathogens in this group include Venezuelan equine encephalitis (VEEV), Western equine encephalitis (WEEV) and Eastern equine encephalitis virus (EEEV). Most alphaviruses that cause debilitating arthralgia belong to the Semliki Forest (SF) complex and include members of the Old World viruses including Semliki Forest virus (SFV), Chikungunya virus (CHIKV), Ross River virus (RRV) and Mayaro virus (MAYV). Human infections are often associated with fever, rash, severe joint pain (arthralgia) and stiffness that can last weeks, months and in some cases years in duration. For the purpose of this thesis, I will focus on the related arthritogenic alphaviruses CHIKV and MAYV which share approximately 66% amino acid identity.

1.4.1 CHIKV and MAYV

As is the case with ZIKV and DENV, acute infection with CHIKV or MAYV results in a febrile-like illness lasting 3 to 5 days with the onset of fever, headache, muscle ache, retroorbital pain and joint pain. However, in about ~50% of infected individuals, severe manifestation can develop and can last greater than 6 months with severe and incapacitating arthralgia, which is referred to as the chronic stage of disease.

The most notable member of the arthritogenic alphaviruses is CHIKV. It was first isolated in Tanzania in 1952 (Mason and Haddow, 1957), followed by sporadic but confined outbreaks in Asia and Africa. In the late 1990s and early 2000s, CHIKV began to emerge on a global scale. In the past fifteen years, an alarming and unprecedented increase in CHIKV spread has occurred with cases reported in more than 100 countries (Vairo et al., 2019). Outbreaks of CHIKV disease have occurred in Africa, Asia, Europe, the Americas and islands in the Indian and Pacific Oceans (**Figure 1.8A**). The rapid increase of CHIKV infection rates is due partly to increased global travel but can also be attributed to its use of mosquito vectors *Aedes aegypti* and *Aedes albopictus*, which are the type of mosquitos typically involved in urban transmission cycles of DENV and ZIKV.

MAYV was originally isolated in 1954 from the serum of a forest worker living in Mayaro County of Trinidad Island. Since then, it has been found in Central and South America (**Figure 1.8B**). Outbreaks of MAYV are sporadic, relatively small, and usually in the vicinity of rainforest areas. The main source of MAYV transmission appears to be forest-dwelling *Haemagogus* species of mosquitoes, however the virus

A.

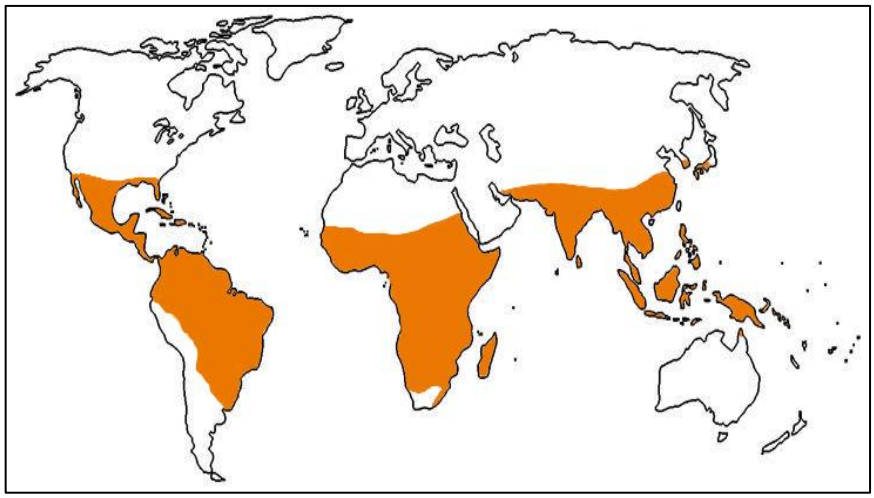

B.

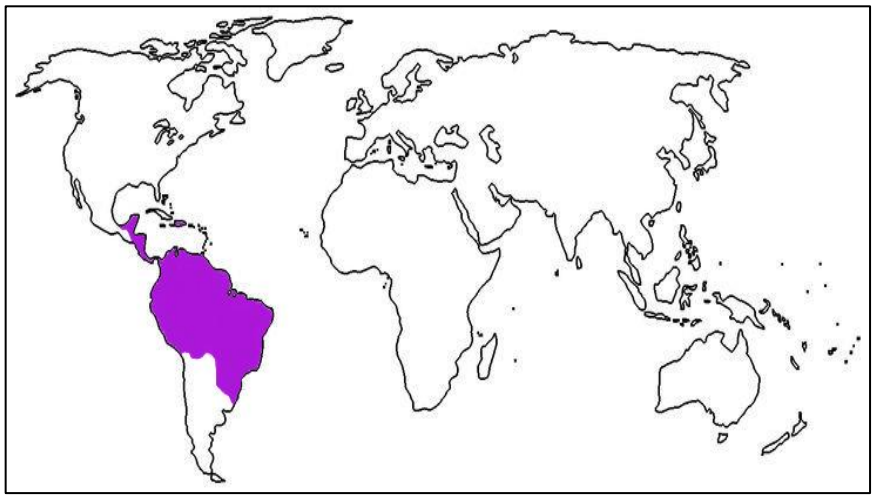

Figure 1.8. Global distribution of A. CHIKV and B. MAYV as of 2020.

can infect and potentially be transmitted by *Aedes aegypti* (Long et al., 2011) and *Aedes albopictus* (Wiggins et al., 2018) mosquitos. This is worrisome as these mosquitoes are typically involved in urban arboviral transmission cycles and thus it has been suggested that the incidence of MAYV will continue to increase. It is also possible that MAYV transmission has been and will continue to be restricted due to individuals harbouring neutralizing antibodies from natural CHIKV infection that potentially cross-neutralize with MAYV (Martins et al., 2019).

There are currently no specific antiviral treatments or vaccines for CHIKV or MAYV and treatment for severe joint pain is limited to anti-inflammatory drugs and physiotherapy. There is a CHIKV live attenuated vaccine candidate (VLA1553) that was granted Fast Track designation by the FDA and is commencing phase 3 clinical trials. Many other promising candidates are undergoing preclinical studies as well (Rezza and Weaver, 2019).

1.4.2 Alphavirus virion and genome organization

Alphaviruses are small icosahedral-shaped enveloped viruses of ~70 nm in diameter (**Figure 1.9)**. The genome is a single-stranded positive sense RNA of approximately 12 kb in length. Alphaviruses have a 5'cap and a poly (A) tail. The genomic RNA consists of two large open reading frames (ORFs); the N-terminal ORF encodes the non-structural polyprotein while the C-terminal ORF encodes the structural polyprotein. The two polyproteins are cleaved post-translationally by viral

A.

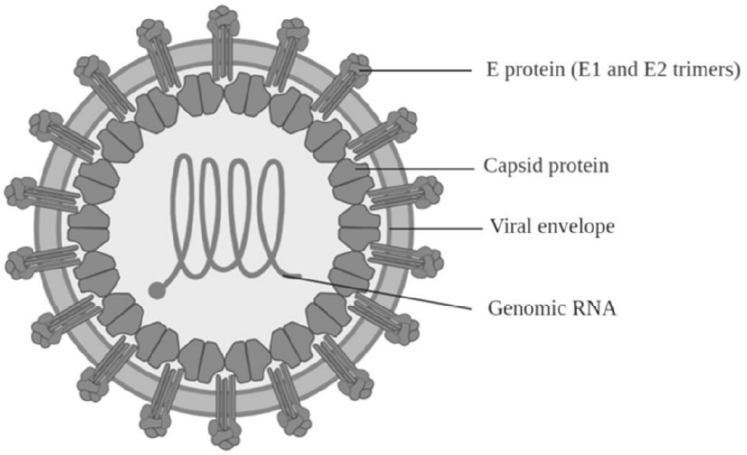

B.

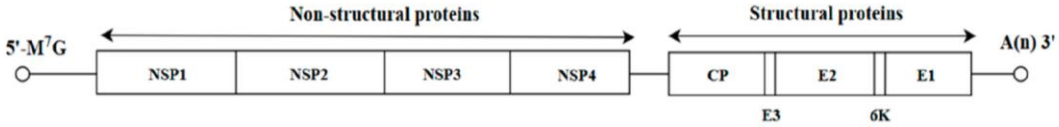

Figure 1.9. Alphavirus virion and genome organization. A. Prototypical alphavirus virion is depicted (~70 nm in diameter). **B.** Schematic representation of the alphavirus genome (~12 kb). The genome contains a type I cap structure at the 5' UTR and a polyadenylated (polyA) tail at the 3'UTR. The N-terminal ORF encodes for the non-structural polyprotein. The C-terminal ORF encodes the structural polyprotein via subgenomic RNA. (Modified from Mandary., et al. 2019)

and host proteases into 4 non-structural (Nsp1, Nsp2, Nsp3, Nsp4), 3 structural proteins (Capsid, E1 and E2) and 2 small cleavage products (E3 and 6K) (Kumar et al., 2018b).

The four non-structural proteins form the replication complex. Nsp1 is the main enzyme involved in alphavirus RNA capping; it contains both guanine-7-methyltransferase and guanylyl transferase activities required for capping and methylation of newly synthesized RNAs (Ahola and Kääriäinen, 1995; Mi and Stollar, 1991). Nsp2 contains nucleoside triphosphatase, RNA triphosphatase, helicase and protease activities (Karpe et al., 2011). The functions of Nsp3 are not well understood but it plays an essential role in RNA replication (LaStarza et al., 1994). The Nsp4 protein functions as the RNA-dependent RNA-polymerase (RdRp) (Chen et al., 2017b).

The E1 and E2 proteins form heterodimers that further associate into trimers that make up the spikes on the viral envelope. E1 mediates fusion of the viral and cellular membranes during viral entry. E2 glycoprotein is responsible for receptor binding but mutations in E1 can affect cellular tropism. This is best represented by analysis of viral isolates of the CHIKV genome during the 2005–2006 Indian Ocean epidemic that revealed a single alanine to valine mutation at position 226 in the E1 glycoprotein (E1-A226V) (Schuffenecker et al., 2006). This mutation was associated with increased fitness of the virus in the atypical vector *Ae. albopictus* mosquitoes (Tsetsarkin et al., 2007), thus greatly increasing the spread of the virus.

1.4.3 Alphavirus replication

The Alphavirus infection cycle can be divided into three stages including virion attachment and entry, translation and replication, viral assembly and exit (**Figure 1.10**).

1.4.3.1 Viral entry and cellular tropism

The alphavirus infection cycle begins by binding of the virion to a cellular receptor. Recently the major cellular receptor for arthralgia-causing alphaviruses including CHIKV, MAYV and RRV was identified as Mxra8 (Zhang et al., 2018). Mxra8 is an adhesion molecule expressed on epithelial, myeloid and mesenchymal cells of mammals, birds and amphibians. As mentioned above, binding of alphavirus virions to the host receptor is primarily mediated by the E2 protein but the T cell immunoglobulin and mucin domain-1 and glycosaminoglycans molecules have also been implicated in CHIKV attachment (Duijl-Richter et al., 2015). Replication of CHIKV has been observed in synovial fibroblasts, skeletal muscle cells, osteoblasts and chondrocytes *in vitro* (Zhang et al., 2018). CHIKV also productively infects human monocyte-derived macrophages but does not infect lymphoid and monocytoid cell lines, primary lymphocytes or monocytes (Sourisseau et al., 2007). Macrophages have been proposed as target cells for MAYV but the relevance to human infections is not clear as mouse macrophage cell lines and mouse primary macrophages were used for these studies (Cavalheiro et al., 2016; de Castro-Jorge et al., 2019). At this point the susceptibility of human macrophages to MAYV-infection and whether the virus can

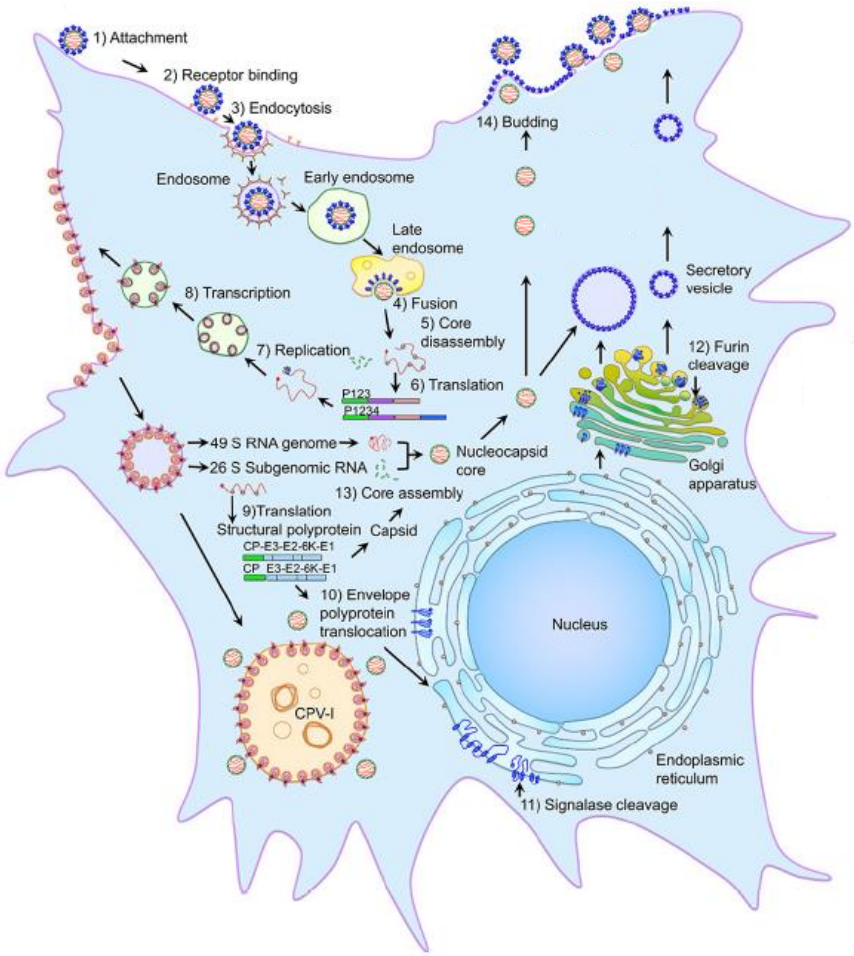

Figure 1.10. Model of alphavirus replication cycle. Following attachment and receptor binding, the virion enters by clathrin-mediated endocytosis. The acidic environment of the endosome lumen triggers conformational changes in the viral spike proteins that result in fusion between the viral and the endosomal membranes allowing release of the nucleocapsid into the cytoplasm. The non-structural polyproteins are translated directly from the viral genomic RNA and form invaginations in the plasma membrane (i.e. replication spherules). Internalization of spherules from the plasma membrane gives rise to type 1 cytopathic vacuoles (CPV-1). As infection progresses negative-strand synthesis is inhibited and synthesis of positive-sense genomic and subgenomic RNA begins. The non-structural polyprotein is produced from a subgenomic RNA. The capsid and envelope polyproteins are translocated to the ER where they are processed by host cell signal peptidase and transported to the Golgi and plasma membrane during which time furin-mediated cleavage of spike proteins occurs in the *trans*Golgi network. Nascent virions bud from the plasma membrane. (Modified from Jose., et al 2017)

persist long-term in these cells, is unknown.

After attachment, virions are internalized via the clathrin-mediated endocytic pathway (Carvalho et al., 2017). In endosomes, the low pH environment leads to structural changes in the envelope glycoproteins that trigger fusion. Specifically, acidic pH destabilizes the interaction between E1 and E2 followed by insertion of the E1 fusion loop into the endosomal membrane resulting in creation of the "fusion pore" (Kielian et al., 2010). The pore increases in size as fusion is completed and the nucleocapsid containing viral RNA is released into the host cell cytoplasm.

1.4.3.2 Translation and replication

After viral uncoating, rapid translation of the RNA yields the polyprotein P1234, which is then processed to release the polymerase, Nsp4. P123 and Nsp4 together form the negative strand RNA polymerase complex. At this time, small single-membrane bulb-shaped invaginations called "spherules" are formed on the external surface of the plasma membrane (reviewed in (Reid et al., 2015)). The fact that dsRNA can be detected inside the spherules and the presence of partially processed non-structural proteins (P123 and Nsp4) on the spherule necks (Frolova et al., 2010), suggests that these plasma membrane-derived structures are the sites of viral RNA synthesis (Spuul et al., 2010). Internalization of spherules by endo-lysosomal membranes gives rise to type 1 cytopathic vacuoles (CPV1) (Grimley et al., 1968). The endosomal origin of CPVs was confirmed by the observation that these structures are

often positive for both endosomal and lysosomal markers (Froshauer et al., 1988). As infection progresses, the non-structural polyprotein precursors are further processed to yield individual non-structural proteins and negative-strand synthesis is inactivated. The fully processed non-structural proteins together form the mature replicase, which is required for efficient synthesis of positive-sense genomic and subgenomic RNA. The structural polyprotein is translated from the subgenomic RNA. Capsid is autocatalytically cleaved off from the polyprotein after which it binds to nascent positive-strand RNA molecules to form nucleocapsids. The envelope proteins are co-translationally translocated into the ER.

1.4.3.3 Virion assembly and exit

In the ER, the E1and E2 glycoproteins interact to form heterodimers that are then transported to the cell surface via the Golgi complex (Leung et al., 2011). In the Golgi, cleavage by furin results in maturation of the E2 protein. Interactions between the capsid protein and the E2 protein drive the budding process (Skoging et al., 1996; Zhao et al., 1994), with E1-E2 heterodimers forming an envelope around nucleocapsid-like particles. Upon release from cells, virions acquire a membrane bilayer derived from the host cell plasma membrane.

1.4.4 Mechanisms of virus-induced arthralgia

The development of virus-induced arthralgia is most likely a consequence of two non-mutually exclusive scenarios. One is that direct and persistent viral replication within joint tissue leads to cellular damage and inflammation. The other takes into account the role of the host immune response in pathogenesis (i.e. recruitment of immune cells to site of tissue damage and secretion of cytokines/chemokines) (**Figure 1.11**). Evidence for persistent replication comes from CHIKV animal studies in which CHIKV RNA was detected in the feet of C57BL/6 mice for 100 days after infection (Poo et al., 2014). Persistent CHIKV RNA was also detected in the spleen but virus was not detected in any tissues of rhesus macaques at 35 days post-infection (Messaoudi et al., 2013). This is consistent with studies that have not been able to isolate infectious virus from human studies of long-term CHIKV infections (Hoarau et al., 2010).

Several cell types have been suggested as target cells for arthritogenic alphavirus replication, including cells from joints, bones, and muscles. However, macrophages appear to play an important role in disease pathology. RRV replication was found to persist in mouse macrophage-derived cell lines, which continually shed virus for over 50 days (La Linn et al., 1996). Moreover, pharmacological depletion of macrophages in mouse models of CHIKV infection ameliorated rheumatic disease but prolonged the viremia (Gardner et al., 2010); thus demonstrating the importance of macrophages for disease progression. Lastly, long-term CHIKV infection in non-human primates suggest that macrophages are the main cellular reservoir during the

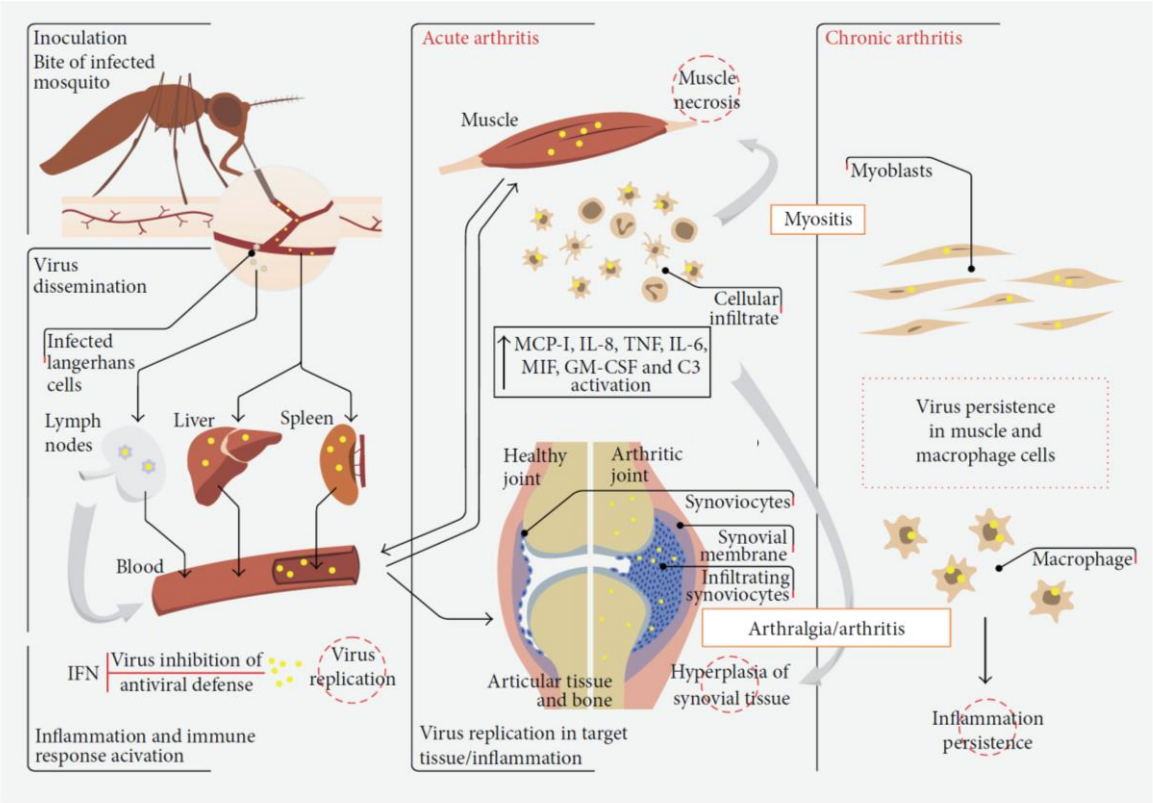

Figure 1.11. Alphavirus-induced arthritis. Initial infection begins with the bite from an infected mosquito that results in local viral replication near the wound. The virus then disseminates and spreads to liver, spleen and lymph nodes which are sites of primary replication. An IFN response is activated but the virus is able to subvert this response and to continue with productive virus replication. The acute phase involves virus replication in target tissues and is characterized by infiltration of macrophages and lymphocytes, NK cells and neutrophils. Persistence of symptoms (i.e chronic phase) may be related to chronic infection or products released by target cells infected with the virus (e.g., MCP-1/CCL2, TNF). (Modified from Assunção-Miranda., et al 2013)

late stages of infection (Labadie et al., 2010). However, the overall contribution of macrophages to disease pathology is not clear. Possible roles for macrophages include maintenance of viral replication and/or the production of inflammatory mediators and soluble factors that contribute to tissue damage and recruitment/activation of lymphocytes and NK cells to target tissues.

All of the discussed studies point to macrophages as key players in virus-induced arthralgia, however, most of the studies have used CHIKV to come to these conclusions. More studies are needed to identify what cells are susceptible to MAYV and to understand how infection of these cells contributes to disease.

1.5 Objectives of Thesis

Due to their minimal genome, arboviruses depend on many host molecules for replication and have evolved multiple strategies to subvert host innate immune defense mechanisms. Thus, the main objective of my thesis research was to identify host factors that are involved in arbovirus replication. Understanding the implications of interactions between viral proteins and host cellular factors may provide insight into virus-host defense evasion strategies and reveal novel therapeutic targets.

The main function of the flavivirus capsid protein is to protect the viral genome, but several studies have suggested that capsid is a multifunctional protein and that it interacts with numerous host factors. To elucidate the functions of capsid, in Chapter

3 and 4 I examine the non-structural functions of flavivirus capsid proteins with the underlying hypothesis that flavivirus capsid proteins subvert the antiviral response.

Previously, our lab demonstrated that the WNV capsid protein inhibits apoptosis through a mechanism that involves phosphatidylinositol 3 kinase (PI3K) activation of Akt. Therefore, the main objective of **Chapter 3** was to determine if this mechanism is conserved among flavivirus capsids and to examine how expression of capsid proteins affect apoptosis and Akt-dependent processes.

In **Chapter 4**, I examine the global transcriptome changes in flavivirus capsid expressing cells by RNA-Seq and identify a potential mechanism by which flavivirus capsids suppress the production of type I interferon. Collectively, the findings presented in Chapter 4 reveal a novel, previously unrecognized role of flavivirus capsids in subverting the innate immune response.

Unlike CHIKV, very little is known about the interactions of MAYV with human cells. Therefore, in **Chapter 5** I investigated the *in vitro* susceptibility of peripheral blood mononuclear cells (PBMCs) and found that MAYV replication was only observed in monocyte-derived macrophages. I proceeded to characterize MAYV infection in primary human macrophages and through RNA-Seq data found that MAYV causes drastic changes in the transcriptome of infected cells.

Chapter 2

Materials and Methods

2.1 Materials

2.1.1 Reagents

Reagents listed below were used as per Manufacturers' instructions unless otherwise stated.

Table 2.1 Commercially prepared reagents

Reagent	Source
40% Acrylamide	Bio-Rad
Accutase Cell detachment solution	BD Biosciences
Agar	Sigma-Aldrich
Agarose, Ultrapure	Invitrogen
Albumin, Bovine Serum Endotoxin-Free	Millipore
Ammonium persulfate	Invitrogen
Ampicillin	Sigma-Aldrich
Anti-DYKDDDDK(FLAG) Magnetic Agarose	Pierce Thermo Scientific
Anti-c-Myc Magnetic Beads	Pierce Thermo Scientific
Bovine-serum albumin (BSA)	Sigma-Aldrich
Bovine-serum albumin (BSA) Endotoxin Free	Millipore
Bromophenol Blue	Sigma-Aldrich
Cd14 MicroBeads	Miltenyi Biotec
Complete^{TM} EDTA-free protease inhibitor	Roche
Crystal violet	Sigma-Aldrich
Dulbecco's modified Eagle's medium (DMEM)	Invitrogen

Ethidium bromide solution	Sigma-Aldrich
Ethanol	Commercial Alcohols
Fetal Bovine Serum	Invitrogen
Formaldehyde 40% (v/v)	Sigma-Aldrich
Glycerol	Thermo Fisher Scientific
Histopaque 1077	Sigma-Aldrich
Hydrochloric acid	Thermo Fisher Scientific
Lipofectamine 2000	Invitrogen
Lipofectamine LTX with Plus Reagent	Invitrogen
LIVE/DEAD fixable Dead Cell stain	Invitrogen
LS Columns for MACS	Miltenyi Biotec
Magnesium chloride hexahydrate	EMD Chemicals
Macrophage Colony-Stimulating Factor human	Sigma-Aldrich
Methanol	Thermo Fisher Scientific
Methylcellulose	Sigma-Aldrich
2-Mercaptoethanol	Thermo Fisher Scientific
N,N,N',N'-tetramethylenediamine (TEMED)	Sigma-Aldrich
OptiMEM	Invitrogen
Paraformaldehye (EM grade)	Electron Microscopy Sciences
PBS, Endotoxin-Free	Millipore
Phorbol 12-myristate 13-acetate (PMA)	Sigma-Aldrich
PhosSTOP	Sigma-Aldrich
2-propanol	Thermo Fisher Scientific
Prolong gold antifade Mountant	Invitrogen
Sodium Chloride	Thermo Fisher Scientific
Sodium dodecyl sulfate (SDS)	Bio-Rad
Sodium hydroxide	Sigma-Aldrich

Transit-LT1	Mirus Bio
Tris-base	EMD Chemicals
Triton X-100	Thermo Fisher Scientific
0.25% Trypsin-EDTA	Invitrogen
Tween 20	Thermo Fisher Scientific
Ultrapure distilled water	Invitrogen

Table 2.2 Molecular Size Standards

Standard	**Source**
GenerRuler, 1kb DNA Ladder (SM0313)	Thermo Fisher Scientific (Fermentas)
GeneRuler 1 kb DNA Ladder Plus (SM1333)	Thermo Fisher Scientific (Fermentas)
PageRuler Pre-stained Protein Ladder (#26616)	Thermo Fisher Scientific (Fermentas)
PageRuler Pre-stained Protein Ladder (#26619)	Thermo Fisher Scientific (Fermentas)

Table 2.3 DNA/RNA modifying enzymes and buffers

Enzyme	**Source**
Antarctic Phosphatase	New England Biolabs
Benzonase	Millipore
Pfu DNA Polymerase	Promega
Platinum Taq DNA polymerase High Fidelity	Invitrogen
Restriction endonucleases	New England Biolabs
Restriction endonucleases	Thermo Fisher Scientific
T4 DNA ligase	Invitrogen

Table 2.4 Detection Systems

System	Source
BD FACSAria III cell sorter	BD Biosciences
Bioanalyzer (model G2939B)	Agilent Scientific Instruments
ImageJ Analysis Software	National Institute of Health
Immobilon-FL PVDF membrane	Millipore
LSRFortessa X20 SORP flow cytometer	BD Biosciences
Moxi-Z Cell Counter	Orflo
Odyssey Infrared Imaging System	LiCor
Qubit	Thermo Fisher Scientific
Synergy 4 Luminescence Reader	BioTek
Ultraviolet transilluminator	Thermo Fisher Scientific
Volocity acquisition and analysis software	Perkin-Elmer

Table 2.5 Multicomponent Systems

System	Source
CellTiter-Glo Luminescent Cell Viability assay kit	Promega
Perfecta SYBR Green Super Mix, Low Rox	Quanta Biosciences
QIAEX II gel extraction kit	Invitrogen
QIAGEN plasmid maxi kit	QIAGEN
QIAprep spin miniprep kit	QIAGEN
QIAquick PCR purification kit	QIAGEN
RNeasy mini kit	QIAGEN
RNAse-Free DNase Set	QIAGEN
Total RNA isolation kit	Mackerey-Nagel
Total DNA kit (maxi)	Mackerey-Nagel

Table 2.6 Commonly used buffers

Name	Composition
5X Protein Sample buffer	62.5 mM Tris-Hcl (pH 6.8), 50% (v/v) glycerol, 2% (w/v) SDS, 0.01% (w/v) bromophenol blue, 5% (v/v) 2-Mercaptoethanol
6X DNA gel loading buffer	Thermo Fisher Scientific
LB growth media	1% (w/v) Bacto-tryptone, 0.5% (w/v) Bactoyeast extract, 0.5% (w/v) NaCl, 0.1% (v/v) 1M NaOH
Phosphate-buffered saline (PBS)	137 mM NaCl, 2.7 mM KCl, 8mM Na2HPO4 (pH 7.4)
PBS-T	137 mM NaCl, 2.7 mM KCl, 8mM Na2HPO4 (pH 7.4), 0.05% Tween-20
SDS-PAGE running buffer (Tris-Glycine)	192 mM glycine, 0.1% (w/v) SDS, 25 mM Tris base (pH 8.3)
TAE	40 mM Tris-Acetate, 1mM EDTA (pH 8.0)
RIPA lysis buffer	5M NaCL, 0.5M EDTA pH 8.0, 1M Tris-HCl pH 8.0, 1% Triton X-100, 10% sodium deoxycholate, 10% SDS
NP-40 lysis buffer	50mM Trist-HCl (pH 7.2), 150mM NaCl, 0.5mM $MnCl_2$, 1% Triton X-100
Western blot transfer buffer	200 mM glycine, 25mM Tris base (pH 8.3), 20% (v/v) methanol, 0.1% (w/v) SDS
Co-IP lysis buffer	50mM Tris-HCL (pH 7.2), 20mM NaCl, 1mM $MgCl_2$, 1% Triton X-100

Table 2.7 Oligonucleotides

Name	Usage, Restriction sites	Sequence (5' → 3')	Section
ZIKV-Cap-myc-Fwd	Cloning, SpeI	ATTAGCACTAGTGCCACCATGGAACAAAAACTCATCTCAGAAGAGGATCTGATGAAAAACCCAAAAAAGAAATCC	Chapter 3
ZIKV-Cap-Rev	Cloning, XhoI	GTACCTCGAGTTATCGTCTCTTCTTCTCCTTCCTAGC	Chapter 3
myc-DENV C - Fw	Cloning, NheI	ATTAGCGCTAGCATGGAACAAAAACTCATCTCAGAAGAGGATCTGAATGACCAACGGAAAAAGGC	Chapter 3
DENV C - Rv	Cloning, BamHI	GTACGGATCCTTATCTGCGTCTCCTATTCAAGA	Chapter 3
myc-JEVC - Fw	Cloning, NheI	ATTAGCGCTAGCATGGAACAAAAACTCATCTCAGAAGAGGATCTGACTAAAAAACCAGGAGGGC	Chapter 3
JEVC - Rv	Cloning, BamHI	GTACGGATCCTTATCTTTTGTTTTGCTTTCTGCC	Chapter 3
myc-MVEV C - Fw	Cloning, NheI	ATTAGCGCTAGCATGGAACAAAAACTCATCTCAGAAGAGGATCTGTCTAAAAAACCAGGAGGAC	Chapter 3
MVEV C - Rv	Cloning, BamHI	GTACGGATCCTTATCTTTTCTTTTGTTTTTTGCC	Chapter 3
myc-WNV C - Fw	Cloning, NheI	ATTAGCGCTAGCATGGAACAAAAACTCATCTCAGAAGAGGATCTGTCTAAGAAACCAGGAGGGCC	Chapter 3
WNV C - Rv	Cloning, BamHI	GATCGGATCCTTATCTTTTCTTTTGTTTTGAGC	Chapter 3
myc-YFV C - Fw	Cloning, NheI	ATTAGCGCTAGCATGGAACAAAAACTCATCTCAGAAGAGGATCTGTCTGGTCGTAAAGCTCAGGG	Chapter 3
YFV C - Rv	Cloning, BamHI	GTACGGATCCTTATTAACGGCGTTTCCTTGAGG	Chapter 3
GLUT 1 - Fw	qRT-PCR	AAC TCT TCA GCC AGG GTC CAC	Chapter 3
GLUT 1 – Rv	qRT-PCR	CAC AGT GAA GAT GAT GAA GAC	Chapter 3
β actin Fw	qRT-PCR	CCT GGC ACC CAG CAC AAT	Chapter 3, 4 and 5

β actin Rv	qRT-PCR	GCC GAT CCA CAC GGA GTA CT	Chapter 3, 4 and 5
IFIT1 Fw	qRT-PCR	TGCAGAACGGCTGCCTAATTT	Chapter 4
IFIT1 Rv	qRT-PCR	CAAGACTCTGTTTTCTAAATCAGGCAT T	Chapter 4
IFNB1 Fw	qRT-PCR	TGTGCCTGGACCATAGTCAGA	Chapter 4
IFNB1 Rv	qRT-PCR	AACAGCATCTGCTGGTTGAAGA	Chapter 4
CCL5 Fw	qRT-PCR	CTCGCTGTCATCCTCATTGCT	Chapter 4
CCL5 Rv	qRT-PCR	GCACTTGCCACTGGTGTAGA	Chapter 4
IFI6 Fw	qRT-PCR	CGCTGCTGTGCCCATCTAT	Chapter 4
IFI6 Rv	qRT-PCR	GCAAGTGAAGAGCAGCAGGTA	Chapter 4
TRIM 22 Fw	qRT-PCR	CTCTGGCTTGGTGAGTGAATCT	Chapter 4
TRIM 22 Rv	qRT-PCR	CCCTTGGCTTCCTTCTGTCTT	Chapter 4
IRF1 Fw	qRT-PCR	CCAGGCTACATGCAGGACTT	Chapter 4
IRF1 Rv	qRT-PCR	GGGTGACACCTGGAAGTTGTA	Chapter 4
STAT2 Fw	qRT-PCR	ATTGACCACGGGTTGGAACA	Chapter 4
STAT2 Rv	qRT-PCR	CGTAGGTCCACCCCTTTGG	Chapter 4
MYD88 Fw	qRT-PCR	CGGGCATCACCACACTTGAT	Chapter 4
MYD88 Rv	qRT-PCR	CAGACACACACAACTTCAGTCGATA	Chapter 4
BAX Fw	qRT-PCR	CCAGCTCTGAGCAGATCATGAA	Chapter 4
BAX Rv	qRT-PCR	GAGACACTCGCTCAGCTTCT	Chapter 4
ZIKV Fw	qRT-PCR	CCTTGGATTCTTGAACGAGGA	Chapter 4
ZIKV Rv	qRT-PCR	AGAGCTTCATTCTCCAGATCAA	Chapter 4
LAMP3 Fw	qRT-PCR	GCAGTCGGGCATTCCTTCA	Chapter 5

LAMP 3 Rv	qRT-PCR	GTGTAGTCAGACGAGCACTCAT	Chapter 5
MAYV Fw	qRT-PCR	AAGCTCTTCCTCTGCATTG	Chapter 5
MAYV Rv	qRT-PCR	TGCTGGAAATGCTCTTTGT	Chapter 5

Table 2.8 Plasmid vectors

Plasmid	**Source**
pCMV-VSV.G	Charles Rice (Rockefeller University)
pGag-Pol	Charles Rice (Rockefeller University)
p8113.1 NY99 WNV replicon	Vladimir Yamshchikov (Oregon Public Health Laboratory)
pFlagCMV2-EFP	Dong-Er Zhang (The Scripps Research Institute)
pTRIP-MCS-AcGFP	Constructed by M. Urbanowski
pTRIP-MCS-AcGFP-myc-WNV Capsid	Constructed by M. Urbanowski
pTRIP-MCS-AcGFP-myc-YFV Capsid	Constructed by M. Urbanowski
pTRIP-MCS-AcGFP-myc-SLEV Capsid	Constructed by M. Urbanowski
pTRIP-MCS-AcGFP-myc-DENV Capsid	Constructed by M. Urbanowski
pTRIP-MCS-AcGFP-myc-JEV Capsid	Constructed by M. Urbanowski
pTRIP-MCS-AcGFP-myc-MVEV Capsid	Constructed by M. Urbanowski
pTRIP-MCS-AcGFP-myc-ZIKV Capsid	Constructed in this study

pcDNA3.1-myc-WNV Capsid	Constructed in this study. Used in Hou et al. 2017
pcDNA3.1-myc-ZIKV Capsid	Constructed in this study. Used in Hou et al. 2017
pcDNA3.1-myc-YFV Capsid	Constructed in this study. Used in Hou et al. 2017
pcDNA3.1-myc-JEV Capsid	Constructed in this study. Used in Hou et al. 2017
pcDNA3.1-myc-DENV Capsid	Constructed in this study. Used in Hou et al. 2017
pcDNA3.1-myc-MVEV Capsid	Constructed in this study. Used in Hou et al. 2017

Table 2.9 Primary Antibodies

Antibody	Dilution	Application	Source
Goat-anti GFP	1:1000	WB	Abcam
Guinea Pig Anti-DENV Capsid	1:1000	WB	T. Hobman, University of Alberta
Guinea Pig anti-WNV Capsid	1:1000	WB	T. Hobman, University of Alberta
Mouse anti-actin	1:2000	WB	Abcam
Mouse anti-CD63	1:500	IF	Novus Biologicals
Mouse anti-CHIKV E2	1:200	FC	M. Diamond, Washington University School of Medicine
Mouse anti-DDX58	1:1000	WB	Abcam
Mouse anti-Flag	1:1000	WB	Sigma-Aldrich
Mouse anti-myc 9e10	1:1000	WB	ATCC
Mouse anti-WNV NS3	1:1000	WB	R & D Systems

Mouse anti-ZIKV NS1	1:100	FC	T. Hobman, University of Alberta
Rabbit anti-Akt (4685)	1:1000	WB	Cell Signaling
Rabbit anti-phosphoAkt (S473)	1:1000	WB	Cell Signaling
Rabbit anti-Flag	1:1000	WB	Cell Signaling
Rabbit anti-GAPDH	1:1000	WB	Abcam
Rabbit anti-GLUT1	1:1000	WB	Sigma-Aldrich
Rabbit anti-human activated caspase-3	1:200	FC	BD Biosciences
Rabbit anti-human activated caspase-8 antibody	1:200	FC	Cell Signaling
Rabbit anti-IRF3	1:1000	WB	Cell Signaling
Rabbit anti-phospho-IRF3 (Ser396)	1:1000	WB	Cell Signaling
Rabbit anti-LAMP3	1:1000	WB	Abcam
Rabbit anti-PPP1CC	1:2000	WB	Bethyl Laboratories
Rabbit anti-TRIM25/EFP	1:2000	WB	Abcam
Rabbit anti-ZIKV Capsid	1:1000	WB	GeneTex
Immunophenotyping Abs			
Alexa Fluor 647 anti-human CD14	1:100	FC	Biolegend
FITC mouse anti-human CD3	1:100	FC	BD Pharmingen
FITC anti-human CD20 Antibody	1:100	FC	Biolegend
PE anti-human CD11c Antibody	1:100	FC	BioLegend

Table 2.10 Secondary Antibodies

Antibody-Conjugate	Dilution	Application	Source
Donkey anti-Mouse Alexa488	1:5000	IF	Invitrogen
Donkey anti-Mouse Alexa680	1:10000	WB	Invitrogen
Donkey anti-Rabbit Alexa488	1:5000	IF	Invitrogen
Donkey Anti-Rabbit 800	1:10000	WB	Li-COR
Donkey Anti-Mouse 800	1:10000	WB	Invitrogen
Goat anti-mouse-Alexa647	1:10000	WB	Invitrogen

Table 2.11 Mammalian cell lines

Cell line	Source
A549	American Type Culture Collection (ATCC)
HEL/18	E. Gönczöl, Wistar Institute
HEK293T	ATCC
Vero	ATCC

Table 2.12 Viruses

Virus	Source
Zika virus (PLCal_ZIKV)	Dr. David Safronetz (Public Health Agency of Canada)
Zika virus (Puerto Rico strain PRVABC-59)	Dr. Mike Diamond (Washington University School of Medicine)
Dengue virus -2 (New Guinea strain)	Dr. Mike Drebot (Public Health Agency of Canada)
Mayaro virus (Venezuela 2010 strain)	Dr. Scott Weaver (University of Texas Medical Branch)

2.2 Methods

2.2.1 Molecular Biology

2.2.1.1 Purification of Plasmid DNA from E.coli

E.coli (DH5α) was transformed with plasmid of interest and then grown in Luria Broth (LB) media with the appropriate selective antibiotic. Plasmid DNA was purified using the Qiagen Qiaprep spin mini prep kit (**Table 2.5**) with overnight cultures of 3-5 mL as per manufacturer's instructions. For larger volumes, the Qiagen Plasmid Maxi kit (**Table 2.5**) with overnight cultures of 100-200 mL was used as per manufacturer's instructions. DNA samples were kept at -20°C for storage.

2.2.1.2 Polymerase chain reaction

The Pfu DNA Polymerase or Platinum Taq DNA polymerase High Fidelity (**Table 2.3**) were used for PCR amplification. A typical reaction contained 100 ng of template DNA, 200 μM of dNTP, 0.4 μM of each primer and 1.25U/ reaction. All reactions were performed on a TC-312 (Techne) or a T100 Thermal cycler (Bio-Rad).

2.2.1.3 Restriction endonuclease digestion

Restriction endonuclease digestion was typically performed with 1-5 μg of plasmid DNA or ~0.2 μg of PCR product in a total volume of 20-30 μL as per manufacturer's instructions.

2.2.1.4 Agarose Gel electrophoresis

Ultrapure agarose of 0.5-1% (w/v) was dissolved in TAE buffer. To visualize, ethidium bromide was added to a final concentration of 0.5 μg/mL and the agarose was poured into a gel casting platform. After cooling and setting, the gel was submerged into an electrophoresis tank with TAE running buffer. Samples were mixed with 6x loading buffer (**Table 2.6**) before loading to the corresponding well. Gels were run at 100 Volts for 30min – 1 hr depending on experiment. A UV transilluminator was used to visualize the separated DNA fragments.

2.2.1.5 Purification of DNA fragments

PCR products were cleaned up using the PCR purification kit (**Table 2.5**) following manufacturer's instructions. For purification of cut DNA fragments prior to cloning, the Qiagen QiaexII gel extraction kit (**Table 2.5**) was used for clean up.

2.2.1.6 Ligation of DNA fragments

All ligation reactions were performed as per manufacturer's protocol using T4 DNA ligase (**Table 2.3**). All ligations were incubated at 16°C overnight.

2.2.1.7 Transformation of E. coli

Chemically competent DH5α *E. coli* cells were thawed on ice, then ~50ng of plasmid was added to the thawed cells in a circular motion followed by a 5 min incubation at room temperature. The cells were then heat shocked for 90 seconds in a 37°C water bath followed by 15 min incubation on ice. SOC media (200 µL) was added to the cells and which were then put in a shaker for 30 min at 37°C. The transformed cells were then plated on LB media agarose plates containing the appropriate selective antibiotic.

2.2.1.8 Construction of recombinant plasmids

Construction of pTRIP-MCS-AcGFP-myc-ZIKV capsid

Primers were designed to amplify ZIKV-capsid (**Table 2.7**) from the template plasmid pcDNA3.1-ZIKVcapsid (Kumar et al., 2016). The forward primer introduced a myc-tag onto the N-terminus of capsid. Platinum *Taq* DNA polymerase High Fidelity (**Table 2.3**) was used for PCR (annealing temperature was 58°C, with 1 min extension at 68°C for 30 cycles). The PCR products were purified using a Qiagen PCR purification kit (**Table 2.5**) and then digested with *SpeI* and *XhoI* to produce a 360 bp fragment that was ligated into *SpeI* and *XhoI* digested pTRIP-MCS-ACGFP vector. The authenticity of the plasmid was verified by DNA sequencing.

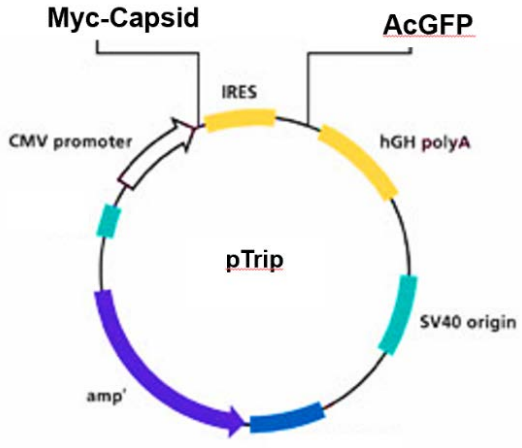

Figure 2.1. Plasmid map of pTRIP-MCS-AcGFP-myc-Capsid.

Construction of pCDNA3.1-Myc-DENVC, pCDNA3.1-Myc-JEVC, pCDNA3.1-Myc-MVEVC, pCDNA3.1-Myc-YFVC, pCDNA3.1-Myc-WNVC

PCR primers were designed to amplify full length cDNA encoding capsid proteins with *NheI* and *BamHI* sites (**Table 2.7**) from the template plasmid pTRIP-MCS-AcGFP-capsid. Platinum *Taq* DNA polymerase High Fidelity (**Table 2.3**) was used for PCR (annealing temperature was 58°C, with 1 min extension at 68°C for 30 cycles). PCR amplification fragments were digested with *NheI* and *BamHI* and subcloned into pCDNA3.1 (-) plasmid between *NheI* and *BamHI* restriction sites. The authenticity of the plasmids was verified by DNA sequencing

Construction of pCDNA3.1-Myc-SLEVC

All steps were identical to that described previously with the exception that SLEV C has a *BamHI* site in the middle of its coding sequence, so a different reverse primer was created with a *HindIII* restriction site (**Table 2.7**). The authenticity of the plasmid was verified by DNA sequencing

2.2.2 RNA techniques

2.2.2.1 RNA isolation

Total RNA was isolated using the Total RNA isolation kit (**Table 2.5**) as per manufacturer's instructions. The kit used for isolation of total RNA for RNA

sequencing was the RNeasy mini kit (**Table 2.5**). Samples were DNase-treated on the column (RNase-Free DNase Set, **Table 2.5**) as per manufacturer's instructions.

2.2.2.2 Quantification of RNA

For RNA samples that were destined for RNA-sequencing, the Agilent 2100 Bioanalyzer instrument was used for assessment of RNA quality and quantity (**Table 2.4**) according to manufacturers' protocol. RNA was also quantified using a Qubit fluorometer (**Table 2.4**). For other purposes, RNA was quantified using a Nano-drop spectrophotometer.

2.2.3 Cell Culture, transfection, and transduction of mammalian cell lines

2.2.3.1 Cell line maintenance

A549, HEK293T and Vero cells were grown in DMEM supplemented with 10% FBS. HEL/18 cells were grown in RPMI-1640 supplemented with 10% FBS and nonessential amino acids. PBMCs, primary monocytes and macrophages were cultured in RPMI supplemented with 15% heat-inactivated FBS and 1% Penicillin-streptomycin. All cultures were incubated in a humidified incubator at 37°C with 5% CO_2.

2.2.3.2 Transfection of cell lines

A549 and HEK293T cells were transiently transfected with lipofectamine 2000 or lipofectamine-LTX transfection reagent (**Table 2.1**) as described by the manufacturer's protocol. In brief, cells were seeded so that they were 80% confluent at time of transfection. Plasmid DNA (1-2 μg), 2 μL of lipofectamine (for lipofectamine LTX: 1 μL of Plus Reagent) were mixed in OptiMEM and incubated with cells for ~4 hours at after which time the media were changed.

2.2.3.3 Generation of AcGFP-Myc-ZIKV capsid expressing stable cell lines

A549 cells were transduced with lentivirus encoding AcGFP or AcGFP-ZIKV capsid. Twenty-four hours post-transduction AcGFP-positive cells were sorted using a BD FACSAria III cell sorter (**Table 2.4**) and plated at 1 cell/well into 96-well plates. Cells were cultured under observation for ~3 weeks after which ten colonies from AcGFP or AcGFP-ZIKV capsid transduced populations were picked and expanded for further analysis. Clones were analyzed by flow cytometry for AcGFP expression. One AcGFP and one AcGFP-ZIKV capsid clone with similar AcGFP expression were picked to use in future experiments. ZIKV capsid expression was verified by immunoblotting (**Chapter 4**).

2.2.3.4 Polyionosinic:Polycytidylic Acid (Poly(I:C)) stimulation

Mock, AcGFP or AcGFP-ZIKV capsid expressing stable cell lines were seeded in 12-well plates ($1x10^5$ cells/well). The next day, cells were transfected with 2µg of Poly(I:C) or 2 µg of pCDNA3.1(-) using TransIT-LT1Transfection Reagent (**Table 2.1**) as per manufacturer's instructions. Twenty-four hours after Poly(I:C) transfection, cells were washed in PBS and harvested for RNA extraction.

2.2.3.5 RNA interference

A549 cells were seeded ($1x10^5$ cells/well) in a 12-well plate. The next day, cells were transfected with small interfering RNAs (siRNAs) or control siRNA (siControl) at 12 nM for TRIM25 studies and at 50 nM for LAMP3 studies. Lipofectamine RNAiMAX reagent (**Table 2.1**) was used for all siRNA transfections. Cells were collected 48 hours post-transfection for further experimentation or analysis.

2.2.3.6 Cell viability assays

To assess how flavivirus capsid expression affected cell viability, levels of ATP, were measured in A549 or HEL-18 cells that were transduced at a MOT of 3 as described in Section 2.2.4. Lysates were collected at 24-, 48- and 72-hours post-transduction and luciferase activities were determined using CellTiter-Glo Luminescent Cell Viability assay kit (**Table 2.5**). Luciferase activity was measured using a Synergy 4 Luminescence Reader (**Table 2.4**).

2.2.4 Virology techniques

2.2.4.1 Production of lentivirus

HEK293T cells were seeded at $3x10^6$ cells in 10cm plates. The next day, cells were transfected as follows: DNA (for VSVG: pHCMVG 1.6µg, HIV gag-pol 5.6µg, TRIP/GFP 5.6µg) was mixed in a tube. In a separate tube 48 µL TransIT-LT1 was added to 800 µL serum-free media (Opti-MEM) and incubated for 5 min at room temperature after which the DNA-transfection reagent mixture was added, mixed and incubated for an additional 20 minutes at room temperature. In parallel, media on the HEK293T cells were ex-changed with 7 mL of pre-warmed DMEM containing 3% FBS. After the 20 min incubation, transfection mixtures were added to cells in a drop-wise manner. The media in the plate were changed after ~6 hours to 10 mL of DMEM with 3% FBS. Cell media were harvested at 48 hours, stored at 4°C overnight, and fresh DMEM with 3% FBS (10 mL) was added to each plate. Media were harvested again at 72 hours and combined with previous supernatants which were then centrifuged at 1000×g for 10 minutes at 4°C. The supernatants were collected and polybrene (10 µg/mL) and HEPES (20mM) were added. Aliquots (1-2 mL) were made and stored at -80°C.

2.2.4.2 Transduction of mammalian cells with lentivirus

A549 or HEL/18 cells were seeded at $2x10^5$ cells/well in 6-well plates 24-hours prior to transduction. Media were removed and replaced with DMEM containing 3%

FBS and 5 μg/mL polybrene. Cells were spin-inoculated at 1,200×g for 1 hour at 37°C, followed by a complete media change to DMEM with 10% FBS.

2.2.4.3 Determination of lentivirus yield

A549 cells were seeded at $2x10^5$ cells/well in 6-well plates and the next day, media were changed to DMEM with 3% FBS and 5 μg/mL of polybrene. The lentivirus stocks were titered by adding 10 μL, 50 μL or 100 μL of lentivirus suspension to each well. The plates were spin inoculated for 1 hour at 1,2000 x g at 37°C. The media were removed and replaced with DMEM containing 10% FBS. Twenty-four hours post-transduction, media were removed, cells were washed once with PBS, detached using trypsin-EDTA, resuspended in DMEM + 10% FBS and then prepared for analyses by flow cytometry. Each positive event is due to a single transducing particle so the percent of GFP-positive cells per well obtained by flow cytometry was multiplied by the total number of cells in each well to give transducing units (TU) per well. This number was then divided by the amount of lentivirus stock added to the well (i.e. 10, 50 or 100 μL) to obtain TU/mL.

Note: only samples that were less than 15% GFP-positive were used to determine TU/mL.

2.2.4.4 Virus infection and quantification

All infections were performed for 1-2 hours in media with 3% FBS. After infection, cells were washed twice with serum-free media before replacing with 10% FBS supplemented media.

Plaque assays were performed on Vero cells seeded at $2x10^5$ cells per well into 24-well plates. Conditioned media from infected cells were serially diluted in serum-free DMEM and 100 µL of supernatant was added to each well in duplicate. Plates were placed in a 37°C with 5% CO_2 incubator for 2 hours after which 1 mL of DMEM containing 0.5% methylcellulose was added to each well. After 2,4 and 6 days (for MAYV, ZIKV, and DENV), cells were fixed with 1 mL of 10% formaldehyde. After 30 minutes, the formaldehyde was removed, plates rinsed in water and tapped to dry. Cells were stained with 1% (w/v) crystal violet in 20% (v/v) methanol for 30 minutes. Staining solution was removed, and plates were rinsed in water. After drying the plates, the plaques were counted.

2.2.5 SDS-Page and Immunoblotting

Cells were collected at designated time points and were washed once in PBS before lysis in cold RIPA buffer (**Table 2.6**) supplemented with Complete Protease inhibitor cocktail (**Table 2.1**) and PhosSTOP phosphatase inhibitor cocktail (**Table 2.1**). Lysates were incubated for 20 min with rotation at 4°C and subsequently cleared by centrifugation for 15 min at 14,000 rpm in a microfuge at 4°C. Laemmli Sample

buffer (**Table 2.6**) was added to the cleared lysates and heated to 95°C for 5 min. Cell lysates were separated by SDS-PAGE and then transferred to polyvinylidene fluoride (PVDF) membranes. Membranes were blocked for at least one hour in 5% bovine serum albumin (BSA) in PBS prior to primary antibody incubation. Primary antibody was diluted in 5% BSA and added to the membrane for overnight incubation at 4°C. The appropriate secondary antibodies were incubated for 1 hour and proteins were visualized using fluorescent LiCor Odyssey detection system (**Table 2.4**).

2.2.6 Immunofluorescence Microscopy

A549 cells were seeded in 12-well plates containing glass coverslips at a concentration of $1x10^5$ cells/well. The next day, the cells were infected with MAYV at an MOI of 3 and infection was allowed to progress for 24 hours after which cells were washed once in PBS followed by fixation for 20 min with 1 mL of 4% PFA in PBS. After fixation, the PFA was removed and the cells were washed 3 times with PBS and then blocked and permeabilized with 0.2% Triton X-100 + 3% BSA in PBS for 1 hour at room temperature. The cells were then incubated with the primary antibody in 3% BSA for 1.5 hours at room temperature or at 4°C overnight in a moist chamber. Coverslips were washed twice for 10 minutes in a solution of 0.2% Triton X-100 + 0.3% BSA after which secondary antibody was added at a dilution of 1:5000 with DAPI at a final concentration of 1 µg/mL in 3% BSA. Secondary antibody was incubated with samples for 1 hour at room temperature and then coverslips were washed once in 0.2% Triton X-100 in PBS for 10 min followed by a final wash in PBS for 10 min.

Alternatively, DAPI was added in the washing steps following the secondary antibody concentration. Finally, the cover slips were mounted onto microscope slide using ProLong Gold antifade mounting solution (**Table 2.1**) and dried overnight at room temperature. Confocal microscopy Z-stack images (0.2 µm thick) were acquired using an Olympus IX-81 spinning-disk confocal microscope with a 60X/1.42 numerical-aperture (NA) oil objective using Volocity acquisition and analysis software (**Table 2.4**). ImageJ Analysis Software was used to analyze images. Intensity quantification was determined by outlining each cell and quantify gray levels for each object using ImageJ software.

2.2.7 Analysis of protein-protein interactions

2.2.7.1 Microcystin-Sepharose pulldowns

A549 cells ($2x10^6$ cells/well) were seeded in 10cm dishes and the next day, were transduced with lentivirus encoding AcGFP only or flavivirus capsid proteins. Forty-eight hours post-transduction, cells were lysed in 1 mL of NP-40 lysis buffer (**Table 2.6**) containing protease inhibitors (**Table 2.1**). Preparation of beads: MC-Sepharose (MC-S) was prepared as previously described (Moorhead et al., 1994; Moorhead et al., 2008). In brief, MC-S was incubated with 7µg of purified recombinant human protein phosphatase-1 (PP-1) catalytic subunit gamma (PP-1cg) for 1 hour at 4ºC with rotation in 300 µL total volume of Buffer A (150mM NaCl, 50mM Tris-HCl, pH 7.4, 0.1mM EDTA, 0.5mM MnCl2, 0.2% β-mercaptoethanol). Then, the beads

were washed twice with 500 µL of Buffer A + 0.1% Tween-20, followed by two washes with 500 µL Buffer A. A portion of the cell lysate (400 µL) was added to the prepared MC-S with Buffer A to a final volume of 800 µL and then incubated overnight at 4ºC with rotation. The next day, samples were washed 3 times with 500 µL of Buffer A + 0.1% Tween-20. Thirty µL of 2X Laemmli sample buffer with 5% β-mercaptoethanol was added to each sample which were then heated for 5 min at 95ºC before loading on SDS-PAGE gels.

2.2.7.2 Co-immunoprecipitation of PP-1 and ZIKV C

A549 cells ($2x10^5$ cells/well) were seeded into 6-well plate and then 20 hours later, cells were transduced with lentiviral stocks prepared from cells transfected with pTRIP-AcGFP or pTRIP-AcGFP-ZIKV-myc capsid at an MOT of 3. Two hours after transduction, cells were transfected with 2.5 µg pEGFP-PP1 plasmid DNA using Lipofectamine 2000 (**Table 2.1**) following manufacturers instructions. Twenty-four hours post-transfection, cells were collected and lysed in 400 µL of Co-IP buffer (Table 2.6) containing protease and phosphatase inhibitors (**Table 2.1**). Cell lysates were rotated for 15 min at 4ºC followed by centrifugation at 15,000×g for 10 minutes. Supernatants were collected and 40 µL aliquots were saved as "input" samples for immunoblotting. Myc-beads prepared as previously described (Lopez-Orozco et al., 2015) were incubated with clarified cell lysates with rotation at 4ºC overnight followed by one wash with 500 µL of Co-IP buffer. Twenty µL of 2X Laemmli sample buffer

with 5% β-mercaptoethanol was added to the beads which were then heated for 5 min at 95ºC before loading on SDS-PAGE gels.

2.2.7.3 Co-immunoprecipitation of TRIM25 and ZIKV C

A549, AcGFP or ZIKV capsid expressing stable cells (1 x 10^6) were pelleted and lysed in 400 µL Co-IP buffer with protease and phosphatase inhibitors (**Table 2.1**) as described in Section 2.2.7.2. Cleared lysates were then loaded onto anti-Myc magnetic beads (**Table 2.1**) and incubated overnight with rotation at 4ºC. Beads were washed twice with 400 µL of Co-IP buffer. Forty µL of 2X Laemmli sample buffer with 5% β -mercaptoethanol was added to the beads which were then heated for 5 min at 95ºC before loading on SDS-PAGE gels. For the reciprocal IP, the same methods were followed with the exception that AcGFP and ZIKV capsid-expressing stables were transfected with a plasmid encoding Flag-TRIM25 (**Table 2.8**) 24 hours prior to cell lysis.

2.2.8 RNA sequencing

2.2.8.1 Sample prep for RNA-sequencing

A549 cells (1 x 10^5 cells/well) were seeded into 6-well plates and transduced as previously described in Section 2.2.4.2 at a multiplicity of transduction (MOT) of 10. Forty-eight hours post-transduction, cells were collected for flow cytometry

analysis or cells were pelleted from duplicate wells, washed with PBS and stored at -80ºC for subsequent RNA extraction.

For analyses of MAYV-infected monocyte-derived macrophages (MDMs), MDMs (1-2x10^6 cells/well) were differentiated for 7 days at which point samples were infected with MAYV at an MOI of 10 for 72 hours. Cells were then subjected to flow cytometry analysis or were pelleted from duplicate wells, washed with PBS and stored at -80°C for subsequent RNA extraction. In both cases, total RNA was extracted using the RNeasy mini kit (**Table 2.5**) with additional DNase-treatment (**Table 2.5**). RNA concentration and quality were determined using a Qubit fluorometer (**Table 2.4**) and Bioanalyzer (**Table 2.4**) respectively prior to sequencing. All samples had an RNA integrity number (RIN) higher than 8.0.

2.2.8.2 Ion Torrent Next-generation sequencing

Genome-wide targeted amplicon amplification was performed using an Ion AmpliSeq™ Transcriptome Human Gene Expression Kit (Thermo-Fisher). In brief, 100 ng of total RNA was used to prepare the libraries as per manufactures protocol and stated elsewhere (Li et al., 2015). Libraries were quantified using an Ion Library TaqMan Quantitation kit (Thermo-Fisher) and then diluted to a total of 100 pM. Sequencing was performed on an Ion S5 sequencer (Thermo-Fisher).

2.2.8.3 Analysis of RNA-Seq (Differential gene expression analysis)

Data from next-generation sequencing were analyzed for differential expression with fold-change using Partek® Flow Software (Partek, St. Louis, MO, USA). In brief, unaligned reads were processed using STAR aligner assembly to human genome 19 and annotated to RefSq Transcripts 84. Gene enrichment analysis was performed with a list of the Differentially expressed genes (DEGs) identified above. The lists were analyzed on the online server GOrilla (Eden et al., 2009), DAVID (Huang et al., 2008; Sherman and Lempicki, 2009) and GO Enrichment Analysis (Geneotology.org) (Ashburner et al., 2000; Consortium, 2018; Mi et al., 2018).

2.2.9 Isolation of primary cells from blood

2.2.9.1 Gradient density centrifugation for purification of PBMC cells

All donors provided written informed consent and study protocols were approved by the Health Research Ethics Board at the University of Alberta. Approximately 80 mL of blood was drawn from healthy adult volunteers. Samples were diluted 2X with sterile PBS and then 20 mL of the diluted blood was carefully added to 20 mL of Histopaque (**Table 2.1**) which was centrifuged at 1800 rpm for 22 min at room temperature in a centrifuge (Brake = 0, acceleration = 1). The interphase layer (buffy coat) was carefully removed using a 10 mL pipette and then transferred to a new tube. Twenty mL of serum-free RPMI was added to each sample which were

then centrifuged at 1200 rpm for 10 min in a centrifuge (Brake=6, acceleration= 6). Supernatants were removed followed by a second wash of the buffy coat with 20 mL of serum-free RPMI. Finally, cells were centrifuged at 800 rpm for 10 min in a centrifuge after which the pellets were resuspend in 10 mL total of RPMI with 15% FBS and 1% Penicillin-Streptomycin.

2.2.9.2 Isolation of $CD14^+$ monocytes and MDM differentiation

$CD14^+$ monocytes were isolated using CD14 Microbeads according to manufacturer's instructions (**Table 2.1**) which reliably resulted in samples of >95% CD14+ purity. M-CSF was added to the media (25 ng/mL) for a total of 7 days. Note, fresh M-CSF-containing media were added on Day 3 or 4 post-seeding. After 7 days with MCSF, cells were infected with MAYV at indicated MOIs.

2.2.10 Flow cytometry

2.2.10.1 Detection of activated caspase-3 and caspase-8 in transduced cells

A549 cells were transduced as described in Section 2.2.4.2, with the exception that an MOT of 3 was used. Briefly, cells were challenged with 250 ng/mL of anti-Fas antibody and 1 μg/mL cycloheximide for 6-8 hours following 48-hours of incubation and a medium change. Cell culture supernatants and adherent cells were collected by trypsinization followed by centrifugation (500×g for 5 minutes). After washing in PBS,

cells were resuspended in PBS containing 2% paraformaldehyde and then placed on ice for a minimum of 1 hour. Cells were pelleted again, washed once with PBS, and permeabilized with PBS containing 0.2% Triton X-100 and 10% FBS for 10 min. Following a wash with PBS, cells were incubated with 0.25 µg of rabbit anti-active caspase-3 or 0.25 µg of rabbit anti-active caspase-8 in 50 µL PBS containing 1% BSA for 60 minutes. Cells were then washed in PBS and incubated for 30 minutes with 0.1 µg of the appropriate fluorescent secondary antibody in PBS containing 1% BSA. Following a single wash in PBS, cells were resuspended in PBS containing 1% BSA, 5mM EDTA and analyzed via flow cytometry utilizing FACS Canto II flow cytometer (BD Biosciences) or LSRFortessa X20 SORP flow cytometer (BD Biosciences). To detect caspase-3 activation in transduced cells treated with LY294002, A549 cells were transduced as described previously but in addition to treatment with anti-Fas antibody and cycloheximide, cells were treated with either 50 µM LY294002 or DMSO alone and incubated for 6 to 8 hours before fixation and permeabilization. Cells were stained with active-caspase-3 antibody as described above. Cells were analyzed via flow cytometry utilizing FACS Canto II flow cytometer (BD Biosciences). Duplicate samples were lysed in 2X Laemmli sample buffer with 5% β-mercaptoethanol and 10mM NaF, followed by heating at 95ºC for 5 min.

2.2.10.2 Detection of caspase-3 in cells co-expressing capsid and WNV replicon

After transduction of A549 cells with lentivirus encoding WNV capsid protein, the cells were transfected with plasmids encoding WNV replicon (p8113.1 WNV

NY99) blue fluorescent protein (pEBFP-N1) or DsRed protein (pDsRed) using Lipofectamine 2000 (**Table 2.1**) following manufacturer's protocol in OptiMEM media. Due to lack of suitable commercially available antibodies to WNV non-structural proteins (to identify replicon expressing cells), a strategy to indirectly identify replicon-expressing cells with a surrogate marker was used. Cells were co-transfected with a plasmid encoding BFP and replicon plasmids at a molar ratio of 1 BFP to 8 replicon plasmids such that any BFP-positive cell was very likely to carry the replicon plasmid. As a proof of concept, transfected plasmids encoding BFP and DsRed plasmids (1 BFP: 8 DsRNA) and FACS analyses revealed that BFP positive cells were also ~99.8% positive for DsRed. We repeated the experiments using replicon plasmids instead of DsRed and then gated on GFP+ (capsid expressing) BFP+ (replicon expressing) cells and assayed which ones were positive for active caspase-3.

2.2.10.3 Flow cytometry analysis of ZIKV-infected cells

A549 cells (2 x 10^5 cells/well) were seeded into 6-well plates and transduced the next day with lentivirus encoding AcGFP or AcGFP-ZIKV capsid at a multiplicity of transduction of 3 (MOT 3) by spinnoculation as described in Section 2.2.4.2. The next day cells were infected with ZIKV Puerto Rico strain (PRVABC-59) at a multiplicity of infection of 5 (MOI 5). Cells were collected 48 hrs post-infection by trypsinization and fixed in 4% paraformaldehyde for a minimum of 1 hour at 4ºC, followed by a PBS wash. Cells were permeabilized and blocked using 0.2% Triton X-100 and 10% FBS for 10 min on ice. Following a PBS wash, cells were incubated with

mouse anti-ZIKV NS1 8F1 antibody for 1 hour at room temperature. Cells were washed once with PBS and then incubated with donkey anti-mouse Alexa Fluor 647 for 30 min. Following a wash in PBS, cells were resuspended in PBS + 1% BSA + 5mM EDTA and analyzed via flow cytometry using a LSRFortessa X20 SORP flow cytometer.

2.2.10.4 Flow cytometry analysis of MAYV-infected cells

The CD14-depleted population or monocytes isolated from peripheral blood samples were seeded in 6-well plates at a density of ~1-2x10^6 cells/well in the presence or absence of M-CSF. The next day, cells were infected with MAYV strain Venezuela 2010 (**Table 2.12**) at a MOI of 10 for 1.5 hr in a humidified incubator at 37ºC with 5% CO_2. Following infection, cells were carefully washed twice in serum-free media prior after which complete media was added to cells. At 48- and 72-hours post-infection, Accutase (**Table 2.1**) together with a cell scraper was used to gently detach remaining cells which were then washed once in PBS, followed by incubation with LIVE/DEAD cell stain kit (**Table 2.1**) for 25 min in the dark. Cells then were washed twice in PBS and stained with T cell marker CD3, B cell marker CD19, or Dendritic cell marker CD11c for 30 min in the dark, followed by washing in PBS once. Cells were permeabilized, blocked and stained as per Section *2.2.10.3* with the exception that mouse anti-CHIKV E2 or rabbit anti-CHIKV capsid primary antibody was used. All centrifugations were carried out at 400×g for 5 min.

Chapter 3

Expression of Flavivirus capsids enhance the cellular environment for viral replication by activating Akt-signalling pathways

A version of this chapter was published in:

"Airo AM*, Urbanowski MD*, Lopez-Orozco J, You JH, Skene-Arnold TD, Holmes C, Yamshchikov V, Malik-Soni N, Frappier L, Hobman TC. 2018. Expression of flavivirus capsids enhance the cellular environment for viral replication by activating Akt-signalling pathways. *Virology*. 516:147-157."

* Authors contributed equally

Figures 3.1, 3.4A, 3.4B and 3.6B were supplied by Dr. Matt Urbanowski. Figure 3.7A was supplied by Dr. Lori Frappier.

3.1 Rationale

Flaviviruses including Dengue virus (DENV) and West Nile virus (WNV) cause significant morbidity and mortality worldwide. Similar to other viruses, they depend on multiple host pathways during their life cycle and have evolved strategies to avoid the innate immune response.

The main function of the capsid protein is to protect the viral genome, but several studies have suggested that capsid is a multifunctional protein and that it interacts with many host factors (reviewed in (Urbanowski et al., 2008; Willows et al., 2013)). One reasoning for this is that capsid is localized to the cytoplasm and nuclei thus permitting spatial access to interact with an abundance of cellular proteins (Reviewed in (Urbanowski et al., 2008)). For example, the capsid protein of WNV has been implicated in non-structural functions such as modulation of apoptosis (Urbanowski and Hobman, 2013; Yang et al., 2002; Yang et al., 2008), modulation of peroxisomes (You et al., 2015) and in induction of neurovirulence (van Marle et al., 2007). It is worth noting that the latter paper used the membrane-anchored form of capsid, which is cleaved by the viral protease and does not exist at appreciable levels in infected cells (Urbanowski and Hobman, 2013). DENV capsid has also been implicated in non-structural functions; including the regulation of lipid metabolism (Carvalho et al., 2012) and modulation of peroxisomes (You et al., 2015). Evidence suggests that flaviviruses activate cell survival signalling shortly after infection (Lee et al., 2005; Scherbik and Brinton, 2010), which in turn may serve to block apoptosis. Previously, our lab demonstrated that the WNV capsid protein inhibits apoptosis

through a mechanism that involves phosphatidylinositol 3 kinase (PI3K) activation of Akt (Urbanowski and Hobman, 2013). To determine if this mechanism was conserved among flaviviruses, we examined how expression of capsid proteins from seven different flaviviruses affect apoptosis and Akt-dependent processes.

3.2 Results

3.2.1 Myc-tagged flavivirus capsids localize to cytoplasmic reticular elements and nuclei

To confirm the expression of myc-tagged capsids, A549 cells were transduced with lentiviruses encoding each capsid followed by immunoblotting. All of the flavivirus capsids were expressed at comparable levels and migrated at the expected size (**Figure 3.1A**). Flavivirus capsids are known to localize to the nucleus or to the endoplasmic reticulum, so next we decided to investigate if these capsids maintained the subcellular localization seen in infection. **Figure 3.1B** demonstrates that all capsids localized to nuclei as well as cytoplasmic reticular and punctate elements.

3.2.2 Expression of flavivirus capsids protects cells from Fas-dependent apoptosis

The WNV capsid protein was previously shown to protect mammalian cells from death receptor-dependent apoptosis (Urbanowski and Hobman, 2013). To determine if this was a conserved phenomenon, we compared the effects of anti-Fas on

A.

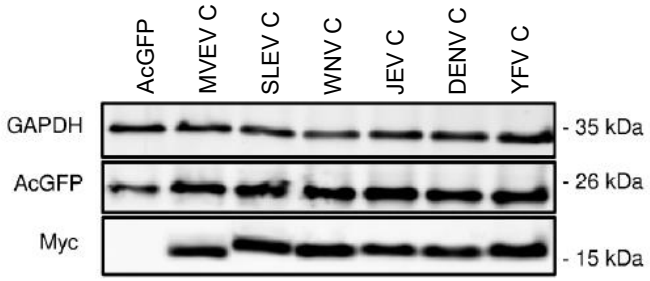

B.

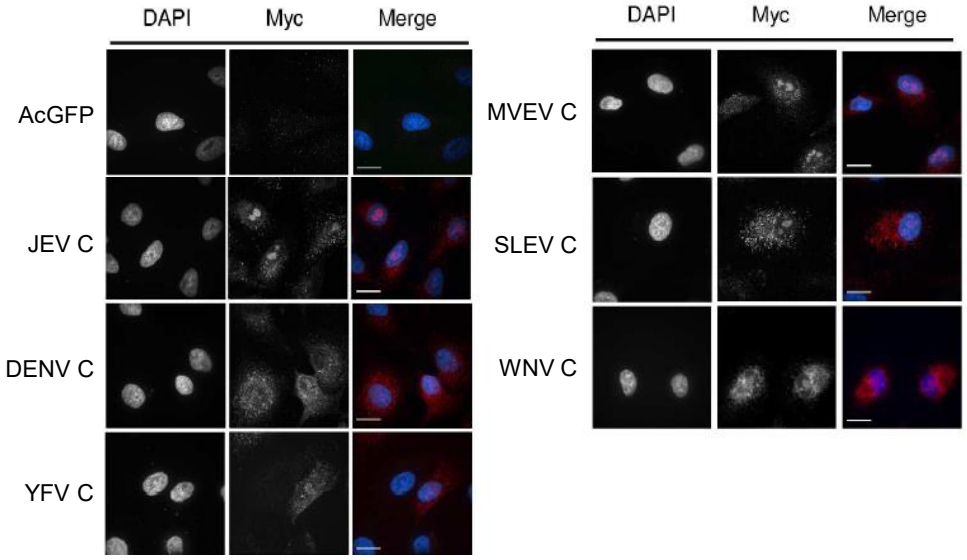

Figure 3.1. Expression and localization of myc-tagged flavivirus capsid proteins. A549 cells were transduced with lentiviruses encoding the indicated capsid proteins and then incubated for 48 hours before analyses by immunoblotting or indirect immunofluorescence. **A.** Capsids were detected using an antibody to the Myc epitope. Levels of AcGFP and GAPDH are shown to illustrate transduction efficiency and lysate loading controls respectively. **B.** Capsid proteins were detected with anti-Myc and nuclei were stained with DAPI. Extended focus images of Z-stacks composed of 0.25µm slices are shown. The white scale bars in the images represent 15 µm. Each channel was pseudo-colored prior to creating the merged images.

cells expressing the myc-tagged capsid proteins from six different flaviviruses. Following anti-Fas challenge, cells expressing myc-tagged MVEV, SLEV, WNV, JEV, DENV and YFV capsids or AcGFP only were fixed and stained with antibodies to active caspase-3 or caspase-8. Transduced cells expressing the capsid proteins were distinguished from non-transduced cells by AcGFP fluorescence. Only the AcGFP-positive cells were included in the analyses (**Figure 3.2A**). All capsid-expressing cells had less active caspase-3 and caspase-8 in response to anti-Fas challenge to varying degrees (**Figure 3.2B, C and D**). SLEV, DENV and JEV capsid-expressing cells demonstrated the most significant level of protection when compared to control with a greater than 60% reduction in active caspase-3. WNV, YFV and MVEV capsid-expressing cells demonstrated a reduction in active caspase-3 of approximately 50%. Finally, activation of the upstream initiator caspase-8 by anti-Fas was reduced by 40% or more in all capsid-expressing cells (**Figure 3.2D**). The relative expression level of capsid proteins as determined by immunoblotting was consistent among capsids (**Figure 3.2E**). These data suggest that flavivirus capsids are pro-survival in response to anti-Fas challenge.

3.2.3 Capsid expression confers a modest but significant protective effect against Fas-dependent apoptosis in replicon-transfected cells

A possible scenario is that during flavivirus replication pools of capsid protein that have not been recruited to virus assembly sites, serve to inhibit apoptosis that can be induced by detection of viral RNA and/or cytopathic effects of non-structural

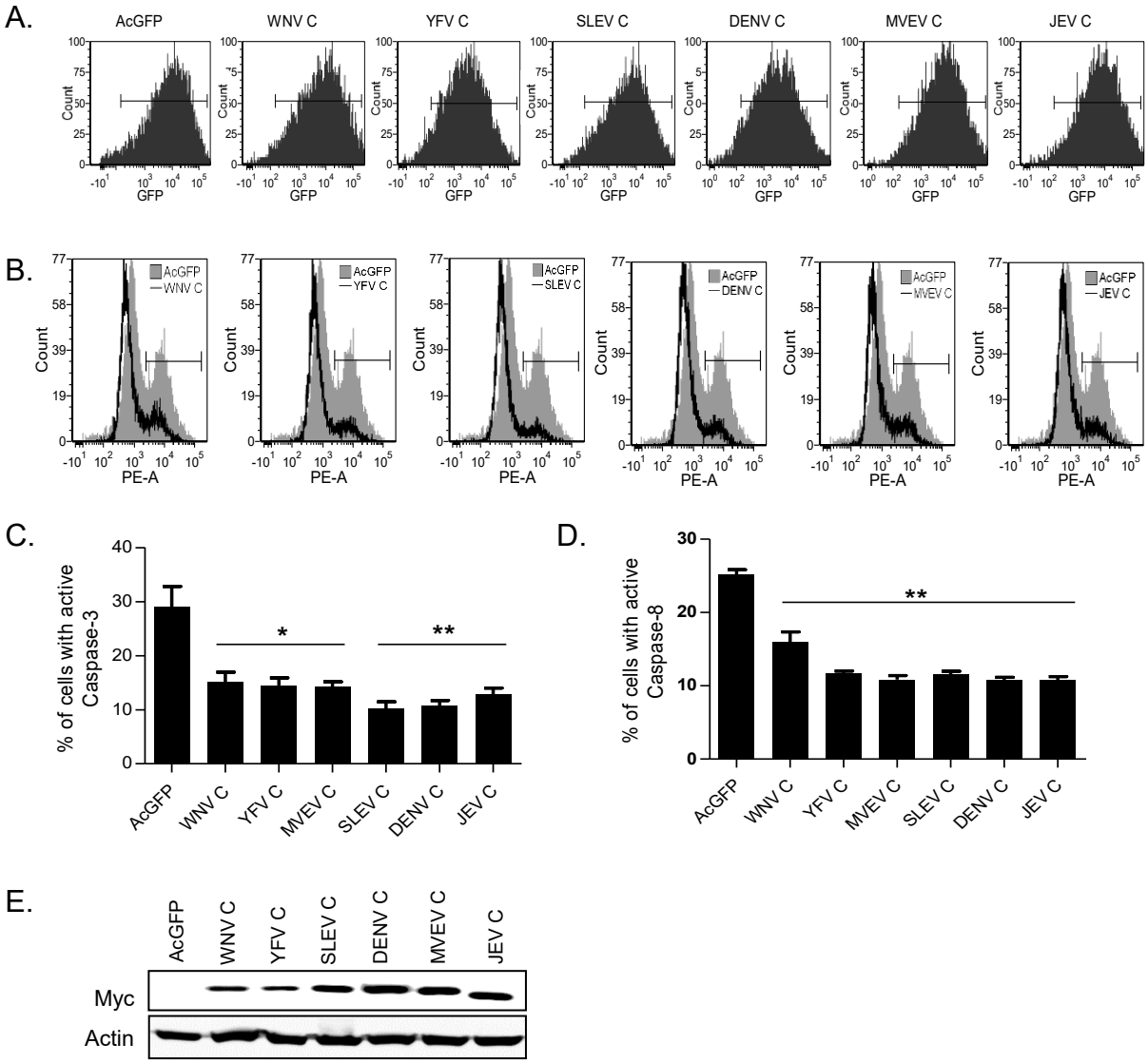

Figure 3.2. Expression of flavivirus capsids protects cells from anti-Fas challenge. A549 cells were transduced with lentiviruses encoding the indicated myc-tagged capsid proteins. Forty-eight hours post-transduction, cells were challenged with anti-Fas, fixed and then subjected to analyses by flow cytometry. **A.** Histograms showing levels of AcGFP fluorescence in each sample. Only the AcGFP-positive cells were included in the analyses. **B**. Histogram plots displaying caspase-3 staining profiles for the indicated capsid proteins overlaid with AcGFP control are shown. **C.** Data from 4 experiments showing levels of active caspase-3 in capsid expressing cells are summarized. **D.** Data from 4 experiments showing levels of active caspase-8 in capsid expressing cells are summarized. **E.** Relative expression levels of capsid proteins as determined by immunoblotting for Myc and actin. Results of statistical analyses (t-test) are indicated (* $P \leq 0.05$) (**, $P \leq 0.01$).

protein expression. To define how expression of non-structural proteins affects the capacity of capsid proteins to inhibit apoptosis, lentivirus-transduced cells expressing AcGFP alone or WNV capsid proteins were transfected with a replicon plasmid encoding the non-structural proteins of WNV (NY99 strain (Borisevich et al., 2006)). We only had access to replicons derived from the NY99 strain of WNV and therefore, co-expression of WNV capsid was most biologically relevant. In parallel, we co-expressed SLEV capsid with the WNV NY99 replicon. SLEV capsid was chosen because in our hands, it had the most potent anti-apoptotic activity and SLEV is part of the Japanese encephalitis group in *Flaviviridae* (as is WNV). After transfection, cells were subsequently challenged with anti-Fas and analyzed for active caspase-3 by flow cytometry. In the absence of Fas-challenge, expression of WNV non-structural proteins induced apoptosis in >35% of cells regardless of whether capsid proteins were co-expressed (**Figure 3.3A and B**). Treatment with anti-Fas resulted in almost twice as many replicon expressing cells undergoing apoptosis. Capsid protein expression conferred a modest but significant protective effect against Fas-stimulation in replicon-transfected cells.

3.2.4 Flavivirus capsids enhance phosphorylation of Akt at serine 473

Activation of the pro-survival kinase Akt can inhibit apoptosis through a number of different mechanisms (Andrabi et al., 2007; Brunet et al., 1999; Wang et al., 2008). It is therefore potentially significant that flaviviruses activate Akt shortly after

A.

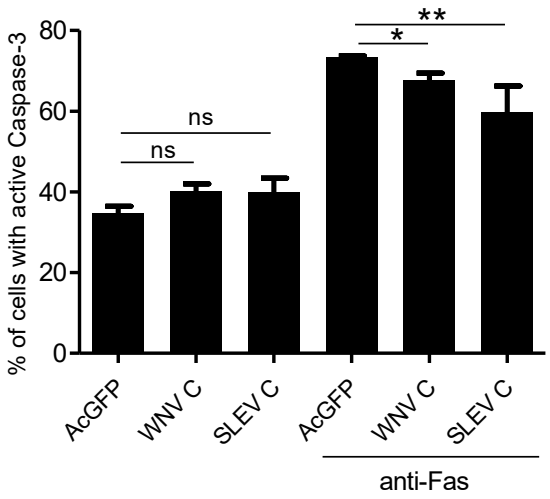

B.

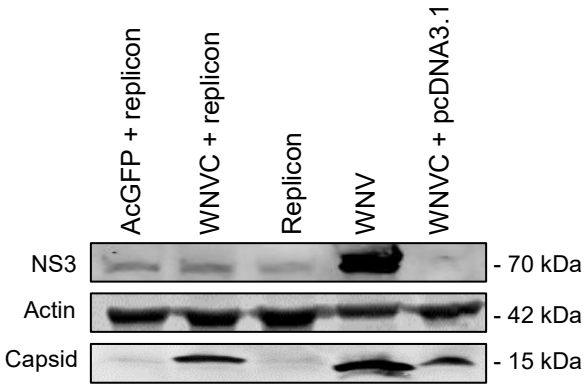

Figure 3.3. Capsid expression confers a modest but significant protective effect against Fas-dependent apoptosis in replicon-transfected cells. **A.** Data from 4 experiments are summarized showing levels of active caspase-3 in cells co-expressing capsid and WNV replicon in the absence or presence of anti-Fas. **B**. Relative expression levels of NS3 and capsid were determined by immunoblotting. Results of statistical analyses (t-test) are indicated (* $P \leq 0.05$) (**, $P \leq 0.01$).

infection (Lee et al., 2005; Scherbik and Brinton, 2010). To determine if Akt phosphorylation correlated with the anti-apoptotic activity of flavivirus capsid proteins, we assessed the phosphorylation state of Akt at serine-473 (S473) in capsid-expressing cells. This phosphorylation event is required for maximal activation of Akt (Hart and Vogt, 2011). Forty-eight hours after lentiviral transduction, cells were shifted to serum-free media for 24 hours before lysates were subjected to immunoblot analyses. Experiments were performed under serum-limiting conditions to more closely mimic the *in vivo* scenario and thus create more physiologically relevant conditions for assessing how capsid expression affects PI3K signalling. Data in **Figure 3.4A** and **Figure 3.4B** show that compared to serum-starved cells expressing AcGFP alone, relative levels of phospho-Akt S473 in a number of capsid expressing cells were significantly higher. Specifically, the phospho-Akt S473 signals in cells expressing capsid proteins from MVEV, SLEV and WNV were 3-4 fold higher than in those expressing AcGFP alone. Conversely, the steady state levels of Akt protein *per se* were not affected by expression of capsid proteins. Although levels of phospho-Akt were higher in serum-starved cells expressing JEV, DENV and YFV capsids, under these experimental conditions the observed increases were not statistically significant. These data suggest that the anti-apoptotic function of flavivirus capsid proteins correlates with the ability to induce/preserve activating phosphorylation of Akt. Next, I confirmed that capsid-induced phosphorylation of Akt at S473 was abrogated in the presence of the PI3K inhibitor LY294002. By blocking PI3K activity, this inhibitor lowers the phosphorylation and activity of Akt. As shown in **Figure 3.4C**, higher concentrations

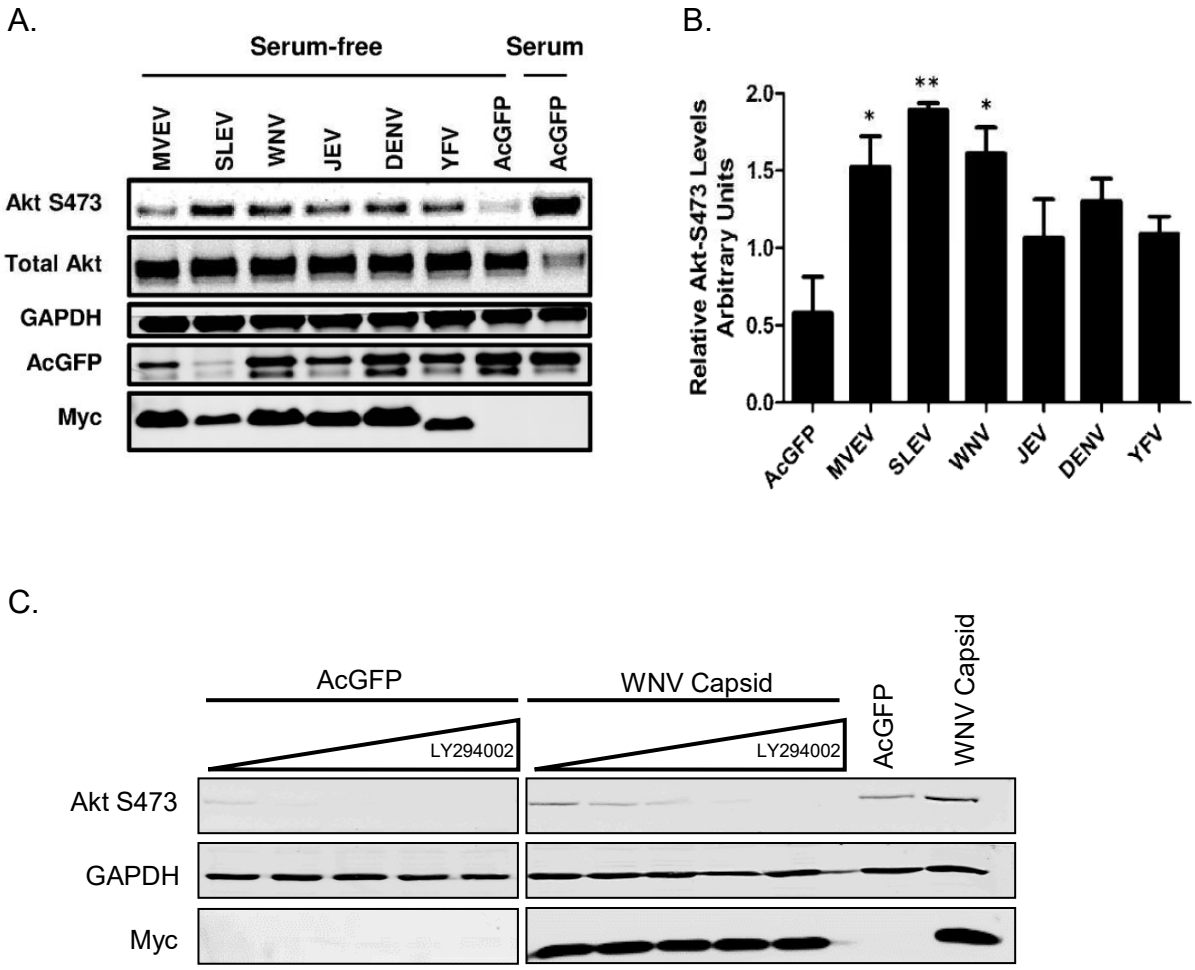

Figure 3.4. Flavivirus capsid expression promotes Akt activation. A. Forty-eight hours post-transduction, A549 cells were serum starved for 24 hours after which lysates were processed for immunoblotting using antibodies to phospho-Akt-S473, Myc, GFP, GAPDH and total Akt. The lane marked "Serum" contains lysate from AcGFP only expressing cells that were maintained in normal growth medium for the entire experimental time period. **B**. Intensities were measured and corrected for total Akt signal and plotted as relative phospho-Akt-S473 levels, with the AcGFP only-expressing cells serving as a control. **C.** Capsid-induced phosphorylation of Akt at S473 was abrogated in the presence of the PI3K inhibitor LY294002 . Forty-eight hours post-transduction A549 cells were treated with increasing concentrations of LY294002 (12.5 – 200 μM). Cell lysates were subjected to SDS-PAGE and immunoblot analysis with antibodies to phospho-Akt, GAPDH and myc was performed. The data from 3 separate experiments were subject to t-test analyses. (* $P \leq 0.05$) (**, $P \leq 0.01$).

of LY294002 were required to abrogate the phosphorylation of Akt at S473 in cells expressing the WNV capsid protein.

3.2.5 Inhibition of PI3K reduces anti-apoptotic activity of flavivirus capsid proteins

To investigate if the phosphorylation level of Akt at S473 influences the pro-survival activities of capsid, transduced cells were treated with the PI3K-inhibitor LY294002. Forty-eight hours post-transduction, capsid-expressing cells were treated for 6-8 hours with anti-Fas with or without LY294002 present. Duplicate samples were collected for analyses by flow cytometry and immunoblotting. Only AcGFP-positive cells were included in the flow cytometry analysis. Immunoblotting was used to confirm that LY294002 indeed depleted the level of phospho-Akt at S473 (**Figure 3.5A**). Results from flow cytometry analyses showed that treatment with LY294002 alone (grey bars) did not result in a significant induction of apoptosis under these experimental conditions. In contrast, cells treated with both anti-Fas (white bars) and LY294002 (black bars) exhibited increased apoptotic death (**Figure 3.5B**). These data suggest that the activity of PI3K is important for the anti-apoptotic functions of flavivirus capsids.

3.2.6 Flavivirus capsid expressing cells are more metabolically active

The PI3K/Akt signalling pathway is known to mediate cellular metabolism (Ward and Thompson, 2012). As such, we next investigated if/how metabolism was

A.

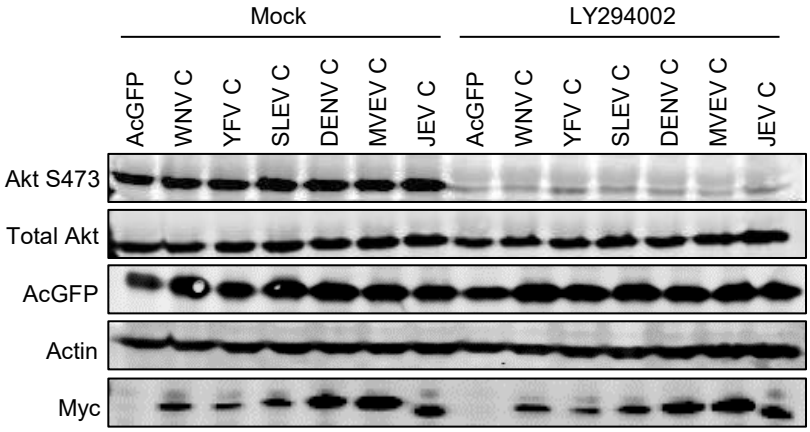

B.

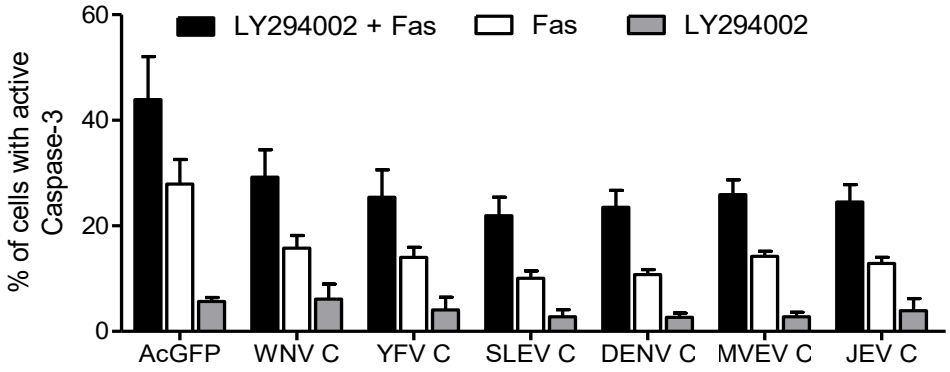

Figure 3.5. Inhibition of PI3K reduces protection by flavivirus capsid proteins to anti-Fas. Forty-eight hours post-transduction A549 cells were treated with DMSO or anti-Fas with or without addition of LY294002. **A.** Cell lysates were subjected to SDS-PAGE and immunoblot analysis with antibodies to total Akt, phospho-Akt, GFP, myc and actin. The addition of the PI3 kinase inhibitor (LY294002) reduces phospho-Akt S473 in control (AcGFP) and capsid-expressing cells. **B.** Cells were processed for intracellular staining with antibodies to active caspase-3 followed by staining with AlexaFluor anti-rabbit 546. Only the GFP positive cells were included in the analysis. Average results from 3 independent experiments are shown

affected by expression of flavivirus capsids. Lysates from A549 cells expressing myc-tagged capsids were prepared at 24, 48- and 72-hours post-transduction and total intracellular ATP levels were measured. All capsid-expressing cells exhibited a significant increase in the levels of intracellular ATP at 48 hours (**Figure 3.6A**). In particular, SLEV and DENV capsids had the strongest effects; cells expressing these capsids had 1.8 to 2-fold more ATP after 72 hours.

To further assess changes in cellular metabolism, AcGFP and capsid-expressing cells were counted and then subjected to Alamar blue assays at 48 hours post-transduction to assess the metabolic activity of mitochondria. The levels of reduced Alamar blue in the transduced cells were measured by fluorimetry. Reduction of Alamar blue is dependent upon the enzyme nicotinamide adenine dinucleotide phosphate-oxidase, the activity of which is required for oxidative respiration, an indicator of cell viability and metabolic activity (Vega-Avila and Pugsley, 2011). We observed that expression of DENV capsid resulted in the highest upregulation of mitochondrial metabolic activity, however, all of the flavivirus capsid proteins resulted in significantly increased mitochondrial activity (**Figure 3.6B**).

3.2.7 Expression of flavivirus capsid proteins increases expression of GLUT1

It was recently reported that DENV induces the glycolytic pathway to support efficient viral replication and the expression of glucose transporter 1 (GLUT1), is upregulated in DENV-infected cells (Fontaine et al., 2015). Because Akt regulates

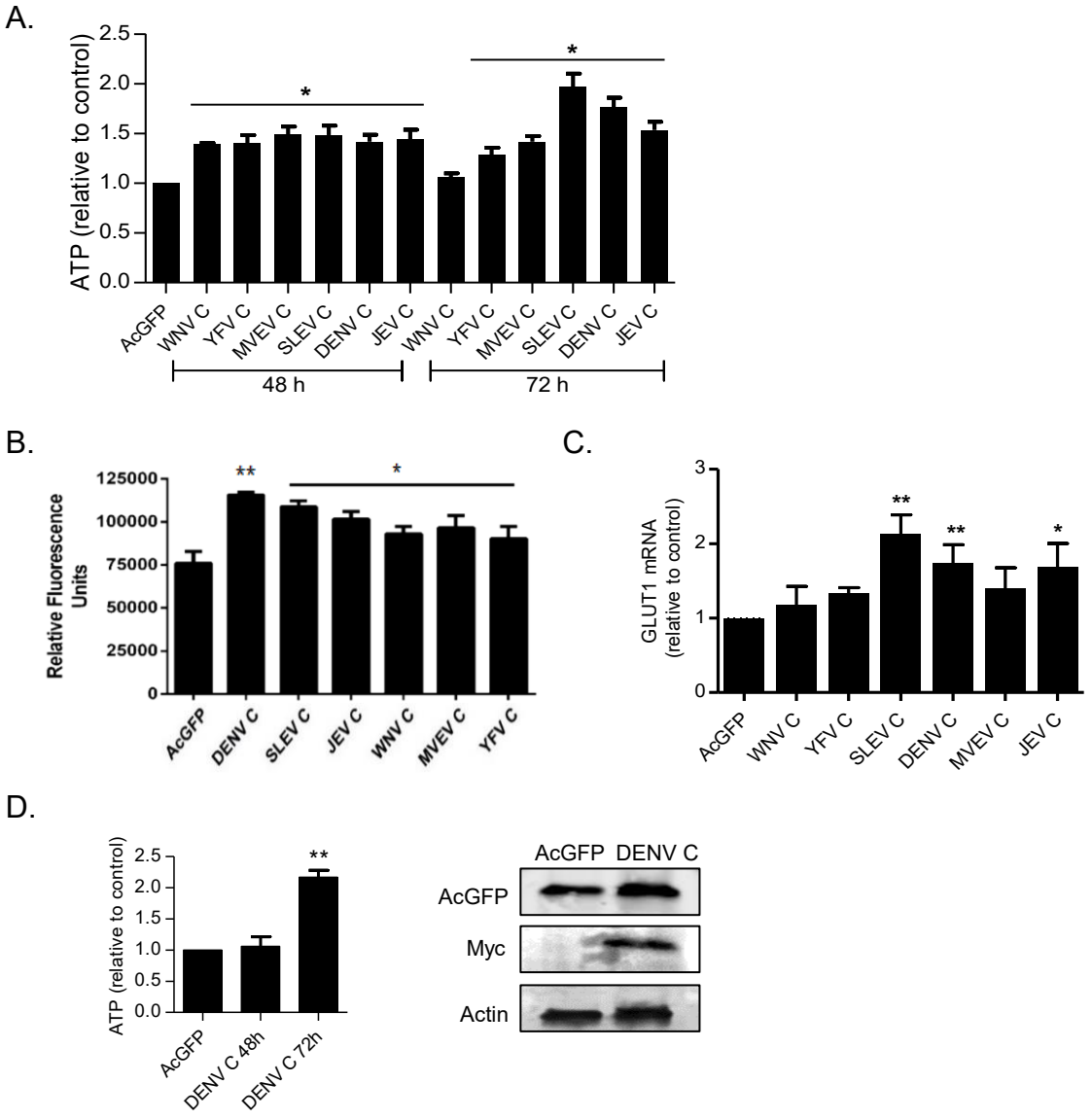

Figure 3.6. Capsid-expressing cells are more metabolically active. A549 cells were transduced with lentiviruses encoding myc-tagged capsids. **A.** Capsid-expressing cells contain higher levels of ATP. Lysates were collected at 48h and 72h post-transduction and ATP levels were determined. **B.** Expression of flavivirus capsids increases mitochondrial metabolic activity. Cells were collected at 48h post-transduction and relative oxidative respiration of mitochondria were determined using an AlamarBlue reduction assay. Fluorescence of the reduced form of AlamarBlue was plotted as relative fluorescence units. **C.** Expression of flavivirus capsids increases expression of GLUT1 mRNA. Total RNA extracted at 72h post-transduction was subjected to qRT-PCR using primers specific for Glucose Transporter 1 (GLUT1). The average values from three independent experiments are shown. **D.** Primary human embryonic lung fibroblasts (HEL-18) expressing DENV capsid contain higher levels of ATP. Results from statistical tests (t-test) are shown. (* $P \leq 0.05$; ** $P \leq 0.01$).

multiple steps in glycolysis (Rathmell et al., 2003), we investigated if GLUT1 levels were altered in capsid-expressing cells. A549 cells were transduced with flavivirus capsids and samples were collected at 24-72 hours post-transduction after which relative GLUT1 mRNA levels were assess by qRT-PCR. Levels of GLUT1 mRNA were not significantly affected by capsid expression between 24- and 48-hours post-transduction (data not shown). However, cells expressing capsid proteins from SLEV, DENV and JEV exhibited significant upregulation in GLUT1 mRNA at 72 hours post-transduction (**Figure 3.6C**). Levels of GLUT1 mRNA were also higher in cells transduced with lentiviruses encoding WNV, YFV and MVEV capsids but the increases were not statistically significant.

To confirm that the observed effects on metabolic activity were not limited to continuous cell lines, we assessed the effect of capsid expression in primary human embryonic lung (HEL-18) fibroblasts (Megyeri et al., 1999). Total intracellular ATP levels increased by more than 2-fold in DENV capsid-expressing HEL-18 cells at 72 hours post-transduction (**Figure 3.6D**).

3.2.8 Dengue virus capsid interacts with protein phosphatase 1

To understand more about the mechanism by which flavivirus capsid proteins activate Akt, we examined a list of host cell proteins that were identified in a proteomic screen for DENV capsid protein interactions (You et al., 2015). Protein phosphatase 1 catalytic subunit (PP-1c) was identified as binding partner for DENV capsid but not

the size-matched negative control protein (**Figure 3.7A**). PP-1 is a serine/threonine phosphatase that interacts with many regulatory subunits to confer specificity for hundreds of substrate proteins including Akt. Dephosphorylation of Akt by PP-1 has been shown to down-regulate the activity of this kinase (Xiao et al., 2010). Accordingly, sequestration of PP-1 by DENV capsid and preventing dephosphorylation of phospho-Akt is a plausible mechanism by which expression of the viral protein increases Akt activity.

To verify the interaction between DENV capsid and PP-1c, we used affinity chromatography with microcystin (MC), a cyanobacterial toxin that covalently binds to the active site of PP-1c thereby inhibiting its activity (MacKintosh et al., 1995). When immobilized on Sepharose beads (MC-Sepharose/MC-S), microcystin can be used to purify proteins that interact with phosphatases. Forty-eight hours post-transduction, A549 cell lysates were subjected to pulldowns with MC-S alone or MC pre-bound with PP-1c followed by immunoblotting with antibodies to PP-1c or DENV capsid. The data in **Figure 3.7B** show that consistent with the mass spectrometry data in **Figure 3.7A**, DENV capsid forms a stable complex with PP-1c.

3.2.9 Zika virus capsid protects cells from Fas-dependent apoptosis and interacts with protein phosphatase 1

With the recent emergence of ZIKV and associated need for understanding pathogenesis, we decided to investigate if ZIKV capsid possessed similar qualities to

A.

	DENV Capsid		CMV UL137	
	UP	SC	UP	SC
Protein phosphatase 1G (PP-1c); IPI00006167	11	21	0	0

UP= unique peptides SC= total spectral counts

B.

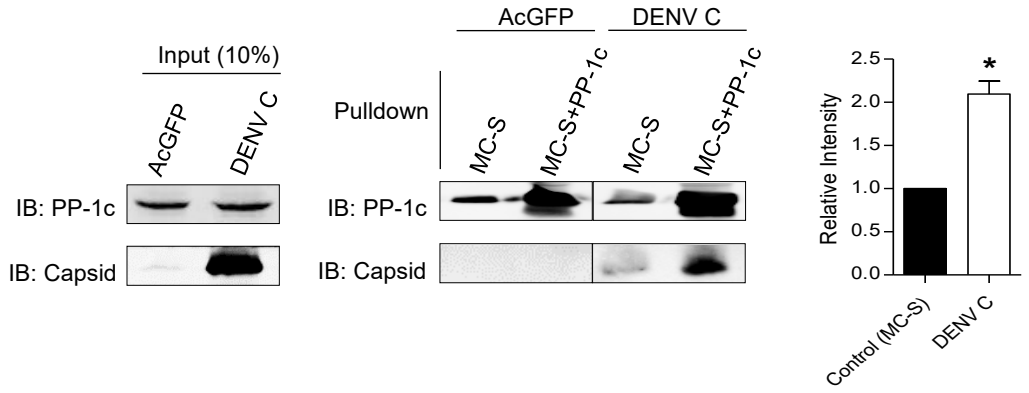

Figure 3.7. Dengue virus capsid interacts with protein phosphatase 1 (PP-1c). A. FLAG-tagged DENV capsids or cytomegalovirus UL137 (size matched negative control) and their associated proteins were isolated by affinity purification from transiently transfected HEK293T cells. Host cell proteins that co-purified with the capsid proteins were identified by tandem mass spectrometry. The number of unique peptides (UP) and the total number of peptides (spectral counts; SC) for PP-1c are shown. **B.** Affinity pull-downs in cells transduced with lentiviruses encoding DENV capsid proteins. Cell lysates collected at 48h post-transduction were incubated with microcystin-sepharose (MC-S) beads with or without pre-bound PP-1c. Shown are the mean relative intensities of the immunoblots based on 3 independent experiments. Results of statistical analyses (t-test) are indicated (* $P \leq 0.05$).

the other capsids tested in this study. The coding region for the capsid from a contemporary Asian strain of ZIKV (PLCal_ZIKV) was modified with an N-terminal myc tag and a recombinant lentivirus harboring this expression construct was produced. The expression of AcGFP and ZIKV capsid in transduced cells was confirmed by immunoblotting (**Figure 3.8A**). Similar to what was observed with other flavirus capsid proteins, expression of ZIKV capsid was protective against challenge with anti-Fas. Specifically, there was a 43% reduction in active caspase-3 in ZIKV capsid expressing cells compared to control cells expressing AcGFP alone (**Figure 3.8B**). The anti-apoptotic activity of ZIKV capsid was largely abrogated but not eliminated when cells were also treated with the PI3K inhibitor LY294002 (**Figure 3.8C**). This suggests that the effect of capsid is mediated in part by PI3K and that other mechanisms may also contribute to the effect of capsid. As was the case with the other capsids tested in this study, expression of ZIKV capsid resulted in increased phosphorylation of Akt (**Figure 3.8A**). Because of the close relationship between ZIKV and DENV, we investigated whether ZIKV capsid interacts with protein phosphatase 1. Cells expressing AcGFP (control) or myc-tagged ZIKV capsid were transfected with a plasmid encoding pEGFP-PP1. Twenty-four hours post-transfection, lysates were subjected to co-immunoprecipitation with anti-myc followed by immunoblotting for PP-1c and ZIKV capsid. Data in **Figure 3.9** show that compared to the control, almost three times as much PP-1c was pulled down by ZIKV capsid. These results are consistent with a scenario in which flavivirus capsid proteins protect infected cells from apoptosis in whole or part by sequestering phosphatases that inactivate Akt.

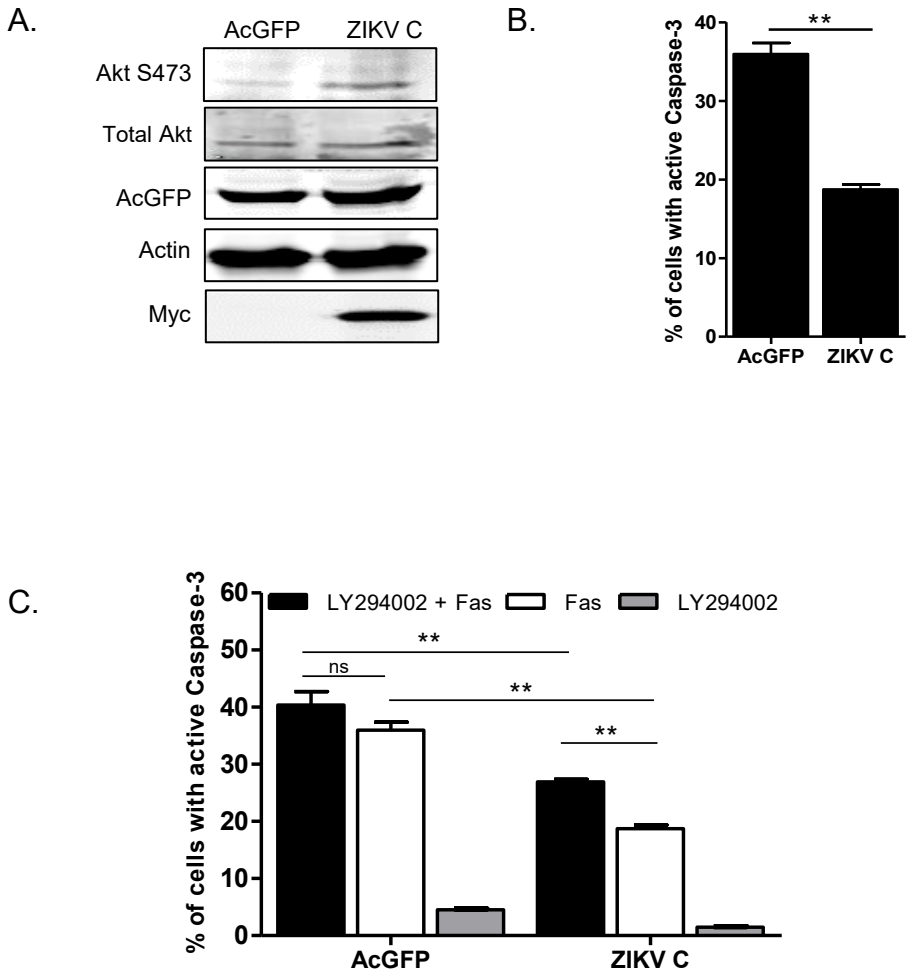

Figure 3.8. Expression of Zika virus capsid increases phospho-Akt and protects cells from anti-Fas challenge. A. Expression of ZIKV-capsid in transduced cells. Myc-tagged ZIKV capsid or AcGFP control was transduced into A549 cells. Lysates were collected at 48h post-transduction and immunoblotted with antibodies to Myc, GFP, total Akt, phospho-Akt, and actin (loading control). **B.** Expression of ZIKV capsid blocks apoptosis. A549 cells were transduced with lentiviral particles encoding ZIKV-capsid protein. Cells were challenged with anti-Fas and then analyzed by flow cytometry using an antibody to active-Caspase 3. Only GFP-expressing cells were included in the analysis. The data from 3 experiments are summarized. **C.** Inhibition of PI3K reduces protection by ZIKV-capsid. Cells were transduced with ZIKV-capsid or AcGFP and treated with anti-Fas and LY294002 followed by flow cytometry analysis using antibody for active-caspase 3. Only GFP-expressing cells were included in the analysis. Data from 3 independent experiments are summarized. Results of statistical analyses (t-test) are indicated (**, $P \leq 0.01$).

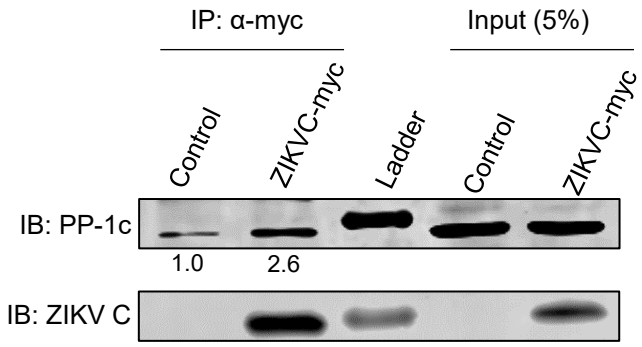

Figure 3.9. Zika virus capsid interacts with protein phosphatase 1 (PP-1c). Myc-tagged ZIKV capsid or AcGFP control were expressed in A549 cells by lentiviral transduction followed by transfection with plasmid encoding GFP-tagged PP-1c. Twenty-four hours later, lysates were subjected to co-immunoprecipitation with anti-Myc followed by immunoblotting for PP-1c and capsid. Shown is a representative immunoblot of 3 independent experiments.

3.2.10 Protein sequence alignment of flavivirus capsid proteins

A protein sequence alignment of all the flavivirus capsid proteins used in this study was made using CLUSTALW (1.83) multiple sequence alignment. As seen in **Figure 3.10**, black and grey boxes represent highly conserved residues and the red boxes represent putative PP-1c binding motifs. The flavivirus capsids used in this study have ~40% conserved amino acid sequence. All capsids except YFV and ZIKV contain a putative PP-1c binding motif "RFVL/KLFM" or "RAVL/GILK" (personal communication with Dr. Tamara Skene-Arnold and Dr. Charles Holmes, University of Alberta). Instead of a "RFVL" motif, ZIKV capsid contains a "RMVL" motif at the same site where all other capsids (except YFV) contain putative PP-1c binding motifs "RFVL" or "KLFM". Interestingly, the amino acid sequence of YFV capsid appears to be the least conserved and in comparison to all capsids in this study, YFV capsid was consistently one of the "weaker" capsids in conferring resistance to apoptosis, induction of phospho-Akt and in stimulation of cellular metabolic activity.

```
DENV    MNNQRK-KARNTPFNMLKRERNRVSTVQQLTKRFSLGMLQGRGPLKLFMALVAFLRFLT
JEV     MTKKPGGPGKNRAINMLKRGLPRVFPLVGV-KRVVMSLLDGRGPVRFVLALITFFKFTA
MVEV    MSKKPGGPGKPRVVNMLKRGIPRVFPLVGV-KRVVMNLLDGRGPIRFVLALLAFFRFTA
SLEV    MSKKPGKPGRNRVVNMLKRGVSRVNPLTGL-KRILGSLLDGRGPVRFILAILTFFRFTA
WNV     MSKKPGGPGKSRAVNMLKRGMPRVLSLIGL-KRAMLSLIDGKGPIRFVLALLAFFRFTA
YFV     MSGRKA-QGKTLGVNMVRRGVRSLSNK--I-KQKTKQIGNRPGPSRGVQGFIFFFLFNI
ZIKV    MKNPKKKSGGFRIVNMLKRGVARVSPFGGL-KRLPAGLLLGHGPIRMVLAILAFLRFTA
        *.      .    .**::*    :     : *:    :    ** : . .:: *: *

DENV    IP---PTAGILKRWGTIKKSKAINVLRGFRKEIGRMLNILNRR-----RR
JEV     LA---PTKALLGRWKAVEKSVAMKHLTSFKRELGTLIDAVNKRGRKQNKR
MVEV    LA---PTKALIRRWKSVNKTTAMKHLTSFKKELGTLIDVVNKRGKKQKKR
SLEV    LQ---PTEALKRRWRAVDKRTALKHLNGFKRDLGSMLDTINRRP--SKKR
WNV     IA---PTRAVLDRWRGVNKQTAMKHLLSFKKELGTLTSAINRRSSKQKKR
YFV     LTGKKITAHLKRLWKMLDPRQGLAALRKVKRVVAGLMRGLSSR----KRR
ZIKV    IK---PSLGLINRWGSVGKKEAMEIIKKFKKDLAAMLRIINARKE-KKRR
        :     :  :   *  :    .:  :  .:: :. :   :. *     :*
```

Figure 3.10. Protein sequence alignment of the flavivirus capsids. Alignment was performed using CLUSTALW Multiple Sequence alignment. Residues shaded in black are conserved in all capsids. (* conserved among all; : conserved in all minus one; . conserved in all minus two). Red boxes highlight putative PP-1c binding motifs "RFVL/KLFM" or "RAVL/GILK".

3.3 Summary

In this chapter we investigated how expression of capsid proteins from seven different flaviviruses affect apoptosis and Akt-dependent processes. All seven of the capsid proteins protected cells from Fas-dependent apoptosis through a mechanism that requires activated Akt. All the flavivirus capsid proteins tested induced phosphorylation of Akt, albeit to different levels. Unexpectedly, co-expression of WNV capsid and the WNV non-structural proteins (replicon) suggested that capsid proteins do not protect cells from the pro-apoptotic effects of non-structural protein expression in the absence of anti-Fas. This could mean that capsid proteins only protect infected cells from extrinsic apoptotic signals rather than cell death signalling that results from cellular detection of viral RNA.

As well as resistance to apoptosis, we also investigated whether capsid expression affected cellular processes that are affected by Akt. We observed elevated ATP levels, increased mitochondrial metabolism and increased expression of glucose transporter 1 (GLUT1) in capsid-expressing cells. Finally, affinity purification of DENV capsid from human cells coupled to mass spectrometry identified protein phosphatase 1 (PP-1), a phosphatase known to inactivate Akt, as a DENV capsid interacting protein. This suggests that DENV capsid expression may activate Akt by sequestering protein phosphatase 1 which results in accumulation of phospho-Akt. Increased Akt activity would also be expected to affect other downstream signalling pathways that affect cell survival and metabolism. We also showed that ZIKV capsid interacts with PP-1, suggesting that this is may be a conserved mechanism among

flavivirus capsids. Together, these data are consistent with a scenario in which flavivirus capsid proteins prepare the host cell for virus replication by increasing the activity of survival and energy producing pathways.

Chapter 4

RNA-sequencing of flavivirus capsid expressing cells reveals novel insights into capsid-mediated subversion of host innate immune responses

4.1 Rationale

The establishment of a robust interferon (IFN) response by the host cell is essential to control viral infection. For example, flavivirus replication is inhibited by pre-treatment of cells with IFNα/β (Ye et al., 2013), thus viruses have evolved elegant strategies to subvert the IFN response. Previous studies have elucidated the molecular mechanisms by which the flavivirus non-structural proteins (NS4A, NS4B, NS1, NS2B-NS3, NS5) (Ashour et al., 2009; Grant et al., 2016; Hu et al., 2019; Jones et al., 2005; Kumar et al., 2016; Ma et al., 2018; Wu et al., 2017) (for a recent review (Lee and Shin, 2019)) subvert IFN induction and IFN signalling. However, it is not clear if any of the structural proteins (C, prM, E) modulate the IFN response.

Previous studies have associated ZIKV capsid to non-structural functions in host cells. For example, it was suggested that ZIKV infection impairs the Nonsense-mediated mRNA decay (NMD) pathway, a mechanism that is believed to involve ZIKV capsid interacting with up-frameshift protein 1 (UPF1) (Fontaine et al., 2018). The YFV capsid as well as other flavivirus capsid proteins were identified as potent suppressors of RNA silencing (Samuel et al., 2016). Additionally, the DEAD Box Helicase 3 X-Linked (DDX3X) protein was identified as a DENV capsid-interacting partner and the authors suggested this may be a potential mechanism for suppression of antiviral functions (albeit the exact mechanism is unknown) (Kumar et al., 2018a). In our lab, it was previously shown that flavivirus infection dramatically reduces the pool of cellular peroxisomes and that this phenotype was largely mediated by the capsid protein (You et al, 2015; Wong et al, 2019). Given that peroxisomes are signalling

platforms for antiviral innate immunity (Dixit et al., 2010), it is temping to speculate that capsid can interfere with the IFN response. However, previous experiments performed by a former PhD student (Dr. Shangmei Hou) showed that capsid expression did not significantly affect the induction of poly (I:C) stimulated IFN-lambda and it was concluded that capsid protein alone was not sufficient to block IFN induction (You et al., 2015). In this chapter, I provide data that suggest that flavivirus capsids in fact do block the production of type I IFN.

4.2 Results

4.2.1 Global gene expression changes in capsid-expressing cells

Multiple studies have assessed ZIKV-induced transcriptomic changes in human cell types such as microglia, fibroblasts, monocyte-derived macrophages, astrocytes and dendritic cells (Kozak et al., 2017; Limonta et al., 2018; Sun et al., 2017b; Tiwari et al., 2017). Collectively, these studies demonstrate that infection with ZIKV in susceptible cells causes massive transcriptional changes, but to my knowledge no studies have examined how expression of a single viral protein affects host mRNA profiles. In this study, RNA-sequencing was used to assess the global transcriptome changes in cells expressing flavivirus capsid proteins. A549 cells were transduced with lentiviral vectors (LV) encoding AcGFP alone or AcGFP and myc-tagged capsid (C) proteins at a MOT of 10 as previously described in Chapter 3. Forty-eight hours post-transduction all samples were ~90% AcGFP-positive and expressed myc-tagged capsid proteins at comparable levels (**Figure 4.1**). Total RNA was extracted from duplicate

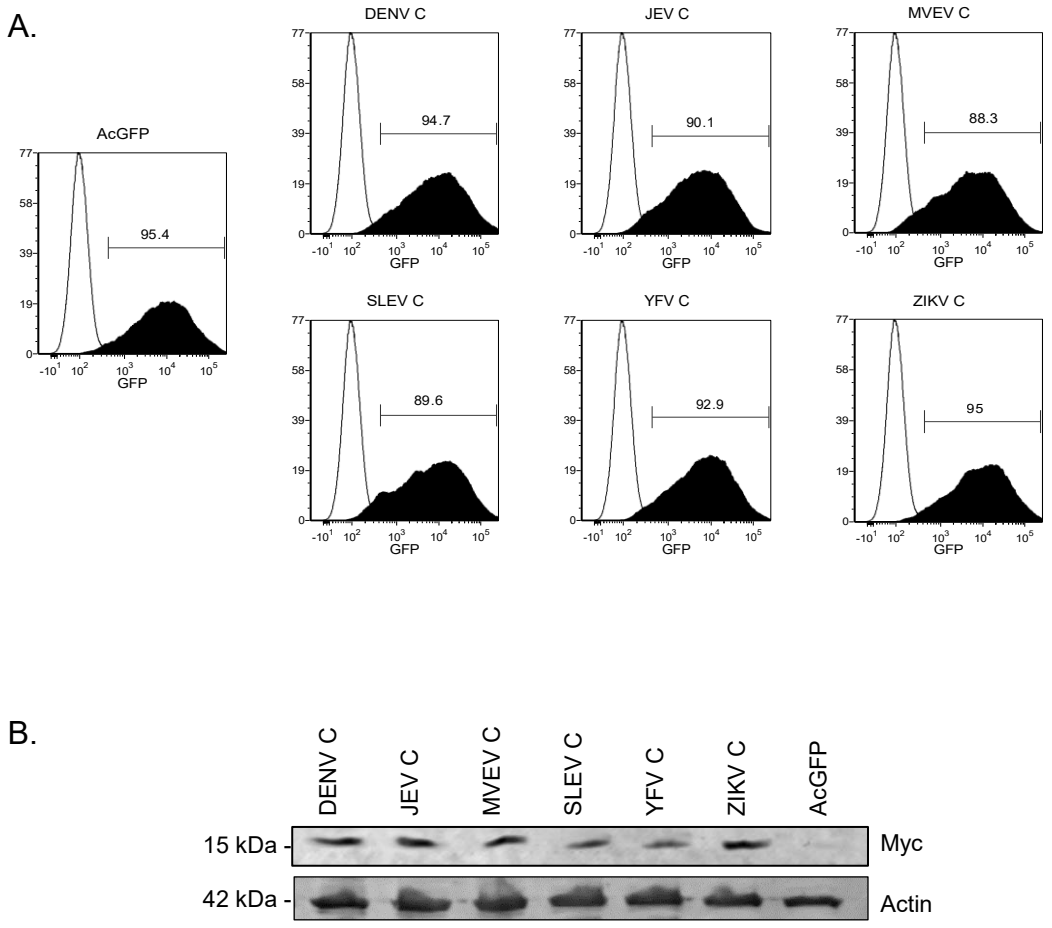

Figure 4.1. Expression of myc-tagged capsid proteins. A549 cells were transduced with lentiviral vectors expressing AcGFP alone or AcGFP and myc-tagged capsid proteins. Cells were collected at 48 hours post-transduction for analysis by flow cytometry and immunoblotting. **A.** GFP expression of transduced cells was measured by flow cytometry. Values shown are % GFP-positive cells relative to mock. **B.** Cell lysates from duplicate samples were analyzed by immunoblotting with anti-Myc and anti-Actin.

samples and RNA-Sequencing was performed using the Thermo-Fisher Ion S5 sequencer. Gene expression analysis in capsid-expressing cells showed that there were 3,546-downregulated and 75-upregulated common differentially expressed genes (DEGs) among all capsids relative to control (fold change > 2, p-value ≤ 0.01) (**Figure 4.2A** and **B**). The top 20 down- and up-regulated genes are listed in **Tables 4.1** and **4.2**, respectively. Strikingly, most of the DEGs that were highly downregulated (≥10-fold) by expression of capsid proteins regardless of the flavivirus, were enriched for genes involved in the interferon response (e.g. *CCL5, MX1, OASL, IFIT2*) (**Figure 4.3**). Gene ontology enrichment analysis was performed on all down-regulated genes ≥10-fold and the top biological processes significantly enriched were identified as "defense response to virus" or "Interferon alpha/beta signalling" (**Figure 4.4A** and **Figure 4.5**). Gene ontology enrichment analysis of up-regulated genes revealed that most were associated with pathways that regulate cell division and cell cycle (**Figure 4.4B**).

4.2.2 QPCR validates transcriptomic changes from RNA-sequencing

To validate the transcriptomic changes identified by RNA-sequencing, cDNAs were prepared from the same RNA samples used for RNA-sequencing. Since most of the DEGs from the RNA-seq were downregulated, eight downregulated genes with fold changes between 1 and 1000 were selected, and qPCR was performed with primers that had the same gene sequence used in the Ion AmpliSeq™ Transcriptome Human Gene Expression kit (Thermo-Fisher). The gene expression changes as measured by qPCR

A.

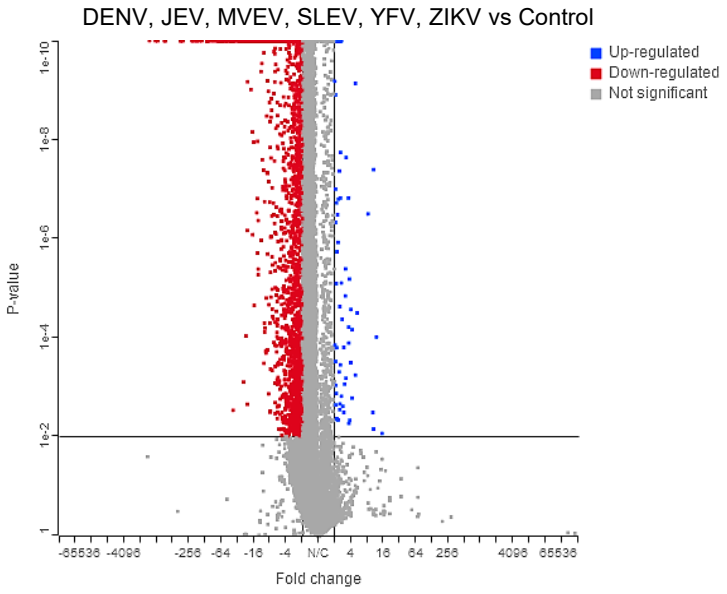

B.

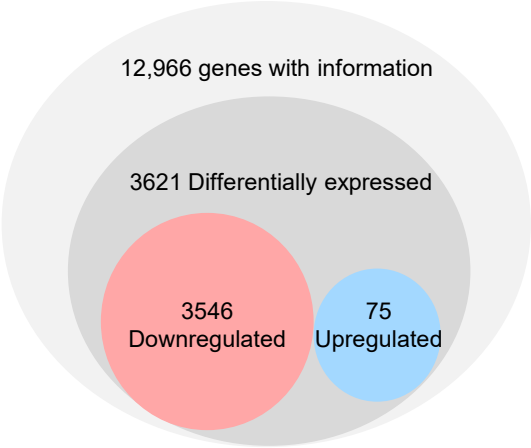

Figure 4.2. Global gene expression changes in capsid expressing cells. A549 cells were transduced with lentiviral vectors expressing AcGFP alone or AcGFP and myc-tagged capsid proteins. Cells were collected at 48 hours post-transduction and then total RNA was extracted and processed for RNA-sequencing. Shown are the global gene expression changes common amongst all capsid-expressing cells relative to control (AcGFP). **A**. Volcano plot displaying differentially expressed genes. Differentially expressed genes with > 2-fold changes and with a p-value ≤ 0.01 are shown. Blue: up-regulated, Red: Down-regulated, Grey: Not significant. **B.** Total common gene expression changes in capsid expressing cells. All genes with a p-value of ≤ 0.01 are included. In total, 3,621 genes were differentially expressed (> 2-fold change).

Gene	Description	Fold Change
CCL5	C-C Motif Chemokine Ligand 5	-1363.33
MX1	MX Dynamin Like GTPase 1	-1055.14
OASL	2'-5'-Oligoadenylate Synthetase Like	-956.56
IFIT2	Interferon Induced Protein With Tetratricopeptide Repeats 2	-718.98
IFIT3	Interferon Induced Protein With Tetratricopeptide Repeats 3	-694.00
IFIT1	Interferon Induced Protein With Tetratricopeptide Repeats 1	-363.25
BST2	Bone Marrow Stromal Cell Antigen 2	-352.47
ISG15	ISG15 Ubiquitin-Like Modifier	-221.56
PLEKHA4	Pleckstrin Homology Domain Containing A4	-212.54
IFI6	Interferon Alpha Inducible Protein 6	-185.33
HSPA6	Heat Shock Protein Family A (Hsp70) Member 6	-159.88
IRF7	Interferon Regulatory Factor 7	-117.75
IFIH1	Interferon Induced With Helicase C Domain 1	-111.11
UBA7	Ubiquitin Like Modifier Activating Enzyme 7	-108.42
HLA-B	Major Histocompatibility Complex, Class I, B	-95.93
ATF3	Activating Transcription Factor 3	-88.65
DDX58	DExD/H-Box Helicase 58	-79.13
PARP10	Poly(ADP-Ribose) Polymerase Family Member 10	-73.80
SAMD9L	Sterile Alpha Motif Domain Containing 9 Like	-68.68
SP110	SP110 Nuclear Body Protein	-67.85

Table 4.1. List of top 20 down-regulated differentially expressed genes (p-value $\leq$ 0.01)

Gene	Description	Fold Change
PRELID2	PRELI Domain Containing 2	14.96
ATP5MD	ATP Synthase Membrane Subunit DAPIT	11.83
SEC31A	SEC31 Homolog A, COPII Coat Complex Component	10.48
TXNDC5	Thioredoxin Domain Containing 5	10.13
ANKS4B	Ankyrin Repeat And Sterile Alpha Motif Domain Containing 4B	8.24
TBC1D22A	TBC1 Domain Family Member 22A	5.22
ITGB3BP	Integrin Subunit Beta 3 Binding Protein	4.80
SCARNA3	Small Cajal Body-Specific RNA 3	4.20
DDC	Dopa Decarboxylase	4.20
PIK3C2A	Phosphatidylinositol-4-Phosphate 3-Kinase Catalytic Subunit Type 2 Alpha	3.99
CENPE	Centromere Protein E	3.96
PLPPR1	Phospholipid Phosphatase Related 1	3.80
TMEM107	Transmembrane Protein 107	3.70
PMS2	PMS1 Homolog 2, Mismatch Repair System Component	3.63
CDC25C	Cell Division Cycle 25C	3.61
EFCAB10	EF-Hand Calcium Binding Domain 10	3.58
NUP43	Nucleoporin 43	3.25
NONO	Non-POU Domain Containing Octamer Binding	3.23
PDK3	Pyruvate Dehydrogenase Kinase 3	3.15
HMMR	Hyaluronan Mediated Motility Receptor	3.13

Table 4.2. List of top 20 up-regulated differentially expressed genes (p-value ≤ 0.01)

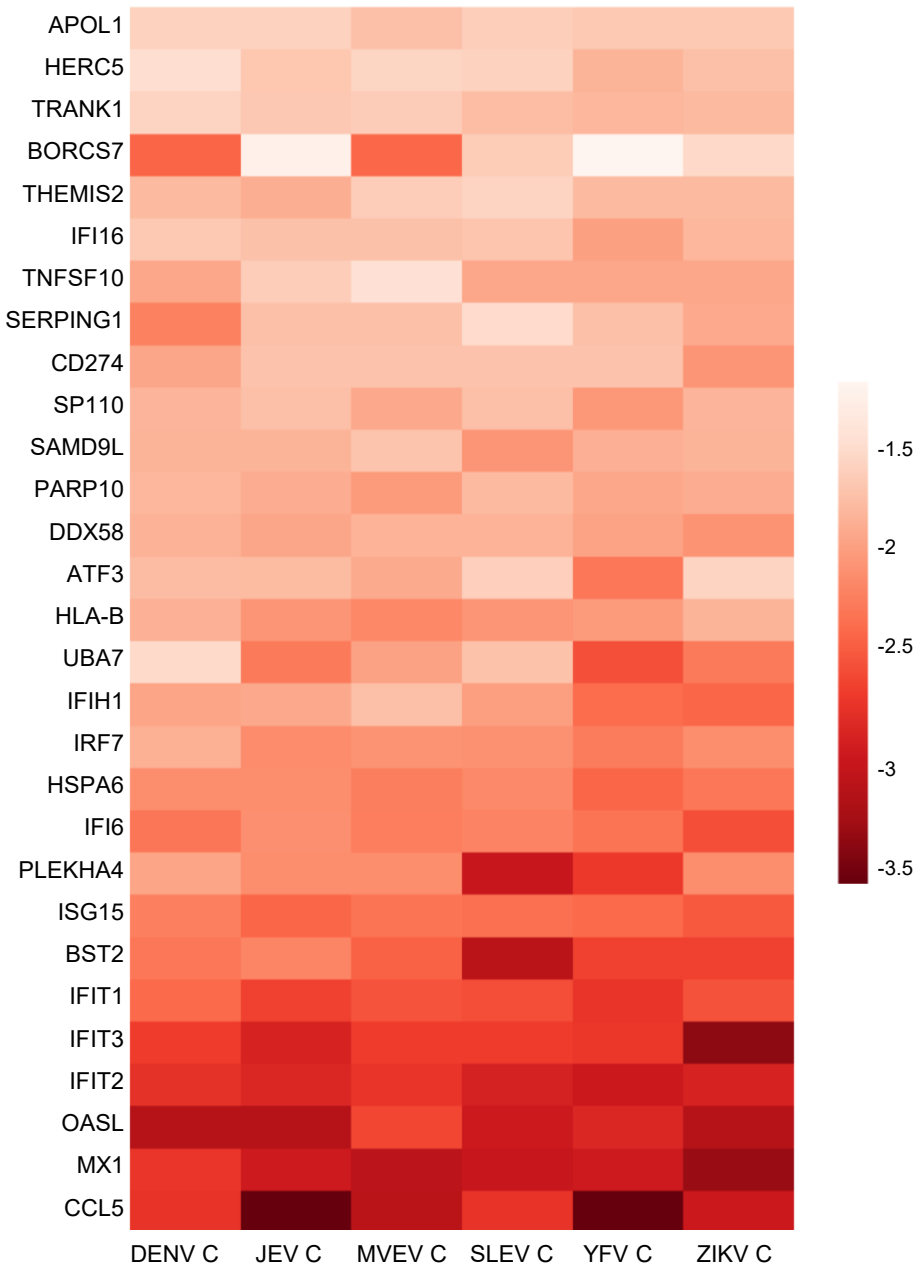

Figure 4.3. Top 30 down-regulated genes in cells transduced with flavivirus capsids. Each panel in the heat map represents a particular gene and the intensity of the colour represents fold change relative to control (all values underwent log 10 transformation).

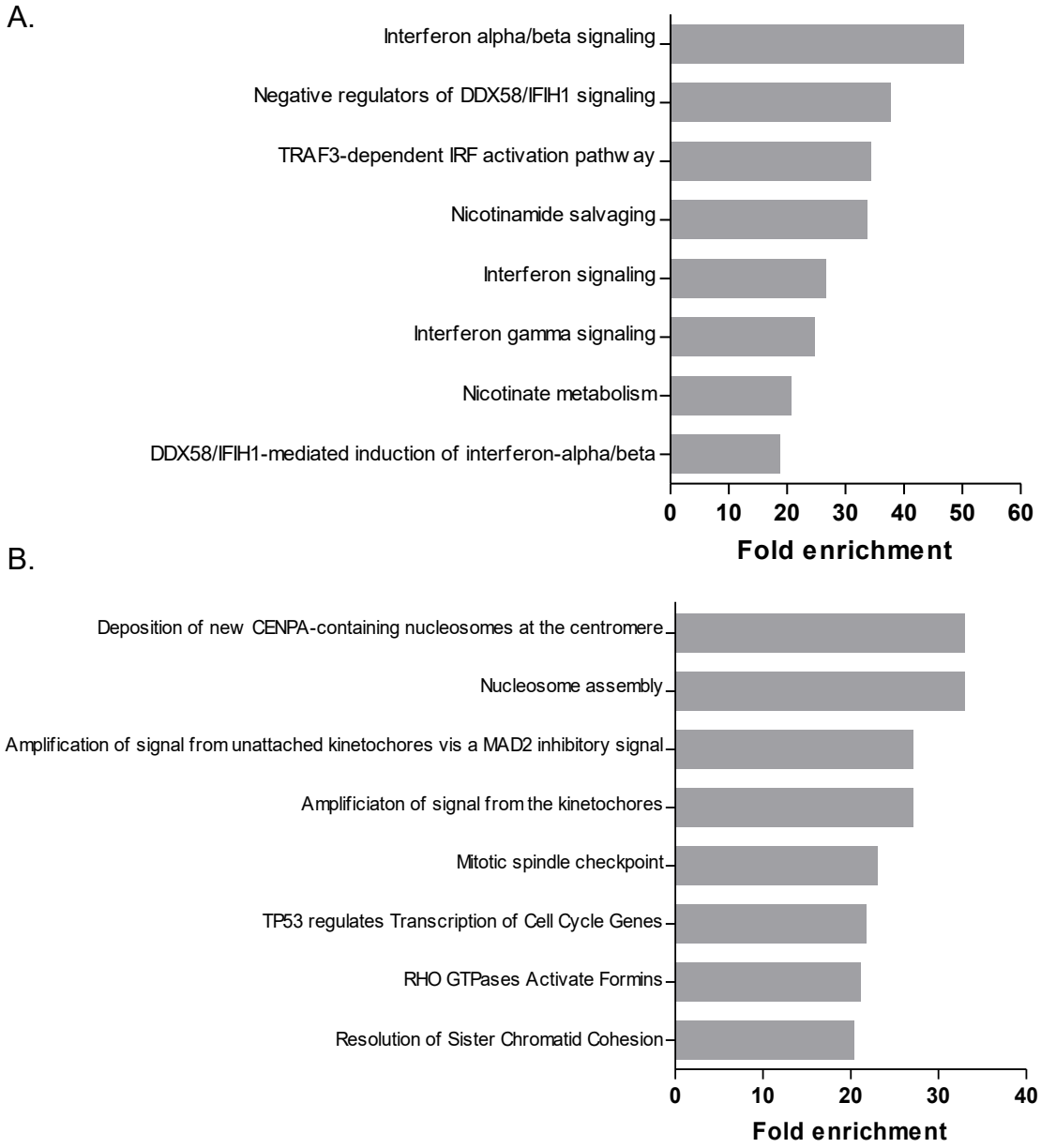

Figure 4.4. Gene ontology enrichment analysis of common differentially expressed genes (DEGs) among capsids. Biological pathways were determined by individually submitting DEG lists of **A.** Down-regulated genes and **B.** Up-regulated genes to the online bioinformatics server (geneontology.org) using the annotation data set "Reactome pathways". Shown are the top eight enriched pathways.

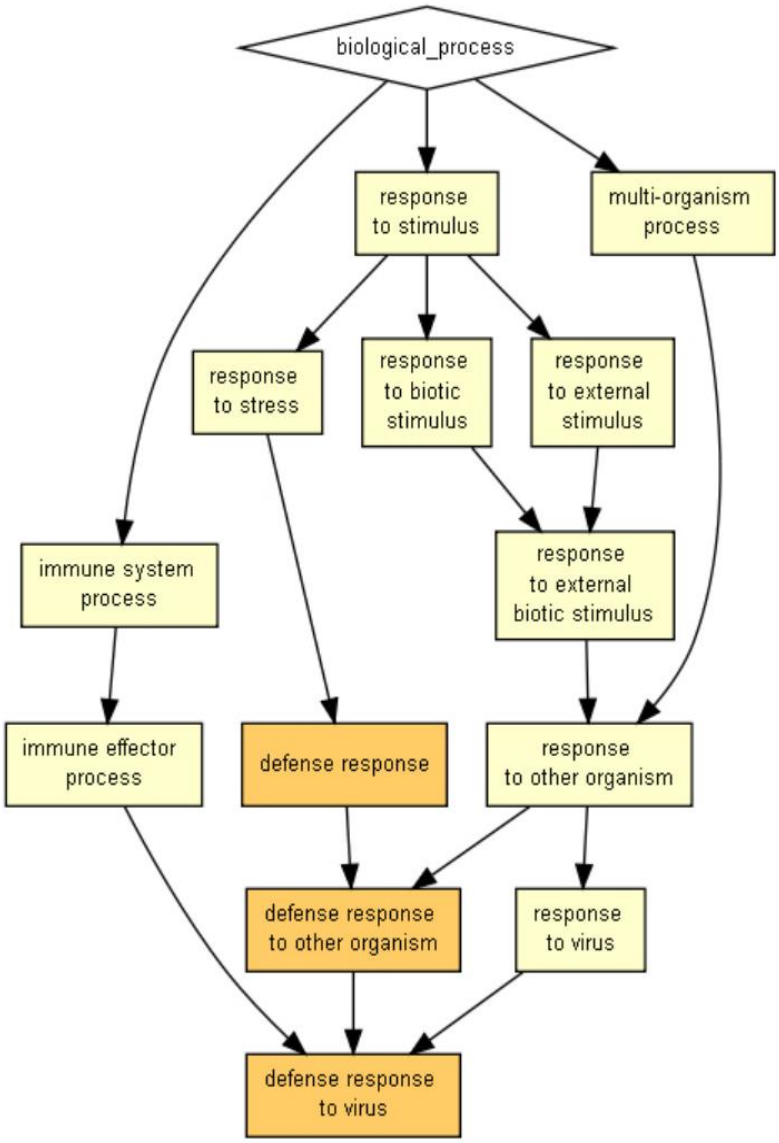

Figure 4.5. Visualization of gene ontology enrichment analysis of common down-regulated differentially expressed genes (DEGs) in capsid-expressing cells. Pathways were determined by submitting the DEG list of down-regulated genes to the online server GOrilla. The colour of the box represents the enrichment p-value (light yellow 10^{-3} to 10^{-5} , dark yellow 10^{-5} to 10^{-7}).

and those derived from RNA-sequencing were very similar for all genes tested (**Figure 4.6A**). The correlation coefficient between the select genes (Pearson's r) was 0.9996 (**Figure 4.6B**). The fact that the transcriptomic changes derived from RNA-sequencing could be validated using an independent assay provide confidence in the data from the RNA-sequencing experiments.

4.2.3 Cells transduced with lentiviral vectors encoding ZIKV capsid suppress IFN-β and are susceptible to infection

Previous studies have shown that lentiviral vectors (LV) can trigger a transient type I Interferon response both *in vitro* (Breckpot et al., 2010) and *in vivo* (Brown et al., 2006) (reviewed in (Nayak and Herzog, 2010)). In dendritic cells, lentivirus transduction leads to TLR activation, is inhibited in TRIF/MyD88 knockout cells, and leads to production of *IFN-β*, *IL-23* and other interferon stimulated genes (ISGs) (Breckpot et al., 2010). To investigate if our LVs were triggering a type I IFN response, I transduced A549 cells with LV expressing AcGFP (control) or AcGFP-Myc-ZIKVC and expression of *IFN-β* was measured by qPCR. Lentivirus-transduced cells expressing AcGFP only resulted in ~150-fold induction of *IFN-β* whereas lentivirus transduced cells expressing AcGFP-Myc-ZIKVC resulted in only ~4-fold induction of *IFN-β* (**Figure 4.7A**). These data suggest that ZIKV capsid expression suppresses lentivirus-induced *IFN-β*. Since transduction of cells with LV expressing AcGFP lead to production of *IFN-β* whereas transduction of cells with LV expressing AcGFP-Myc-ZIKVC did not, I next hypothesized that cells expressing AcGFP-Myc-ZIKVC would

A.

GENE ID	Fold change (RNA-Seq)	Fold change (qPCR)
CCL5	-986.51	-1056.44
IFIT1	-338.25	-362.04
IFI6	-154.19	-134.36
TRIM22	-47.25	-37.14
IRF1	-32.96	-29.65
STAT2	-24.33	-20.39
MYD88	-8.79	-6.96
BAX	-1.79	-1.25

B.

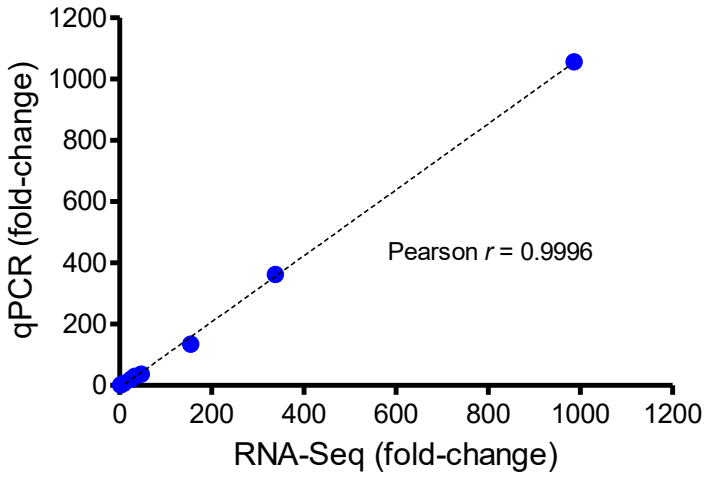

Figure 4.6. Validation of RNA-Sequencing. A. Shown is the fold change of select genes that were generated from RNA-seq and qPCR for DENV capsid expressing cells. **B.** The fold-change obtained from RNA-Seq and qPCR were plotted with a line of best fit.

A.

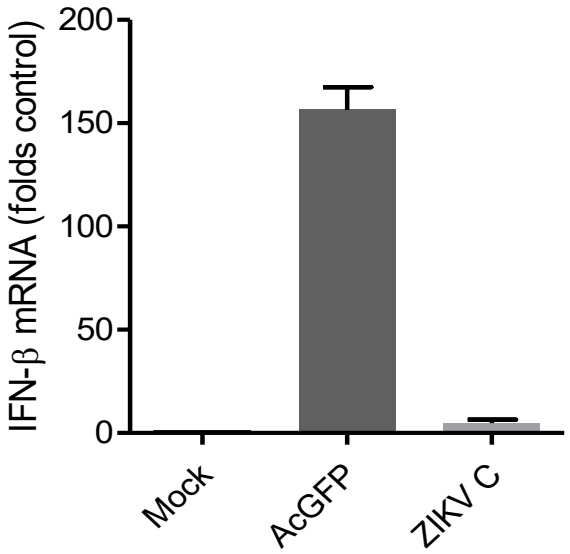

B.

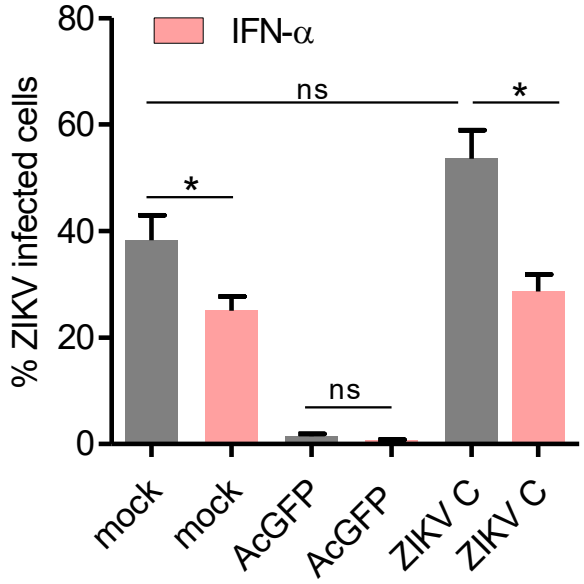

Figure 4.7. ZIKV capsid expressing cells suppress IFN-β and are highly susceptible to infection. A549 cells were transduced with lentivirus expressing AcGFP or AcGFP-Myc-ZIKVC (MOT of 10). **A.** AcGFP expressing cells have high levels of IFN-β mRNA. Cells were collected at 48 hours post-transduction and the levels of IFN-β mRNA in mock, AcGFP or ZIKV C-expressing cells were determined by qRT-PCR. **B.** ZIKV C expressing cells are permissive to ZIKV infection but are sensitive to pre-treatment with IFN-α. Transduced cells were infected with ZIKV at an MOI of 3 (grey bars) or pre-treated with IFN-α prior to ZIKV infection (pink bars). All cells were collected 48 hours post-infection and stained with anti-ZIKV NS1 antibody. Only the GFP-positive cells were included in the analysis. Average results from 3 independent experiments are shown. Results of statistical analyses (t-test) are indicated (* $P \leq 0.05$).

be susceptible to infection whereas AcGFP-expressing cells would be resistant to infection. To address this hypothesis, A549 cells were transduced with LV expressing AcGFP or AcGFP-Myc-ZIKVC after which they were infected with ZIKV. Samples were collected for flow cytometry analysis at 48 hours post-infection. Cells transduced with LV expressing AcGFP alone were highly resistant to ZIKV-infection. In contrast, cells transduced with LV expressing AcGFP-Myc-ZIKVC were highly permissive to infection (**Figure 4.7B**). In fact, AcGFP-Myc-ZIKVC-expressing cells were more permissive to ZIKV infection than mock-transduced cells, albeit this was not statistically significant. Pre-treatment with IFN-α prior to ZIKV infection resulted in decreased infection in all samples (pink bars in **Figure 4.7B**), suggesting that capsid-expressing cells are sensitive to IFN-α and thus not actively subverting type I IFN signalling.

4.2.4 ZIKV capsid expressing cells subvert IFN induction

To further examine how flavivirus capsid expression affects IFN induction, I created stable cell lines expressing AcGFP or AcGFP-Myc-ZIKVC (**Figure 4.8A**). QRT-PCR-based analyses of these cell lines revealed that their basal level of ISGs were comparable to mock treated cells (**Figure 4.8B**). Accordingly, I deemed that they would be suitable for subsequent IFN induction studies. AcGFP-Myc-ZIKVC expressing cells exhibited significantly lower transcript levels of *IFIT1, CCL5* and *IFN*-β compared to mock and AcGFP-expressing cells following poly (I:C) transfection (**Figure 4.8B**). The transcription factor IRF-3 is required for evocation

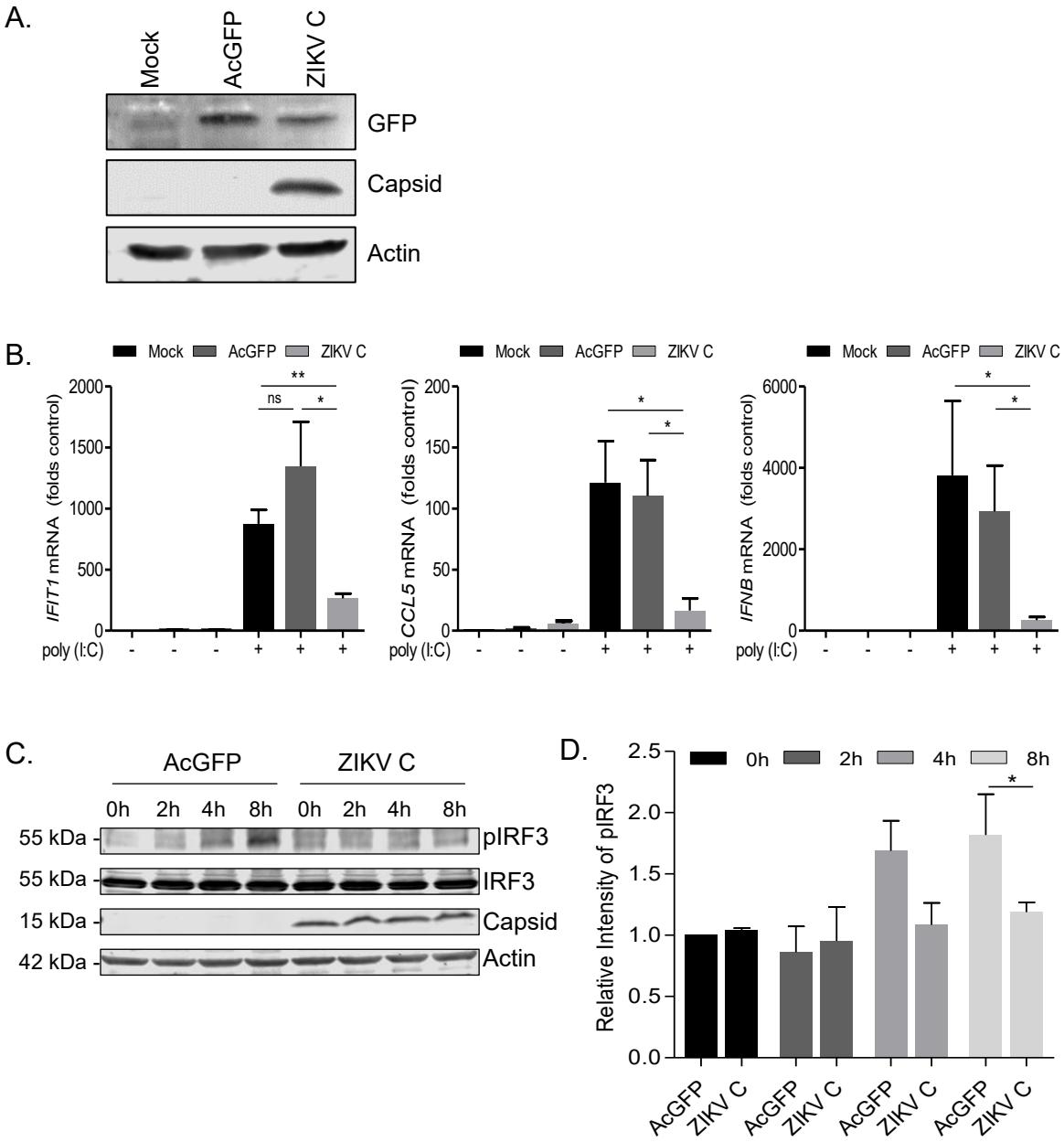

Figure 4.8. ZIKV capsid expressing cells suppress IFN induction. A. Immunoblot blot of GFP, ZIKV capsid and actin in cell lysates from AcGFP or AcGFP-ZIKV capsid expressing stable cell lines. **B.** Expression of select ISGs in AcGFP and ZIKV C-expressing cells. Cells were transfected with poly (I:C) for 24 hours, total RNA was extracted and used to quantify *IFIT1, CCL5, IFN-β* gene expression by qRT-PCR. Shown are normalized values relative to mock cells (control). Data were from three independent experiments. **C.** Time course of p-IRF3 in AcGFP or ZIKV C stables following poly (I:C) transfection. Western blot with antibodies that detect pIRF3, IRF3, ZIKV capsid, and actin are shown. **D.** Mean relative intensity of western blots based on 3 independent experiments. Results of statistical analyses (t-test) are indicated (* $P \leq 0.05$) (**, $P \leq 0.01$).

of type I IFN responses both *in vitro* and *in vivo* (Yanai et al., 2018). To investigate if capsid protein expression affects the activation of IRF-3, cell lysates were collected from stable cells expressing either AcGFP or AcGFP-Myc-ZIKVC after poly (I:C) transfection at several time points and immunoblotted for phospho-IRF3. AcGFP-Myc-ZIKVC-expressing cells had less phospho-IRF3 compared to AcGFP-expressing cells after poly (I:C) stimulation (**Figure 4.8C and D**).

4.2.5 ZIKV capsid interacts with TRIM25

TRIM25 is an E3 Ubiquitin ligase enzyme that is best known for its regulation of RIG-I signalling by K63-linked polyubiquitination (Martín-Vicente et al., 2017). Upon recognition of viral RNA, RIG-I undergoes a conformational change that exposes the CARD domain. RIG-I then homo-oligomerizes on RNA after which it is polyubiquitinated by TRIM25. This facilitates interaction with MAVS, activation of IRF3, and induction of innate immune signalling (Sánchez-Aparicio et al., 2018). An interactomic screen performed in collaboration with Dr. Lorri Frappier (University of Toronto) identified TRIM25 as a ZIKV capsid interacting partner. First, it was important to validate the interaction between ZIKV capsid and TRIM25. Cell lysates from A549 cells expressing AcGFP-Myc-ZIKVC or AcGFP (control) were subjected to co-immunoprecipitation with anti-myc followed by immunoblotting with anti-TRIM25 and anti-ZIKVC antibodies. **Figure 4.9A** shows that TRIM25 forms a stable complex with ZIKV capsid**.** The reciprocal co-immunoprecipitation using cell lysates from A549 cells expressing AcGFP-myc-ZIKVC or AcGFP (control) with or without

A.

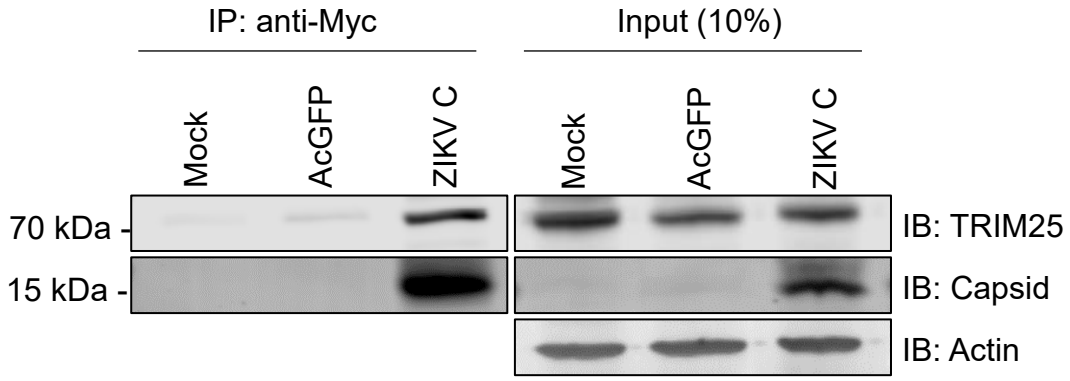

B.

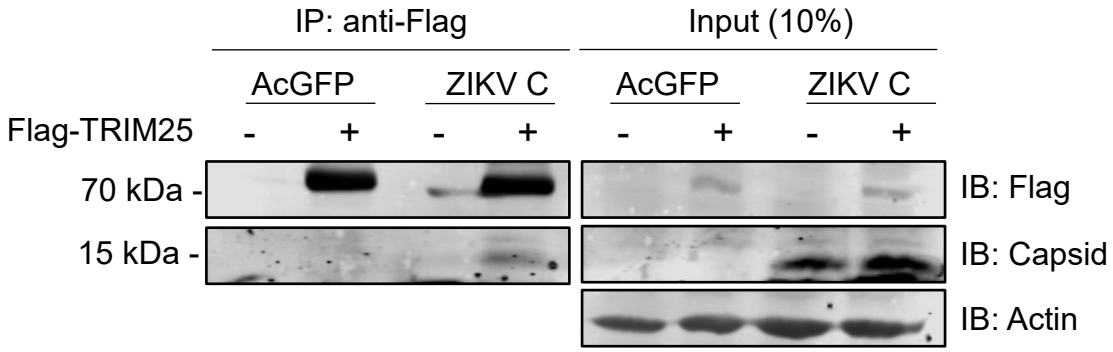

Figure 4.9. ZIKV capsid interacts with TRIM25. A. Myc-tagged ZIKV capsid expressing cells were lysed and co-immunoprecipitation was performed using anti-Myc beads. Immunoblots were probed for TRIM25, capsid and actin. Shown is a representative immunoblot of 3 independent experiments. **B.** Flag-TRIM25 expressing cells were lysed and co-immunoprecipitation was performed using anti-Flag beads. Immunoblots were probed for flag, capsid and actin. Shown is a representative immunoblot of 2 independent experiments.

Flag-TRIM25 were subjected to co-immunoprecipitation with anti-Flag followed by immunoblotting with anti-Flag and anti-ZIKVC antibodies (**Figure 4.9B)**.

4.2.6 TRIM25 protein levels are not significantly changed during ZIKV-infection

Many viruses degrade host cell-encoded viral restriction factors as a means to impair the innate immune response. To test whether TRIM25 is targeted for degradation during ZIKV infection, A549 cells were infected with ZIKV and cellular lysates were collected for western blot analysis at 24- and 48-hours post-infection. The levels of TRIM25 protein did not significantly change during ZIKV infection (**Figure 4.10**).

4.2.7 Knockdown of TRIM25 enhances ZIKV replication

To further analyze the role of TRIM25 during ZIKV infection, we utilized dicer-substrate siRNA (DsiRNA) targeting TRIM25 (siTRIM25) or a non-targeting DsiRNA control (siControl). A549 cells were transfected with DsiRNA for 48 hours and cell lysates were analyzed for TRIM25 levels by western blotting (**Figure 4.11A**). The protein level of TRIM25 was reduced by ~75% following siTRIM25 transfection. Next, cells were infected with ZIKV and 48 hours post-infection cellular RNA was extracted and cell supernatants were collected for qRT-PCR and viral plaque assays respectively. Knockdown of TRIM25 resulted in a small (~2-fold) but statistically

A.

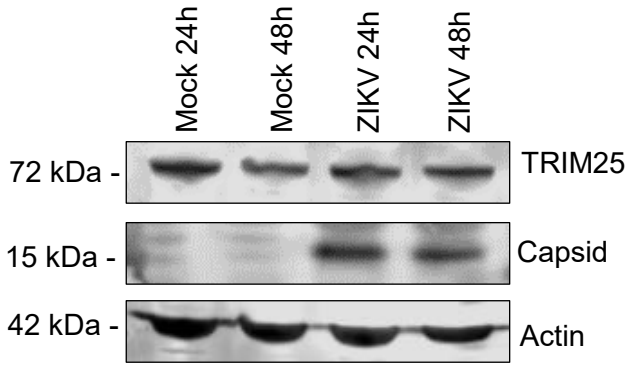

B.

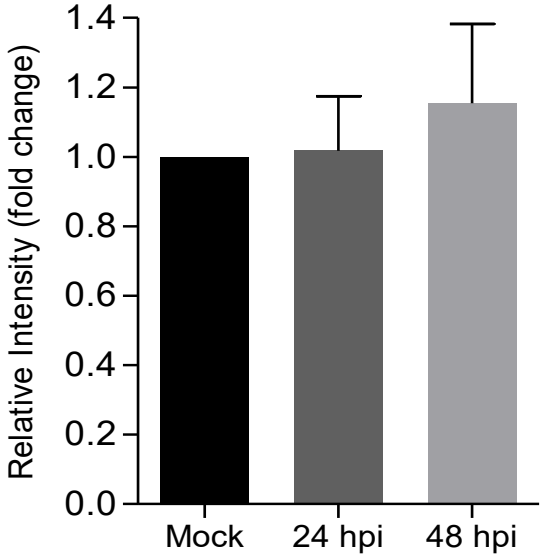

Figure 4.10. TRIM25 is not degraded during ZIKV infection. A549 cells were infected with ZIKV (MOI of 3) and cell lysates were collected 24 and 48 hours post-infection**. A.** Western blot of cell lysates from Mock or ZIKV-infected cells at 24 or 48 hours post-infection. Antibodies specific to TRIM25, ZIKV capsid or Actin were used. **B.** Relative intensity (fold change) of TRIM25 levels by immunoblotting as determined from 3 independent-experiments.

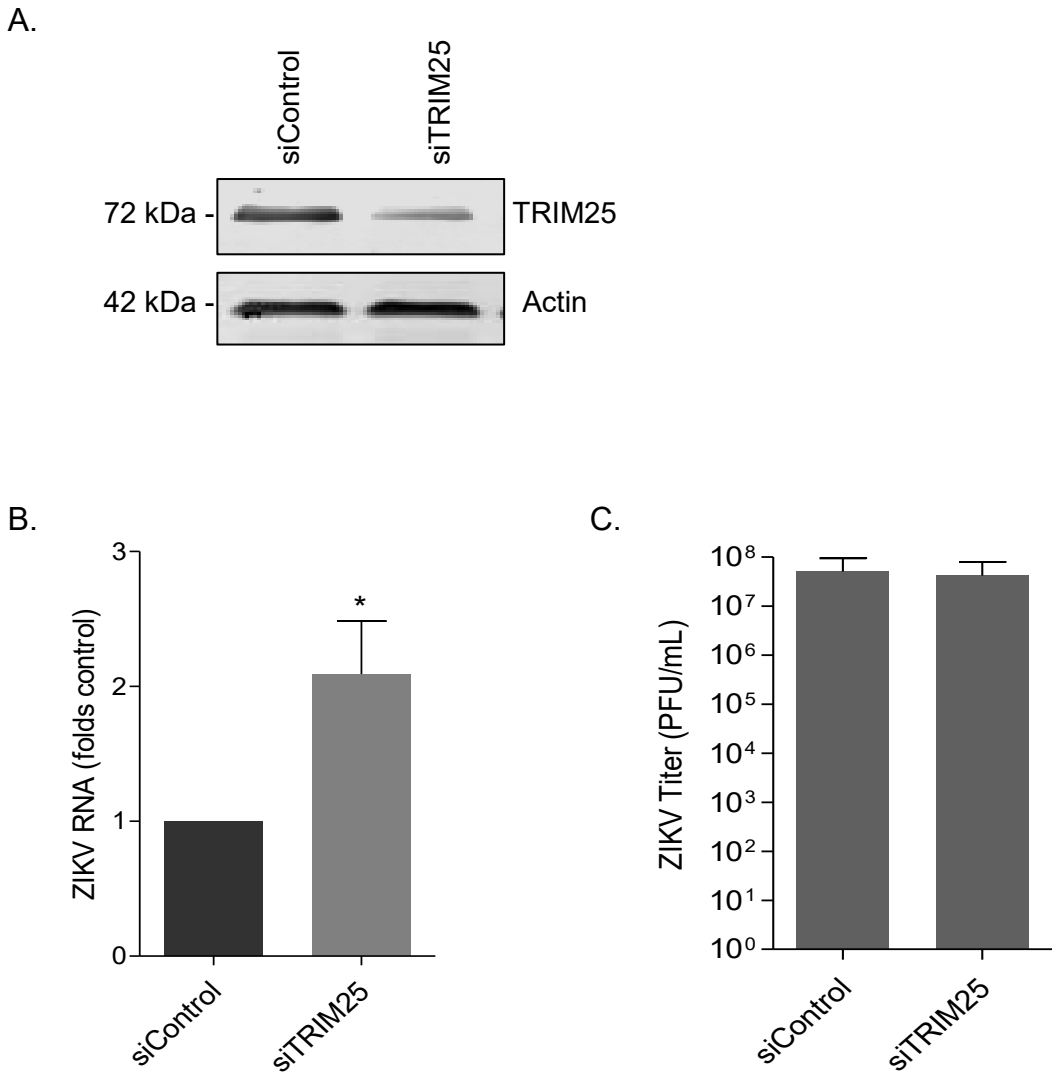

Figure 4.11. Knockdown of TRIM25 enhances ZIKV infection. A549 cells were transfected with siNon-targeting control (siControl) or siTRIM25 for 48 hours followed by infection with ZIKV (MOI of 3). **A.** Western blots of cell lysates 48 hours post-transfection with desired siRNA and probed with antibodies for TRIM25 and Actin. **B**. Cellular RNA was extracted at 48 hours post-infection and qRT-PCR using ZIKV specific primers was performed. **C**. Supernatant was collected for quantification by plaque assay. The average values from 3 independent experiments are shown. All data were subject to t-test analyses (* $P \leq 0.05$).

significant increase in ZIKV replication as determined by qRT-PCR using specific primers to ZIKV genomic RNA (**Figure 4.11B**). However, knockdown of TRIM25 did not have a significant affect on viral titers (**Figure 4.11C**).

4.3 Summary

In this chapter I investigated the global transcriptional changes in host cells induced by expression of flavivirus capsid proteins. This indicates that expression of the capsid proteins from DENV, JEV, SLEV, MVEV, YFV, and ZIKV results in large transcriptional changes that were common amongst all capsids. Analysis of common DEGs in capsid-expressing cells showed that there were 3,546-downregulated and 75-upregulated DEGs in capsid-expressing cells relative to control. Gene ontology enrichment analysis of top downregulated genes identified the top significantly enriched biological processes as "defense response to virus" or "Interferon alpha/beta signalling". Gene ontology enrichment analysis of up-regulated genes were mainly enriched in pathways associated with cell division and cell cycle regulation.

As lentiviral vectors (LV) can trigger a transient type I IFN response (Breckpot et al., 2010), I investigated if the LVs used in these experiments triggered a type I IFN response. Compared to transduced cells expressing AcGFP alone in which significant induction of *IFN-β* was observed, transduced cells expressing AcGFP-Myc-ZIKVC had very low levels of *IFN-β* mRNA. In addition, transduced cells expressing AcGFP were resistant to ZIKV infection, whereas transduced cells expressing AcGFP-Myc-ZIKVC were highly permissive to ZIKV infection. Of note, both AcGFP and AcGFP-Myc-ZIKVC transduced cells were sensitive to pre-treatment with IFN-α.

To further examine how the capsid protein subverts IFN induction, I took advantage of the fact that the type I IFN response generated to lentiviral transduction is transient. I created cell lines stably expressing AcGFP or AcGFP Myc-ZIKVC and

I confirmed that the created cell line had low basal levels of ISGs comparable to untransduced cells. Following poly (I:C) stimulation, the cells stably expressing ZIKV capsid demonstrated suppressed *IFN-β* production and IRF3 phosphorylation relative to mock and cells stably expressing AcGFP alone.

Lastly, I showed that ZIKV capsid interacts with TRIM25 by co-immunoprecipitation. To further define the role of TRIM25, I infected A549s with ZIKV and analyzed the level of TRIM25 during infection by immunoblotting. The protein levels of TRIM25 were unchanged during ZIKV infection. DsiRNA-mediated knockdown of TRIM25 followed by subsequent ZIKV infection resulted in a small increase in viral replication (~2-fold increase) as measured by qRT-PCR using ZIKV specific primers, suggesting that TRIM25 may act as a viral restriction factor.

Collectively, the findings in Chapter 4 reveal a novel, previously unrecognized role of flavivirus capsids in subverting the innate immune response. Future studies will focus on elucidating the interaction of ZIKV capsid with TRIM25 and how this interaction affects downstream antiviral signalling.

Chapter 5

Characterization of Mayaro virus infection in primary human macrophages

5.1 Rationale

The emergence of mosquito-transmitted alphaviruses such as Chikungunya virus (CHIKV) and Mayaro virus (MAYV) poses significant concern in many parts of the world. Infection by these pathogens generally does not result in fatality, however, in a large proportion of people, persistent and severe MAYV-induced arthralgia can develop.

It is unclear why long-term arthralgia develops in infected patients but it is thought to be a consequence of persistent viral replication at joint sites or continuous expression of proinflammatory immune cytokines (Esposito and da Fonseca, 2017). One study examined long-term CHIKV infection in non-human primates and the results suggested that CHIKV can persist mainly in mononuclear cells; specifically macrophages appeared to be the main cellular reservoir during the late stages of CHIKV infection (Labadie et al., 2010). This is in agreement with what has been previously shown *in vitro*; CHIKV can infect monocyte-derived macrophages and primary fibroblasts but cannot replicate in lymphoid or monocytoid cells lines, primary lymphocytes, monocytes or monocyte-derived dendritic cells (Sourisseau et al., 2007). In contrast to CHIKV, there are comparatively few published studies on MAYV replication and tissue tropism is largely unknown. A very recent study characterized MAYV infection in mouse bone-marrow derived-macrophages and found that MAYV infection induces the expression of inflammasome proteins such as Caspase-1 (de Castro-Jorge et al., 2019) but the susceptibility of human cells to MAYV remains unknown. Thus, in this chapter I describe the use of peripheral blood mononuclear cells

(PBMCs) isolated from healthy adult donors to investigate the susceptibility of specific cell types in blood to MAYV. In addition, I used $CD14^+$ monocytes differentiated into macrophages isolated from healthy adult donors to characterize MAYV replication in these cells with the aim of understanding how MAYV infection alters the inflammatory profile of macrophages.

5.2 Results

5.2.1. MAYV replicates in Vero and A549 cell lines

There are limited studies showing MAYV replication in cell types and as such, my first approach was to assess MAYV-replication in common cell lines used in the lab. I infected Vero and A549 epithelial cells with MAYV at a MOI of 1 or 0.1 and collected supernatants at several time points post-infection. Vero cells were found to be highly susceptible to infection (**Figure 5.1A**). This is not very surprising as Vero cells are IFN deficient (Desmyter et al., 1968). A549 cells were also susceptible but the rate of MAYV replication was slower in comparison to Vero cells (**Figure 5.1B)** even though the virus replicated to similarly high titers (~10^6-10^7 pfu/mL) in both cell types.

A.

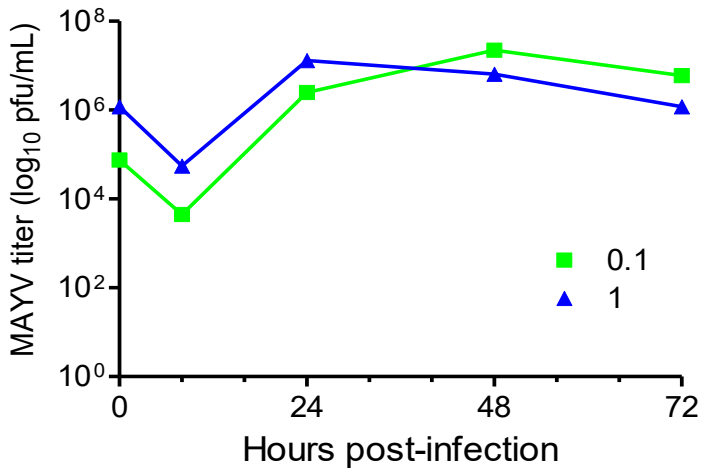

B.

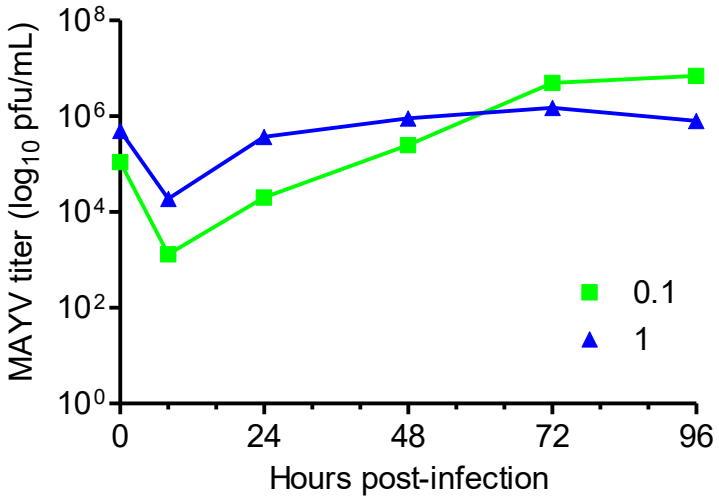

Figure 5.1. **MAYV replication in cell lines**. **A**. Vero or **B.** A549 cells were infected with MAYV at an MOI of 0.1 or 1 and culture supernatants were collected 8, 24, 48, 72 and 96 hours post-infection. Viral titers (shown as $\log_{10}$ pfu/mL) were determined by plaque assay. Average values from two independent experiments are shown.

5.2.2 Flow cytometric analysis of MAYV-infected cells in peripheral blood mononuclear cells

To investigate the susceptibility of human PBMCs to MAYV *in vitro*, PBMCs were obtained from adult healthy donors from the buffy coats following Histopaque density centrifugation. The $CD14^+$ monocytes were sequentially isolated from the buffy fraction using CD14-specific magnetic beads (for details on purification protocol refer to Materials and Methods section 2.2.9). The $CD14^+$ monocytes were infected with MAYV as were cells that were differentiated into macrophages with M-CSF treatment for 7 days prior to infection. Meanwhile, the CD14-depleted population was infected with MAYV. All suspension and adherent cells were collected 48 hours post-MAYV infection. Cells were stained with the LIVE/DEAD cell viability dye and surface stained for either CD14, CD3, CD19 or CD11c prior to fixation and permeabilization. Rabbit anti-capsid antibody was used for intracellular staining prior to analysis by flow cytometry. As shown in **Figure 5.2A**, MAYV antigen (i.e. capsid) was not detected in monocytes, T cells, B cells or Dendritic cells but was detected in monocyte-derived macrophages (MDMs).

5.2.3 Monocyte-derived macrophages (MDMs) are susceptible to MAYV

To investigate viral replication dynamics in MDMs, $CD14^+$ monocytes were isolated and differentiated into macrophages as previously described. MDMs were infected with MAYV and cells were collected at 24, 48- and 72-hours post-infection.

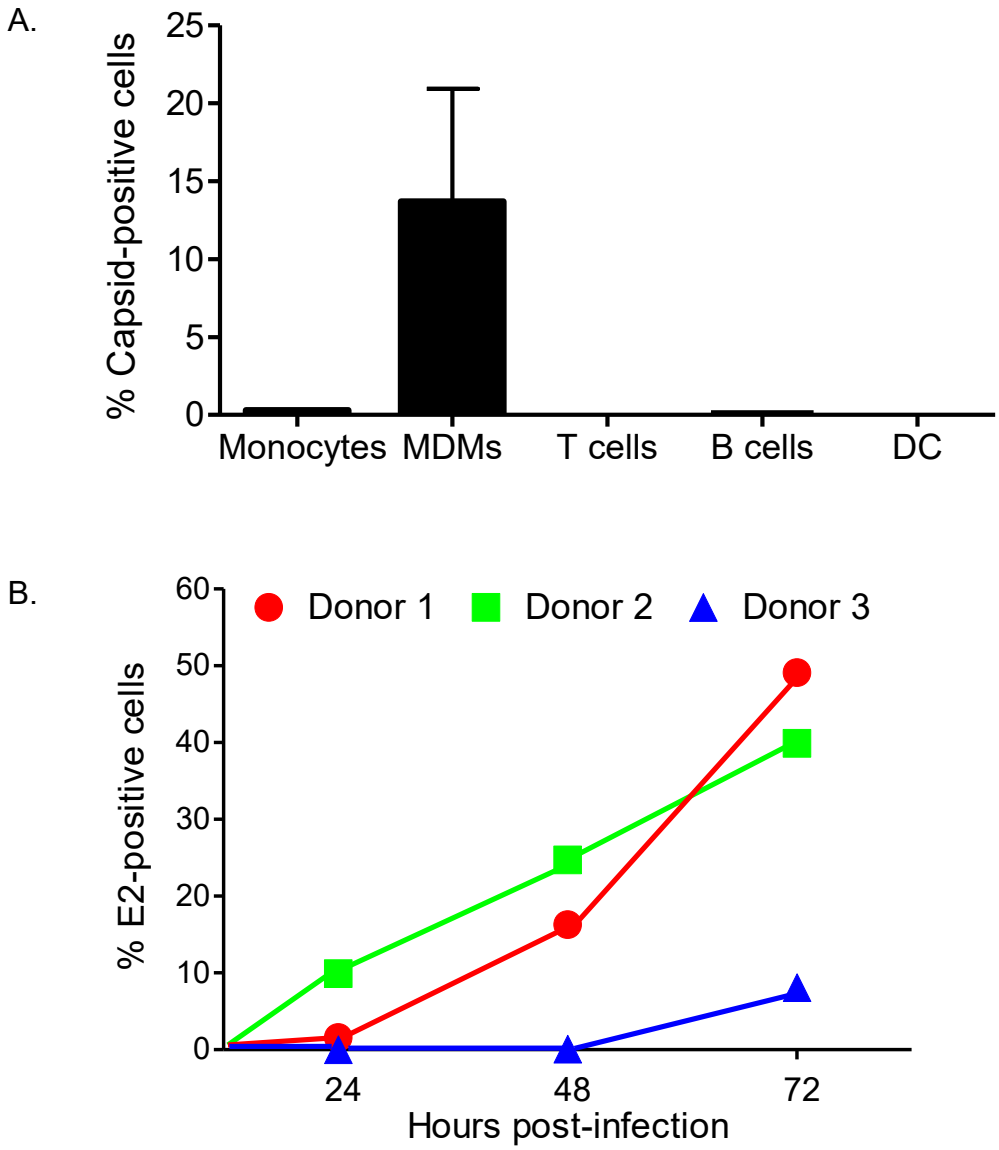

Figure 5.2. Monocyte-derived macrophages (MDMs) are susceptible to MAYV. **A.** MAYV infection of indicated cells as determined by flow cytometry at 48 hours post-infection. **B.** MAYV infection in MDMs as determined by flow cytometry at indicated time points. PBMCs were obtained from adult healthy donors and $CD14^+$ cells were isolated (>95% purity) and infected with MAYV or differentiated into macrophages then infected with MAYV. Meanwhile, the CD14-depleted population was infected with MAYV. All infections were performed at a MOI of 10. The infected CD14-depleted population was surface stained for T cell marker CD3, B cell marker CD19, or Dendritic cell marker CD11c. Cells were then fixed and permeabilized prior to staining for MAYV infection with rabbit anti-capsid antibody or mouse anti-envelope antibody prior to analysis by flow cytometry. Dead cells were excluded by staining with the LIVE/DEAD fixable Near-IR Dead Cell stain kit.

Cells were stained with a viability dye prior to fixation and permeabilization and subsequently stained with an antibody to the viral envelope protein 2 (E2). Shown in **Figure 5.2B** are the data collected from three adult healthy donors. Cells from each of the three donors demonstrated a time-dependent increase in the proportion of cells expressing E2 (**Figure 5.2B**), suggesting that MDMs are permissive to MAYV infection. Some donors demonstrated higher levels of infection (Donor 1 and 2 ~40-50%; Donor 3 ~10%).

To further assess susceptibility of MDMs to MAYV, virus growth curves from supernatant of infected MDMs were performed. In brief, primary $CD14^+$ monocytes were differentiated into macrophages as described previously and infected with MAYV at an MOI of 0.5 or 10. Supernatants were collected from independent wells at several time points post-infection. Data in **Figure 5.3A** and **B** show that viral titers in the supernatants of MAYV-infected MDMs did not increase over time suggesting that infection of this cell type does not result in a productive infection.

5.2.4 Global gene expression changes in MAYV-infected MDMs

To determine how MAYV infection of macrophages affected host cell transcription, RNA sequencing was utilized. $CD14^+$ monocytes were isolated from eight healthy adult donors (4 Female; 4 Male) and differentiated into macrophages as previously described. MDMs were infected with MAYV at a MOI of 10 and duplicate samples were collected 72 hours post-infection for flow analysis and total RNA

A.

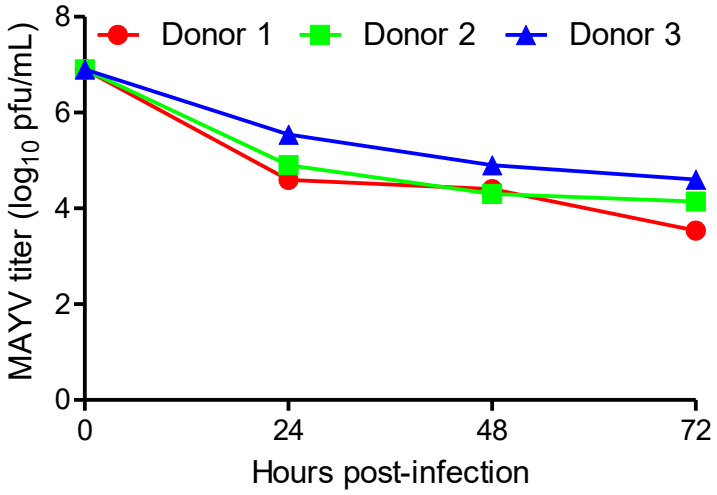

B.

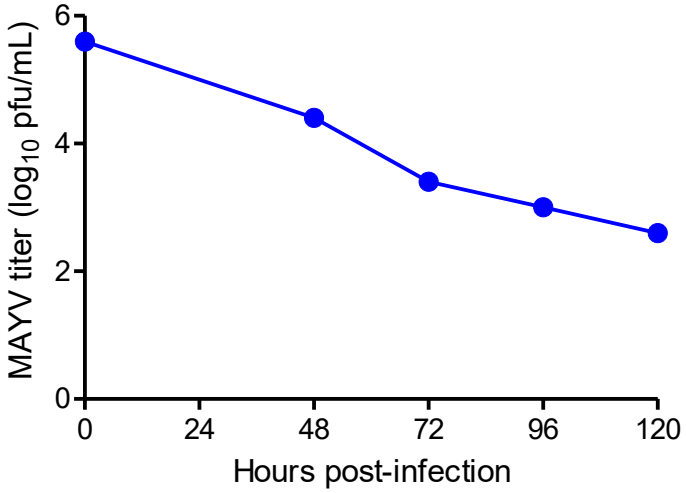

Figure 5.3. Growth curves of MAYV-infected MDMs. CD14^{+} monocytes were isolated from adult healthy donors using CD14-specific magnetic beads and were differentiated into macrophages with M-CSF treatment for 7 days. Cells were infected with MAYV at desired MOI and supernatant was collected at indicated time points. **A.** High MOI growth curve (MOI 10) and **B.** Low MOI growth curve (MOI 0.5).

isolation (**Figure 5.4)**. Flow cytometry analysis of MAYV-infected macrophages revealed donor-specific differences in susceptibility to MAYV, but this was expected (**Figure 5.5)**. The percent infection ranged from ~5-50% among donors (**Figure 5.5A**). Since I am using an antibody to the viral envelope protein 2 (E2) to assess infection in macrophages, I assessed the potential scenario that leftover MAYV virions are phagocytosed by macrophages thus leading to an increase in E2-positive cells in the absence of replication. To address this scenario, I used ultraviolet (UV)-inactivated MAYV (UV-MAYV) as a control and I confirmed that UV-MAYV was inactive by plaque assay. The addition of UV-MAYV to MDMs did not result in an increase of E2-positive cells or cause cell death (**Figures 5.5A and B**). Surprisingly, the level of infection also did not appear to correlate with MAYV-induced cell death (**Figure 5.5B**). The total RNA was isolated and MAYV RNA was detected in all infected samples by qRT-PCR using specific primers to MAYV (**Figure 5.5C**). Total RNA was used for library preparation and RNA-sequencing using a transcriptome panel that detects expression of over 20,000 human genes. There were ~1300 upregulated and ~1500 down-regulated differentially expressed genes (DEGs) (fold change > 2, p-value < 0.05) resulting from MAYV infection of MDMs (**Figure 5.6**). A scatter plot of common DEGs between female and male donors revealed that there were no large gender-based differences in response to virus infection (**Figure 5.7**).

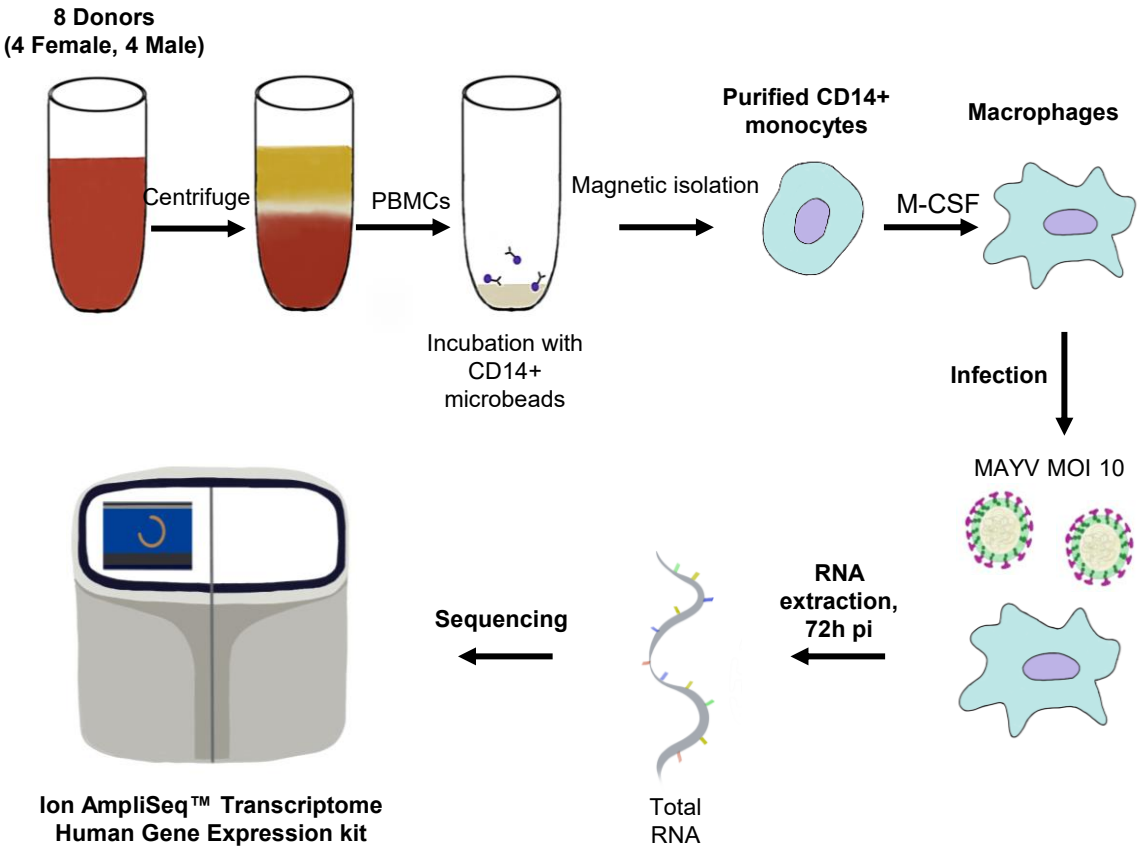

Figure 5.4. Diagram of sample preparation used for RNA-sequencing. $CD14^+$ monocytes were purified from whole PBMCs and differentiated into macrophages with M-CSF treatment for 7 days. Cells were subsequently infected with MAYV (MOI of 10) and total RNA was extracted 72 hours post-infection. Changes in the transcriptome were determined using the Ion AmpliSeq™ Transcriptome Human Gene expression kit and sequenced on the Thermo Fisher Ion S5™ Sequencer.

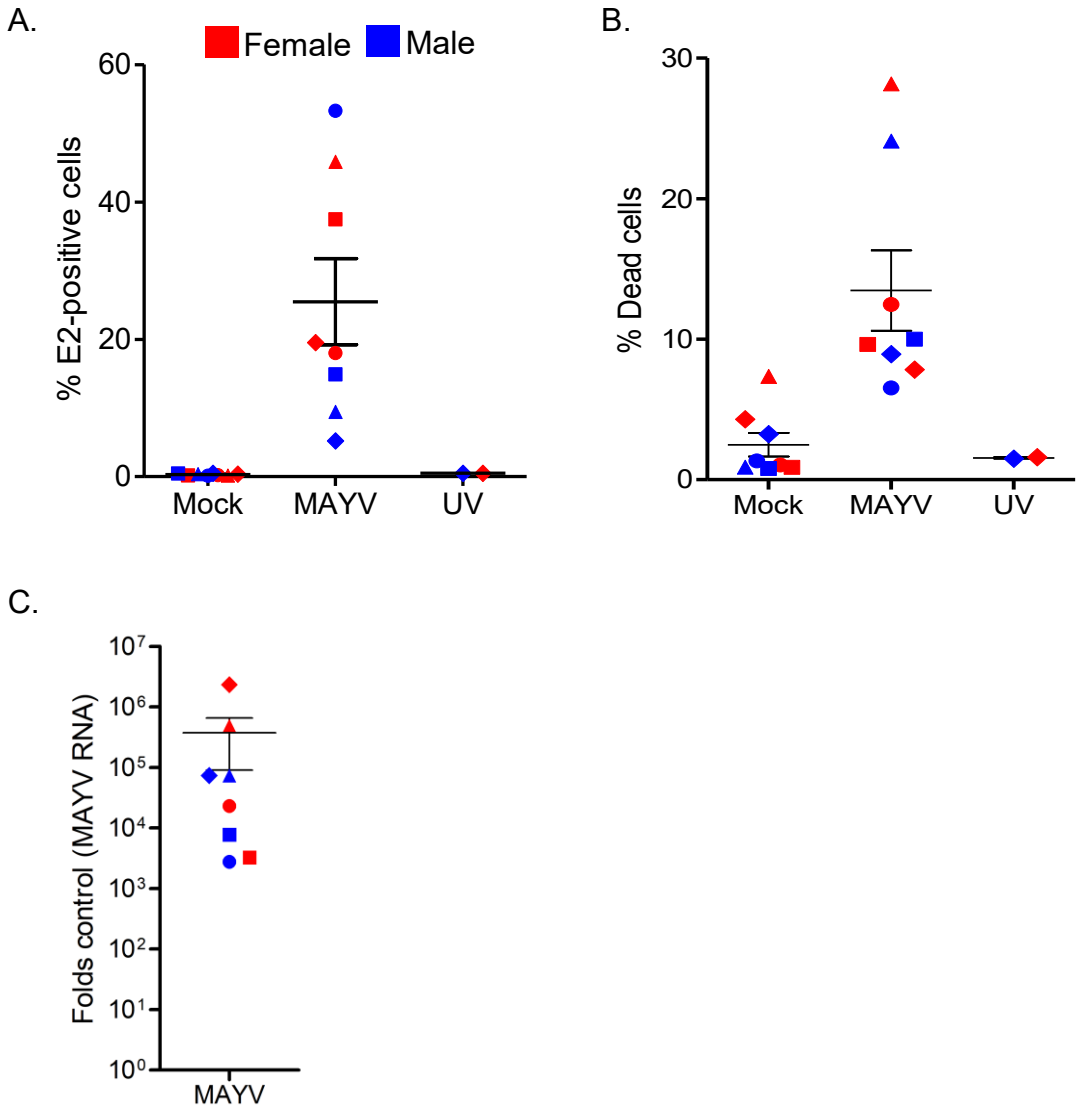

Figure 5.5. MDMs from eight healthy donors show different levels of susceptibility to MAYV. CD14$^+$ monocytes were purified from whole PBMCs and differentiated into macrophages with M-CSF treatment for 7 days prior to infection. Cells were infected with MAYV (MOI 10) and collected at 72 hours post-infection for RNA-Seq and duplicate samples were taken for flow cytometry analysis. **A.** Percentage of cells infected with MAYV in female (Red boxes, n=4) and male donors (Blue boxes, n=4). **B.** Percent of dead cells as determined by staining with the LIVE/DEAD fixable Near-IR Dead Cell stain kit. **C.** Levels of MAYV RNA in donors were determined by qRT-PCR using primers specific for MAYV.

A.

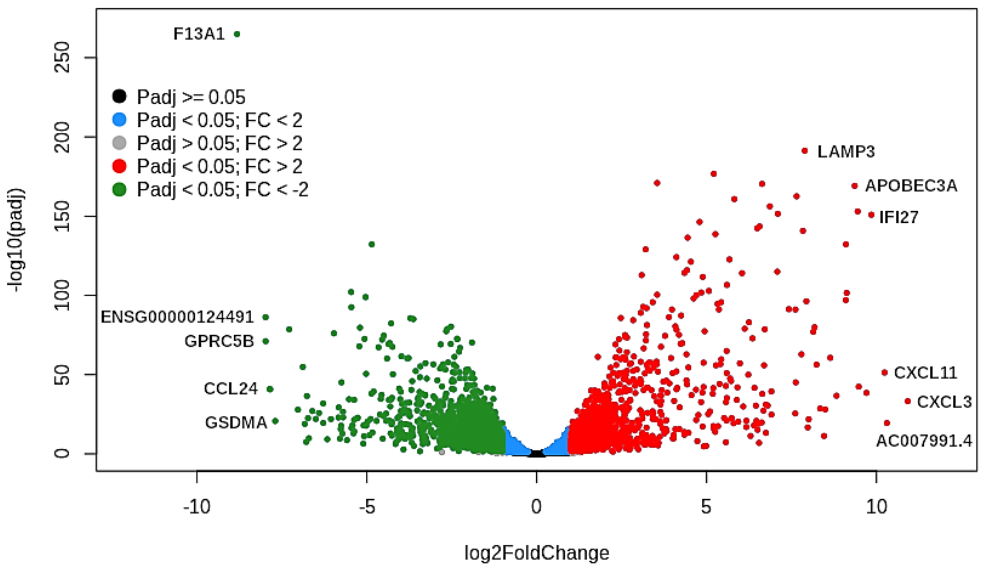

B.

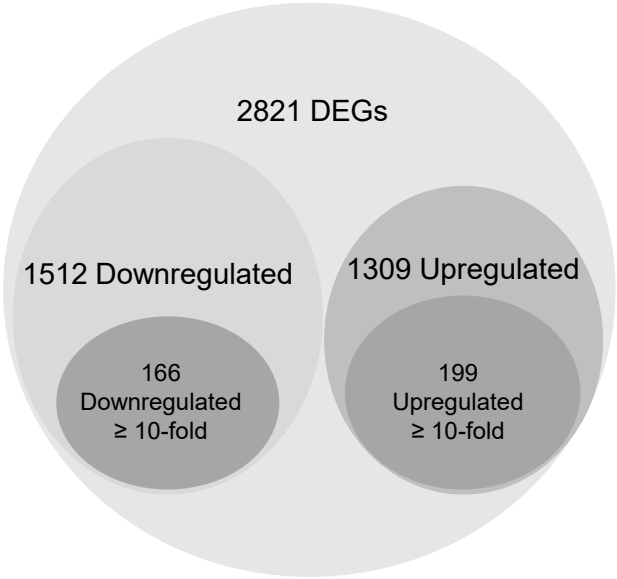

Figure 5.6. MAYV induces dramatic changes in the transcriptome of macrophages. A. Volcano Plot displaying differentially expressed genes (DEGs). Red = Upregulated > 2-fold, Green = down-regulated > 2-fold. **B.** Total global gene expression changes in MAYV-infected MDM cells. All genes with a p-value of < 0.05 are included. In total, 2,821 genes were significantly differentially expressed.

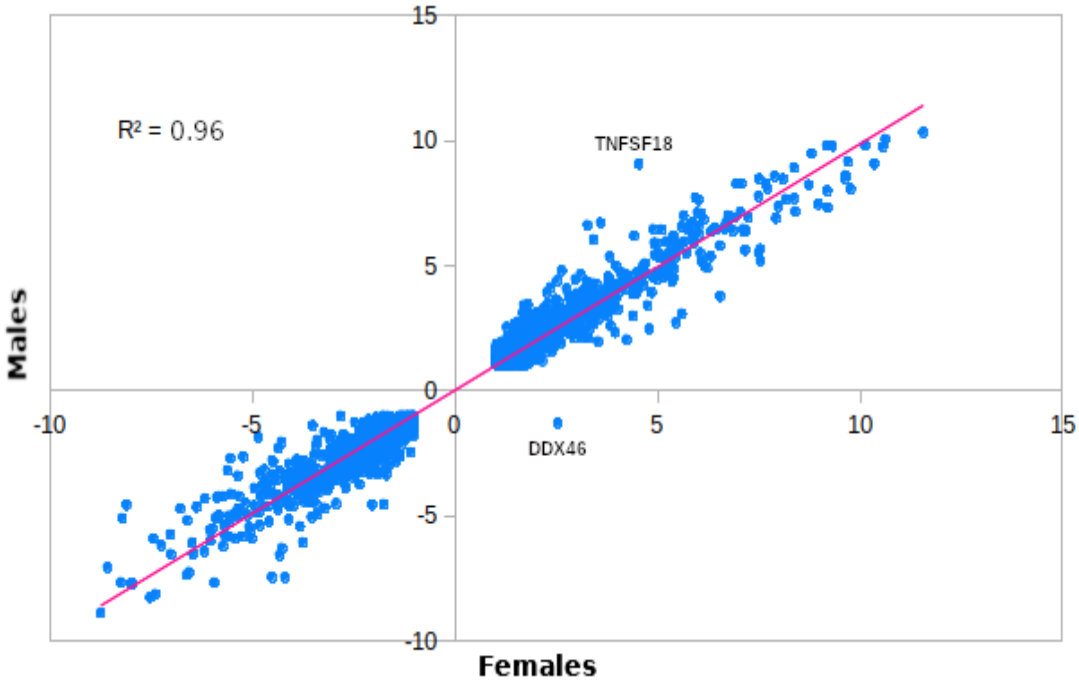

Figure 5.7. Scatter Plot of common DEGs between female and male donors. All DEGs with a p-value of < 0.05 and > 2-fold changes are included. DEGs derived from female donors are plotted on the x-axis, DEGs derived from Male donors are plotted on the y-axis. Values shown are log2FoldChange.

5.2.5 Gene ontology enrichment analysis of upregulated DEGs in MDMs

Gene ontology enrichment analysis was performed on DEGs that were upregulated ≥10-fold (199 genes). Of the top biological processes significantly enriched were 'Interleukin-12 secretion', and 'myeloid dendritic cell chemotaxis' (**Figure 5.8A**). The top molecular functions significantly enriched were 'CXCR3 chemokine receptor binding' and 'CCR chemokine receptor binding' (**Figure 5.8B**). The list of upregulated DEGs was compared against an Interferome database (http://www.interferome.org/interferome/home.jspx) demonstrated that most genes induced by MAYV are regulated by type I and II IFN as can be seen in the Venn diagram in **Figure 5.8C.** The top 20 upregulated DEGs are listed in **Table 5.1.** Interestingly, the highest upregulated genes were chemotactic cytokines (chemokines), a group that included *CXCL13*, *CXCL11,* and *CXCL10.* Together, these data suggest that MAYV-infection of MDMs induces pro-inflammatory genes, many of which are involved in chemotaxis of leukocytes and lymphocytes and thus may play an important role in infiltration of inflammatory cells to sites of infection.

5.2.6 Gene ontology enrichment analysis of downregulated DEGs in MDMs

Gene ontology enrichment analysis was also performed on all down-regulated DEGs ≥10-fold (155 genes) and the top biological processes significantly enriched were 'creatine biosynthetic process', and 'negative regulation of complement activation'. Many of the DEGs were also associated with cell cycle regulation (**Figure 5.9A**). Analysis of down-regulated DEGs using the online server GOrilla showed an enrichment of genes associated with regulation of inflammatory response (**Figure**

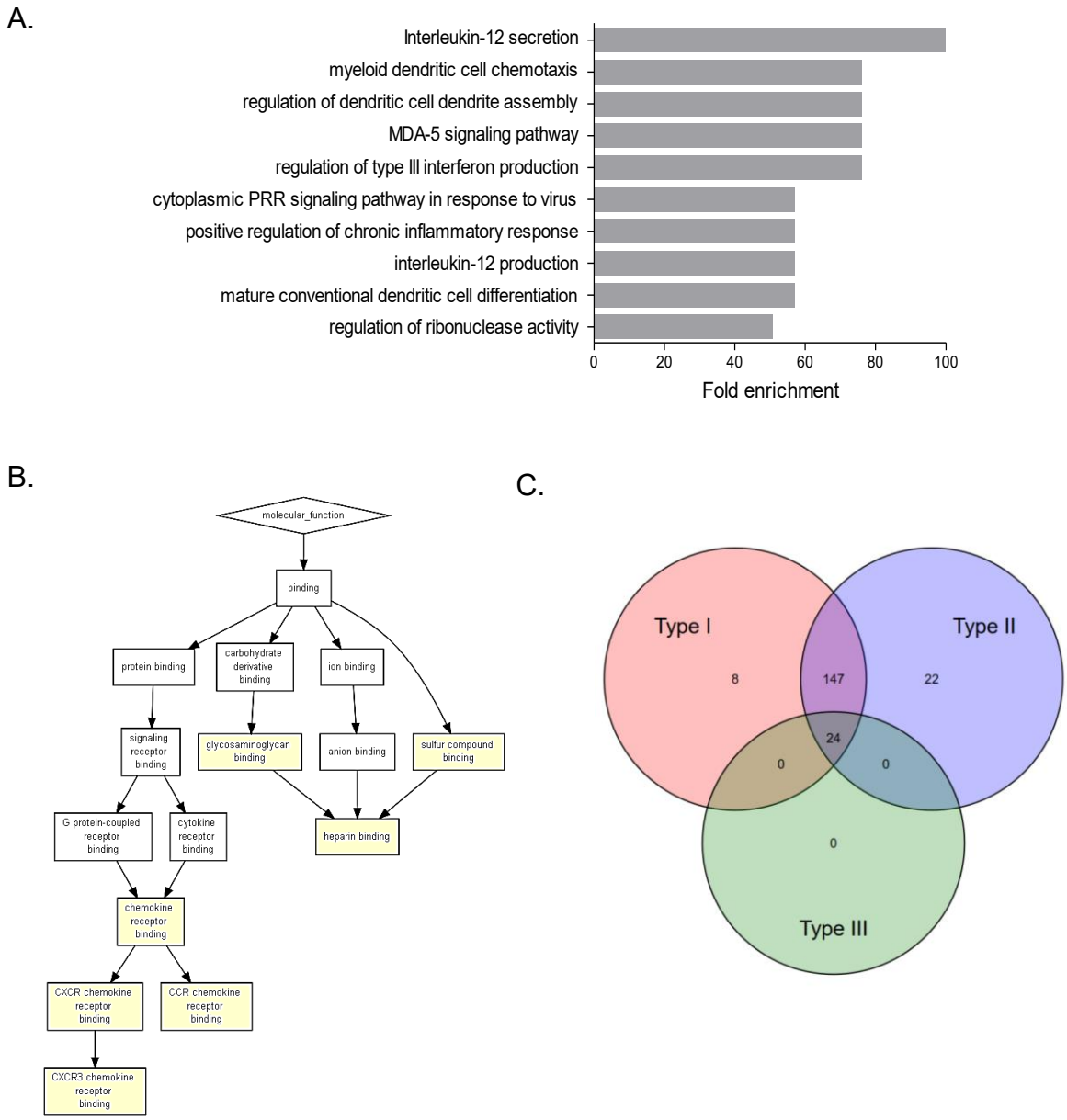

Figure 5.8. Gene Ontology enrichment analysis of up-regulated DEGs in MAYV-infected MDMs. Analysis of all significantly upregulated DEGs ≥ 10-fold analyzed. **A.** Bar chart showing the top enriched terms for 'biological process' ranked by fold enrichment (geneontology.org). **B.** Visualization of DEGs for 'molecular function' using the online server GOrilla. The colour of the box represent the enrichment p-value (light yellow 10^{-3} to 10^{-5}). **C.** Venn diagram of all interferon-associated genes using the Interferome database (http://www.interferome.org/interferome/home.jspx).

Gene	Description	Fold Change
CXCL13	C-X-C motif chemokine ligand 13	1938
CXCL11	C-X-C motif chemokine ligand 11	1207
IFI27	interferon alpha inducible protein 27	922
IDO1	indoleamine 2,3-dioxygenase 1	834
CXCL10	C-X-C motif chemokine ligand 10	712
APOBEC3A	apolipoprotein B mRNA editing enzyme catalytic subunit 3A	697
LAMP3	lysosomal associated membrane protein 3	656
ABTB2	ankyrin repeat and BTB domain containing 2	557
RSAD2	radical S-adenosyl methionine domain containing 2	549
C1S	complement C1s	548
ZBP1	Z-DNA binding protein 1	453
GBP1P1	guanylate binding protein 1 pseudogene 1	399
CCR7	C-C motif chemokine receptor 7	360
CCL19	C-C motif chemokine ligand 19	351
NEURL3	neuralized E3 ubiquitin protein ligase 3	324
ANKRD1	ankyrin repeat domain 1	302
TMEM171	transmembrane protein 171	282
HSH2D	hematopoietic SH2 domain containing	257
DEFB1	defensin beta 1	252
OASL	2'-5'-oligoadenylate synthetase like	245

Table 5.1. List of top 20 up-regulated DEGs (p-value < 0.05).

A.

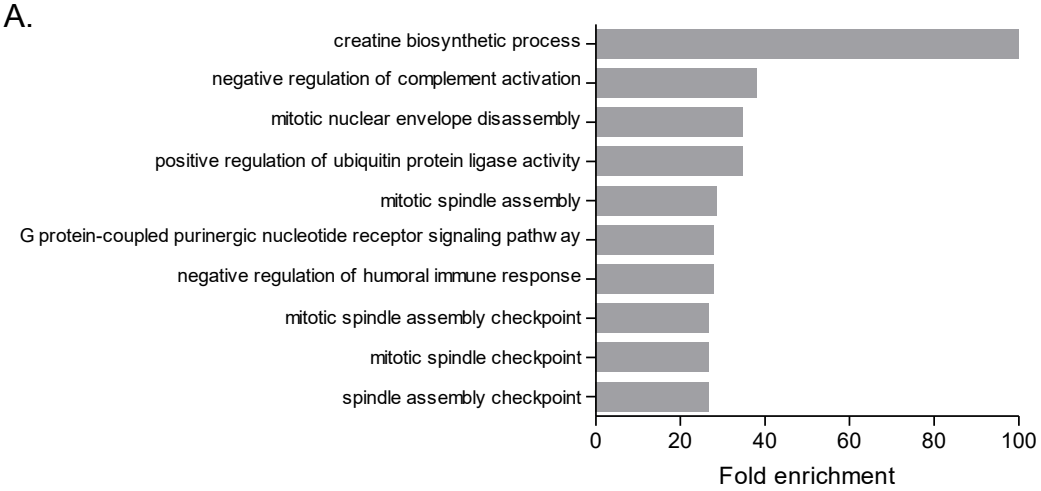

B.

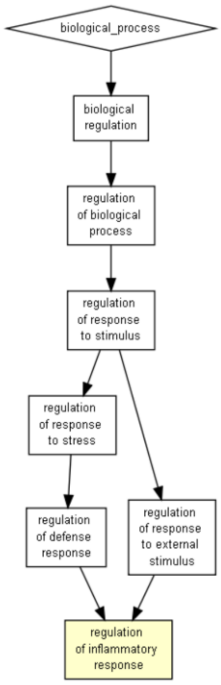

Figure 5.9. Gene Ontology enrichment analysis of down-regulated DEGs in MAYV-infected MDMs. Analysis of all significantly downregulated DEGs ≥ 10-fold were analyzed. **A.** Bar chart showing the top enriched terms for 'biological process' ranked by fold enrichment (geneontology.org). **B.** Visualization of DEGs for 'biological process' using the online server GOrilla. The colour of the box represent the enrichment p-value (light yellow 10^{-3} to 10^{-5}).

5.9B). Shown in **Table 5.2** are the top 20 down-regulated genes. Interestingly, the genes that were down-regulated the most were Coagulation Factor XIII A Chain (F13A1) and G Protein-Coupled Receptor Class C Group 5 Member B (GPRC5B), both of which appear to play important roles in inflammatory disease pathologies (Raghu et al., 2015; Wang et al., 2019). These data suggest that MAYV-infection of primary macrophages causes dysregulation of genes involved in mitosis, metabolism, and inflammatory responses.

5.2.7 LAMP3/CD63 is upregulated in MAYV-infected cells

One of the most significantly upregulated genes (~660-fold) was LAMP3/CD63 which encodes Lysosomal Associated Membrane Protein 3 (LAMP3). LAMP3 is a tetraspanin protein that localizes to the plasma membrane, late endosomal and lysosomal membranes and has been reported to play a role in other viral infections such as Influenza A (Zhou et al., 2011) and Epstein Barr virus (Hurwitz et al., 2017). Moreover, it was shown that the alphavirus envelope proteins E1and E2 trafficked to a LAMP3-positive compartment and incorporated this protein into virions (Ng et al., 2008). I used qRT-PCR as an independent method to validate that the transcript level of LAMP3 is in fact upregulated in MAYV-infected macrophages (**Figure 5.10A**) and A549 cells (**Figure 5.10B**). To investigate if the observed increase of *LAMP3* was IFN-regulated, I infected Vero cells (which lack the ability to produce IFN (Desmyter et al., 1968)) and quantified the transcript level of LAMP3 by qRT-PCR. LAMP3 transcripts were upregulated ~25-fold in MAYV-infected Vero cells (**Figure 5.10C**), which may

Gene	Description	Fold Change
F13A1	coagulation factor XIII A chain	-453
GPRC5B	G protein-coupled receptor class C group 5 member B	-253
SPTLC3	serine palmitoyltransferase long chain base subunit 3	-234
CCL24	C-C motif chemokine ligand 24	-230
GSDMA	gasdermin A	-208
HGF	hepatocyte growth factor	-156
GPR34	G protein-coupled receptor 34	-131
ADAMTS10	ADAM metallopeptidase with thrombospondin type 1 motif 10	-118
CACNA2D3	Calcium voltage-gated channel auxiliary subunit alpha2delta3	-114
RRM2	ribonucleotide reductase regulatory subunit M2	-110
ASPM	Abnormal spindle microtubule assembly	-109
COBLL1	Cordon-blue WH2 repeat protein like 1	-106
MKI67	Marker of proliferation Ki-67	-105
BIRC5	Baculoviral IAP repeat containing 5	-97
MAMDC2	MAM domain containing 2	-91
DLGAP5	DLG associated protein 5	-78
KIF20A	Kinesin family member 20A	-78
P2RY13	Purinergic receptor P2Y13	-72
RGS18	Regulator of G protein signaling 18	-67
IGF1	Insulin like growth factor 1	-63

Table 5.2. List of top 20 down-regulated DEGs (p-value < 0.05).

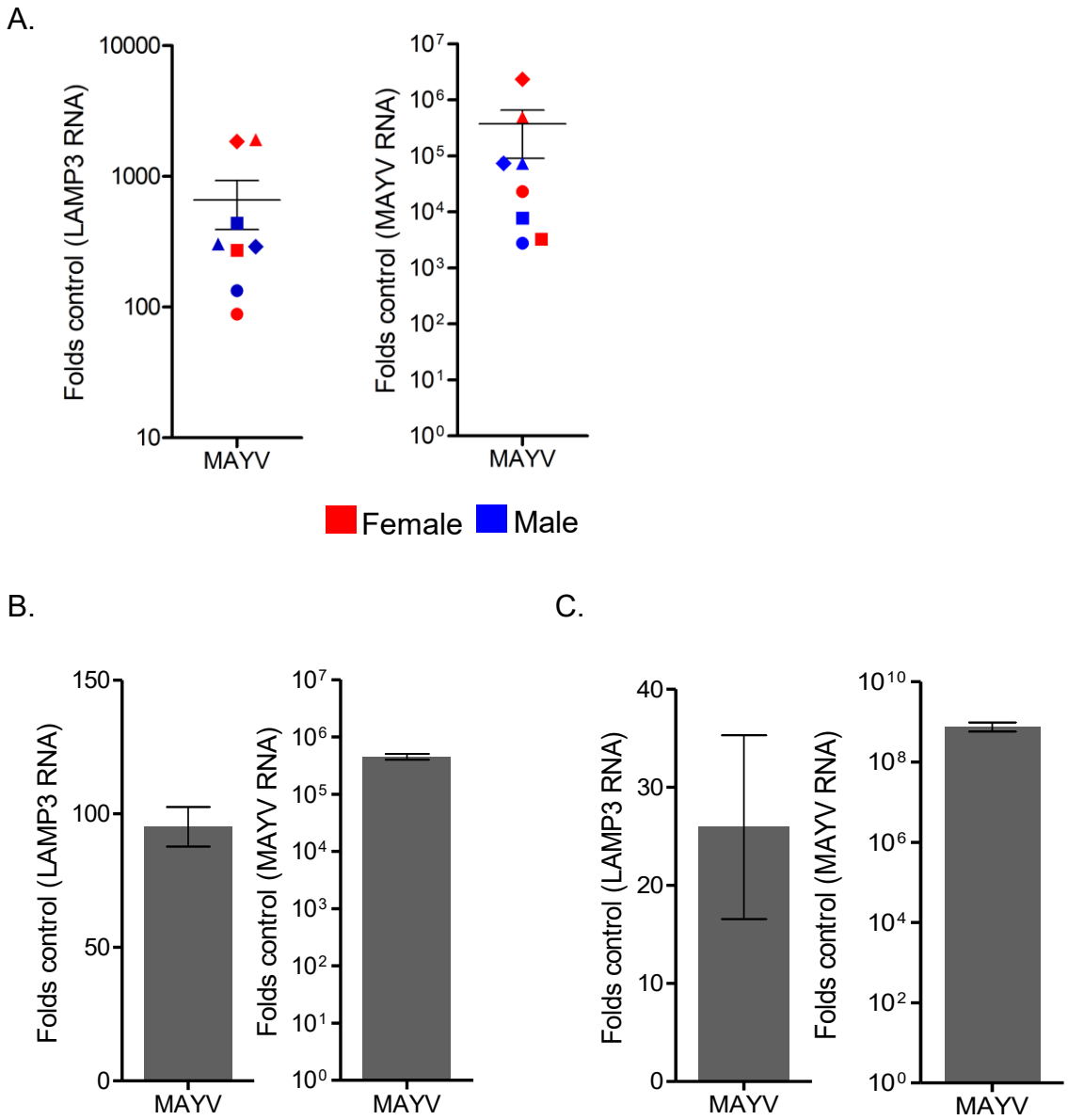

Figure 5.10. LAMP3/CD63 is transcriptionally upregulated in MAYV-infected cells. Cells were infected with MAYV at an MOI of 10, total RNA was extracted and subjected to qRT-PCR with primers for MAYV RNA and LAMP3 in **A.** MDMs **B.** A549 or **C.** Vero cells. The results from 2 independent experiments are shown.

indicate that upregulation of *LAMP3* involves a mechanism independent of IFN and/or that transcriptional changes induced by MAYV are cell type dependent.

To examine if the protein level of LAMP3 was upregulated in MAYV-infected cells, A549 cells were infected and were observed by immunofluorescence microscopy using antibodies to LAMP3 and capsid. As depicted in **Figure 5.11**, there was a ~2-fold increase in the total gray value per cell of LAMP3 in MAYV-infected cells.

5.2.8 LAMP3 protein levels persist despite small interfering RNA-mediated knockdown

To further examine the role of LAMP3 on MAYV replication, I used two different small interfering RNAs (siRNAs) to knockdown expression of LAMP3 prior to infection. In brief, A549 cells were transfected with siNon-targeting control (siControl) or siLAMP3 #1 or siLAMP3 #2 for 48 hours. Samples for RNA and western blot analysis were collected at 48 hours post-siRNA transfection or cells were infected with MAYV and supernatants were collected at 48 hours post-infection for plaque assay. The mRNA level of LAMP3 in siLAMP3-transfected cells decreased ~80% (**Figure 5.12A**), however, the protein level of LAMP3 was not affected (**Figure 5.12B**). The results of the plaque assay are shown in **Figure 5.12C**. Of note, follow-up experiments using a set of four pooled siRNA to knockdown LAMP3 were also unsuccessful due to the inability to knockdown protein levels sufficiently (>50%) without affecting cell viability. Thus, the role that LAMP3 plays on MAYV-infection is yet to be elucidated.

A.

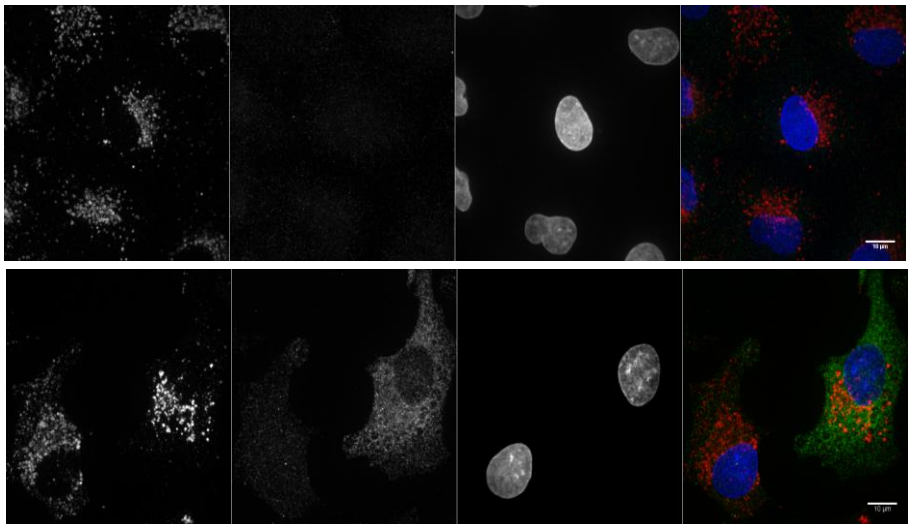

B.

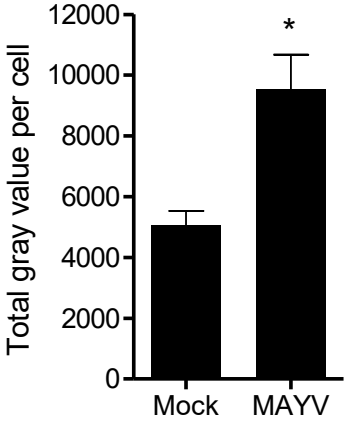

Figure 5.11. LAMP3/CD63 is upregulated in MAYV-infected cells. A. A549 cells were infected with MAYV and fixed 24 hours post-infection. Anti-CD63 antibody and anti-Capsid antibody were used for staining. Shown is 60x magnification. **B.** Analysis of mock and MAYV-infected cells. Shown is the total gray value per cell of CD63-stained cells. Total gray value was determined by calculating the sum of gray values of all pixels in an outlined cell and then normalized by dividing by the area of selection (total cell area). At least 30 cells for each condition was included in the analysis. Only cells positive for Capsid staining were included in the analysis of infected cells. Scale Bar represents 10 µm. Data were subject to t-test analyses (* $P \leq 0.05$).

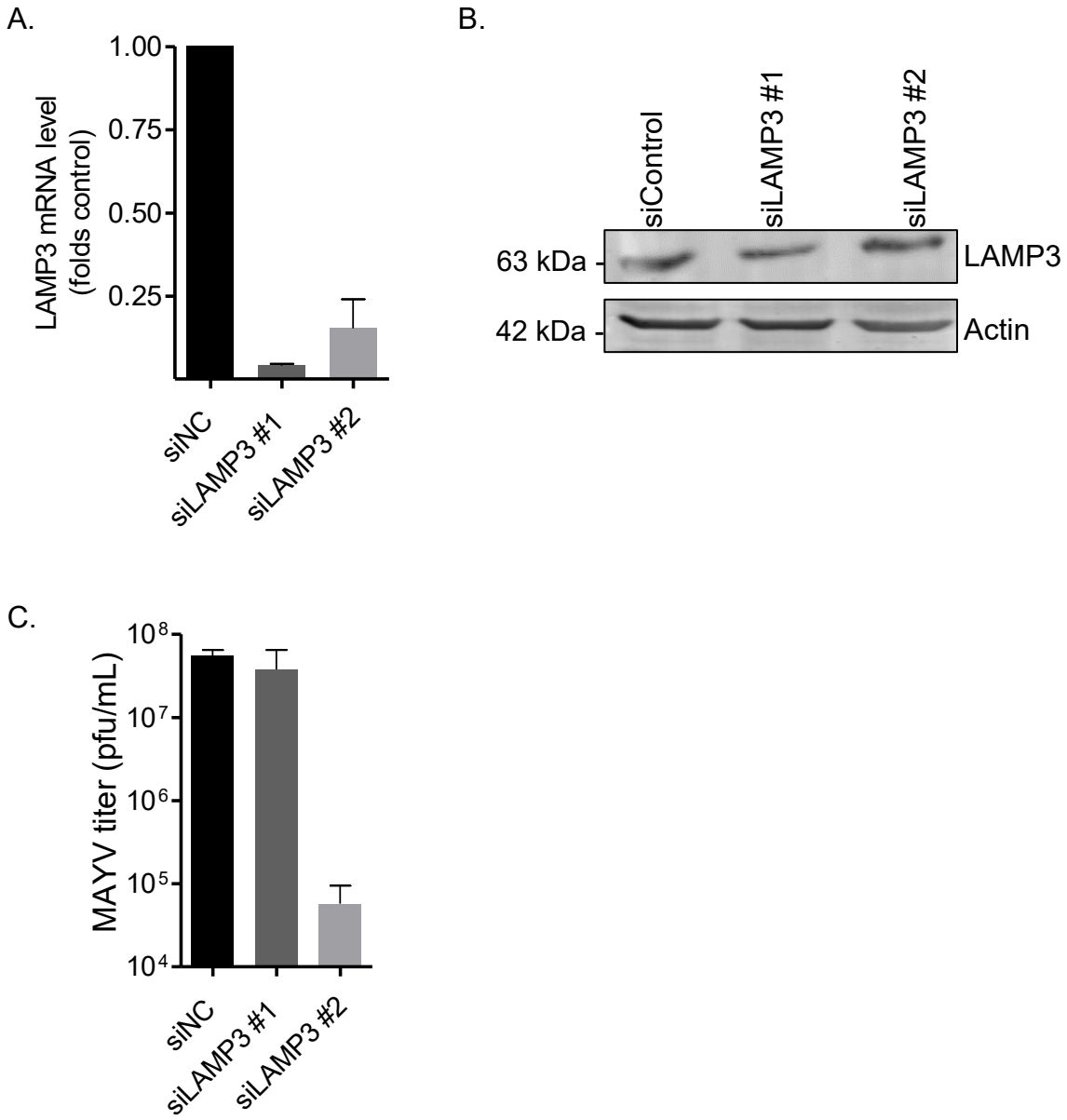

Figure 5.12. siRNA mediated knockdown of LAMP3. A549 cells were transfected with siControl, siLAMP3 #1 or siLAMP3 #2, 48 hours post-transfection cells were infected with MAYV and supernatant was collected at 48 hours post-infection. **A.** Transcript level of LAMP3. **B.** Protein level of LAMP3. **C.** MAYV titer as determined by plaque assay. Shown are averages from two experiments. The results from 2 independent experiments are shown.

5.3 Summary

Identifying the host cells that are susceptible to MAYV will aid in understanding the pathogenesis and in development of novel therapeutics. Vero and A549 cells were found to be highly susceptible to MAYV-infection. To investigate which human primary cells were permissive to MAYV infection, I isolated and infected PBMCs from healthy adult donors and gated on major immune subsets by flow cytometry. Additional staining for MAYV capsid protein demonstrated that virus antigen was not detectable in monocytes, dendritic cells, B cells or T cells, however, monocyte-derived macrophages were permissive for infection based on the observation that they stained positive for the viral capsid protein. Next, RNA-sequencing of MAYV-infected macrophages was performed using total RNA isolated from four female and male adult healthy donors. The data in this chapter show that there were large differences in MAYV susceptibility among the donors, but MAYV-infection led to modest induction of cell death and MAYV RNA was detected in all donors.

MAYV-infection lead to dramatic changes in the host transcriptome of MAYV-infected macrophages with ~1300 upregulated and ~1500 down-regulated DEGs. RNA-sequencing of samples revealed that there were no major gender-based differences in response to viral infection. Most of the upregulated DEGs were chemotactic cytokines and included *CXCL13*, *CXCL11,* and *CXCL10.* The top biological processes significantly enriched was 'IL-12 secretion'. Gene ontology enrichment analysis was performed on all down-regulated DEGs and the most enriched process was 'creatine biosynthetic process' but many genes involved in cell cycle

regulation were also identified. Collectively, these data suggest that MAYV-infection of MDMs induces a robust dysregulation of genes involved in proinflammatory responses that can lead to chronic inflammation and associated pathology.

Transcripts encoding the tetraspanin protein LAMP3 (also known as CD63) was also upregulated by MAYV infection. Follow up LAMP3-knockdown experiments were unsuccessful thus the role that LAMP3 plays on MAYV-infection is yet to be elucidated.

This is the first study to examine the effect of MAYV-infection in primary human macrophages. In this chapter I show that MDMs are susceptible to MAYV, that infection leads to a modest amount of cell death, and that MAYV-infection of MDMs leads to large global gene expression changes. Collectively, the data presented in this chapter provides insight into the role macrophages play in MAYV-induced chronic inflammation and disease pathology.

Chapter 6

Discussion and Perspectives

6.1 Synopsis

My thesis work focused on identifying the mechanisms by which arboviruses hijack cellular pathways and cause disease. In Chapter 3, I showed that expression of seven different flavivirus capsid proteins induced phosphorylation of Akt and protected cells from Fas-dependent apoptosis through a mechanism that requires activated Akt. As such, I will begin this chapter by discussing the numerous ways that viruses manipulate the PI3K/Akt signalling pathway and how this is beneficial for completion of viral replication cycles.

In Chapter 4, I showed that expression of flavivirus capsid proteins causes global transcriptional changes in host cells and further identified a plausible mechanism by which ZIKV capsid subverts the interferon induction pathway. As such, I will discuss mechanisms by which ZIKV and other flaviviruses subvert the IFN induction pathway. Moreover, I will discuss the various mechanisms that have been proposed for flavivirus capsid-mediated evasion of innate immunity.

Lastly, in Chapter 5, I identified monocyte-derived macrophages (MDMs) as cells that are permissive to MAYV infection and observed that MAYV-infection causes a robust dysregulation in the host transcriptome of these cells. I will examine how MAYV-infection alters macrophages, the consequences, and extrapolation to chronic inflammation and associated virus-induced pathology. I will finish this section by examining the role of the protein LAMP3/CD63 in MAYV, alphavirus and other viral infections.

6.2 Viral activation of PI3K/Akt-signalling

To thrive in the host cell environment, viruses must at least temporarily elude multiple anti-viral defence systems that become activated shortly after infection. A common strategy used by DNA and RNA viruses involves activation of the pro-survival kinase Akt (Buchkovich et al., 2008; Diehl and Schaal, 2013). Once activated, the PI3K/Akt pathway regulates several key cellular functions including protein synthesis, cell growth, glucose metabolism, and inflammation (Liu and Cohen, 2015). Thus, viruses have found diverse ways to hijack this pathway to exert an effect in host cells.

6.2.1 Viral entry

Several viruses exploit the PI3K/Akt pathway to facilitate viral entry. For example, Zaire Ebola virus (ZEBOV) induces phosphorylation of Akt shortly after exposure of cells to both active and radiation-inactivated ZEBOV (Saeed et al., 2008). This suggests that PI3K-mediated signalling is necessary for ZEBOV entry, albeit the precise mechanism by which Akt is activated remains unknown. Human cytomegalovirus (HCMV) activates PI3K shortly post-infection and like ZEBOV, viral replication is not required to induce PI3K activity (Johnson et al., 2001). Hepatitis C virus (HCV) also transiently activates Akt during the early stages of viral infection by a mechanism that again, does not require viral replication (Liu et al., 2012). It is thought that this activation is mediated by interaction between HCV E2 and its two co-receptors

CD81 and claudin-1. Interestingly, flaviviruses such as JEV and DENV activate Akt within 1 hour post-infection and when PI3K was blocked using an inhibitor, apoptosis was seen to occur at an early stage of infection (Lee et al., 2005). The activation of PI3K/Akt by flaviviruses is rapid, thus binding of virion to host cell receptors appears to be sufficient for this process. However, it is likely that a more sustained phase of Akt activation occurs later in infection.

6.2.2 Cell survival

Akt kinase plays multiple roles in preventing cell death, one of which is through inhibitory phosphorylation of the pro-apoptotic Bcl-2 family member Bad (Datta et al., 1997; Fiandalo and Kyprianou, 2012). Akt also phosphorylates and inactivates Forkhead box O (FOXO) transcription factors (Brunet et al., 1999). As well as inactivating them, phosphorylation of FOXO transcription factors results in their nuclear exclusion and degradation in the cytoplasm which in turn prevents transcription of FOXO-dependent genes that induce apoptosis. Moreover, Akt can directly phosphorylate and inhibit caspase-9 (Cardone et al., 1998). Finally, expression of a constitutively active Akt was shown to increase c-FLIP expression in tumor cells and this led to resistance to apoptosis (Panka et al., 2001).

Both DNA and RNA viruses have evolved to encode proteins that function to activate PI3K/Akt signalling after entry occurs. For example, Vaccinia virus and Cowpox virus activate Akt signalling to keep infected cells alive (Soares et al., 2009)

whereas HCV activates this pathway to enhance both entry and translation through a mechanism that requires binding of the viral protein NS5A to PI3K (He et al., 2002). Binding of NS5A stimulates of PI3K-mediated signalling and protects HCV-infected cells from apoptosis (Shi et al., 2016; Street et al., 2004). Influenza A virus NS1 also binds to and activates PI3K, leading to an inhibition of caspase-9 and limiting virus-induced cell death (Ehrhardt et al., 2007). Previous research in our lab showed that expression of the WNV capsid protein protects cells from Fas-mediated apoptosis through a mechanism that requires PI3K activity (Urbanowski and Hobman, 2013). Data shown in Chapter 3 supports a model in which capsid activates Akt by sequestration of Protein Phosphatase 1 (PP-1), a phosphatase that is known to inhibit the activity of Akt (Xiao et al., 2010). Accordingly, in cells expressing capsid protein (as well as in WNV-infected cells), PP-1 cannot dephosphorylate Akt, and thus remains in an active state where it can function in anti-apoptotic pathways (**Figure 6.1**).

In this thesis, I showed that ZIKV and other flavivirus capsid proteins are anti-apoptotic (Airo et al., 2018), however, others have reported contradictory observations. Several papers have suggested that capsid protein is involved in WNV-induced cell death (Bhuvanakantham et al., 2010; Oh et al., 2006; Yang et al., 2008). It is worth noting that these studies used the membrane-anchored form of capsid (123 amino acids), instead of the mature form of capsid (105 amino acids) used in the experiments in this thesis. Only the mature form of capsid is detectable in WNV infected cells, which puts into question the relevance of studies using the membrane-anchored form of capsid to WNV biology (Urbanowski and Hobman, 2013). Moreover, it was

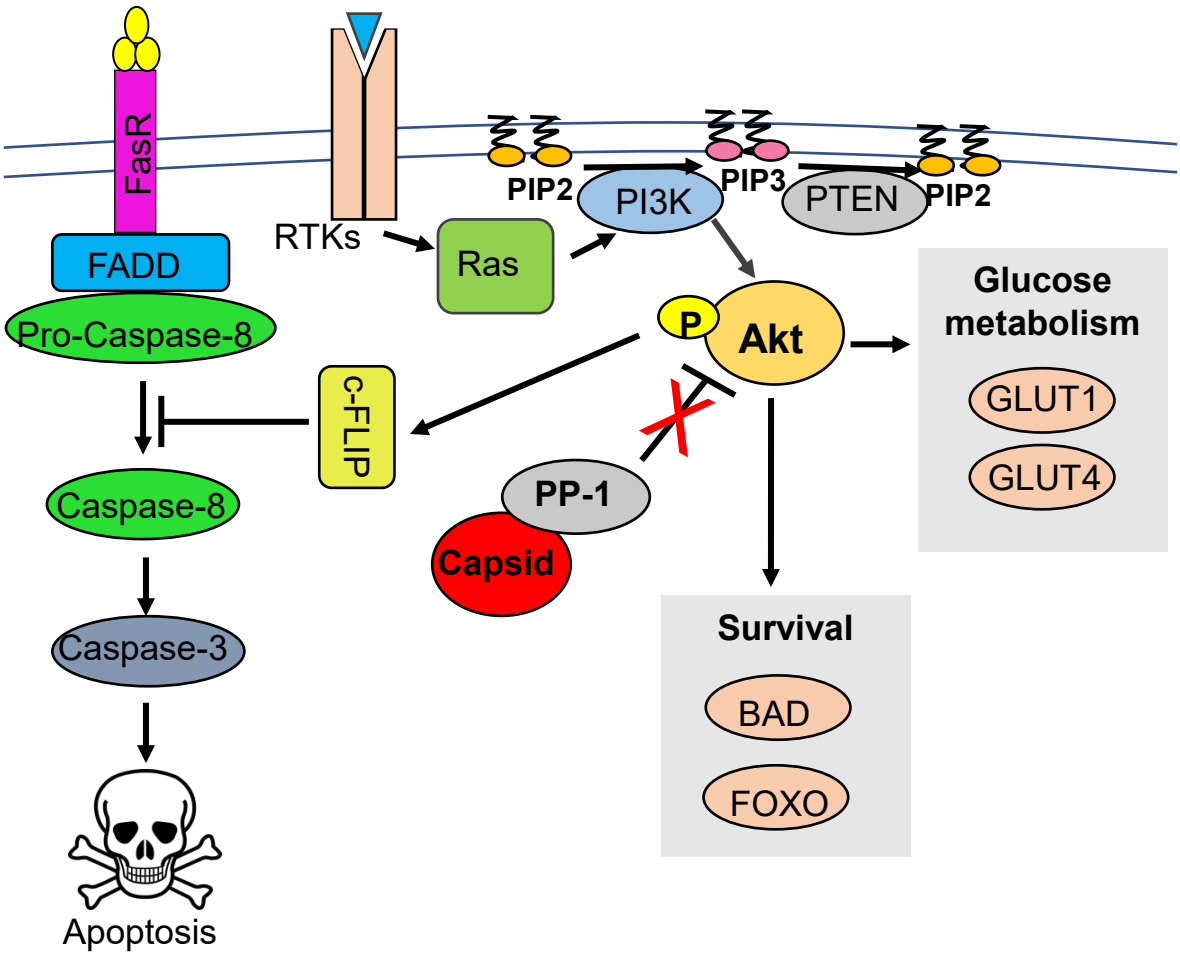

Figure 6.1. Model of how flavivirus capsid proteins increase levels of phospho-Akt. The model is based on the demonstrated interaction between DENV and ZIKV capsid proteins and the phosphatase PP-1. Interaction of phosphatases such as PP-1 that dephosphorylate Akt are prevented by capsid-dependent sequestration, resulting in higher levels of active Akt. Phospho-Akt activates multiple downstream signalling pathways that affect cell survival and metabolism.

recently shown that ZIKV capsid induces ribosomal stress and apoptosis in rat and human neuroprogenitor cells (Slomnicki et al., 2017). The latter paper used the mature form of capsid and thus the discrepancy may be attributed to the use of constructs encoding different capsid strains or to the use of different cells lines.

6.2.3 Metabolism

Many viruses activate PI3K/Akt signalling pathways likely in part to satisfy the energy requirements of viral replication. For example, Mazzon *et al.*, demonstrated that the alphaviruses Semliki Forest (SFV) and Ross River (RRV) increase glycolysis by activating the PI3K/Akt signalling pathway (Mazzon et al., 2018). This process is mediated by the viral protein Nsp3, which binds directly to PI3K and activates PI3K/Akt signalling. Nsp3 contains the well characterized PI3K activation motif "YXXM" and the introduction of a Y369F mutation in this motif resulted in the inability to activate Akt, reduced glycolysis and reduced viral replication. The functions of Nsp3 are not well understood, but it is essential for RNA replication (LaStarza et al., 1994), thus one possibility is that the Y369F mutation affects this function. However, pharmacological inhibition of Akt resulted in reduced SFV replication, highlighting the importance of the PI3K/Akt signalling pathway in SFV replication. One mechanism by which the activation of PI3K/Akt signalling increases glycolysis is by enhancing transcription and membrane translocation of glucose transporters (Chan et al., 2012) such as GLUT1(Barthel et al., 1999), thus facilitating increased transport of glucose into the cytoplasm. This phenomenon is not limited to

RNA viruses as infection of cells with the DNA virus Kaposi sarcoma-associated herpes virus induces Akt hyperphosphorylation resulting in increased GLUT1 trafficking to the plasma membrane (Gonnella et al., 2013).

In keeping with our data, analysis of the transcriptomic landscape of ZIKV-infected cells showed that ZIKV altered genes involved in cellular metabolism in infected cells (Tiwari et al., 2017). These changes are consistent with the concept that viruses have substantial metabolic requirements in order to achieve sustained viral production. For example, DENV infection results in upregulated glycolysis in host cells (Fontaine et al., 2015). Of note, it was reported that interaction of DENV NS1 with glyceraldehyde 3-phosphate dehydrogenase (GAPDH) results in increased energy production (Allonso et al., 2015), however, this process may involve more than one mechanism as Akt activation occurs rapidly in flavivirus-infected cells (Lee et al., 2005). Data presented in this thesis suggest that capsid expression alone is sufficient to increase the metabolic activity of cells by a mechanism that requires PI3K activity.

6.2.4 Perspective: the role of flavivirus capsids in the PI3K/Akt pathway

The primary role of flavivirus capsids is to protect the viral genome during entry and egress from host cells. However, my research indicates that these proteins are also involved in the establishment of a favourable environment conducive to viral replication. It achieves this by in part by subversion of programmed cell death pathways to allow completion of the viral life cycle, and to induce metabolic pathways

that are required to fulfill the high energy cost of viral replication. Data in Chapter 3 show that over expression of capsid alone is sufficient to induce Akt by a mechanism that requires PI3K activity. I also found that capsid expressing cells have increased mitochondrial metabolism, elevated ATP levels and increased expression of GLUT1. Interestingly, capsid proteins did not protect cells from the pro-apoptotic effects of non-structural protein expression. This could mean that capsid proteins only protect infected cells from extrinsic apoptotic signals rather than cell death signalling that can result from cellular detection of viral RNA.

Consistent with our findings, it was recently reported that AR-12, a potent inhibitor of PI3K/Akt signalling, down-regulates DENV-induced Akt activity and limits virus replication (Chen et al., 2017a). AR-12 also showed efficacy against ZIKV both *in vitro* and *in vivo* (Chan et al., 2018). Specifically, ZIKV-infected A129 mice treated with AR-12 at one hour post-infection showed significantly higher survival rates, less body weight loss and lower blood and tissue ZIKV RNA loads (Chan et al., 2018). From a clinical perspective, it would be interesting to determine whether Akt-targeting drugs would be useful for treatment of flavivirus-infected patients. Several compounds have been proven to inhibit Akt with a small number entering clinical evaluation mostly for anticancer therapy (Nitulescu et al., 2018). Combination antiviral treatment using direct acting (virus-targeting) and indirect acting (host-targeting) drugs is an interesting avenue and should be evaluated further.

6.3 Subversion of interferon induction by flaviviruses

In the following section, I will discuss how the ZIKV capsid inhibits production of IFN as a mechanism to avoid recognition by the innate immune response.

6.3.1 Subversion of Type I IFN induction by ZIKV and other flaviviruses

Many studies have characterized the molecular mechanisms by which flavivirus non-structural proteins subvert IFN induction. For example, the NS4A protein of ZIKV binds directly to MAVS via the N-terminal caspase activation and recruitment domain (CARD) that blocks the interaction between RIG-I/MAVS, which is required for induction of type I IFNs (Hu et al., 2019; Ma et al., 2018). The NS3 protein of ZIKV encodes a conserved binding motif for the chaperone protein 14-3-3 and this serves to block 14-3-3-mediated cytosol to mitochondria translocation of RIG-I and MDA5 (Riedl et al., 2019). This is the same strategy used by DENV NS3 (Chan and Gack, 2016). The NS1 and NS4B proteins of ZIKV also inhibit IFN induction but by direct interaction with TBK1; thus, blocking TBK1 oligomerization that is required for IFN induction. Moreover, NS5 of ZIKV inhibits the IFN pathway by interaction with IKKε, a protein upstream of IRF-3 (Lundberg et al., 2019). **Figure 6.2** depicts the multiple ways in which ZIKV non-structural proteins inhibit IFN induction. Curiously, it is not only flavivirus proteins that have been shown to interfere with production of IFN. For example, the subgenomic flavivirus RNA (sfRNA) derived from the 3'UTR of genomic RNA of a DENV epidemic strain can play a role in immune evasion

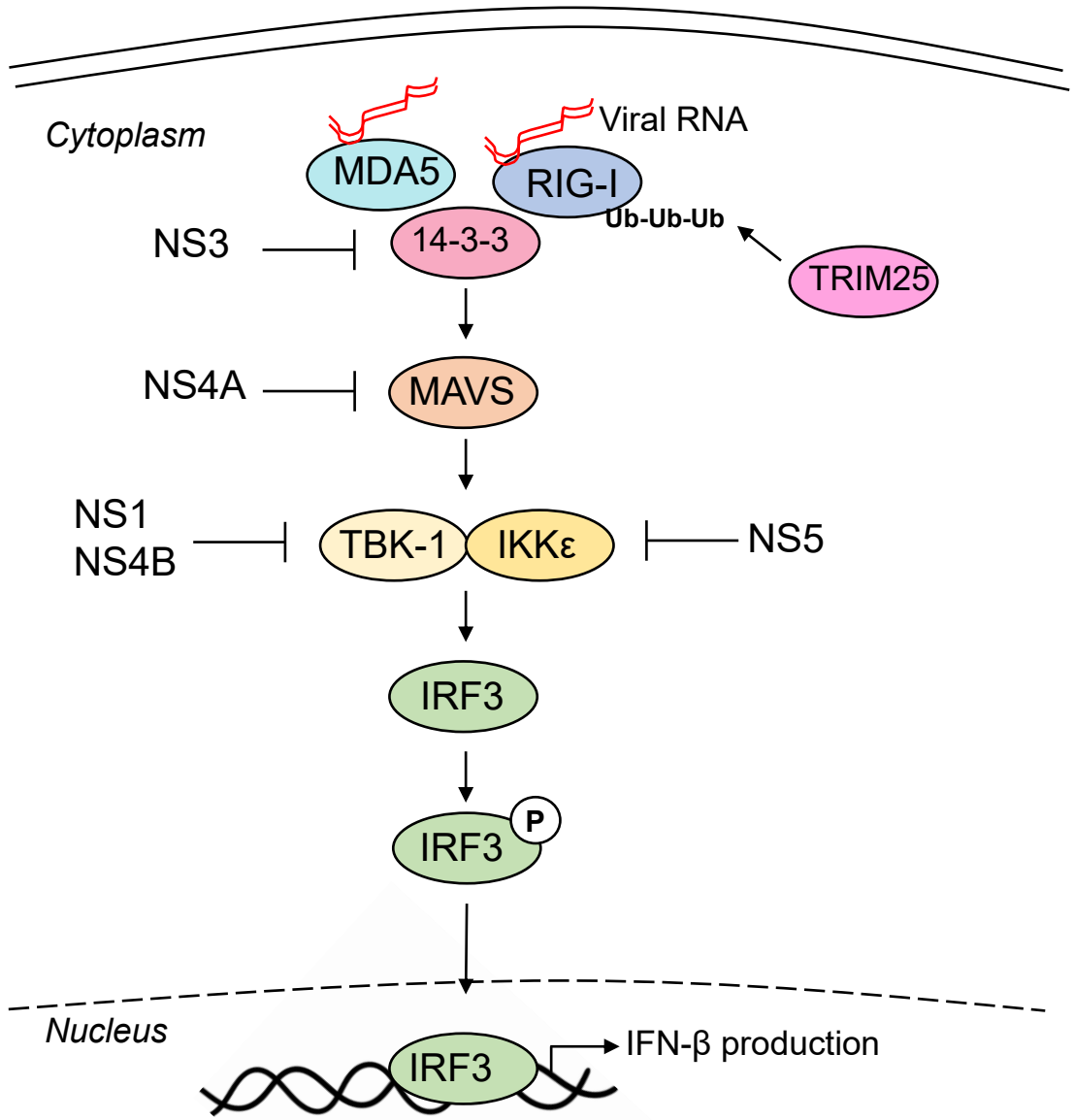

Figure 6.2 Depiction of how ZIKV non-structural proteins inhibit IFN-induction. ZIKV genomic RNA is recognized by the cytoplasmic pathogen recognition receptors MDA5 and RIG-I. MDA5 and RIG-I are activated upon binding of viral RNA. Activation of RIG-I is dependent on polyubiquitination by E3 Ubiquitin ligase TRIM25. The 14-3-3 chaperone protein is required for translocation of MDA5 and RIG-I to the mitochondria, where interaction with adaptor protein MAVS takes place. MAVS leads directly to activation of TBK-1 and IKKε which then phosphorylates the transcription factor IRF-3. Phosphorylated IRF-3 homodimerizes and moves into the nucleus to induce transcription of *IFN* genes.

(Manokaran et al., 2015). It is thought that the sfRNA physically interacts with TRIM25 and blocks TRIM25 mediated polyubiquitination of RIG-I, albeit the details by which this occurs are not clear.

In line with my data, a previous study in our lab reported that transient expression of capsid did not affect the activity of the IFIT1 promoter, suggesting there was no effect on IFN signalling. However, capsid-expression did decrease IFN-β and IRF-3 promoter activity, suggesting that capsid subverts IFN induction, albeit these data were not statistically significant (Kumar et al., 2016). The discrepancy may be explained by the use of different cell lines, such as HEK293T versus A549 cells used in this thesis; or different methods such as a transient over-expression approach versus the lentivirus transduction approach used in this thesis. Of note, the use of chemical-based products such as calcium phosphate or liposomes that are used in transient over-expression approach can lead to cytotoxicity and thus may interfere with the results of sensitive assays.

6.3.2. Flavivirus capsids subvert IFN induction

Several recent papers have suggested a role for flavivirus capsids in the subversion of the innate immune response. Samuel *et al*., identified YFV capsid as well as other flavivirus capsid proteins as potent suppressors of RNA silencing, a possible mechanism to counteract immune responses in both mammalian and insect hosts (Samuel et al., 2016). Previous work identified DEAD Box Helicase 3 X-linked

(DDX3X) as a DENV capsid-interacting protein (Kumar et al., 2018a). DDX3X is an interacting partner of TBK1 and is required for induction of IFN (Soulat et al., 2008), thus, the authors hypothesized that capsid-mediated degradation of DDX3X was a plausible mechanism of IFN subversion, however, this hypothesis did not hold as follow up experiments showed that knock-down of DDX3X did not affect the induction of type I interferon response upon DENV infection. Interestingly, Faustino *et al.,* recently identified influenza virus non-structural protein 1 (NS1) as a structurally similar protein to DENV capsid (Faustino et al., 2019). The authors noted that among its many roles, NS1 is a viral immune-suppressor and they postulated that DENV capsid may also act as an immune-suppressor. Intriguingly, one mechanism by which influenza virus NS1 suppresses the immune system is by interacting with TRIM25 (Gack et al., 2009).

In Chapter 4, data was presented showing that ZIKV capsid interacts with TRIM25, but the molecular details and result of this interaction are unknown. TRIM25-mediated polyubiquitination of RIG-I is required to initiate a signalling cascade that leads to phosphorylation of transcription factors IRF3 and NF-kB (Gack et al., 2007; Okamoto et al., 2018). Thus, one possible scenario is that ZIKV capsid sequesters TRIM25 and subsequently prevents its interaction with and/or ubiquitination of RIG-I.

Our lab reported that flavivirus capsid proteins interfere with biogenesis of peroxisomes (Wong et al., 2019; You et al., 2015). This process is mediated by capsid-dependent sequestration of the peroxisome factor Pex19, which is essential for

formation of new peroxisomes. Since a pool of MAVS is targeted to peroxisomes, these organelles serve as signalling platforms in RIG-I-like receptor (RLR) antiviral immunity (Dixit et al., 2010). It makes sense from a viral perspective to degrade peroxisomes, but previous findings in our lab suggested that capsid did not block the induction of IFN-λ although, to my knowledge, IFN-α/β signalling was not tested. In addition, ZIKV capsid inhibited stress granule assembly by interaction via caprin-1 and G3BP1 (Hou et al., 2017). This is also a potential mechanism of antiviral subversion as it is generally thought that stress granules can restrict viral access to translational machinery (Hou et al., 2017). Interestingly, the stress granule protein G3BP1 binds viral dsRNA and RIG-I to enhance the IFN-β response (Kim et al., 2019). For an overview of the identified ZIKV capsid-interacting proteins involved in IFN induction, see **Figure 6.3**.

6.3.3 Perspective: Examining the role of Flavivirus capsids on evasion of innate immunity

In this study I identified TRIM25 as a ZIKV capsid-interacting partner. Interestingly, knockdown of TRIM25 in cells resulted in increased ZIKV RNA but no effect on titer was observed. Overall, these data suggest that TRIM25 may act a viral restriction factor, however, a full knockout approach may be required to accurately assess the effect of TRIM25 on ZIKV replication. It is also plausible that capsid uses TRIM25-independent mechanisms to subvert the IFN response. Interestingly, in an integrated proteomics approach, Scaturro *et al.,* identified TRIM26 as a ZIKV capsid

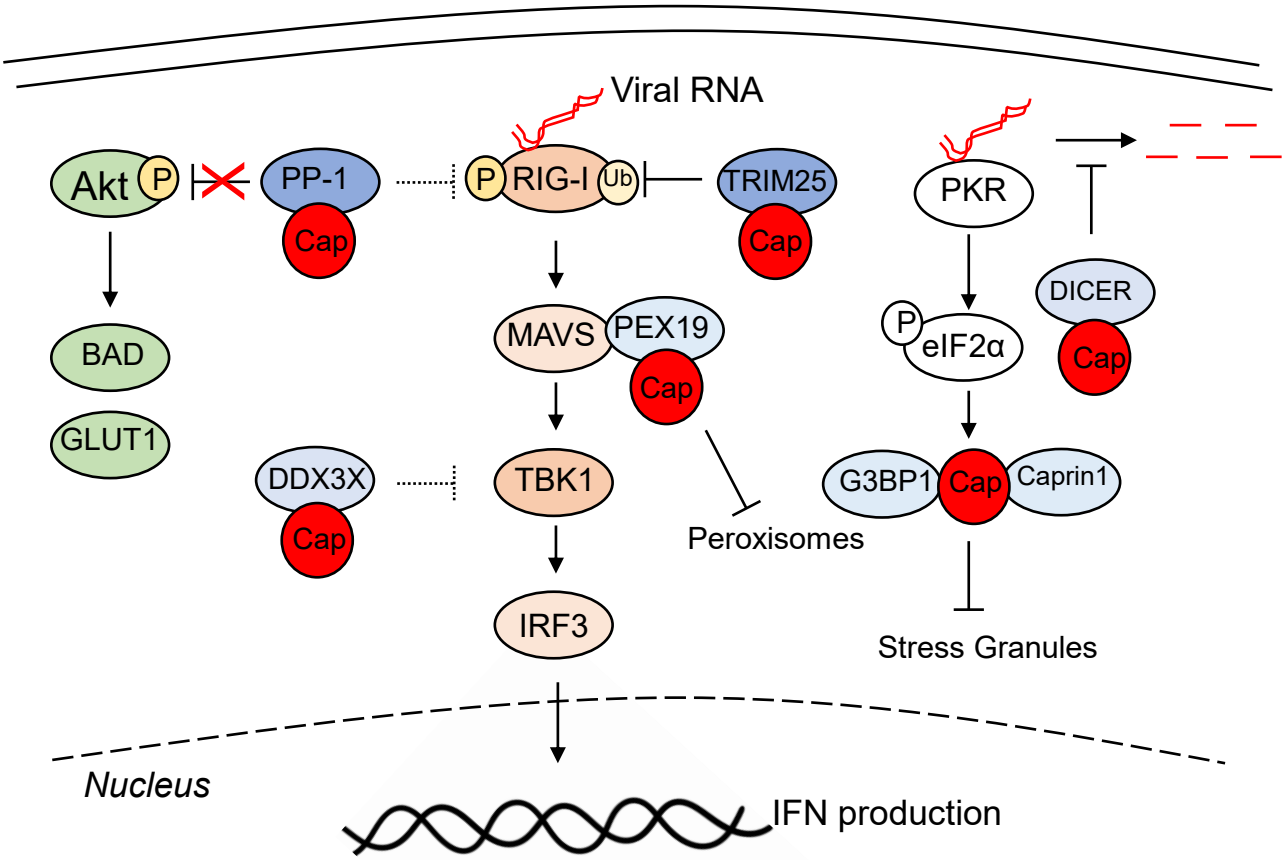

Figure 6.3. Model for how flavivirus capsid proteins inhibit innate immune responses. Proteins depicted in royal blue represent capsid-binding proteins identified in this thesis. Proteins depicted in light blue represent capsid-binding proteins reported in the literature. Proteins depicted in light red represent inhibited pathways. Proteins depicted in green represent activated pathways. Dashed lines represent speculative mechanisms that require further validation.

interacting protein in the cytoplasm (Scaturro et al., 2018). Unlike TRIM25, the role of TRIM26 on innate immune evasion is not clearly defined, but it is possible that a similar mechanism is utilized. In addition, PP-1 is a phosphatase that can dephosphorylate and activate RIG-I (Wies et al., 2013). Intriguingly, we and others found that ZIKV capsid interacts with PP-1, as previously discussed in Chapter 3 (Airo et al., 2018; Scaturro et al., 2018). Thus, it is plausible that flavivirus capsids have evolved several approaches that act synergistically to inhibit the innate immune response.

These studies help elucidate the mechanisms by which flaviviruses such as ZIKV cause human disease. Molecular knowledge of how viruses evade antiviral responses can aid in the rational design of future vaccines and/or therapeutics and in the development of better animal models for future pathogenesis studies.

6.4 Characterization of MAYV infection in primary human macrophages

The studies discussed in the following section focus on the tropism of MAYV infection and how MAYV infection alters the inflammatory profile of human monocyte derived macrophages (MDMs).

6.4.1 Macrophages are target cells of MAYV-infection

Data in Chapter 5 show that while MDMs are permissive for MAYV, infection of these cells did not result in increasing viral titers over time. In contrast, Sourisseau

et al., showed that the closely related alphavirus CHIKV, productively infects MDMs (Sourisseau et al., 2007). Consistent with our findings on MAYV though, CHIKV does not infect lymphoid and monocytoid cell lines, primary lymphocytes or monocytes. Of note, I also infected MDMs with CHIKV and did not observe an increase in viral titer over time which would be expected of a productive infection. There are several possibilities for the observed disparities including different MDM differentiation/culturing methods or different quantification assays to measure virus production. Sourisseau *et al*., isolated and differentiated MDMs in the same manner used in this thesis with the exception that human serum was used in place of fetal bovine serum. It is plausible that replication of CHIKV in the presence of human serum more accurately represents the situation during human infection and that this microenvironment can alter cell physiology. However, a more likely explanation for the observed difference is that Sourisseau *et al*., measured levels of infectious virions by limiting dilution on Vero cells (expressed as TCID50/mL). This method involved scoring the cytopathic effect (CPE) 5 days after infection and the titer was calculated by determining the last dilution giving 50% cells displaying CPE. It is important to note that this assay measures cell death rather than viral replication. Curiously, data by Sourisseau *et al*. showed higher viral load (as measured by TCID50/mL and viral RNA in supernatant) are achieved in macrophages infected with a high MOI, but viral load decreases as the MOI is lowered. This suggests that viral replication is inefficient and restricted, possibly due to the secretion of IFN or cytokines generated by infected macrophages.

As mentioned above, I did not observe evidence of productive infection when MDMs were exposed to MAYV. This could be due to: i) Failure of nascent virions to bud from and/or be released from host cells; or ii) Inefficient/low viral replication in macrophages. The latter explanation is more unlikely as relatively high values of genomic viral RNA were observed in infected macrophages. It would be interesting to compare MAYV-infected MDMs to highly susceptible cells such as MAYV-infected Vero cells by electron microscopy to examine the number of viral replication complexes and viral particles in infected cells.

Macrophages have been proposed as target cells for MAYV but the relevance to human infections is unclear because mouse macrophage cell lines and mouse primary macrophages were used in the initial studies (Cavalheiro et al., 2016; de Castro-Jorge et al., 2019). Cavalheiro *et al*. concluded that MAYV-infection of mouse macrophages induced the production of the cytokine TNFα (Cavalheiro et al., 2016). Since TNFα promotes an inflammatory profile characteristic of arthritis, MAYV-induced production of TNFα may contribute to the pathogenesis of MAYV. Results from the RNA-Seq in Chapter 5 revealed that while *TNFα* transcripts were upregulated ~15-fold in MAYV-infected MDMs, transcripts encoding the TNFα-induced protein 6 (*TNFAIP6*) were increased almost 200-fold. This may be of relevance to pathogenesis as TNFAIP6 is induced by TNFα and is commonly found in the synovial fluid of patients with osteoarthritis and rheumatoid arthritis (Wisniewski et al., 1994). Monocytes and macrophages are sources of TNFα but T and B lymphocytes, mast cells, NK, neutrophils, endothelial cells, fibroblasts and osteoclasts can also produce the

cytokine (Bradley, 2008). Examining levels of TNFα and TNFAIP6 proteins in the media of MAYV-infected MDMs by ELISA would provide additional information regarding the inflammatory profile of infected macrophages.

A recent study corroborated that mouse macrophages are susceptible to MAYV but in this case it was found that infection led to induction of inflammasome proteins such as NLRP3, ASC, AIM2 and Caspase-1 (de Castro-Jorge et al., 2019). The authors suggested that the NLRP3 inflammasome may be linked to MAYV pathogenesis, however, data from my RNA-seq analyses in Chapter 5 are not in agreement with this conclusion. Specifically, while *IL-1β* was upregulated ~3-fold, there was no change in *caspase-1* levels and expression of *NLRP3* was reduced ~3 fold. Together these data suggest that MAYV-infection of human MDMs does not lead to the induction of the NLRP3 inflammasome.

While macrophages do not appear to be productively infected by MAYV, it is tempting to speculate that they may serve as viral reservoirs. Persistent low-grade infection of macrophages may result in production of pro-inflammatory cytokine/chemokines that contributed to the virus-associated pathology as discussed further in the next section.

6.4.2 Examining the role of MAYV-infected macrophages in arthralgia

Approximately 50% of MAYV-diagnosed cases go on to present with arthralgia (Halsey et al., 2013; Mourão et al., 2012) but the molecular mechanisms behind this

process are largely unknown. CHIKV-induced arthralgia is thought to be the consequence of infection of multiple cell types in the joint and infiltration of mainly mononuclear cells (Suhrbier, 2019). Several studies that have examined the cytokine profiles of MAYV or CHIKV-infected patients provide clues regarding the key mediators behind joint inflammation and arthralgia. In a one year longitudinal study of individuals with confirmed MAYV infection, it was reported that patients elicited a strong immune response with secretion of proinflammatory mediators such as IL-6, IL-7, IL-8, IL-12p70, IL-15, IP-10/CXCL10, TNFα and MCP-1/CCL2 (Santiago et al., 2015). Another study evaluated the expression of cytokines/chemokines in patients with CHIKV and concluded that TNFα, IL-6, IL-8 and MCP-1/CCL2 play a role in persistent arthralgia whereas TNFα, IL-12, and MCP-1/CCL2 inflammatory markers are associated with chronic disease and severity of symptoms (Ninla-Aesong et al., 2019). Another study found that disease severity is associated with levels of CXCL9 and IP-10/CXCL10 at 6-months post-CHIKV infection (Kelvin et al., 2011). Unfortunately, due to the relatively small sample sizes, it is difficult to make reliable conclusions from the cytokine profiles of patients from small outbreaks, but there are overlapping data among these reports that give key insights into biomarkers for disease severity and arthralgia. Interestingly, CXCL10, IL-15, TNFα, CCL2 were all found to be transcriptionally upregulated in MAYV-infected MDMs and IL-12 signalling was the most significantly enriched biological process identified (Chapter 5). Of note, CXCL10, IL-15, TNFα and CCL2, as well as the top up-regulated gene from the RNA-seq in Chapter 5, CXCL13, are all strongly associated with inflammatory diseases and are important players in joint inflammation and arthritis (Greisen et al., 2014;

Gschwandtner et al., 2019; Karin and Razon, 2018; Yamanaka, 2015; Yang et al., 2015). Finally, I found that many of the MAYV-induced transcripts encoded chemo-attractant molecules suggesting that immune cell migration, differentiation, and cell activation may be important processes of viral pathogenesis. Together, these data suggest that MAYV-infection of human macrophages induces key proinflammatory mediators that may contribute to virus-induced arthralgia.

6.4.3 The role of LAMP3/CD63 on alphavirus infection

Lysosomal-Associated Membrane Protein 3 (LAMP3/CD63) belongs to the tetraspanin superfamily that localizes to endosomes, lysosomes, secretory vesicles, as well as the plasma membrane (Duffield et al., 2003). In experiments described in Chapter 5, I saw a dramatic increase in *LAMP3* expression in response to MAYV infection whereas significant changes in *LAMP1* or *LAMP2* transcript levels did not occur. MAYV-induced expression of *LAMP3* did not appear to be the result of IFN induction as *LAMP3* was increased during infection of IFN-deficient cells.

Tetraspanin proteins can form microdomains that mediate viral attachment, entry, intracellular trafficking, virus assembly and exit sites (Florin and Lang, 2018). Since LAMP3/CD63 is also found on the plasma membrane, it is possible that it functions in virus entry/signalling but to my knowledge, it has never been identified as an alphavirus receptor. Many viruses, including HIV, Influenza A virus, HPV, and Lujo virus, localize to CD63-positive endosomes during entry and knockdown of CD63 inhibits virus replication (Fu et al., 2015; Gräßel et al., 2016; Raaben et al., 2017; Zhou

et al., 2011). Collectively, most of these studies suggest that CD63 plays a role in the early stages of viral infection. One possibility is that CD63 acts as an endolysosomal receptor that facilitates the fusion of the viral envelope with the endosomal membrane. Another enveloped virus, Lassa virus, employs such strategy; it uses α-dystroglycan as a primary receptor but then switches to LAMP1 in the endosomal compartment and this switch is important, but not essential, for infectivity (Cohen-Dvashi et al., 2016). Another tetraspanin protein TSPAN9, was identified as a host factor that promotes infection of alphaviruses such as Sindbis virus, SFV and CHIKV but not for the flavivirus, DENV (Ooi et al., 2013; Stiles and Kielian, 2016). Depletion of TSPAN9 decreased SFV membrane fusion in endosomes but the mechanism or if TSPAN9 interacts with the viral envelope protein to mediate fusion of viral and cellular membranes is unknown. Finally, it has been reported that the spike glycoproteins E2 and E1 of Sindbis virus E1/E2 are transported to a CD63-positive compartment and that CD63 is incorporated into nascent virions (Ng et al., 2008). The latter suggests a role for LAMP3/CD63 in viral exit, however, the significance of this is not clear.

As shown in **Figure 5.12**, LAMP3 targeting siRNA #2 but not siRNA #1, inhibited MAYV replication despite no observed changes in LAMP3 total protein levels. SiRNA#1 targets the 3' UTR whereas siRNA#2 targets the coding region (CDS) of the mature transcript. It is unclear if the potency of siRNA targeting the coding region or the 3'-UTR of mRNA differs (Lai et al., 2013) but I will speculate that the observed differences could be due to lack of specificity and off-target effects. One possibility is that siRNA #2 targets other members of the LAMP family that possess a

similar sequence thus can cause regulation of unintended transcripts through partial sequence complementarity. Future studies using a monoclonal antibody that inhibits LAMP3/CD63 or the use of alternative knock-down strategies targeting LAMP3 in cells will help to elucidate the role LAMP3/CD63 plays in MAYV-infection.

6.4.2 Perspective: Physiological consequences of macrophage infection

In this study, I focused on identifying the target cells of MAYV-infection and how this virus alters global gene expression in macrophages. Arthralgia is a common complication following MAYV infection, but the underlying molecular mechanisms that contribute to this process are unknown. Macrophages appear to play a pivotal role in autoimmune diseases such as rheumatoid arthritis. This is because macrophages are important players in both pathogen detection/response and their pro-inflammatory, tissue damaging and remodeling capabilities can contribute to acute and chronic disease (Kinne et al., 2000). As such, understanding how macrophages are altered during MAYV-infection may lead to therapies that alleviate chronic inflammation. A first step in this process is identifying dysregulated cytokines/chemokines that can cause tissue damage (such as TNFα, CCL2), and secondly, providing treatment to counteract the dysregulation. For example, CCL2 is thought to act as a proinflammatory agent by promoting in the migration and accumulation of leukocytes and monocytes in the knee joints of rheumatoid arthritis patients (Zhang et al., 2015). Of note, anti-TNF treatment has been used in patients with chronic joint symptoms but

the effectiveness of this therapy is controversial and only suggested if other treatments have failed (Sutaria et al., 2018).

6.5 Concluding remarks

Due to their minimal genome, arboviruses such as Zika, Dengue and Mayaro viruses depend on many host molecules for replication and have evolved multiple strategies to subvert host innate immune defense mechanisms. As demonstrated in this thesis, the capsid protein of flaviviruses is multifunctional. The main function of the capsid protein is to protect the viral genome, but my data suggests that capsid plays additional roles in evasion of antiviral systems including inhibition of apoptosis and suppression of the IFN response. Moreover, in this thesis I examine MAYV tropism and characterize MAYV-infection in primary human macrophages. The data in this thesis provides insight into the role macrophages play in MAYV-induced chronic inflammation and disease pathology. Understanding the molecular mechanisms by which viruses hijack cellular pathways provide insight into host-virus biology that can lead to advances in vaccine design or discovery of novel therapeutic targets.

REFERENCES

Ackermann, M., Padmanabhan, R., 2001. De novo synthesis of RNA by the dengue virus RNA-dependent RNA polymerase exhibits temperature dependence at the initiation but not elongation phase. Journal of Biological Chemistry 276, 39926-39937.

Acosta, E.G., Castilla, V., Damonte, E.B., 2011. Infectious dengue-1 virus entry into mosquito C6/36 cells. Virus research 160, 173-179.

Ahola, T., Kääriäinen, L., 1995. Reaction in alphavirus mRNA capping: formation of a covalent complex of nonstructural protein nsP1 with 7-methyl-GMP. Proceedings of the National Academy of Sciences 92, 507-511.

Airo, A.M., Urbanowski, M.D., Lopez-Orozco, J., You, J.H., Skene-Arnold, T.D., Holmes, C., Yamshchikov, V., Malik-Soni, N., Frappier, L., Hobman, T.C., 2018. Expression of flavivirus capsids enhance the cellular environment for viral replication by activating Akt-signalling pathways. Virology 516, 147-157.

Alessi, D.R., Deak, M., Casamayor, A., Caudwell, F.B., Morrice, N., Norman, D.G., Gaffney, P., Reese, C.B., MacDougall, C.N., Harbison, D., 1997. 3-Phosphoinositide-dependent protein kinase-1 (PDK1): structural and functional homology with the Drosophila DSTPK61 kinase. Current biology 7, 776-789.

Allonso, D., Andrade, I.S., Conde, J.N., Coelho, D.R., Rocha, D.C., da Silva, M.L., Ventura, G.T., Silva, E.M., Mohana-Borges, R., 2015. Dengue virus NS1 protein modulates cellular energy metabolism by increasing glyceraldehyde-3-phosphate dehydrogenase activity. Journal of virology 89, 11871-11883.

Amberg, S.M., Rice, C.M., 1999. Mutagenesis of the NS2B-NS3-mediated cleavage site in the flavivirus capsid protein demonstrates a requirement for coordinated processing. Journal of virology 73, 8083-8094.

Ammosova, T., Yedavalli, V.R., Niu, X., Jerebtsova, M., Van Eynde, A., Beullens, M., Bollen, M., Jeang, K.-T., Nekhai, S., 2011. Expression of a protein phosphatase 1 inhibitor, cdNIPP1, increases CDK9 threonine 186 phosphorylation and inhibits HIV-1 transcription. Journal of Biological Chemistry 286, 3798-3804.

Andrabi, S., Gjoerup, O.V., Kean, J.A., Roberts, T.M., Schaffhausen, B., 2007. Protein phosphatase 2A regulates life and death decisions via Akt in a context-dependent manner. Proceedings of the National Academy of Sciences 104, 19011-19016.

Angleró-Rodríguez, Y.I., Pantoja, P., Sariol, C.A., 2014. Dengue Virus Subverts the Interferon Induction Pathway via NS2B/3 Protease-IκB Kinase ε Interaction. Clin. Vaccine Immunol. 21, 29-38.

Ashburner, M., Ball, C.A., Blake, J.A., Botstein, D., Butler, H., Cherry, J.M., Davis, A.P., Dolinski, K., Dwight, S.S., Eppig, J.T., 2000. Gene ontology: tool for the unification of biology. Nature genetics 25, 25.

Ashour, J., Laurent-Rolle, M., Shi, P.-Y., García-Sastre, A., 2009. NS5 of dengue virus mediates STAT2 binding and degradation. Journal of virology 83, 5408-5418.

Assenberg, R., Mastrangelo, E., Walter, T.S., Verma, A., Milani, M., Owens, R.J., Stuart, D.I., Grimes, J.M., Mancini, E.J., 2009. Crystal structure of a novel conformational state of the flavivirus NS3 protein: implications for polyprotein processing and viral replication. Journal of virology 83, 12895-12906.

Assunção-Miranda, I., Cruz-Oliveira, C., Da Poian, A.T., 2013. Molecular mechanisms involved in the pathogenesis of alphavirus-induced arthritis. BioMed research international 2013.

Barrows, N.J., Campos, R.K., Liao, K.-C., Prasanth, K.R., Soto-Acosta, R., Yeh, S.-C., Schott-Lerner, G., Pompon, J., Sessions, O.M., Bradrick, S.S., 2018. Biochemistry and molecular biology of flaviviruses. Chemical reviews 118, 4448-4482.

Barthel, A., Okino, S.T., Liao, J., Nakatani, K., Li, J., Whitlock, J.P., Roth, R.A., 1999. Regulation of GLUT1 gene transcription by the serine/threonine kinase Akt1. Journal of Biological Chemistry 274, 20281-20286.

Beatty, P.R., Puerta-Guardo, H., Killingbeck, S.S., Glasner, D.R., Hopkins, K., Harris, E., 2015. Dengue virus NS1 triggers endothelial permeability and vascular leak that is prevented by NS1 vaccination. Science translational medicine 7, 304ra141-304ra141.

Bhatt, S., Gething, P.W., Brady, O.J., Messina, J.P., Farlow, A.W., Moyes, C.L., Drake, J.M., Brownstein, J.S., Hoen, A.G., Sankoh, O., 2013. The global distribution and burden of dengue. Nature 496, 504.

Bhuvanakantham, R., Cheong, Y.K., Ng, M.-L., 2010. West Nile virus capsid protein interaction with importin and HDM2 protein is regulated by protein kinase C-mediated phosphorylation. Microbes and infection 12, 615-625.

Biswal, S., Reynales, H., Saez-Llorens, X., Lopez, P., Borja-Tabora, C., Kosalaraksa, P., Sirivichayakul, C., Watanaveeradej, V., Rivera, L., Espinoza, F., 2019. Efficacy of a tetravalent dengue vaccine in healthy children and adolescents. New England Journal of Medicine 381, 2009-2019.

Borisevich, V., Seregin, A., Nistler, R., Mutabazi, D., Yamshchikov, V., 2006. Biological properties of chimeric West Nile viruses. Virology 349, 371-381.

Bradley, J., 2008. TNF-mediated inflammatory disease. The Journal of Pathology: A Journal of the Pathological Society of Great Britain and Ireland 214, 149-160.

Breckpot, K., Escors, D., Arce, F., Lopes, L., Karwacz, K., Van Lint, S., Keyaerts, M., Collins, M., 2010. HIV-1 lentiviral vector immunogenicity is mediated by Toll-like receptor 3 (TLR3) and TLR7. Journal of virology 84, 5627-5636.

Brown, B.D., Sitia, G., Annoni, A., Hauben, E., Sergi, L.S., Zingale, A., Roncarolo, M.G., Guidotti, L.G., Naldini, L., 2006. In vivo administration of lentiviral vectors triggers a type I interferon response that restricts hepatocyte gene transfer and promotes vector clearance. Blood 109, 2797-2805.

Brunet, A., Bonni, A., Zigmond, M.J., Lin, M.Z., Juo, P., Hu, L.S., Anderson, M.J., Arden, K.C., Blenis, J., Greenberg, M.E., 1999. Akt promotes cell survival by phosphorylating and inhibiting a Forkhead transcription factor. cell 96, 857-868.

Buchkovich, N.J., Yu, Y., Zampieri, C.A., Alwine, J.C., 2008. The TORrid affairs of viruses: effects of mammalian DNA viruses on the PI3K–Akt–mTOR signalling pathway. Nature Reviews Microbiology 6, 266-275.

Cao-Lormeau, V.-M., Roche, C., Teissier, A., Robin, E., Berry, A.-L., Mallet, H.-P., Sall, A.A., Musso, D., 2014. Zika virus, French polynesia, South pacific, 2013. Emerging infectious diseases 20, 1085.

Cardone, M.H., Roy, N., Stennicke, H.R., Salvesen, G.S., Franke, T.F., Stanbridge, E., Frisch, S., Reed, J.C., 1998. Regulation of cell death protease caspase-9 by phosphorylation. Science 282, 1318-1321.

Carvalho, C.A., Silva, J.L., Oliveira, A.C., Gomes, A.M., 2017. On the entry of an emerging arbovirus into host cells: Mayaro virus takes the highway to the cytoplasm through fusion with early endosomes and caveolae-derived vesicles. PeerJ 5, e3245.

Carvalho, F.A., Carneiro, F.A., Martins, I.C., Assunção-Miranda, I., Faustino, A.F., Pereira, R.M., Bozza, P.T., Castanho, M.A., Mohana-Borges, R., Da Poian, A.T., 2012. Dengue virus capsid protein binding to hepatic lipid droplets (LD) is potassium ion dependent and is mediated by LD surface proteins. Journal of virology 86, 2096-2108.

Cavalheiro, M.G., COSTA, L.S.D., Campos, H.S., Alves, L.S., Assuncao-Miranda, I., POIAN, A.T., 2016. Macrophages as target cells for Mayaro virus infection: involvement of reactive oxygen species in the inflammatory response during virus replication. Anais da Academia Brasileira de Ciências 88, 1485-1499.

Chan, C.-H., Li, C.-F., Yang, W.-L., Gao, Y., Lee, S.-W., Feng, Z., Huang, H.-Y., Tsai, K.K., Flores, L.G., Shao, Y., 2012. The Skp2-SCF E3 ligase regulates Akt

ubiquitination, glycolysis, herceptin sensitivity, and tumorigenesis. Cell 149, 1098-1111.

Chan, J.F.-W., Zhu, Z., Chu, H., Yuan, S., Chik, K.K.-H., Chan, C.C.-S., Poon, V.K.-M., Yip, C.C.-Y., Zhang, X., Tsang, J.O.-L., 2018. The celecoxib derivative kinase inhibitor AR-12 (OSU-03012) inhibits Zika virus via down-regulation of the PI3K/Akt pathway and protects Zika virus-infected A129 mice: A host-targeting treatment strategy. Antiviral research 160, 38-47.

Chan, Y.K., Gack, M.U., 2016. A phosphomimetic-based mechanism of dengue virus to antagonize innate immunity. Nature immunology 17, 523.

Chazal, M., Beauclair, G., Gracias, S., Najburg, V., Simon-Lorière, E., Tangy, F., Komarova, A.V., Jouvenet, N., 2018. RIG-I recognizes the 5′ region of Dengue and Zika virus genomes. Cell reports 24, 320-328.

Chee, H.-Y., AbuBakar, S., 2004. Identification of a 48 kDa tubulin or tubulin-like C6/36 mosquito cells protein that binds dengue virus 2 using mass spectrometry. Biochemical and biophysical research communications 320, 11-17.

Chen, H.-H., Chen, C.-C., Lin, Y.-S., Chang, P.-C., Lu, Z.-Y., Lin, C.-F., Chen, C.-L., Chang, C.-P., 2017a. AR-12 suppresses dengue virus replication by down-regulation of PI3K/AKT and GRP78. Antiviral research 142, 158-168.

Chen, M.W., Tan, Y.B., Zheng, J., Zhao, Y., Lim, B.T., Cornvik, T., Lescar, J., Ng, L.F.P., Luo, D., 2017b. Chikungunya virus nsP4 RNA-dependent RNA polymerase core domain displays detergent-sensitive primer extension and terminal adenylyltransferase activities. Antiviral research 143, 38-47.

Cheng, E.H.-Y., Nicholas, J., Bellows, D.S., Hayward, G.S., Guo, H.-G., Reitz, M.S., Hardwick, J.M., 1997. A Bcl-2 homolog encoded by Kaposi sarcoma-associated virus, human herpesvirus 8, inhibits apoptosis but does not heterodimerize with Bax or Bak. Proceedings of the National Academy of Sciences 94, 690-694.

Cohen-Dvashi, H., Israeli, H., Shani, O., Katz, A., Diskin, R., 2016. Role of LAMP1 binding and pH sensing by the spike complex of Lassa virus. Journal of virology 90, 10329-10338.

Consortium, G.O., 2018. The gene ontology resource: 20 years and still GOing strong. Nucleic acids research 47, D330-D338.

Datta, S.R., Dudek, H., Tao, X., Masters, S., Fu, H., Gotoh, Y., Greenberg, M.E., 1997. Akt phosphorylation of BAD couples survival signals to the cell-intrinsic death machinery. Cell 91, 231-241.

Datta, S.R., Katsov, A., Hu, L., Petros, A., Fesik, S.W., Yaffe, M.B., Greenberg, M.E., 2000. 14-3-3 proteins and survival kinases cooperate to inactivate BAD by BH3 domain phosphorylation. Molecular cell 6, 41-51.

Davis, C.W., Nguyen, H.-Y., Hanna, S.L., Sánchez, M.D., Doms, R.W., Pierson, T.C., 2006. West Nile virus discriminates between DC-SIGN and DC-SIGNR for cellular attachment and infection. Journal of virology 80, 1290-1301.

Davis, M.E., Wang, M.K., Rennick, L.J., Full, F., Gableske, S., Mesman, A.W., Gringhuis, S.I., Geijtenbeek, T.B., Duprex, W.P., Gack, M.U., 2014. Antagonism of the phosphatase PP1 by the measles virus V protein is required for innate immune escape of MDA5. Cell host & microbe 16, 19-30.

de Castro-Jorge, L.A., de Carvalho, R.V., Klein, T.M., Hiroki, C.H., Lopes, A.H., Guimarães, R.M., Fumagalli, M.J., Floriano, V.G., Agostinho, M.R., Slhessarenko, R.D., 2019. The NLRP3 inflammasome is involved with the pathogenesis of Mayaro virus. PLoS pathogens 15, e1007934.

Desmyter, J., Melnick, J.L., Rawls, W.E., 1968. Defectiveness of interferon production and of rubella virus interference in a line of African green monkey kidney cells (Vero). Journal of virology 2, 955-961.

Dick, G., Kitchen, S., Haddow, A., 1952. Zika virus (I). Isolations and serological specificity. Transactions of the royal society of tropical medicine and hygiene 46, 509-520.

Diehl, N., Schaal, H., 2013. Make yourself at home: viral hijacking of the PI3K/Akt signaling pathway. Viruses 5, 3192-3212.

Dixit, E., Boulant, S., Zhang, Y., Lee, A.S., Odendall, C., Shum, B., Hacohen, N., Chen, Z.J., Whelan, S.P., Fransen, M., 2010. Peroxisomes are signaling platforms for antiviral innate immunity. Cell 141, 668-681.

Duffield, A., Kamsteeg, E.-J., Brown, A.N., Pagel, P., Caplan, M.J., 2003. The tetraspanin CD63 enhances the internalization of the H, K-ATPase β-subunit. Proceedings of the National Academy of Sciences 100, 15560-15565.

Duffy, M.R., Chen, T.-H., Hancock, W.T., Powers, A.M., Kool, J.L., Lanciotti, R.S., Pretrick, M., Marfel, M., Holzbauer, S., Dubray, C., 2009. Zika virus outbreak on Yap Island, federated states of Micronesia. New England Journal of Medicine 360, 2536-2543.

Duijl-Richter, V., Mareike, K., Hoornweg, T.E., Rodenhuis-Zybert, I.A., Smit, J.M., 2015. Early events in chikungunya virus infection—from virus cellbinding to membrane fusion. Viruses 7, 3647-3674.

Eden, E., Navon, R., Steinfeld, I., Lipson, D., Yakhini, Z., 2009. GOrilla: a tool for discovery and visualization of enriched GO terms in ranked gene lists. BMC bioinformatics 10, 48.

Ehrhardt, C., Wolff, T., Pleschka, S., Planz, O., Beermann, W., Bode, J.G., Schmolke, M., Ludwig, S., 2007. Influenza A virus NS1 protein activates the PI3K/Akt pathway to mediate antiapoptotic signaling responses. Journal of virology 81, 3058-3067.

Elmore, S., 2007. Apoptosis: a review of programmed cell death. Toxicologic pathology 35, 495-516.

Elshuber, S., Allison, S.L., Heinz, F.X., Mandl, C.W., 2003. Cleavage of protein prM is necessary for infection of BHK-21 cells by tick-borne encephalitis virusFN1. Journal of General Virology 84, 183-191.

Errett, J.S., Suthar, M.S., McMillan, A., Diamond, M.S., Gale, M., 2013. The essential, nonredundant roles of RIG-I and MDA5 in detecting and controlling West Nile virus infection. Journal of virology 87, 11416-11425.

Esposito, D.L.A., da Fonseca, B.A.L., 2017. Will Mayaro virus be responsible for the next outbreak of an arthropod-borne virus in Brazil? The Brazilian Journal of Infectious Diseases.

Faria, N.R., da Silva Azevedo, R.d.S., Kraemer, M.U., Souza, R., Cunha, M.S., Hill, S.C., Thézé, J., Bonsall, M.B., Bowden, T.A., Rissanen, I., 2016. Zika virus in the Americas: early epidemiological and genetic findings. Science 352, 345-349.

Faria, N.R., Quick, J., Claro, I., Theze, J., de Jesus, J.G., Giovanetti, M., Kraemer, M.U., Hill, S.C., Black, A., da Costa, A.C., 2017. Establishment and cryptic transmission of Zika virus in Brazil and the Americas. Nature 546, 406.

Faustino, A.F., Martins, A.S., Karguth, N., Artilheiro, V., Enguita, F.J., Ricardo, J.C., Santos, N.C., Martins, I.C., 2019. Structural and Functional Properties of the Capsid Protein of Dengue and Related Flavivirus. International journal of molecular sciences 20, 3870.

Fiandalo, M., Kyprianou, N., 2012. Caspase control: protagonists of cancer cell apoptosis. Experimental oncology 34, 165.

Fitzsimmons, L., Cartlidge, R., Chang, C., Sejic, N., Galbraith, L.C., Suraweera, C.D., Croom-Carter, D., Dewson, G., Tierney, R.J., Bell, A.I., 2019. EBV BCL-2 homologue BHRF1 drives chemoresistance and lymphomagenesis by inhibiting multiple cellular pro-apoptotic proteins. Cell Death Differ.

Florin, L., Lang, T., 2018. Tetraspanin assemblies in virus infection. Frontiers in immunology 9, 1140.

Fontaine, K.A., Leon, K.E., Khalid, M.M., Tomar, S., Jimenez-Morales, D., Dunlap, M., Kaye, J.A., Shah, P.S., Finkbeiner, S., Krogan, N.J., 2018. The cellular NMD pathway restricts Zika virus infection and is targeted by the viral capsid protein. MBio 9, e02126-02118.

Fontaine, K.A., Sanchez, E.L., Camarda, R., Lagunoff, M., 2015. Dengue virus induces and requires glycolysis for optimal replication. Journal of virology 89, 2358-2366.

Fredericksen, B.L., Keller, B.C., Fornek, J., Katze, M.G., Gale, M., 2008. Establishment and maintenance of the innate antiviral response to West Nile Virus involves both RIG-I and MDA5 signaling through IPS-1. Journal of virology 82, 609-616.

Frolova, E.I., Gorchakov, R., Pereboeva, L., Atasheva, S., Frolov, I., 2010. Functional Sindbis virus replicative complexes are formed at the plasma membrane. Journal of virology 84, 11679-11695.

Froshauer, S., Kartenbeck, J., Helenius, A., 1988. Alphavirus RNA replicase is located on the cytoplasmic surface of endosomes and lysosomes. The Journal of cell biology 107, 2075-2086.

Fu, E., Pan, L., Xie, Y., Mu, D., Liu, W., Jin, F., Bai, X., 2015. Tetraspanin CD63 is a regulator of HIV-1 replication. International journal of clinical and experimental pathology 8, 1184.

Gack, M.U., Albrecht, R.A., Urano, T., Inn, K.-S., Huang, I.-C., Carnero, E., Farzan, M., Inoue, S., Jung, J.U., García-Sastre, A., 2009. Influenza A virus NS1 targets the ubiquitin ligase TRIM25 to evade recognition by the host viral RNA sensor RIG-I. Cell host & microbe 5, 439-449.

Gack, M.U., Shin, Y.C., Joo, C.-H., Urano, T., Liang, C., Sun, L., Takeuchi, O., Akira, S., Chen, Z., Inoue, S., 2007. TRIM25 RING-finger E3 ubiquitin ligase is essential for RIG-I-mediated antiviral activity. Nature 446, 916-920.

Galluzzi, L., Vitale, I., Aaronson, S.A., Abrams, J.M., Adam, D., Agostinis, P., Alnemri, E.S., Altucci, L., Amelio, I., Andrews, D.W., 2018. Molecular mechanisms of cell death: recommendations of the Nomenclature Committee on Cell Death 2018. Cell Death & Differentiation 25, 486-541.

Garcia-Blanco, M.A., Vasudevan, S.G., Bradrick, S.S., Nicchitta, C., 2016. Flavivirus RNA transactions from viral entry to genome replication. Antiviral research 134, 244-249.

Gardner, J., Anraku, I., Le, T.T., Larcher, T., Major, L., Roques, P., Schroder, W.A., Higgs, S., Suhrbier, A., 2010. Chikungunya virus arthritis in adult wild-type mice. Journal of virology 84, 8021-8032.

Gillespie, L.K., Hoenen, A., Morgan, G., Mackenzie, J.M., 2010. The endoplasmic reticulum provides the membrane platform for biogenesis of the flavivirus replication complex. Journal of virology 84, 10438-10447.

Gollins, S.W., Porterfield, J.S., 1986. pH-dependent fusion between the flavivirus West Nile and liposomal model membranes. Journal of General Virology 67, 157-166.

Gonnella, R., Santarelli, R., Farina, A., Granato, M., D'Orazi, G., Faggioni, A., Cirone, M., 2013. Kaposi sarcoma associated herpesvirus (KSHV) induces AKT hyperphosphorylation, bortezomib-resistance and GLUT-1 plasma membrane exposure in THP-1 monocytic cell line. Journal of Experimental & Clinical Cancer Research 32, 1.

Grant, A., Ponia, S.S., Tripathi, S., Balasubramaniam, V., Miorin, L., Sourisseau, M., Schwarz, M.C., Sánchez-Seco, M.P., Evans, M.J., Best, S.M., 2016. Zika virus targets human STAT2 to inhibit type I interferon signaling. Cell host & microbe 19, 882-890.

Gräßel, L., Fast, L.A., Scheffer, K.D., Boukhallouk, F., Spoden, G.A., Tenzer, S., Boller, K., Bago, R., Rajesh, S., Overduin, M., 2016. The CD63-Syntenin-1 complex controls post-endocytic trafficking of oncogenic human papillomaviruses. Scientific reports 6, 32337.

Greisen, S.R., Schelde, K.K., Rasmussen, T.K., Kragstrup, T.W., Stengaard-Pedersen, K., Hetland, M.L., Hørslev-Petersen, K., Junker, P., Østergaard, M., Deleuran, B., 2014. CXCL13 predicts disease activity in early rheumatoid arthritis and could be an indicator of the therapeuticwindow of opportunity'. Arthritis research & therapy 16, 434.

Grimley, P.M., Berezesky, I.K., Friedman, R.M., 1968. Cytoplasmic structures associated with an arbovirus infection: loci of viral ribonucleic acid synthesis. Journal of virology 2, 1326-1338.

Gschwandtner, M., Derler, R., Midwood, K.S., 2019. More than just attractive: how CCL2 influences myeloid cell behavior beyond chemotaxis. Frontiers in Immunology 10, 2759.

Gubler, D.J., Vasilakis, N., Musso, D., 2017. History and emergence of Zika virus. The Journal of infectious diseases 216, S860-S867.

Guirakhoo, F., Heinz, F.X., Mandl, C.W., Holzmann, H., Kunz, C., 1991. Fusion activity of flaviviruses: comparison of mature and immature (prM-containing) tick-borne encephalitis virions. Journal of General Virology 72, 1323-1329.

Gutsche, I., Coulibaly, F., Voss, J.E., Salmon, J., d'Alayer, J., Ermonval, M., Larquet, E., Charneau, P., Krey, T., Mégret, F., 2011. Secreted dengue virus nonstructural protein NS1 is an atypical barrel-shaped high-density lipoprotein. Proceedings of the National Academy of Sciences 108, 8003-8008.

Habjan, M., Hubel, P., Lacerda, L., Benda, C., Holze, C., Eberl, C.H., Mann, A., Kindler, E., Gil-Cruz, C., Ziebuhr, J., 2013. Sequestration by IFIT1 impairs translation of 2′ O-unmethylated capped RNA. PLoS pathogens 9.

Halsey, E.S., Siles, C., Guevara, C., Vilcarromero, S., Jhonston, E.J., Ramal, C., Aguilar, P.V., Ampuero, J.S., 2013. Mayaro virus infection, Amazon basin region, Peru, 2010–2013. Emerging infectious diseases 19, 1839.

Halstead, S., O'Rourke, E., Allison, A., 1977. Dengue viruses and mononuclear phagocytes. Infection.

Harrison, S.C., 2008. Viral membrane fusion. Nature structural & molecular biology 15, 690-698.

Hart, J.R., Vogt, P.K., 2011. Phosphorylation of AKT: a mutational analysis. Oncotarget 2, 467.

Hawkes, R., 1964. Enhancement of the infectivity of arboviruses by specific antisera produced in domestic fowls. Australian Journal of Experimental Biology and Medical Science 42, 465-482.

Hayman, T.J., Hsu, A.C., Kolesnik, T.B., Dagley, L.F., Willemsen, J., Tate, M.D., Baker, P.J., Kershaw, N.J., Kedzierski, L., Webb, A.I., 2019. RIPLET, and not TRIM25, is required for endogenous RIG-I-dependent antiviral responses. Immunology and cell biology 97, 840-852.

He, Y., Nakao, H., Tan, S.-L., Polyak, S.J., Neddermann, P., Vijaysri, S., Jacobs, B.L., Katze, M.G., 2002. Subversion of cell signaling pathways by hepatitis C virus nonstructural 5A protein via interaction with Grb2 and P85 phosphatidylinositol 3-kinase. Journal of virology 76, 9207-9217.

Hilgard, P., Stockert, R., 2000. Heparan sulfate proteoglycans initiate dengue virus infection of hepatocytes. Hepatology 32, 1069-1077.

Hoarau, J.-J., Bandjee, M.-C.J., Trotot, P.K., Das, T., Li-Pat-Yuen, G., Dassa, B., Denizot, M., Guichard, E., Ribera, A., Henni, T., 2010. Persistent chronic inflammation

and infection by Chikungunya arthritogenic alphavirus in spite of a robust host immune response. The Journal of Immunology 184, 5914-5927.

Hou, S., Kumar, A., Xu, Z., Airo, A.M., Stryapunina, I., Wong, C.P., Branton, W., Tchesnokov, E., Götte, M., Power, C., 2017. Zika virus hijacks stress granule proteins and modulates the host stress response. Journal of Virology 91, e00474-00417.

Hu, Y., Dong, X., He, Z., Wu, Y., Zhang, S., Lin, J., Yang, Y., Chen, J., An, S., Yin, Y., 2019. Zika virus antagonizes interferon response in patients and disrupts RIG-I–MAVS interaction through its CARD-TM domains. Cell & Bioscience 9, 46.

Huang, D.W., Sherman, B.T., Lempicki, R.A., 2008. Bioinformatics enrichment tools: paths toward the comprehensive functional analysis of large gene lists. Nucleic acids research 37, 1-13.

Hurwitz, S.N., Nkosi, D., Conlon, M.M., York, S.B., Liu, X., Tremblay, D.C., Meckes, D.G., 2017. CD63 regulates epstein-barr virus LMP1 exosomal packaging, enhancement of vesicle production, and noncanonical NF-κB signaling. Journal of virology 91, e02251-02216.

Ilinykh, P.A., Tigabu, B., Ivanov, A., Ammosova, T., Obukhov, Y., Garron, T., Kumari, N., Kovalskyy, D., Platonov, M.O., Naumchik, V.S., 2014. Role of protein phosphatase 1 in dephosphorylation of Ebola virus VP30 protein and its targeting for the inhibition of viral transcription. Journal of Biological Chemistry 289, 22723-22738.

Johnson, A.J., Roehrig, J.T., 1999. New mouse model for dengue virus vaccine testing. Journal of virology 73, 783-786.

Johnson, R.A., Wang, X., Ma, X.-L., Huong, S.-M., Huang, E.-S., 2001. Human cytomegalovirus up-regulates the phosphatidylinositol 3-kinase (PI3-K) pathway: inhibition of PI3-K activity inhibits viral replication and virus-induced signaling. Journal of virology 75, 6022-6032.

Jones, M., Davidson, A., Hibbert, L., Gruenwald, P., Schlaak, J., Ball, S., Foster, G.R., Jacobs, M., 2005. Dengue virus inhibits alpha interferon signaling by reducing STAT2 expression. Journal of virology 79, 5414-5420.

Jose, J., Taylor, A.B., Kuhn, R.J., 2017. Spatial and temporal analysis of alphavirus replication and assembly in mammalian and mosquito cells. MBio 8, e02294-02216.

Kale, J., Osterlund, E.J., Andrews, D.W., 2018. BCL-2 family proteins: changing partners in the dance towards death. Cell Death & Differentiation 25, 65-80.

Karin, N., Razon, H., 2018. Chemokines beyond chemo-attraction: CXCL10 and its significant role in cancer and autoimmunity. Cytokine 109, 24-28.

Karpe, Y.A., Aher, P.P., Lole, K.S., 2011. NTPase and 5′-RNA triphosphatase activities of Chikungunya virus nsP2 protein. PloS one 6.

Kato, H., Takeuchi, O., Sato, S., Yoneyama, M., Yamamoto, M., Matsui, K., Uematsu, S., Jung, A., Kawai, T., Ishii, K.J., 2006. Differential roles of MDA5 and RIG-I helicases in the recognition of RNA viruses. Nature 441, 101.

Kaufmann, S.H., Earnshaw, W.C., 2000. Induction of apoptosis by cancer chemotherapy. Experimental cell research 256, 42-49.

Kawasaki, T., Kawai, T., 2014. Toll-like receptor signaling pathways. Frontiers in immunology 5, 461.

Kelvin, A.A., Banner, D., Silvi, G., Moro, M.L., Spataro, N., Gaibani, P., Cavrini, F., Pierro, A., Rossini, G., Cameron, M.J., 2011. Inflammatory cytokine expression is associated with chikungunya virus resolution and symptom severity. PLoS neglected tropical diseases 5.

Khromykh, A.A., Varnavski, A.N., Sedlak, P.L., Westaway, E.G., 2001. Coupling between replication and packaging of flavivirus RNA: evidence derived from the use of DNA-based full-length cDNA clones of Kunjin virus. Journal of virology 75, 4633-4640.

Kielian, M., Chanel-Vos, C., Liao, M., 2010. Alphavirus entry and membrane fusion. Viruses 2, 796-825.

Kim, S.S.-Y., Sze, L., Lam, K.-P., 2019. The stress granule protein G3BP1 binds viral dsRNA and RIG-I to enhance interferon-β response. Journal of Biological Chemistry 294, 6430-6438.

Kinne, R.W., Bräuer, R., Stuhlmüller, B., Palombo-Kinne, E., Burmester, G.-R., 2000. Macrophages in rheumatoid arthritis. Arthritis Research & Therapy 2, 189.

Kozak, R., Majer, A., Biondi, M., Medina, S., Goneau, L., Sajesh, B., Slota, J., Zubach, V., Severini, A., Safronetz, D., 2017. MicroRNA and mRNA dysregulation in astrocytes infected with Zika virus. Viruses 9, 297.

Krammer, P.H., 2000. CD95's deadly mission in the immune system. Nature 407, 789.

Krauer, F., Riesen, M., Reveiz, L., Oladapo, O.T., Martinez-Vega, R., Porgo, T.V., Haefliger, A., Broutet, N.J., Low, N., Group, W.Z.C.W., 2017. Zika virus infection as a cause of congenital brain abnormalities and Guillain–Barré syndrome: systematic review. PLoS medicine 14, e1002203.

Kumar, A., Hou, S., Airo, A.M., Limonta, D., Mancinelli, V., Branton, W., Power, C., Hobman, T.C., 2016. Zika virus inhibits type-I interferon production and downstream signaling. EMBO reports 17, 1766-1775.

Kumar, R., Singh, N., Abdin, M.Z., Patel, A.H., Medigeshi, G.R., 2018a. Dengue virus capsid interacts with DDX3X–a potential mechanism for suppression of antiviral functions in dengue infection. Frontiers in cellular and infection microbiology 7, 542.

Kumar, S., Kumar, A., Mamidi, P., Tiwari, A., Kumar, S., Mayavannan, A., Mudulli, S., Singh, A.K., Subudhi, B.B., Chattopadhyay, S., 2018b. Chikungunya virus nsP1 interacts directly with nsP2 and modulates its ATPase activity. Scientific reports 8, 1-14.

La Linn, M., Aaskov, J.G., Suhrbier, A., 1996. Antibody-dependent enhancement and persistence in macrophages of an arbovirus associated with arthritis. Journal of General Virology 77, 407-411.

Labadie, K., Larcher, T., Joubert, C., Mannioui, A., Delache, B., Brochard, P., Guigand, L., Dubreil, L., Lebon, P., Verrier, B., 2010. Chikungunya disease in nonhuman primates involves long-term viral persistence in macrophages. The Journal of clinical investigation 120, 894-906.

Lai, C.-F., Chen, C.-Y., Au, L.-C., 2013. Comparison between the repression potency of siRNA targeting the coding region and the 3′-untranslated region of mRNA. BioMed research international 2013.

LaStarza, M.W., Lemm, J.A., Rice, C.M., 1994. Genetic analysis of the nsP3 region of Sindbis virus: evidence for roles in minus-strand and subgenomic RNA synthesis. Journal of virology 68, 5781-5791.

Lazear, H.M., Govero, J., Smith, A.M., Platt, D.J., Fernandez, E., Miner, J.J., Diamond, M.S., 2016. A mouse model of Zika virus pathogenesis. Cell host & microbe 19, 720-730.

Lazear, H.M., Nice, T.J., Diamond, M.S., 2015. Interferon-λ: immune functions at barrier surfaces and beyond. Immunity 43, 15-28.

Lee, C.-J., Liao, C.-L., Lin, Y.-L., 2005. Flavivirus activates phosphatidylinositol 3-kinase signaling to block caspase-dependent apoptotic cell death at the early stage of virus infection. Journal of virology 79, 8388-8399.

Lee, J.K., Shin, O.S., 2019. Advances in Zika virus–host cell interaction: Current knowledge and future perspectives. International journal of molecular sciences 20, 1101.

Leung, J.Y.-S., Ng, M.M.-L., Chu, J.J.H., 2011. Replication of alphaviruses: a review on the entry process of alphaviruses into cells. Advances in virology 2011.

Li, Q., Zheng, Z., Liu, Y., Zhang, Z., Liu, Q., Meng, J., Ke, X., Hu, Q., Wang, H., 2016. 2C proteins of enteroviruses suppress IKKβ phosphorylation by recruiting protein phosphatase 1. Journal of virology 90, 5141-5151.

Li, W., Turner, A., Aggarwal, P., Matter, A., Storvick, E., Arnett, D.K., Broeckel, U., 2015. Comprehensive evaluation of AmpliSeq transcriptome, a novel targeted whole transcriptome RNA sequencing methodology for global gene expression analysis. BMC genomics 16, 1069.

Li, Y., Zhang, C., Chen, X., Yu, J., Wang, Y., Yang, Y., Du, M., Jin, H., Ma, Y., He, B., 2011. ICP34. 5 protein of herpes simplex virus facilitates the initiation of protein translation by bridging eukaryotic initiation factor 2α (eIF2α) and protein phosphatase 1. Journal of biological chemistry 286, 24785-24792.

Li, Y., Zhang, C., Chen, X., Yu, J., Wang, Y., Yang, Y., Du, M., Jin, H., Ma, Y., He, B., 2011. ICP34. 5 protein of herpes simplex virus facilitates the initiation of protein translation by bridging eukaryotic initiation factor 2α (eIF2α) and protein phosphatase 1. Journal of biological chemistry 286, 24785-24792.

Limonta, D., Jovel, J., Kumar, A., Airo, A., Hou, S., Saito, L., Branton, W., Ka-Shu Wong, G., Mason, A., Power, C., 2018. Human Fetal Astrocytes Infected with Zika Virus Exhibit Delayed Apoptosis and Resistance to Interferon: Implications for Persistence. Viruses 10, 646.

Lindenbach, B.D., Thiel, H.-J., Rice, C.M., Thiel, H., Rice, C., Chanock, R., 2007. Flaviviridae: the viruses and their replication.

Liu, W.J., Chen, H.B., Khromykh, A.A., 2003. Molecular and functional analyses of Kunjin virus infectious cDNA clones demonstrate the essential roles for NS2A in virus assembly and for a nonconservative residue in NS3 in RNA replication. Journal of virology 77, 7804-7813.

Liu, X., Cohen, J.I., 2015. The role of PI3K/Akt in human herpesvirus infection: from the bench to the bedside. Virology 479, 568-577.

Liu, Z., Tian, Y., Machida, K., Lai, M.M., Luo, G., Foung, S.K., Ou, J.-h.J., 2012. Transient activation of the PI3K-AKT pathway by hepatitis C virus to enhance viral entry. Journal of Biological Chemistry 287, 41922-41930.

Lobigs, M., Lee, E., 2004. Inefficient signalase cleavage promotes efficient nucleocapsid incorporation into budding flavivirus membranes. Journal of virology 78, 178-186.

Long, K.C., Ziegler, S.A., Thangamani, S., Hausser, N.L., Kochel, T.J., Higgs, S., Tesh, R.B., 2011. Experimental transmission of Mayaro virus by Aedes aegypti. The American journal of tropical medicine and hygiene 85, 750-757.

Lopez-Orozco, J., Pare, J.M., Holme, A.L., Chaulk, S.G., Fahlman, R.P., Hobman, T.C., 2015. Functional analyses of phosphorylation events in human Argonaute 2. RNA 21, 2030-2038.

Loreto, C., La Rocca, G., Anzalone, R., Caltabiano, R., Vespasiani, G., Castorina, S., Ralph, D.J., Cellek, S., Musumeci, G., Giunta, S., 2014. The role of intrinsic pathway in apoptosis activation and progression in Peyronie's disease. BioMed research international 2014.

Lubick, K.J., Robertson, S.J., McNally, K.L., Freedman, B.A., Rasmussen, A.L., Taylor, R.T., Walts, A.D., Tsuruda, S., Sakai, M., Ishizuka, M., 2015. Flavivirus antagonism of type I interferon signaling reveals prolidase as a regulator of IFNAR1 surface expression. Cell host & microbe 18, 61-74.

Lundberg, R., Melén, K., Westenius, V., Jiang, M., Österlund, P., Khan, H., Vapalahti, O., Julkunen, I., Kakkola, L., 2019. Zika Virus Non-Structural Protein NS5 Inhibits the RIG-I Pathway and Interferon Lambda 1 Promoter Activation by Targeting IKK Epsilon. Viruses 11, 1024.

Ma, J., Ketkar, H., Geng, T., Lo, E., Wang, L., Xi, J., Sun, Q., Zhu, Z., Cui, Y., Yang, L., 2018. Zika virus non-structural protein 4A blocks the RLR-MAVS signaling. Frontiers in microbiology 9, 1350.

MacKay, C.R., Wang, J.P., Kurt-Jones, E.A., 2014. Dicer's role as an antiviral: still an enigma. Current opinion in immunology 26, 49-55.

Mackenzie, J.M., Khromykh, A.A., Jones, M.K., Westaway, E.G., 1998. Subcellular localization and some biochemical properties of the flavivirus Kunjin nonstructural proteins NS2A and NS4A. Virology 245, 203-215.

MacKintosh, R.W., Dalby, K.N., Campbell, D.G., Cohen, P.T., Cohen, P., MacKintosh, C., 1995. The cyanobacterial toxin microcystin binds covalently to cysteine-273 on protein phosphatase 1. FEBS letters 371, 236-240.

Mandary, M.B., Masomian, M., Poh, C.L., 2019. Impact of RNA Virus Evolution on Quasispecies Formation and Virulence. International journal of molecular sciences 20, 4657.

Manning, B.D., Toker, A., 2017. AKT/PKB signaling: navigating the network. Cell 169, 381-405.

Manokaran, G., Finol, E., Wang, C., Gunaratne, J., Bahl, J., Ong, E.Z., Tan, H.C., Sessions, O.M., Ward, A.M., Gubler, D.J., 2015. Dengue subgenomic RNA binds TRIM25 to inhibit interferon expression for epidemiological fitness. Science 350, 217-221.

Martín-Vicente, M., Medrano, L.M., Resino, S., García-Sastre, A., Martínez, I., 2017. TRIM25 in the regulation of the antiviral innate immunity. Frontiers in immunology 8, 1187.

Martins, K.A., Gregory, M.K., Valdez, S.M., Sprague, T.R., Encinales, L., Pacheco, N., Cure, C., Porras-Ramirez, A., Rico-Mendoza, A., Chang, A., 2019. Neutralizing antibodies from convalescent Chikungunya virus patients can cross-neutralize Mayaro and Una viruses. The American journal of tropical medicine and hygiene 100, 1541-1544.

Mason, P., Haddow, A., 1957. An epidemic of virus disease in Southern Province, Tanganyika Territory, in 1952–1953: An additional note on Chikungunya virus isolations and serum antibodies. Transactions of the Royal Society of Tropical Medicine and Hygiene 51, 238-240.

Mazeaud, C., Freppel, W., Chatel-Chaix, L., 2018. The multiples fates of the Flavivirus RNA genome during pathogenesis. Frontiers in genetics 9, 595.

Mazzon, M., Castro, C., Thaa, B., Liu, L., Mutso, M., Liu, X., Mahalingam, S., Griffin, J.L., Marsh, M., McInerney, G.M., 2018. Alphavirus-induced hyperactivation of PI3K/AKT directs pro-viral metabolic changes. PLoS pathogens 14, e1006835.

Meertens, L., Carnec, X., Lecoin, M.P., Ramdasi, R., Guivel-Benhassine, F., Lew, E., Lemke, G., Schwartz, O., Amara, A., 2012. The TIM and TAM families of phosphatidylserine receptors mediate dengue virus entry. Cell host & microbe 12, 544-557.

Megyeri, K., Berencsi, K., Halazonetis, T.D., Prendergast, G.C., Gri, G., Plotkin, S.A., Rovera, G., Gönczöl, E., 1999. Involvement of a p53-dependent pathway in rubella virus-induced apoptosis. Virology 259, 74-84.

Meier, K.C., Gardner, C.L., Khoretonenko, M.V., Klimstra, W.B., Ryman, K.D., 2009. A mouse model for studying viscerotropic disease caused by yellow fever virus infection. PLoS pathogens 5, e1000614.

Messaoudi, I., Vomaske, J., Totonchy, T., Kreklywich, C.N., Haberthur, K., Springgay, L., Brien, J.D., Diamond, M.S., DeFilippis, V.R., Streblow, D.N., 2013. Chikungunya virus infection results in higher and persistent viral replication in aged rhesus macaques due to defects in anti-viral immunity. PLoS neglected tropical diseases 7.

Mi, H., Muruganujan, A., Ebert, D., Huang, X., Thomas, P.D., 2018. PANTHER version 14: more genomes, a new PANTHER GO-slim and improvements in enrichment analysis tools. Nucleic acids research 47, D419-D426.

Mi, S., Stollar, V., 1991. Expression of Sindbis virus nsP1 and methyltransferase activity inEscherichia coli. Virology 184, 423-427.

Miller, J.L., Dewet, B.J., Martinez-Pomares, L., Radcliffe, C.M., Dwek, R.A., Rudd, P.M., Gordon, S., 2008. The mannose receptor mediates dengue virus infection of macrophages. PLoS pathogens 4.

Modhiran, N., Watterson, D., Muller, D.A., Panetta, A.K., Sester, D.P., Liu, L., Hume, D.A., Stacey, K.J., Young, P.R., 2015. Dengue virus NS1 protein activates cells via Toll-like receptor 4 and disrupts endothelial cell monolayer integrity. Science translational medicine 7, 304ra142-304ra142.

Moorhead, G., MacKintosh, R.W., Morrice, N., Gallagher, T., MacKintosh, C., 1994. Purification of type 1 protein (serine/threonine) phosphatases by microcystin-Sepharose affinity chromatography. FEBS letters 356, 46-50.

Moorhead, G.B., Trinkle-Mulcahy, L., Nimick, M., De Wever, V., Campbell, D.G., Gourlay, R., Lam, Y.W., Lamond, A.I., 2008. Displacement affinity chromatography of protein phosphatase one (PP1) complexes. BMC biochemistry 9, 28.

Morrison, T.E., Diamond, M.S., 2017. Animal models of Zika virus infection, pathogenesis, and immunity. Journal of virology 91, e00009-00017.

Mourão, M.P.G., Bastos, M.d.S., de Figueiredo, R.P., Gimaque, J.B.L., dos Santos Galusso, E., Kramer, V.M., de Oliveira, C.M.C., Naveca, F.G., Figueiredo, L.T.M., 2012. Mayaro fever in the city of Manaus, Brazil, 2007–2008. Vector-borne and Zoonotic Diseases 12, 42-46.

Nan, Y., Nan, G., Zhang, Y.-J., 2014. Interferon induction by RNA viruses and antagonism by viral pathogens. Viruses 6, 4999-5027.
Nayak, S., Herzog, R.W., 2010. Progress and prospects: immune responses to viral vectors. Gene therapy 17, 295.

Neufeldt, C.J., Cortese, M., Acosta, E.G., Bartenschlager, R., 2018. Rewiring cellular networks by members of the Flaviviridae family. Nature Reviews Microbiology 16, 125.

Ng, C.G., Coppens, I., Govindarajan, D., Pisciotta, J., Shulaev, V., Griffin, D.E., 2008. Effect of host cell lipid metabolism on alphavirus replication, virion morphogenesis, and infectivity. Proceedings of the National Academy of Sciences 105, 16326-16331.

Ngan, N.T.T., Kim, S.-J., Lee, J.Y., Myoung, J., 2019. Zika Virus Proteins NS2A and NS4A Are Major Antagonists that Reduce IFN-β Promoter Activity Induced by the MDA5/RIG-I Signaling Pathway. Journal of Microbiology and Biotechnology 29, 1665-1674.

Ninla-Aesong, P., Mitarnun, W., Noipha, K., 2019. Proinflammatory Cytokines and Chemokines as Biomarkers of Persistent Arthralgia and Severe Disease After Chikungunya Virus Infection: A 5-Year Follow-Up Study in Southern Thailand. Viral immunology 32, 442-452.

Nitulescu, G.M., Van De Venter, M., Nitulescu, G., Ungurianu, A., Juzenas, P., Peng, Q., Olaru, O.T., Grădinaru, D., Tsatsakis, A., Tsoukalas, D., 2018. The Akt pathway in oncology therapy and beyond. International journal of oncology 53, 2319-2331.
Nomaguchi, M., Teramoto, T., Yu, L., Markoff, L., Padmanabhan, R., 2004.

Requirements for West Nile virus (–)-and (+)-strand subgenomic RNA synthesis in vitro by the viral RNA-dependent RNA polymerase expressed in Escherichia coli. Journal of Biological Chemistry 279, 12141-12151.

Oh, W., Yang, M.-R., Lee, E.-W., Park, K.-m., Pyo, S., Yang, J.-s., Lee, H.-W., Song, J., 2006. Jab1 mediates cytoplasmic localization and degradation of West Nile virus capsid protein. Journal of Biological Chemistry 281, 30166-30174.

Okamoto, M., Kouwaki, T., Fukushima, Y., Oshiumi, H., 2018. Regulation of RIG-I activation by K63-linked polyubiquitination. Frontiers in Immunology 8, 1942.

Ooi, Y.S., Stiles, K.M., Liu, C.Y., Taylor, G.M., Kielian, M., 2013. Genome-wide RNAi screen identifies novel host proteins required for alphavirus entry. PLoS pathogens 9.

Orange, J.S., Wang, B., Terhorst, C., Biron, C.A., 1995. Requirement for natural killer cell-produced interferon gamma in defense against murine cytomegalovirus infection and enhancement of this defense pathway by interleukin 12 administration. The Journal of experimental medicine 182, 1045-1056.

Panka, D.J., Mano, T., Suhara, T., Walsh, K., Mier, J.W., 2001. Phosphatidylinositol 3-kinase/Akt activity regulates c-FLIP expression in tumor cells. Journal of Biological Chemistry 276, 6893-6896.

Peti, W., Nairn, A.C., Page, R., 2013. Structural basis for protein phosphatase 1 regulation and specificity. The FEBS journal 280, 596-611.

Pham, A.M., Santa Maria, F.G., Lahiri, T., Friedman, E., Marie, I.J., Levy, D.E., 2016. PKR transduces MDA5-dependent signals for type I IFN induction. PLoS pathogens 12.

Pichlmair, A., Lassnig, C., Eberle, C.-A., Górna, M.W., Baumann, C.L., Burkard, T.R., Bürckstümmer, T., Stefanovic, A., Krieger, S., Bennett, K.L., 2011. IFIT1 is an antiviral protein that recognizes 5′-triphosphate RNA. Nature immunology 12, 624.

Poland, G.A., Ovsyannikova, I.G., Kennedy, R.B., 2019. Zika vaccine development: current status, Mayo Clinic Proceedings. Elsevier, pp. 2572-2586.

Poo, Y.S., Rudd, P.A., Gardner, J., Wilson, J.A., Larcher, T., Colle, M.-A., Le, T.T., Nakaya, H.I., Warrilow, D., Allcock, R., 2014. Multiple immune factors are involved in controlling acute and chronic chikungunya virus infection. PLoS neglected tropical diseases 8.

Popgeorgiev, N., Jabbour, L., Gillet, G., 2018. Subcellular localization and dynamics of the Bcl-2 family of proteins. Frontiers in cell and developmental biology 6, 13.

Raaben, M., Jae, L.T., Herbert, A.S., Kuehne, A.I., Stubbs, S.H., Chou, Y.-y., Blomen, V.A., Kirchhausen, T., Dye, J.M., Brummelkamp, T.R., 2017. NRP2 and CD63 are host factors for Lujo virus cell entry. Cell host & microbe 22, 688-696. e685.

Raghu, H., Cruz, C., Rewerts, C.L., Frederick, M.D., Thornton, S., Mullins, E.S., Schoenecker, J.G., Degen, J.L., Flick, M.J., 2015. Transglutaminase factor XIII promotes arthritis through mechanisms linked to inflammation and bone erosion. Blood, The Journal of the American Society of Hematology 125, 427-437.

Rathmell, J.C., Fox, C.J., Plas, D.R., Hammerman, P.S., Cinalli, R.M., Thompson, C.B., 2003. Akt-directed glucose metabolism can prevent Bax conformation change and promote growth factor-independent survival. Molecular and cellular biology 23, 7315-7328.

Reid, C.R., Airo, A.M., Hobman, T.C., 2015. The virus-host interplay: biogenesis of+ RNA replication complexes. Viruses 7, 4385-4413.

Reyes-del Valle, J., Chávez-Salinas, S., Medina, F., del Angel, R.M., 2005. Heat Shock Protein 90 and Heat Shock Protein 70 Are Components of Dengue Virus Receptor Complex in Human Cells. Journal of Virology 79, 4557-4567.

Rezza, G., Weaver, S.C., 2019. Chikungunya as a paradigm for emerging viral diseases: Evaluating disease impact and hurdles to vaccine development. PLoS neglected tropical diseases 13.

Riedl, W., Acharya, D., Lee, J.-H., Liu, G., Serman, T., Chiang, C., Chan, Y.K., Diamond, M.S., Gack, M.U., 2019. Zika virus NS3 mimics a cellular 14-3-3-binding motif to antagonize RIG-I-and MDA5-mediated innate immunity. Cell host & microbe 26, 493-503. e496.

Rivera, J., Abrams, C., Hernáez, B., Alcázar, A., Escribano, J.M., Dixon, L., Alonso, C., 2007. The MyD116 African swine fever virus homologue interacts with the catalytic subunit of protein phosphatase 1 and activates its phosphatase activity. Journal of virology 81, 2923-2929.

Saeed, M.F., Kolokoltsov, A.A., Freiberg, A.N., Holbrook, M.R., Davey, R.A., 2008. Phosphoinositide-3 kinase-Akt pathway controls cellular entry of Ebola virus. PLoS pathogens 4.

Safa, A., 2012. c-FLIP, a master anti-apoptotic regulator. Experimental oncology 34, 176.

Saito, T., Hirai, R., Loo, Y.-M., Owen, D., Johnson, C.L., Sinha, S.C., Akira, S., Fujita, T., Gale, M., 2007. Regulation of innate antiviral defenses through a shared repressor domain in RIG-I and LGP2. Proceedings of the National Academy of Sciences 104, 582-587.

Samuel, G.H., Wiley, M.R., Badawi, A., Adelman, Z.N., Myles, K.M., 2016. Yellow fever virus capsid protein is a potent suppressor of RNA silencing that binds double-stranded RNA. Proceedings of the National Academy of Sciences 113, 13863-13868.

Samuel, M.A., Diamond, M.S., 2005. Alpha/beta interferon protects against lethal West Nile virus infection by restricting cellular tropism and enhancing neuronal survival. Journal of virology 79, 13350-13361.

Sánchez-Aparicio, M.T., Feinman, L.J., García-Sastre, A., Shaw, M.L., 2018. Paramyxovirus V proteins interact with the RIG-I/TRIM25 regulatory complex and inhibit RIG-I signaling. Journal of Virology 92, e01960-01917.

Sanchez, J.G., Chiang, J.J., Sparrer, K.M., Alam, S.L., Chi, M., Roganowicz, M.D., Sankaran, B., Gack, M.U., Pornillos, O., 2016. Mechanism of TRIM25 catalytic activation in the antiviral RIG-I pathway. Cell reports 16, 1315-1325.

Santiago, F.W., Halsey, E.S., Siles, C., Vilcarromero, S., Guevara, C., Silvas, J.A., Ramal, C., Ampuero, J.S., Aguilar, P.V., 2015. Long-term arthralgia after Mayaro virus infection correlates with sustained pro-inflammatory cytokine response. PLoS neglected tropical diseases 9, e0004104.

Scaturro, P., Stukalov, A., Haas, D.A., Cortese, M., Draganova, K., Płaszczyca, A., Bartenschlager, R., Götz, M., Pichlmair, A., 2018. An orthogonal proteomic survey uncovers novel Zika virus host factors. Nature 561, 253.

Schalich, J., Allison, S.L., Stiasny, K., Mandl, C.W., Kunz, C., Heinz, F.X., 1996. Recombinant subviral particles from tick-borne encephalitis virus are fusogenic and provide a model system for studying flavivirus envelope glycoprotein functions. Journal of virology 70, 4549-4557.

Scherbik, S.V., Brinton, M.A., 2010. Virus-induced Ca2+ influx extends survival of west nile virus-infected cells. Journal of virology 84, 8721-8731.

Schneider, W.M., Chevillotte, M.D., Rice, C.M., 2014. Interferon-stimulated genes: a complex web of host defenses. Annual review of immunology 32, 513-545.

Schoggins, J.W., MacDuff, D.A., Imanaka, N., Gainey, M.D., Shrestha, B., Eitson, J.L., Mar, K.B., Richardson, R.B., Ratushny, A.V., Litvak, V., 2014. Pan-viral specificity of IFN-induced genes reveals new roles for cGAS in innate immunity. Nature 505, 691-695.

Schuffenecker, I., Iteman, I., Michault, A., Murri, S., Frangeul, L., Vaney, M.-C., Lavenir, R., Pardigon, N., Reynes, J.-M., Pettinelli, F., 2006. Genome microevolution of chikungunya viruses causing the Indian Ocean outbreak. PLoS medicine 3.

Schug, Z.T., Gonzalvez, F., Houtkooper, R., Vaz, F.M., Gottlieb, E., 2011. BID is cleaved by caspase-8 within a native complex on the mitochondrial membrane. Cell Death & Differentiation 18, 538-548.

Schulz, O., Diebold, S.S., Chen, M., Näslund, T.I., Nolte, M.A., Alexopoulou, L., Azuma, Y.-T., Flavell, R.A., Liljeström, P., e Sousa, C.R., 2005. Toll-like receptor 3 promotes cross-priming to virus-infected cells. Nature 433, 887-892.

Serman, T.M., Gack, M.U., 2019. Evasion of Innate and Intrinsic Antiviral Pathways by the Zika Virus. Viruses 11, 970.

Shang, Z., Song, H., Shi, Y., Qi, J., Gao, G.F., 2018. Crystal structure of the capsid protein from Zika virus. Journal of molecular biology 430, 948-962.

Sherman, B.T., Lempicki, R.A., 2009. Systematic and integrative analysis of large gene lists using DAVID bioinformatics resources. Nature protocols 4, 44-57.

Shi, Q., Hoffman, B., Liu, Q., 2016. PI3K-Akt signaling pathway upregulates hepatitis C virus RNA translation through the activation of SREBPs. Virology 490, 99-108.

Shresta, S., Kyle, J.L., Snider, H.M., Basavapatna, M., Beatty, P.R., Harris, E., 2004. Interferon-dependent immunity is essential for resistance to primary dengue virus infection in mice, whereas T-and B-cell-dependent immunity are less critical. Journal of virology 78, 2701-2710.

Skoging, U., Vihinen, M., Nilsson, L., Liljeström, P., 1996. Aromatic interactions define the binding of the alphavirus spike to its nucleocapsid. Structure 4, 519-529.

Slomnicki, L.P., Chung, D.-H., Parker, A., Hermann, T., Boyd, N.L., Hetman, M., 2017. Ribosomal stress and Tp53-mediated neuronal apoptosis in response to capsid protein of the Zika virus. Scientific reports 7, 16652.

Smit, J.M., Moesker, B., Rodenhuis-Zybert, I., Wilschut, J., 2011. Flavivirus cell entry and membrane fusion. Viruses 3, 160-171.

Smith, C.A., Davis, T., Wignall, J.M., Din, W.S., Farrah, T., Upton, C., McFadden, G., Goodwin, R.G., 1991. T2 open reading frame from the Shope fibroma virus encodes a soluble form of the TNF receptor. Biochemical and biophysical research communications 176, 335-342.

Soares, J.A., Leite, F.G., Andrade, L.G., Torres, A.A., De Sousa, L.P., Barcelos, L.S., Teixeira, M.M., Ferreira, P.C., Kroon, E.G., Souto-Padrón, T., 2009. Activation of the PI3K/Akt pathway early during vaccinia and cowpox virus infections is required for both host survival and viral replication. Journal of virology 83, 6883-6899.

Soulat, D., Bürckstümmer, T., Westermayer, S., Goncalves, A., Bauch, A., Stefanovic, A., Hantschel, O., Bennett, K.L., Decker, T., Superti-Furga, G., 2008. The DEAD-box helicase DDX3X is a critical component of the TANK-binding kinase 1-dependent innate immune response. The EMBO journal 27, 2135-2146.

Sourisseau, M., Schilte, C., Casartelli, N., Trouillet, C., Guivel-Benhassine, F., Rudnicka, D., Sol-Foulon, N., Le Roux, K., Prevost, M.-C., Fsihi, H., 2007. Characterization of reemerging chikungunya virus. PLoS Pathog 3, e89.

Spuul, P., Balistreri, G., Kääriäinen, L., Ahola, T., 2010. Phosphatidylinositol 3-kinase-, actin-, and microtubule-dependent transport of Semliki Forest Virus replication complexes from the plasma membrane to modified lysosomes. Journal of virology 84, 7543-7557.

Srisutthisamphan, K., Jirakanwisal, K., Ramphan, S., Tongluan, N., Kuadkitkan, A., Smith, D.R., 2018. Hsp90 interacts with multiple dengue virus 2 proteins. Scientific reports 8, 1-13.

Stadler, K., Allison, S.L., Schalich, J., Heinz, F.X., 1997. Proteolytic activation of tick-borne encephalitis virus by furin. Journal of virology 71, 8475-8481.

Stiasny, K., Fritz, R., Pangerl, K., Heinz, F.X., 2011. Molecular mechanisms of flavivirus membrane fusion. Amino acids 41, 1159-1163.

Stiles, K.M., Kielian, M., 2016. Role of TSPAN9 in alphavirus entry and early endosomes. Journal of virology 90, 4289-4297.

Stocks, C., Lobigs, M., 1998. Signal peptidase cleavage at the flavivirus C-prM junction: dependence on the viral NS2B-3 protease for efficient processing requires determinants in C, the signal peptide, and prM. Journal of virology 72, 2141-2149.

Street, A., Macdonald, A., Crowder, K., Harris, M., 2004. The Hepatitis C virus NS5A protein activates a phosphoinositide 3-kinase-dependent survival signaling cascade. Journal of Biological Chemistry 279, 12232-12241.

Suhrbier, A., 2019. Rheumatic manifestations of chikungunya: emerging concepts and interventions. Nature Reviews Rheumatology 15, 597-611.

Sun, B., Sundström, K.B., Chew, J.J., Bist, P., Gan, E.S., Tan, H.C., Goh, K.C., Chawla, T., Tang, C.K., Ooi, E.E., 2017a. Dengue virus activates cGAS through the release of mitochondrial DNA. Scientific reports 7, 1-8.

Sun, X., Hua, S., Chen, H.-R., Ouyang, Z., Einkauf, K., Tse, S., Ard, K., Ciaranello, A., Yawetz, S., Sax, P., 2017b. Transcriptional changes during naturally acquired Zika virus infection render dendritic cells highly conducive to viral replication. Cell reports 21, 3471-3482.

Sutaria, R.B., Amaral, J.K., Schoen, R.T., 2018. Emergence and treatment of chikungunya arthritis. Current opinion in rheumatology 30, 256-263.

Swiecki, M., Colonna, M., 2011. Type I interferons: diversity of sources, production pathways and effects on immune responses. Current opinion in virology 1, 463-475.

Tewari, K., Nakayama, Y., Suresh, M., 2007. Role of direct effects of IFN-γ on T cells in the regulation of CD8 T cell homeostasis. The Journal of Immunology 179, 2115-2125.

Thomas, S.J., 2015. NS1: A corner piece in the dengue pathogenesis puzzle? Science translational medicine 7, 304fs337-304fs337.

Tiwari, S.K., Dang, J., Qin, Y., Lichinchi, G., Bansal, V., Rana, T.M., 2017. Zika virus infection reprograms global transcription of host cells to allow sustained infection. Emerging microbes & infections 6, 1-10.

Tsetsarkin, K.A., Vanlandingham, D.L., McGee, C.E., Higgs, S., 2007. A single mutation in chikungunya virus affects vector specificity and epidemic potential. PLoS pathogens 3.

Urbanowski, M.D., Hobman, T.C., 2013. The West Nile virus capsid protein blocks apoptosis through a phosphatidylinositol 3-kinase-dependent mechanism. Journal of virology 87, 872-881.

Urbanowski, M.D., Ilkow, C.S., Hobman, T.C., 2008. Modulation of signaling pathways by RNA virus capsid proteins. Cellular signalling 20, 1227-1236.

Vairo, F., Haider, N., Kock, R., Ntoumi, F., Ippolito, G., Zumla, A., 2019. Chikungunya: Epidemiology, Pathogenesis, Clinical Features, Management, and Prevention. Infectious Disease Clinics 33, 1003-1025.

Van Der Schaar, H.M., Rust, M.J., Chen, C., van der Ende-Metselaar, H., Wilschut, J., Zhuang, X., Smit, J.M., 2008. Dissecting the cell entry pathway of dengue virus by single-particle tracking in living cells. PLoS pathogens 4.

van Marle, G., Antony, J., Ostermann, H., Dunham, C., Hunt, T., Halliday, W., Maingat, F., Urbanowski, M.D., Hobman, T., Peeling, J., 2007. West Nile virus-induced neuroinflammation: glial infection and capsid protein-mediated neurovirulence. Journal of virology 81, 10933-10949.

Vega-Avila, E., Pugsley, M.K., 2011. An overview of colorimetric assay methods used to assess survival or proliferation of mammalian cells, Proc West Pharmacol Soc, p. e4.

Villordo, S.M., Gamarnik, A.V., 2009. Genome cyclization as strategy for flavivirus RNA replication. Virus research 139, 230-239.

Walczak, H., Krammer, P.H., 2000. The CD95 (APO-1/Fas) and the TRAIL (APO-2L) apoptosis systems. Experimental cell research 256, 58-66.

Wang, X., Chen, W., Zeng, W., Bai, L., Tesfaigzi, Y., Belinsky, S.A., Lin, Y., 2008. Akt-mediated eminent expression of c-FLIP and Mcl-1 confers acquired resistance to TRAIL-induced cytotoxicity to lung cancer cells. Molecular cancer therapeutics 7, 1156-1163.

Wang, X., Iyer, A., Lyons, A.B., Korner, H., Wei, W., 2019. Emerging Roles For G-protein Coupled Receptors in Development and Activation of Macrophages: An update! Frontiers in Immunology 10, 2031.

Ward, P.S., Thompson, C.B., 2012. Signaling in control of cell growth and metabolism. Cold Spring Harbor perspectives in biology 4, a006783.

Wies, E., Wang, M.K., Maharaj, N.P., Chen, K., Zhou, S., Finberg, R.W., Gack, M.U., 2013. Dephosphorylation of the RNA sensors RIG-I and MDA5 by the phosphatase PP1 is essential for innate immune signaling. Immunity 38, 437-449.

Wiggins, K., Eastmond, B., Alto, B., 2018. Transmission potential of Mayaro virus in Florida Aedes aegypti and Aedes albopictus mosquitoes. Medical and veterinary entomology 32, 436-442.

Willows, S., Hou, S., Hobman, T.C., 2013. RNA virus capsid proteins: more than just a shell. Future Virology 8, 435-450.

Wisniewski, H.-G., Burgess, W.H., Oppenheim, J.D., Vilcek, J., 1994. TSG-6, an Arthritis-Associated Hyaluronan Binding Protein, Forms a Stable Complex with the Serum Protein Inter-. alpha.-inhibitor. Biochemistry 33, 7423-7429.

Wolf, D., Witte, V., Laffert, B., Blume, K., Stromer, E., Trapp, S., d'Aloja, P., Schürmann, A., Baur, A.S., 2001. HIV-1 Nef associated PAK and PI3-kinases stimulate Akt-independent Bad-phosphorylation to induce anti-apoptotic signals. Nature medicine 7, 1217-1224.

Wong, C.P., Xu, Z., Hou, S., Limonta, D., Kumar, A., Power, C., Hobman, T.C., 2019. Interplay between Zika Virus and Peroxisomes during Infection. Cells 8, 725.

World-Health-Organization, Research, S.P.f., Diseases, T.i.T., Diseases, W.H.O.D.o.C.o.N.T., Epidemic, W.H.O., Alert, P., 2009. Dengue: guidelines for diagnosis, treatment, prevention and control. World Health Organization.

Wu, Y., Liu, Q., Zhou, J., Xie, W., Chen, C., Wang, Z., Yang, H., Cui, J., 2017. Zika virus evades interferon-mediated antiviral response through the co-operation of multiple nonstructural proteins in vitro. Cell discovery 3, 1-14.

Xiao, L., Gong, L., Yuan, D., Deng, M., Zeng, X., Chen, L., Zhang, L., Yan, Q., Liu, J., Hu, X., 2010. Protein phosphatase-1 regulates Akt1 signal transduction pathway to control gene expression, cell survival and differentiation. Cell Death & Differentiation 17, 1448-1462.

Xie, X., Zou, J., Zhang, X., Zhou, Y., Routh, A.L., Kang, C., Popov, V.L., Chen, X., Wang, Q.-Y., Dong, H., 2019. Dengue NS2A protein orchestrates virus assembly. Cell host & microbe 26, 606-622. e608.

Xing, H., Xu, S., Jia, F., Yang, Y., Xu, C., Qin, C., Shi, L., 2020. Zika NS2B is a crucial factor recruiting NS3 to the ER and activating its protease activity. Virus research 275, 197793.

Yamanaka, H., 2015. TNF as a target of inflammation in rheumatoid arthritis. Endocrine, Metabolic & Immune Disorders-Drug Targets (Formerly Current Drug Targets-Immune, Endocrine & Metabolic Disorders) 15, 129-134.

Yanai, H., Chiba, S., Hangai, S., Kometani, K., Inoue, A., Kimura, Y., Abe, T., Kiyonari, H., Nishio, J., Taguchi-Atarashi, N., 2018. Revisiting the role of IRF3 in inflammation and immunity by conditional and specifically targeted gene ablation in mice. Proceedings of the National Academy of Sciences 115, 5253-5258.

Yang, J.-S., Ramanathan, M.P., Muthumani, K., Choo, A.Y., Jin, S.-H., Yu, Q.-C., Hwang, D.S., Choo, D.K., Lee, M.D., Dang, K., 2002. Induction of inflammation by West Nile virus capsid through the caspase-9 apoptotic pathway. Emerging infectious diseases 8, 1379.

Yang, M.R., Lee, S.R., Oh, W., Lee, E.W., Yeh, J.Y., Nah, J.J., Joo, Y.S., Shin, J., Lee, H.W., Pyo, S., 2008. West Nile virus capsid protein induces p53-mediated apoptosis via the sequestration of HDM2 to the nucleolus. Cellular microbiology 10, 165-176.

Yang, X.-K., Xu, W.-D., Leng, R.-X., Liang, Y., Liu, Y.-Y., Fang, X.-Y., Feng, C.-C., Li, R., Cen, H., Pan, H.-F., 2015. Therapeutic potential of IL-15 in rheumatoid arthritis. Human immunology 76, 812-818.

Ye, J., Zhu, B., Fu, Z.F., Chen, H., Cao, S., 2013. Immune evasion strategies of flaviviruses. Vaccine 31, 461-471.

Yoneyama, M., Kikuchi, M., Natsukawa, T., Shinobu, N., Imaizumi, T., Miyagishi, M., Taira, K., Akira, S., Fujita, T., 2004. The RNA helicase RIG-I has an essential function in double-stranded RNA-induced innate antiviral responses. Nature immunology 5, 730.

You, J., Hou, S., Malik-Soni, N., Xu, Z., Kumar, A., Rachubinski, R.A., Frappier, L., Hobman, T.C., 2015. Flavivirus infection impairs peroxisome biogenesis and early antiviral signaling. Journal of virology 89, 12349-12361.

Zevini, A., Olagnier, D., Hiscott, J., 2017. Crosstalk between cytoplasmic RIG-I and STING sensing pathways. Trends in immunology 38, 194-205.

Zhang, L., Yu, M., Deng, J., Lv, X., Liu, J., Xiao, Y., Yang, W., Zhang, Y., Li, C., 2015. Chemokine signaling pathway involved in CCL2 expression in patients with rheumatoid arthritis. Yonsei medical journal 56, 1134-1142.

Zhang, R., Kim, A.S., Fox, J.M., Nair, S., Basore, K., Klimstra, W.B., Rimkunas, R., Fong, R.H., Lin, H., Poddar, S., 2018. Mxra8 is a receptor for multiple arthritogenic alphaviruses. Nature 557, 570-574.

Zhang, X., Jia, R., Shen, H., Wang, M., Yin, Z., Cheng, A., 2017. Structures and functions of the envelope glycoprotein in flavivirus infections. Viruses 9, 338.

Zhang, X., Xie, X., Xia, H., Zou, J., Huang, L., Popov, V.L., Chen, X., Shi, P.-Y., 2019. Zika Virus NS2A-Mediated Virion Assembly. mBio 10, e02375-02319.

Zhao, H., Lindqvist, B., Garoff, H., Von Bonsdorff, C., Liljeström, P., 1994. A tyrosine-based motif in the cytoplasmic domain of the alphavirus envelope protein is essential for budding. The EMBO Journal 13, 4204-4211.

Zhou, Z., Xue, Q., Wan, Y., Yang, Y., Wang, J., Hung, T., 2011. Lysosome-associated membrane glycoprotein 3 is involved in influenza A virus replication in human lung epithelial (A549) cells. Virology journal 8, 384.

Zmurko, J., Neyts, J., Dallmeier, K., 2015. Flaviviral NS4b, chameleon and jack-in-the-box roles in viral replication and pathogenesis, and a molecular target for antiviral intervention. Reviews in medical virology 25, 205-223.